Towards fine-tuning the surface corona of inorganic and organic nanomaterials to control their properties at nano-bio interface

A thesis submitted in fulfilment of the requirements for the degree of Doctor of Philosophy

By
Hemant Kumar Daima
B.Sc. (Life Sciences), M.Sc. (Biotechnology)

School of Applied Sciences
College of Science, Engineering and Health
RMIT University
March 2013

Towards fine-tuning the surface corona of inorganic and organic nanomaterials to control their properties at nano-bio interface

A thesis submitted in fulfilment of the requirements for the degree of Doctor of Philosophy (Applied Biology and Biotechnology)

By

Hemant Kumar Daima

B.Sc. (Life Sciences), M.Sc. (Biotechnology), GATE (Life Sciences)

(National Overseas Scholar, Government of India)

School of Applied Sciences

College of Science, Engineering and Health

RMIT University, Melbourne (Australia)

March 2013

Declaration

I, Hemant Kumar Daima, declare that except where due acknowledgements have been made, this work is that of myself alone; this work has not been submitted previously, in whole or in part, to qualify for any other academic award; and the content of the thesis is the result of work that has been carried out since the official commencement date of the approved research programme; and, any editorial work, paid or unpaid, carried out by a third party is acknowledged.

Hemant Kumar Daima

Date 14.06.2013

Acknowledgements

Working toward Ph.D. has been a wonderful and overwhelming experience and I am indebted to many people, who supported me during this marathon event. I would like to thank all of them for their generous support and help throughout this experience.

First of all, I sincerely express my gratitude to my research supervisors, Prof. S. K. Bhargava and Associate Prof. Vipul Bansal, for sharing their knowledge, and constantly motivating me to strive for greater heights in life. I feel humbled to have worked under your guidance and both of you have been great mentors. Along with my research guides, I must thank Dr. PR. Selvakannan for introducing me to the fascinating area of Nanobiotechnology and helping me throughout this research marathon. Today, I feel lucky to have you all in my life because whenever, I was in dark, I found that you were standing with me to support and encourage. Once I read that "you are not alone during your PhD, your supervisor are with you and your success is their success." You made these words true to me. I am thankful to you for making the time working on my PhD an unforgeable experience.

Dr. Shiv, Dr. Anthony, Dr. Ravi and Ahmad, I am also thankful to you for helping and assisting me with some experiments and data analysis presented in this thesis. Dr. Andrew and Dr. Selvakannan thank you very much for your considerable time to proof-read this thesis. Also, I must thank Prof. Andrew Smith (Dean, School of Applied Sciences) for his priceless suggestions during thesis writing. Special words of indebtedness are due to technical staff Zahra, Paul, Phil, Frank, Peter, Diana, and to all the duty microscopists, who were available whenever I needed them. Thank you all for your technical expertise and support throughout the years. I also express my gratitude to administrative and laboratory staff Karl, Karina, Dr. Lisa, Alexendra, Ruth, Nadia, Howard and Samira for all the help provided over the years.

During my stay in Melbourne, I have met some fantastic individuals, I thank Dr. James, Dr. Mamad, Dr. Sarvesh, Dr. Sampa, Dr. Lily, Dr. Helen, Dr. Devendra, Dr. Frew, Dr. Samuel, Dr. Steven, Dr. Kshudiram, Dr. Neda, Dr. Gopa, Dr. Ylias, Dr. Mukund, Dr.

Andrew, Dr. Rajesh, Dr. Julie, Dr. Sheshnath, Dr. Jammi, Dr. Colin, Dr. Deepa, Dr. Travor, Dr. Greg, Dr. Srinivash, Dr. Jyoti, Dr. Jarrod, Hailey, Jackie, Jos, Emma, Andrew, Andreas, Vivian, Blake, Rahul, Katie, Scott, Fiona, Vishal, Kavitha, Nicola, Ilija, Manika, Akshi, Mahasha, Nafisha, Nura, Addi, Vinni, Sami, Chewe, Blagoj, Kae, Grace, ST, Kim, Linda, Rose, Ben, Den, Meth, Melissa and Adam. You all have unique personality and I will always treasure our friendship and it was a pleasant time for me. You all have been very kind, welcoming and accommodating and it was truly fantastic working and staying with you. Also, I must thank my house owner Chalie and current and previous house mates (Kasif, Mohammad, Tsion, Parul, Ali, Polin, Thakashi, Sonam, Hadi and Yumi) for their cooperation and support at home. Thank you all for always being just a phone call away.

I extend my genuine gratitude to MSJE, Government of India, New Delhi (India) for National Overseas Scholarship, which enabled me to pursue doctoral studies at RMIT University, Melbourne (Australia). Also, I would like to convey my special gratitude to all the staff members of the Indian Consulate at Melbourne, for their constant support and encouragement throughout my stay in Australia. I am also thankful to the DPVC travel grants for funding my two international trips to USA and India for giving me opportunity to present my work at international conferences and RACI graduate travel award.

Finally, I would like to acknowledge the people, who mean the world to me, my parents Shri R. C. Daima and Smt. S. Devi for everything. Many thanks to my naughty brother Lokesh and lovely sister in-law Aarti, for their infinite love. At the end, special words are due to Kalpana for her love, encouragement, patience & above all her support. Your support and inspiration made me to believe in myself & helped me to achieve my dream. I cannot pay back the sacrifices done by you all. Thank you for being in my life.

Last but not least, I thank all those who have helped me directly & indirectly for the successful completion of my research work. Finally, I thank the Almighty for giving me the strength & patience to work through all these years so that today I can stand proud. ***Hemant Kumar Daima***

This dissertation is dedicated to my lovely sister Urmila, who is in some other world now.

Dearest Urmila, although you are in a better place now, I wish you were around to witness my accomplishment. You are always in my thoughts.

Dearest Dad, Mom, Lokesh, Kalpana and Aarti this journey would not have been possible without your love, support, patience and sacrifices. Thank you for being my pillars of strength.

Table of Contents

List of figures xi

List of tables xvii

List of abbreviation and acronyms xviii

Abstract xx

Chapter I. Introduction 1-51

1.1. Nanosciences to nanobiotechnology 2

1.2. What is 'NANO' and why it is different? 4

1.3. Nano-bio interface, toxicity and fabrication of nanomaterials 5

1.4. Interactions between nanoparticles and bacterial cells 9

1.4.1. Structure of Gram positive and negative bacterial cell wall ... 10

1.4.2. Antibiotics, antimicrobial peptides and nanomaterial as antibacterial agents 12

1.5. Other applications of nanobiotechnology 15

1.6. Production of nanoparticles by top-down or bottom-up approach ... 17

1.7. Metal nanoparticles formation and their stability 18

1.8. Surface plasmon of metallic Au and Ag nanoparticles 20

1.9. Objective of the thesis 22

1.10. Outline of thesis 24

1.11. References 26

Chapter II. Characterization techniques 52-71

2.1. Introduction 53

2.2. Microscopy techniques 54

2.2.1. Transmission electron microscopy (TEM) 54

2.2.2. Scanning electron microscopy (SEM) 56

2.3. Spectroscopy techniques 59

2.3.1. Ultraviolet-visible (UV-vis) spectroscopy 59

2.3.2. Fourier transform infrared (FTIR) spectroscopy 60

2.3.3. Other spectroscopic techniques 61

2.3.3.1. Atomic absorption spectroscope (AAS) 61

2.3.3.2. Inductively coupled plasma mass spectroscopy 62

2.4. X-ray based characterization techniques 63

2.4.1. X-Ray photoemission spectroscopy (XPS) 63

2.4.2. Energy dispersive X-ray analysis (EDX) 65

2.5. Particles size analyser 65

2.5.1. Dynamic light scattering (DLS) 66

2.6. Zeta potential measurement (particles charge analyser) 67

2.7. Electrochemical studies using cyclic voltammetry (CV) 68

2.8. References 69

Chapter III. Influence of composition and surface functionalization of nanomaterials towards their biological activities 72-141

3.1. Introduction 73

3.2. Scheme of the work 79

3.3. Experimental section 81

3.3.1. Synthesis of Au, Ag and Au-Ag alloy nanoparticles 81

3.3.2. Processing of nanoparticles by concentration and dialysis 82

3.3.3. Peroxidase-like activity of Au, Ag and Au-Ag nanoparticles ... 82

3.3.4. Antibacterial assays of Au, Ag and Au-Ag alloy nanoparticles 83

3.4. Results and discussion 84

3.4.1. UV-visible spectral studies of Au, Ag and Au-Ag alloy nanoparticles 85

3.4.2. TEM studies of amino acid reduced Au, Ag and Au-Ag alloy nanoparticles 88

3.4.3. Estimation of the metal content present in dialysed nanoparticle solutions 91

3.4.4. Zeta potential measurements of Au, Ag and Au-Ag alloy nanoparticles 92

3.4.5. X-ray photoemission spectroscopy analysis of Au, Ag and Au-Ag alloy nanoparticles 93

3.4.6. FTIR analysis for the confirmation of amino acid shell 98

3.4.7. Electrochemical behaviour of amino acid capped Au, Ag and their alloy nanoparticles 100

3.5. Rational behind employing these nanomaterials for biological applications 104

3.5.1. *In vitro* peroxidase-like behaviour of amino acids capped Au, Ag and Au-Ag alloy nanoparticles 104

3.5.2. Antibacterial assays of amino acid capped nanoparticles 112

3.5.2.1. Antibacterial effects of nanoparticles and influence of surface functionalization 113

3.5.2.2. Effect of metal composition on antibacterial activity employing Au-Ag alloy nanoparticles 116

3.5.2.3. Morphological studies of Au and Ag nanoparticles treated *E. coli* and *S. albus* bacterial cells 119

3.6. Conclusions 125

3.7. References 126

Chapter IV. Sequential surface functionalization of metal nanoparticles using polyoxometalates and lysine to controllably enhance their antibacterial potential 142-191

4.1. Introduction 143

4.2. Scheme of the work 148

4.3. Experimental section 149

4.3.1. Synthesis of gold and silver nanoparticles 149

4.3.2. Processing and dialysis of tyrosine capped nanoparticles 150

4.3.3. Sequential surface functionalization with POMs and lysine 150

4.3.4. Antibacterial activity of POMs and lysine functionalized nanoparticles 151

4.4. Results and discussion 152

4.4.1. Surface charge measurements of POMs and lysine functionalized Au and Ag nanoparticles using zeta potential 153

4.4.2. Estimation of metal content using AAS and ICP-MS studies 155

4.4.3. UV-visible spectroscopic analysis of sequential surface functionalized nanoparticles 156

4.4.4. TEM and DLS measurements of functionalized Au and Ag nanoparticles 159

4.4.5. FTIR spectral analysis to understand surface corona of functionalized nanoparticles 163

4.4.6. XPS analysis of POMs and lysine functionalized nanoparticles 167

4.5. Antibacterial applications of functionalized nanoparticles 170

4.5.1. Assessment of antibacterial activities of gold, silver and their POMs and lysine functionalized nanoparticles 170

4.5.2. Morphological changes in bacterial cell after their treatments with gold, silver and functionalized nanoparticles 176

4.6. Conclusions 180

4.7. References 181

Chapter V. Self-assembled soft nanostructures of plasmid DNA and tri-block copolymer as non-viral DNA delivery vehicle 192-221

5.1. Introduction 193

5.2. Scheme of the work 197

5.3. Experimental section 198

5.3.1. Isolation of pDNA and purification 198

5.3.2. Preparation of pDNA and PEO-PPO-PEO complex 199

5.3.3. Preparation of competent cells 200

5.3.4. Transformation and gene expression 201

5.4. Results and discussion 201

5.4.1. TEM studies of self-assembled structures of pDNA and PEO-PPO-PEO with varying weight ratios 202

5.4.2. FTIR spectral analysis to recognize chemical interaction of self-assembled pDNA and PEO-PPO-PEO complex 204

5.4.3. XPS spectral analysis of self-assembled structures of pDNA and PEO-PPO-PEO 206

5.5. PEO_{20}-PPO_{69}-PEO_{20} mediated transformation and expression of GFP in transformed colonies 209

5.6. Conclusions 213

5.7. References 214

Chapter VI. Conclusions & scope for the future research 222-228

6.1. Summary and conclusions 223-226

6.2. Scope for future work 226-228

Appendices 229-236

List of Figures

Figure.1.1. Comparative sizes of biological components at nanoscale dimension 2

Figure.1.2. Schematic representation of various dimensions of materials at nanoscale 5

Figure.1.3. Schematic representation of various physicochemical properties of nanomaterials which influences nanoparticle-cell interaction 6

Figure.1.4. Schematic representation of peptidoglycan structure 10

Figure.1.5. Schematic diagram of the structure of Gram positive bacterial cell wall 11

Figure.1.6. Schematic representation of Gram negative bacterial cell wall 11

Figure.1.7. Schematic representation of mechanism of antibacterial activities exerted by nanoparticles 14

Figure.1.8. Schematic representation of the 'bottom-up' and 'top-down' synthesis processes of nanomaterials with the popular techniques 17

Figure.1.9. Scheme illustrating the stabilization of metal nanoparticles by (A) electrostatic and (B) steric interactions 19

Figure.1.10. Schematic representation of the interaction of light with metal nanoparticles 21

Figure.2.1. Schematic representation of the major components of the optical systems of a TEM (equivalent terms of light and electron microscopy are also shown) 55

Figure.2.2. Schematic representation of electron-sample interaction in SEM 57

Figure.2.3. Schematic representation of scanning electron microscope 58

Figure.2.4. Schematic representation of the XPS process, showing photo-ionization of an atom by the ejection of a 1s electron 63

Figure.2.5. Schematic representation of the electrical double layer on the surface of nanoparticle 67

Figure.3.1. Chemical structures of tryptophan and tyrosine amino acids . 79

Figure.3.2. Schematic representation of synthesis of Au, Ag and their alloy nanoparticles with different compositions and surface functionality 80

Figure.3.3. UV-visible absorbance spectra of (A) tryptophan (Trp) and tyrosine (Tyr), (B) tryptophan- and (C) tyrosine- reduced Au, Ag and Au-Ag alloy nanoparticles, respectively 85

Figure.3.4. Digital photographs of metal nanoparticle solutions synthesised using (A) tryptophan and (B) tyrosine 87

Figure.3.5. TEM images and particle size distribution histogram of tryptophan reduced Au, Ag and their alloy nanoparticles. Average particle sizes along with standard deviations are also shown 89

Figure.3.6. TEM images and particle size distribution histogram of tyrosine reduced Au, Ag and Au-Ag alloy nanoparticles. Corresponding average particle sizes along with standard deviations are also shown 90

Figure.3.7. Core level Au4f and Ag3d spectra of tryptophan and tyrosine synthesised Au and Ag nanoparticles (A-D) and core level Au4f (E) and Ag3d (F) spectra arising from $Au_{50}Ag_{50}^{Trp}$ alloy nanoparticles, respectively 94

Figure.3.8. Core level XPS spectra of C1s in pristine tryptophan (A), tyrosine (B), Au_{100}^{Trp}(C) and Au_{100}^{Tyr} (D) respectively. Core level N1s (E) and K2p (F) spectra of tryptophan synthesised Au_{100}^{Trp}, respectively 96

Figure.3.9. FTIR spectral analysis of (A) tryptophan- (curve 1) and (B) tyrosine- (curve 1) reduced Au_{100} (curve 2); $Au_{75}Ag_{25}$ (curve 3); $Au_{50}Ag_{50}$ (curve 4); $Au_{25}Ag_{75}$ (curve 5) and Ag_{100} (curve 6) nanoparticles, respectively 98

Figure.3.10. Cyclic voltametric profiles of tryptophan- (A) and tyrosine (B) synthesised nanoparticles recorded at 5 mV s^{-1} in 1 M H_2SO_4 101

Figure.3.11. Cyclic voltametric profiles of (A) typical gold oxide formation and reduction (B) CV profile of 1 mM tryptophan in 1 M H_2SO_4 and (C) CV profile of tyrosine oxidation 102

Figure.3.12. Schematic representation of oxidation of TMB by H_2O_2 catalysed by nanoparticles 106

Figure.3.13. Peroxidase-like behaviour of tryptophan- and tyrosine- capped Au, Ag and Au-Ag alloy nanoparticles with different concentrations 106

Figure.3.14. Temperature dependent peroxidase-like activity of tryptophan- and tyrosine- capped Au and Ag nanoparticles In all the panels, curve 1, 2, 3 and 4 correspond to Au_{100}^{Trp}, Au_{100}^{Tyr}, Ag_{100}^{Trp} and Ag_{100}^{Tyr}, respectively 107

Figure.3.15. Temperature dependent peroxidase-like activity of tryptophan (Panel A, B and C) and tyrosine (Panel D, E and F) capped Au-Ag nanoalloys. In all the panels, curve 1, 2 and 3 correspond to $Au_{75}Ag_{25}$, $Au_{50}Ag_{50}$ and $Au_{25}Ag_{75}$ respectively 111

Figure.3.16. Assessment of antibacterial potential of amino acid capped Au and Ag nanoparticles against (A) *E. coli* and (B) *S. albus*, respectively 115

Figure.3.17. Antibacterial activity of Au-Ag alloy nanoparticles synthesized by tryptophan and tyrosine against *E. coli* (A) and *S. albus* (B) 117

Figure.3.18. SEM micrographs of *E. coli* before and after their treatments with tryptophan and tyrosine synthesised nanoparticles 121

Figure.3.19. SEM micrographs of *S. albus* before and after their treatments with tryptophan and tyrosine synthesised nanoparticles 122

Figure.3.20. Schematic illustration of antibacterial activity of Au and Ag nanoparticles toward *E. coli* and *S. albus* 124

Figure.4.1. Schematic representation of sequential functionalization of tyrosine capped gold nanoparticles by polyoxometalates and lysine 149

Figure.4.2. UV-visible absorbance spectra of $AuNPs^{Tyr}$ and after their surface functionalization with (A) PTA/lysine and (B) PMA/lysine molecules 157

Figure.4.3. UV-visible absorbance spectra of $AgNPs^{Tyr}$ and after their surface functionalization with (A) PTA/lysine and (B) PMA/lysine molecules 158

Figure.4.4. TEM images and particle size distribution histograms of (A) $AuNPs^{Tyr}$, (B) $AuNPs^{Tyr@PTA}$, (C) $AuNPs^{Tyr@PTA\text{-}Lys}$, (D) $AuNPs^{Tyr@PMA}$ and (E) $AuNPs^{Tyr@PMA\text{-}Lys}$ 160

Figure.4.5. TEM images and corresponding particle size distribution histograms of (A) $AgNPs^{Tyr}$, (B) $AgNPs^{Tyr@PTA}$, (C) $AgNPs^{Tyr@PTA\text{-}Lys}$, (D) $AgNPs^{Tyr@PMA}$ and (E) $AgNPs^{Tyr@PMA\text{-}Lys}$ 162

Figure.4.6. FTIR spectra in Panel A: tyrosine, $AuNPs^{Tyr}$ and $AgNPs^{Tyr}$; in Panel B: PTA, $AuNPs^{Tyr@PTA}$, $AuNPs^{Tyr@PTA\text{-}Lys}$, $AgNPs^{Tyr@PTA}$ and $AgNPs^{Tyr@PTA\text{-}Lys}$; and in Panel C: PMA, $AuNPs^{Tyr@PMA}$, $AuNPs^{Tyr@PMA\text{-}Lys}$, $AgNPs^{Tyr@PMA}$ and $AgNPs^{Tyr@PMA\text{-}Lys}$, respectively 164

Figure.4.7. Schematic representation of formation of quinone type structure during reduction of Ag^{+} ions 165

Figure.4.8. Core level spectra of Au4f (A-E), recorded in $AuNPs^{Tyr}$, $AuNPs^{Tyr@PTA}$, $AuNPs^{Tyr@PTA-Lys}$, $AuNPs^{Tyr@PMA}$ and $AuNPs^{Tyr@PMA-Lys}$ samples, respectively. Core level spectra of C1s (F), W4f (G-H), Mo4f (I-J) recorded in $AuNPs^{Tyr}$, $AuNPs^{Tyr@PTA}$, $AuNPs^{Tyr@PTA-Lys}$, $AuNPs^{Tyr@PMA}$ and $AuNPs^{Tyr@PMA-Lys}$, respectively 168

Figure.4.9. Core level spectra of Ag3d (A), W4f (B-C), Mo4f (D-E) recorded in $AgNPs^{Tyr}$, $AgNPs^{Tyr@PTA}$, $AgNPs^{Tyr@PTA-Lys}$, $AgNPs^{Tyr@PMA}$ and $AgNPs^{Tyr@PMA-Lys}$ samples, respectively 169

Figure.4.10. Dose dependent antibacterial activity of PTA (Panels A), PMA (Panels B) and lysine functionalized Au nanoparticles 172

Figure.4.11. Dose dependent antibacterial activity of PTA (Panels A), PMA (Panels B) and lysine functionalized Ag nanoparticles 175

Figure.4.12. SEM micrographs of *Escherichia coli* cells (A) untreated and after their treatments with (B) $AuNPs^{Tyr}$, (C) $AuNPs^{Tyr@PTA}$, (D) $AuNPs^{Tyr@PTA-Lys}$, (E) $AuNPs^{Tyr@PMA}$, and (F) $AuNPs^{Tyr@PMA-Lys}$ 177

Figure.4.13. SEM micrographs of *Escherichia coli* cells (A) untreated and after treatments with (B) $AgNPs^{Tyr}$, (C) $AgNPs^{Tyr@PTA}$, (D) $AgNPs^{Tyr@PTA-Lys}$, (E) $AgNPs^{Tyr@PMA}$, and (F) $AgNPs^{Tyr@PMA-Lys}$ 178

Figure.4.14. Interaction of Au, Ag and their POMs and lysine surface functionalized nanoparticles with *E. coli* bacterial cells 179

Figure.5.1. Chemical structure of tri-block copolymer (PEO-PPO-PEO) ... 196

Figure.5.2. Schematic representation of self-assembly process of A-B-A type tri-block copolymer and pDNA 197

Figure.5.3. TEM images of as-formed (A-C) PEO-PPO-PEO micelles at different concentrations and after their complex formation with pDNA (D-F) 203

Figure.5.4. FTIR spectra of PEO-PPO-PEO (curve 1), pDNA (curve 2), and after their complexation at 1:1 and 1:10 ratios (curve 3 and 4), respectively 204

Figure.5.5. Core level XPS spectra of four principal elements present in pDNA 207

Figure.5.6. XPS spectra of C1s, O1s (tri-block copolymer), N1s and C1s in pDNA: PEO_{20}-PPO_{69}-PEO_{20} at 1:1 and 1: 10 ratios, respectively 208

Figure.5.7. Number of transformed colonies grown on ampicillin plates for varying ratios of pDNA and PEO_{20}-PPO_{69}-PEO_{20} 210

Figure.5.8. Representative transformed colonies grown on ampicillin plates showing expression of GFP gene. pDNA (A), pDNA:PEO_{20}-PPO_{69}-PEO_{20} complexes (B-D) at 1:1 (B), 1:5 (C), and 1:10 (D) ratios, respectively 211

Figure.5.9. Schematic representation of transformation by pDNA/polymer complex 212

List of tables

Table.3.1. Concentration of $HAuCl_4$ and $AgNO_3$ used for the synthesis of Au, Ag and Au-Ag alloy nanoparticles using tryptophan and tyrosine 81

Table.3.2: Molar ratios (%) of Au and Ag estimated from AAS and zeta potential measurements of nanoparticle solutions 92

Table.4.1. Relative concentrations of Au and W or Mo present on the surface of functionalized Au nanoparticles, as used for antibacterial studies 171

Table.4.2. Relative concentrations of Ag and W or Mo present on the surface of functionalized Ag nanoparticles, as used for antibacterial studies 174

Table.5.1. Weight ratios of pDNA and PEO_{20}-PPO_{69}-PEO_{20} employed to prepare self-assembled nanostructures 199

Table.5.2. Atomic % of oxygen, carbon and nitrogen present in pDNA, PEO-PPO-PEO and in the nanostructures of pDNA and PEO-PPO-PEO 209

List of abbreviation and acronyms

a.a. : Amino acid

AAS : Atomic absorption spectroscopy

Ag : Silver

AgNPs : Silver nanoparticles

$AgNPs^{PMA}$: Ag nanoparticles functionalized with phosphomolybdic acid

$AgNPs^{PTA}$: Ag nanoparticles functionalized with phosphotungstic acid

$AgNPs^{PMA@Lys}$: Lysine modified phosphomolybdic acid functionalized AgNPs

$AgNPs^{PTA@Lys}$: Lysine modified phosphotungstic acid functionalized AgNPs

AuNPs : Gold nanoparticles

$AuNPs^{PMA}$: Au nanoparticles functionalized with phosphomolybdic acid

$AuNPs^{PTA}$: Au nanoparticles functionalized with phosphotungstic acid

$AuNPs^{PMA@Lys}$: Lysine modified phosphomolybdic acid functionalized AuNPs

$AuNPs^{PTA@Lys}$: Lysine modified phosphotungstic acid functionalized AuNPs

CFU : Colony forming unit

DNA : Deoxyribonucleic acid

E. coli : *Escherichia coli*

FTIR : Fourier transform infrared

GFP : Green fluorescent protein

LB : Luria broth

Lys (K) : Lysine

nm : nanometer

NPs : nanoparticles

OD : Optical density

pDNA : Plasmid DNA

POM : Polyoxometalates

PMA : Phosphomolybdic acid

PTA : Phosphotungstic acid

S. albus : *Staphylococcus albus*

SERS : Surface enhanced Raman scattering

SEM : Scanning electron microscopy

ROS : Reactive oxygen species

SPR : Surface plasmon resonance

TEM : Transmission electron microscopy

Trp (W) : Tryptophan

Tyr (Y) : Tyrosine

UV-Vis : Ultraviolet-visible

XPS : X-ray photoelectron spectroscopy

XRD : X-ray diffraction

Abstract

Designing nanomaterials for biological applications has become an emerging interdisciplinary area of science; however that raises the need to understand the materials interaction with different biological components at the nano-bio interface. Such basic understanding required for the development of nanomaterials-based diagnosis, therapy and medicine. Majority of recent work have focussed on how the size, shape, stability, surface charge and composition of inorganic nanomaterials control their interaction with the biological entity, whereas other parameters pertaining to the nanoparticles surface such as the surface layer consisting of molecules, ions, hydrophilic or hydrophobic nature and their synergistic effects are often overlooked. Therefore, the major focus of the thesis is to understand that how the variation in surface functionalization in conjunction with inorganic nanoparticles composition reflects on their ability to produce reactive oxygen species and imparts non-specific or selective toxicity against different bacterial strains. However, presence of organic component hinders their application in gene delivery; therefore additionally, organic nanostructures were employed to understand their interaction with DNA and bacterial transformation.

First focus was to develop the synthetic methodologies in controlling the surface functionalization and composition of nanoparticles in a single step using green and eco-friendly routes. Tryptophan and tyrosine amino acids were employed as reducing and stabilizing agents to synthesize gold, silver and their bimetallic alloy nanoparticles. These amino acid

functionalized nanoparticles have been chosen in the research work because the side functional groups present in the amino acids reduce either single metal ions or two different types of metal ions to form monometallic and bimetallic nanoparticles, respectively, while leaving the amine and carboxylic acid groups intact. Hence these nanoparticles can be viewed as amino acid functional groups anchored on a nanoparticles surfaces, which can render these surfaces similar to enzymes. In the context of biological application, usually nanoparticles exhibit toxicity due to their ability to induce production of reactive oxygen species. This can be evaluated by their peroxidise-like activity by catalysing the oxidation of chromogenic substrate. Therefore, these amino acid surface functionalized nanoparticles were subjected to investigate their intrinsic peroxidise enzyme-like behaviour. The peroxidise-like activity was found to be composition, temperature and surface functionalization dependant and it was revealed that the peroxidise-like behaviour originates from the synergistic effects of Ag fraction of the nanoparticles and the amino acid shell. Further, antibacterial studies of these nanoparticles demonstrated that toxicity against Gram positive bacteria (*Staphylococcus albus*) originates only from the amino acid shell present on the nanoparticles surface and composition of nanoparticles doesn't have any significant role. Conversely, antibacterial activity against Gram negative bacterium (*Escherichia coli*) was composition dependent and capping of amino acids had little influence. Morphological studies of nanoparticles treated bacterial cells revealed that after interaction with amino acid surface functionalized nanoparticles, most of the bacterial cells lost their integrity and confirmed level of damage. These findings established

correlation between the surface corona and metal composition of nanoparticles and their antibacterial activities against two different bacterial strains.

Moreover, in order to demarcate how this surface functionalization plays a critical role; non-toxic Au nanoparticles were chosen and revealed significant influence of surface functionalization against Gram negative bacteria. Tyrosine reduced Au nanoparticles that were found to be non-toxic to *E. coli*, turns out to be a potential antibacterial agent after they were sequentially functionalized by polyoxometalates and lysine. Functional polyoxometalate ions imparted antibacterial potential on the surface of tyrosine synthesized Au nanoparticles and the cationic nature of lysine worked as guide to target negatively charged bacterial cells for antibacterial activities. The same sequential surface functionalization was extended to Ag nanoparticles, wherein these nanoparticles showed very high antibacterial activity even in smaller concentrations. These nanoparticle-based functional antibacterial agents seen to employ a physical mode of action against bacteria by causing pore formation, cell wall cleavage and cell lysis.

As-mentioned earlier, inorganic nanoparticles are not suitable for DNA delivery applications and bacterial transformation studies due to their inherent toxicity as well as long residence time of the inorganic nanomaterials within the living system. Moreover, it is not easy to clear inorganic nanomaterials from the living systems due to their strong association with different cellular components. Therefore, DNA delivery vector requies an organic nanomaterial that encapsulate the DNA instead of inorganic nanomaterials. Another reason to choose organic nanostructures

is they can be broken down by enzymatic reactions within the bacterial cells. In this context, organic materials based nanostructures were employed for DNA delivery applications and to understand their interaction with DNA. Tri-block copolymer (PEO_{20}-PPO_{69}-PEO_{20}) was used as the organic material and it is known to undergo self-assembly to form micelles in water. When plasmid DNA was mixed along with the polymer, they form self-assembled structures and these nanostructures are used as non-viral DNA delivery vehicles. The electrostatic interaction between the phosphate group (PO_4^{3-}) of pDNA and the hydrophilic segment (PEO) of tri-block polymer drives the self-assembly process. Different weight ratios of DNA and polymer were screened to find out the optimum weight ratio to achieve highest level of bacterial transformation. At 1:10 weight ratio of DNA and polymer the bacterial transformation was found to be the maximum and it was over 6 folds higher transformation. Furthermore, during transformation studies, the integrity and functionality of the green fluorescent protein (GFP) pDNA in nanostructures were also demonstrated within the cellular environment by the expression of GFP gene.

Chapter I

Introduction

This chapter provides a general introduction about the historical development of nanoscience, nanobiotechnology and nanotoxicology. Special emphasis is given on the cell-nanomaterial interaction at the nano-bio interface and how various physicochemical properties of nanomaterials influence this interaction. Subsequently, a variety of mechanisms by which nanomaterials illustrate antibacterial activities have been discussed and basic differences between Gram positive and Gram negative bacterial strains are discussed. Additionally, synthesis, stability and important physicochemical properties of metallic nanoparticles have been discussed. In the later part of this chapter, the aims of the thesis have been designed to address the gaps in the aforementioned area. Finally, a chapter wise summary of the thesis has been presented.

1.1. Nanosciences to nanobiotechnology

On December 29 1959, an influential lecture "There's plenty of room at the bottom" was delivered by Professor Richard Feynman at the American Physical Society meeting at California Institute of Technology (Caltech), where he initiated the need to implement miniaturization in future technologies. His lecture provoked curiosity to fabricate future devices, which can be portable, powered by small energy devices, using less materials etc.[1] Since that day, the potential of nanotechnology was realized, as we are witnessing the fact that almost each and every electronic, optical, magnetic, sensing, energy and volumetric devices are made as small as possible to support the concept of miniaturization given by Prof. Feynman in his legendary lecture.[1]

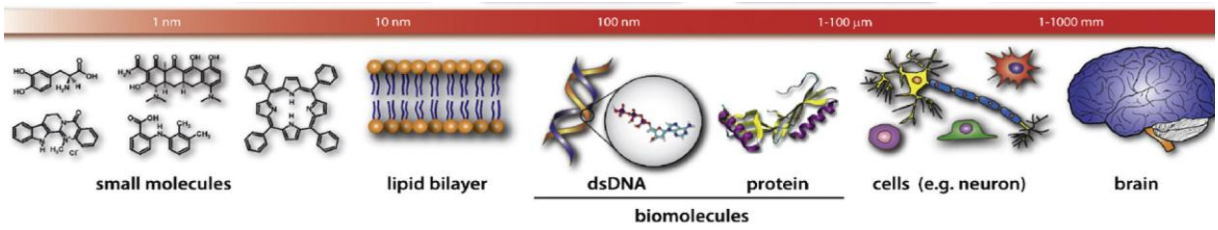

Figure.1.1. Comparative sizes of biological components at nanoscale dimension (adopted from reference [2])

In addition to technological devices, other significant developments in the field of nanosciences have shown extensive impact on almost all areas of natural and applied sciences including material science, physics, chemistry, biology, medicine, microbiology, biotechnology and engineering.[3-7] In the context of biomedical sciences, this influence is possible because the basic biological entities and biomolecules like enzymes, DNA, membrane, motor

proteins etc are complex biological components, and fall in the nanoscale dimension as illustrated in Figure 1.1.[2]

Furthermore, the potential applications of nanoscience in biotechnology, bio-sensing, medicine and microbiology gave birth to the new field called "nanobiotechnology" [8] because most of the biological systems can be integrated with nanomaterials due to their comparable sizes. Moreover, the integration of nanomaterials with biomolecules have illustrated excellent applications in biomedicine that can potentially reach to previously inaccessible targets [9-11] due to multi functionality and higher sensitivity [8] of hybrid nanobiomaterials with desired physical and chemical properties.[12-14]

Thus, the interdisciplinary nature of nanobiotechnology opens up a new avenue of multifunctional hybrid nanomaterials to resolve biological problems. In this perspective, conceivably the most striking example of employing nanomaterials is to control infections. Some of the most common and lethal infections are caused by bacteria and a variety of nanomaterials have been evaluated for their antimicrobial properties that are used to control bacterial growth including those bacterial strains that have evolved resistance to antibiotics.[15-19] Therefore, it is essential to develop nanomaterials for antibacterial applications and to understand the interaction of these nanomaterials with bacterial cells, which is the major focus of this thesis. Moreover, the medicinal potential and environmental impact of nanomaterials could be fully realized only after extensive investigations at the interface of nanobiotechnology. Therefore, this research work has been undertaken to examine that how properties of nanomaterials

influence their interaction with bacterial cells and what happens to the bacteria after being in contact with nanomaterials. These understandings may assist to evaluate biological impacts of functionalized nanomaterials and their potential applications.

1.2. What is 'NANO' and why it is different?

According to the International standard organization (ISO), a nanomaterial is any object with at least one, two or all the three dimensions in the nanoscale range (1 to 100 nm). At the range of nano meter level, materials begin to show distinct mechanical, electrical, optical, magnetic, electro-optical, magneto-optical, physical, and chemical properties, which are different from their bulk and molecular counterparts. Therefore, nanotechnology enables to change some basic properties of a material such as functionality, shape, size, and surface charge without changing its chemical composition [10, 20, 21] and these nano objects may have higher toxicity, greater catalytically activity and different characteristics.

Nanoparticles and composite nanomaterials are found to have wide applications in magnetic storage devices, electronics, optics, catalysis and sensing etc. [3, 4, 22-27] and in the context of biology and medicine nanomaterials have shown outstanding and promising applications.[10, 28-33] Nanomaterials can be explored for novel applications where the properties of the atomic or bulk material are unsuitable. Moreover, during synthesis, growth of nanomaterials can be restricted to obtain 1, 2 or 3 dimensional object thus nanomaterials can be nanoparticles, nanoplates or nanofibres respectively, having 3, 2 or 1 dimensions within the nano-scale

as illustrated in Figure 1.2. Additional terms nanoprism or nanocube have been used to discuss polyhedral nanoparticles. For nanofibres the object may be referred as nanorods or nanotubes, depending upon whether the structure is hollow or solid. Along with nano-size, dimensions of nanomaterials have considerable influence on their properties and biological activities.[25, 33-42]

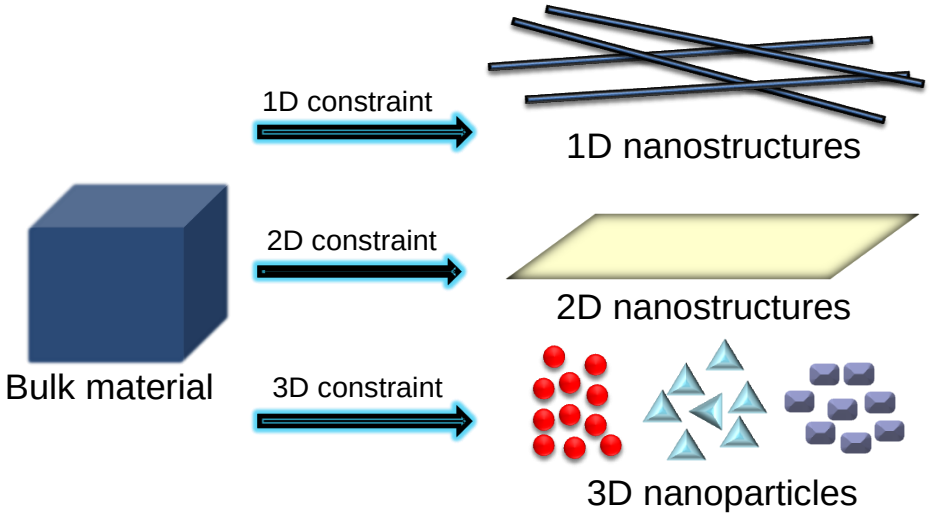

Figure.1.2. Schematic representation of various dimensions of materials at nanoscale

1.3. Nano-bio interface, toxicity and fabrication of nanomaterials

It is imperative to understand that nanotechnology is not just a new step toward miniaturization. Recent advances in the field of nanotechnology have revealed that this is a powerful transformative technology and this is evident from the utilization of nanotechnology based products in every sector of the society and strong influence of nanotechnology on the future of mankind has been predicted.[43-45] There are numerous areas where nanoparticulate systems have shown great technological and scientific significance. For instance, applications of nanotechnology have potential to transform the field of biotechnology, agriculture, manufacturing,

information technology, telecommunication, electronic, materials, medical and other sciences.[10, 30-32, 43, 46-48]

In milieu of biological applications, the major objective of nanotechnology is to engineer and manufacture nanomaterials at the atomic or molecular level to exhibit entirely novel therapeutic applications with better functionality, efficiency and specificity.[49] Since, cells are highly sensitive to their environment [50] and basic biological components are functional configurations at nanometer level, nanobiotechnology has the potential to tailor material's physiochemical properties to achieve the desired level of sensitivity with improved functionality, efficiency and specificity.

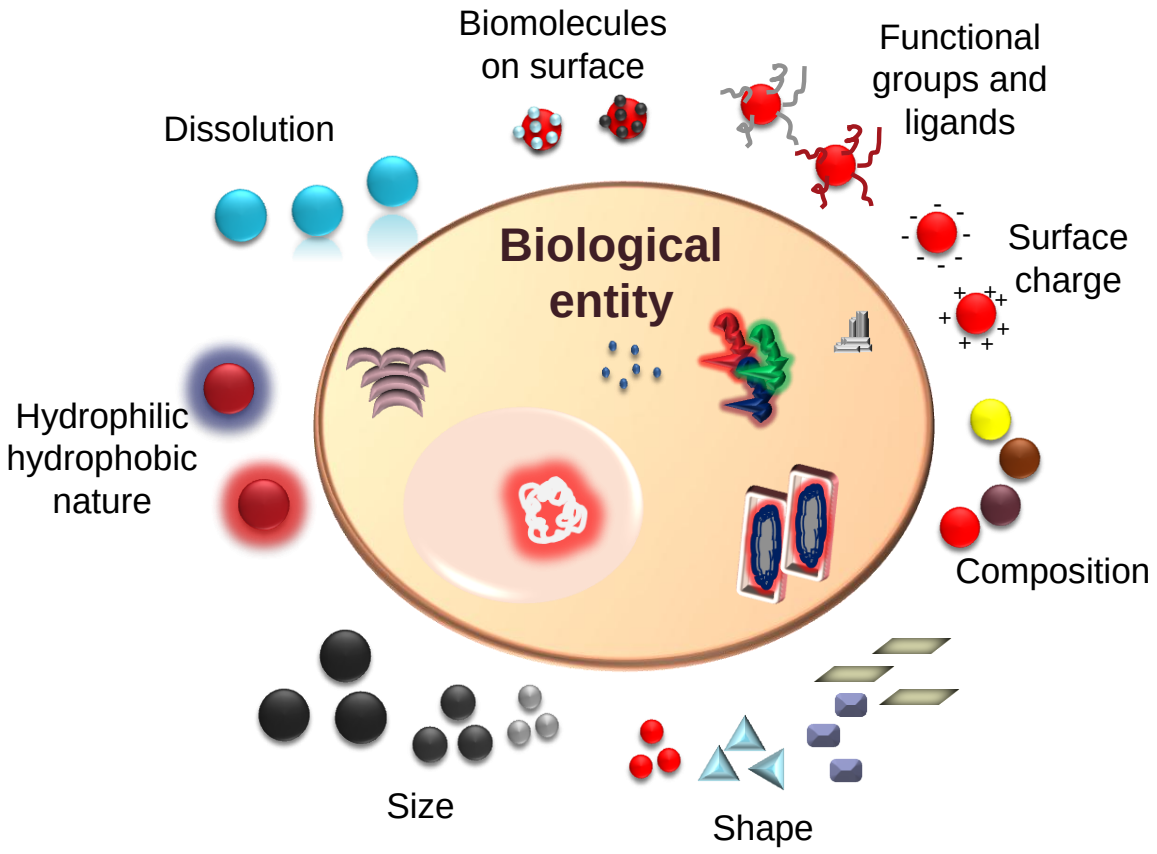

Figure.1.3. Schematic representation of various physicochemical properties of nanomaterials which influences nanoparticle-cell interaction

Various physical and chemical properties of nanomaterials such as surface charge, composition, shape, size, hydrophilic or hydrophobic nature and dissolution effect, presence of biomolecules, functional groups or ligand on the surface of nanomaterials have significant influence at nano-bio interface.[51-56] For instance, cell membranes possess negative charge and if nanomaterials have the similar surface charge, due to the effective repulsion, interaction between cell-nanomaterial will not be possible, while positive surface charge on nanomaterials can provide an opportunity to interact with membrane due to the electrostatic attraction. Further, nanomaterials have intrinsic potential to produce reactive oxygen species (ROS) within or outside of the cell which can challenge cellular integrity and cell survival. After internalization, due to the dissolution effect of nanoparticles cellular functions may be affected severely leading to toxic effects of nanomaterials.[51, 52, 57-59]

Furthermore, presence of diverse functional groups or ligands on the surface of nanomaterials can determine the level of interaction at the nano-bio interface and may damage cells by physical action or by interaction with sub cellular units and genetic material.[2, 59-66] In general, surface expressed bio-molecules, drugs or pharmaceutical chemicals dominate the biological impacts and presence of these molecules on the surface of nanoparticles could be highly significant.[67] Chemical moieties present on the nanoparticles surface have impact on their interaction with biological system therefore strong control over nanoparticles-cell interactions could be primarily controlled by tailoring surface properties of nanomaterials.[68-86]

This discussion illustrates that the principles governing the interactions between biological species and nanomaterials are of significant importance. Therefore, it is imperative to understand that the interactions of designer made functional nanoparticles within biological systems (living organisms) is multidimensional and understanding of these interactions is critically important for further development of nanobiotechnology for biomedical applications and in terms of nano-safety to achieve a particular and controlled biological action.[69, 79, 87]

Nanotoxicology is a vital and emerging part of nanobiotechnology which refers to the study of interactions of engineered nanomaterials with biological system or environment. In nanotoxicology, particular emphasis is on the correlation between the physicochemical properties of nanomaterials with induction of toxic biological responses.[88] Additionally, this field aims to find favourable characteristic of nanoparticulate systems which render them more amenable for the use in biological environment.[31, 89]

In this perspective, Dawson and co-workers have revealed that at the interface of cell and nanoparticles, the effective unit of interaction is not the nanoparticles itself, but the corona present around the nanoparticles is the unit of interest.[67, 70, 90] Surface corona is the key unit of interest for a living entity which ultimately exhibits biological action.[69, 91-94] Likewise, it have been shown that nanomaterials offer large surface areas and their controlled structure and surface functionality can make them outstanding scaffolds for biomedical applications.[55, 71, 78, 79, 84, 85] Furthermore, it has been demonstrated that nanoparticles can be effectively fabricated by amino acid functionalization to afford tailored surfaces for peptide

reorganization, DNA receptors, sensing, imaging and drug or gene delivery applications.[71-73, 83] Moreover, functionalized nanoparticles recognize target biomolecular surfaces via complementary interactions, which can lead toward a desired nanoparticle-cell interaction for biomedical applications.

1.4. Interactions between nanoparticles and bacterial cells

The major objective of this thesis is to investigate how functionalized nanoparticles interact with different bacterial strains and try to understand the impact of nanoparticles surface corona in conjugation with composition on bacterial cells. Therefore, well-known model microorganisms *Staphylococcus albus* (Gram positive) and *Escherichia coli* (Gram negative) were used in this study. Both the bacterial strains used in this thesis possess a strong cell wall, which gives them shape and protects from osmotic lysis and it is the site of action of some antibiotics.[95] Therefore, it is essential to understand the basic structure of these bacterial cell walls before probing the interaction between nanoparticles and bacteria.[95]

After Christian Gram developed the Gram staining technique, bacteria are divided into two major groups based on their response to the Gram stain procedure.[96] Gram positive bacteria stained purple, while Gram negative bacteria were coloured pink or red by this technique [96-98] due to the structural difference between these two groups of bacteria. The Gram positive cell wall consists of a single 20 to 80 nm thick homogeneous peptidoglycan or murein layer outside the plasma membrane. In contrast, the Gram negative cell wall is quite complex and has a 2 to 7 nm

peptidoglycan layer surrounded by a 7 to 8 nm thick outer membrane.[99]

1.4.1. Structure of Gram positive and negative bacterial cell wall

Peptidoglycan is a polymer composed of two sugar derivatives (N-acetylglucosamine [NAG] and N-acetylmuramic acid [NAM]) and several different amino acids, especially three of which viz. D-glutamic acid, D-alanine and *meso*-diaminopimelic acid, are not found in proteins. The backbone of this polymer is composed of alternating NAG and NAM residues as presented in Figure 1.4.[95] A peptide chain of four alternating D- and L-amino acids is connected to the carboxyl group of NAM. Chains of linked peptidoglycan subunits are joined by cross linkers between the peptides. Often the carboxylic group of the terminal D-alanine is connected directly to the amino group of diaminopimelic acid, but a peptide inter-bridge may be used instead. Most Gram negative cell wall peptidoglycan lacks the peptide inter-bridge.

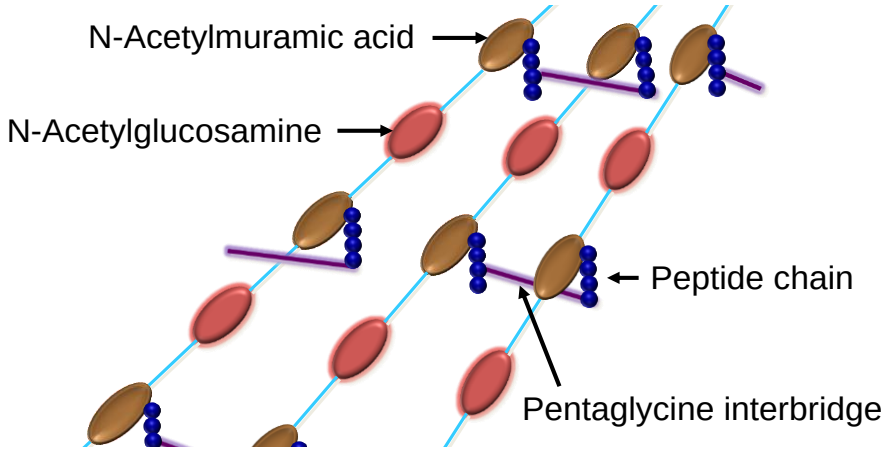

Figure.1.4. Schematic representation of peptidoglycan structure

As illustrated in Figure 1.5 a Gram-positive bacterium has thick and homogeneous cell wall which is composed of peptidoglycan and contains a peptide inter-bridge and large amount of teichoic acids (polymers of glycerol

or ribitol joined by phosphate groups).[99] Amino acids such as D-alanine or sugars like glucose are attached to the glycerol and ribitol groups. The teichoic acids are connected to either peptidoglycan itself by a covalent bond with the six hydroxyl of NAM or to plasma membrane lipids (called lipoteichoic acids). Teichoic acid extends to the surface of the peptidoglycan, and because of its negative charge it gives the Gram-positive cell wall its negative charge. Teichoic acid is not present in Gram negative bacteria.

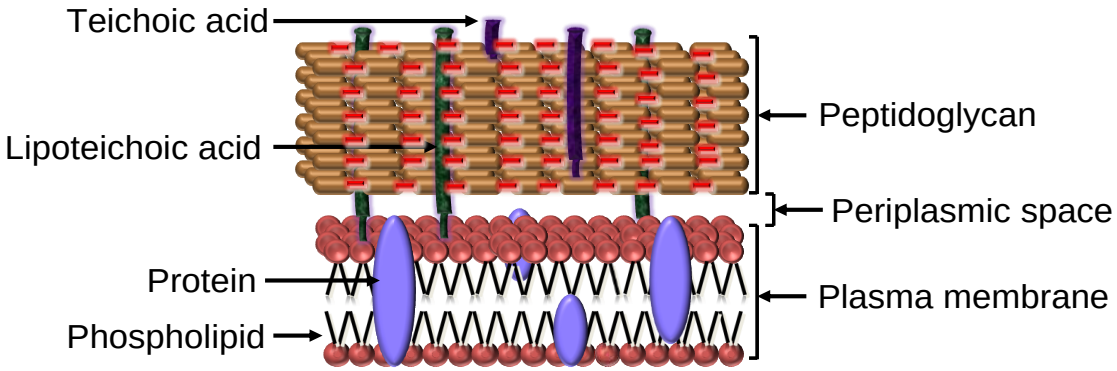

Figure.1.5. Schematic diagram of the structure of Gram positive bacterial cell wall

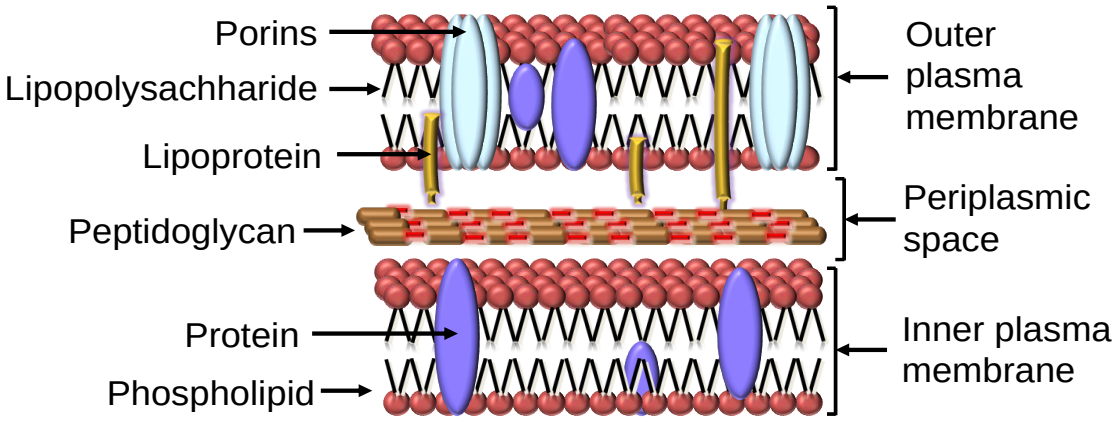

Figure.1.6. Schematic representation of Gram negative bacterial cell wall

In *Escherichia coli*, thin peptidoglycan layer next to the plasma membrane constitute 5-10 % of the wall weight and it is about 2-7 nm thick.

The outer membrane lies outside the thin peptidoglycan layer as shown in Figure 1.6. The outer membrane of Gram negative bacteria is more permeable than the plasma membrane and permits the passage of small molecules like glucose and other monosaccharide. This is due to the presence of special porin proteins. Three porin molecules clusters together and span the outer membrane to form a narrow channel through which molecules smaller than about 600-700 Daltons can pass. Large and complex lipopolysaccharides (LPSs) contain both lipids and carbohydrates and considered unusual constituent of the outer membrane. The most abundant membrane proteins in Gram negative bacteria are Braun's lipoprotein, a small lipoprotein covalently joined to the underlying peptidoglycan and embedded in the outer membrane by its hydrophobic end. The outer membrane and peptidoglycan are so firmly linked by this lipoprotein such that they can be isolated as one unit.

1.4.2. Antibiotics, antimicrobial peptides and nanomaterial as antibacterial agents

In bacterial cells, the most important function of cell wall is to serve as a protective barrier as discussed. It prevents or slows the entry of salts, antibiotics and other toxic substances that are lethal / toxic to the bacterium. Antibiotics and antimicrobial peptides interact with bacterial cells through a variety of mechanism to kill or control bacterial growth.

Conventional antibiotics such as ciprofloxacin, doxycycline and ceftazidime penetrate into bacteria and act on a particular sub-cellular target to inhibit bacterial growth. Rather than causing physical damage to

the cell wall, these antibiotics typically interact chemically with bacterial genetic material, block cell-division and sometimes trigger autolysis in target microorganism. In this manner, bacterial morphology is preserved and therefore, bacterial species may develop resistance.

On the other hand, antimicrobial peptides are an abundant and diverse group of molecules which have potential to damage and kill microorganism by pore formation. The composition of amino acids, amphipathicity, cationic charge and small size of these antimicrobial peptides make them suitable class of antibacterial agents.[100] Due to cationic changes these interact with the cell wall through an electrostatic interaction which causes physical damage to the bacterial cells by forming pores. This physical action prevents microbes from developing resistance and indeed it has been demonstrated that cationic antimicrobial peptides and nanomaterials can overcome bacterial resistance.[101-103]

Moreover, silver (Ag) has long been known for its antibacterial activity and applications due to its considerably lower toxicity toward human cells then to bacteria.[86, 104-108] Additionally, antibacterial nanoparticles have been synthesised from copper, iron, cerium oxide, zinc oxide, titanium oxide and silicon dioxide.[16, 109-120] In general, it has been demonstrated that nanoparticles cause disruption of cell wall, cell lysis, release Ag^{+} ions, denature bacterial surface proteins, interact with genetic material and generate reactive oxygen species (ROS) and thereby exert antimicrobial activities as illustrated in Figure 1.7.[16, 104, 111, 120-128]

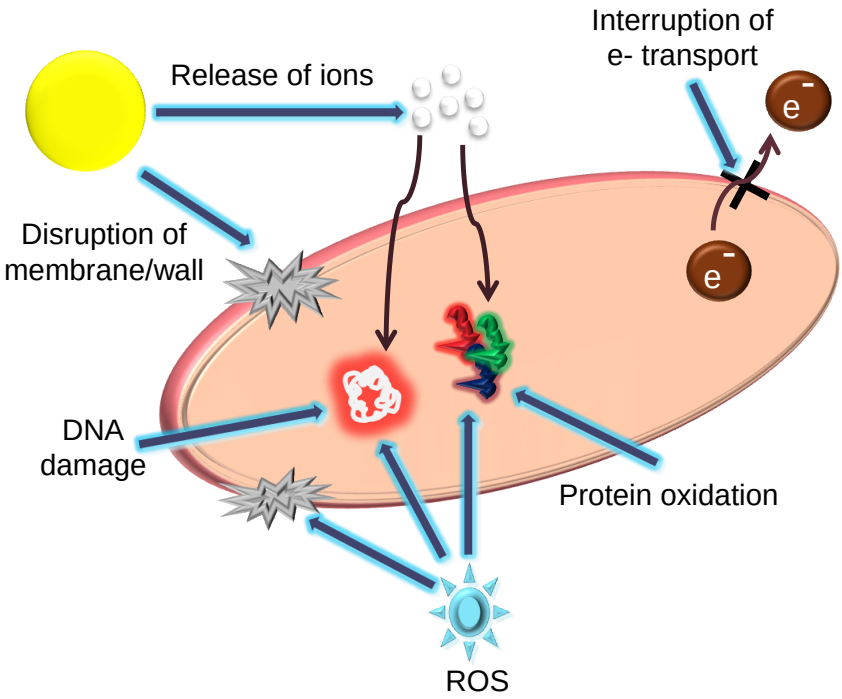

Figure.1.7. Schematic representation of mechanism of antibacterial activities exerted by nanoparticles

In this perspective of antibacterial applications of nanoparticles, gold nanoparticles are considered relatively inactive.[82] Interestingly, the inert Au nanoparticles were found to exhibit antibacterial activities after their surface functionalization with antibiotics and ionic surfactant.[74, 82, 129-131] In this thesis, Au and Ag nanoparticles were chosen to tailor their surface properties in conjugation with Au-Ag composition to formulate controlled antibacterial nanoparticles and effects of Au-Ag composition and surface functionalization was studied at the interface of nanoparticles and bacterial cells. Furthermore, since the presence of peptidoglycan layer is a specific membrane feature of bacterial species (not mammalian cells), therefore it was predicted that if the antibacterial effect of nanoparticles is associated with the cell wall; it may be more appropriate to use such nanoparticles as an antibacterial agent under *in-vivo* environment.[132]

1.5. Other applications of nanobiotechnology

In addition to develop antimicrobial agents for infectious disease, nanobiotechnology has many other biomedical applications.[133-137] For instance, nanomaterials are being used for electrochemical bioassays, DNA and protein detection (Au and Ag metal based), quantum dots (QDs) bioconjugates in cell and tissue imaging, immunological assays, nanoscale localized surface plasmon resonance biosensors, catalysis, *in-vitro* diagnosis of cancer and other disease etc.[8, 13, 14, 29, 135, 138-154]

In addition to the above mentioned applications, nanobiotechnology has prototypical applications in bacterial transformation. In molecular biology, the study of bacterial transformation is a routine practice, which involves introduction of foreign genetic material to other bacteria for a variety of applications. Moreover, gene therapy is one of the most frequently used approach in medicine, wherein foreign DNA is introduced into cells of patients to express the pharmaceutical proteins and nucleic acid based drugs to control gene expression. Likewise, antisense therapy involves transfer of oligonucleotides, which can be used to suppress the expression of the disease causing genes. Therefore, these therapies can be regarded as promising and ultimate cure for many life threatening and debilitating diseases including cancer.[155, 156] Therefore, it is necessary to develop efficient DNA delivery vectors and to understand their interaction with DNA in order to realize the full potential of these therapies.

Conventionally, viral vectors have been used for introduction of genetic material from one species to other but due to their possible side

effects [157] and development in nanobiotechnology have influenced design of a variety of functional nanomaterials for such application, which includes functional Au nanoparticles, silica materials, QDs, plant based vesicles and polymers.[71, 155, 158-170] Although, the major objective of this thesis is to explore interaction of functionalized metal nanoparticles with different bacterial cells at nano-bio interface, employing the same nanoparticles for DNA delivery is limited because it is difficult to remove these inorganic nanomaterials from the biological systems and the metal based nanoparticles may exhibit toxicity. Hence, it is imperative to utilize organic materials based nanostructures for such biological applications because compared to inorganic nanostructures, organic nanostructures can be broken down within the biological system. Therefore, polymer based nanostructures were additionally employed to understand the interactions governing DNA-polymer self-assembly and furthermore for transformation studies.

The applications of nanobiotechnology described here may have significant potential but based on the theme of this thesis a variety of Au and Ag nanoparticles are fabricated to understand the influence of surface functionalization and metal composition on bacterial cells and their enzyme-like activities. Therefore, the next part of this chapter discusses about the available nanoparticles synthesise methodologies, their stability, special surface plasmon resonance property, etc.

1.6. Production of nanoparticles by top-down or bottom-up approach

In general, nanomaterials synthesis can be done by employing either a 'top-down' or 'bottom-up' approach as illustrated in Figure 1.8. Initially, these terms were introduced by the Foresight Institute (1989) in the field of nanotechnology.[171] In the top-down strategy, traditional methods such as mechanical grinding, erosion or controlled tools are used to mill, cut and shape materials in to a desired structure.[137, 172] Conversely, in the bottom-up approach chemical methods are applied to assemble useful nanostructures based on the concept of molecular self-assembly or molecular recognition.

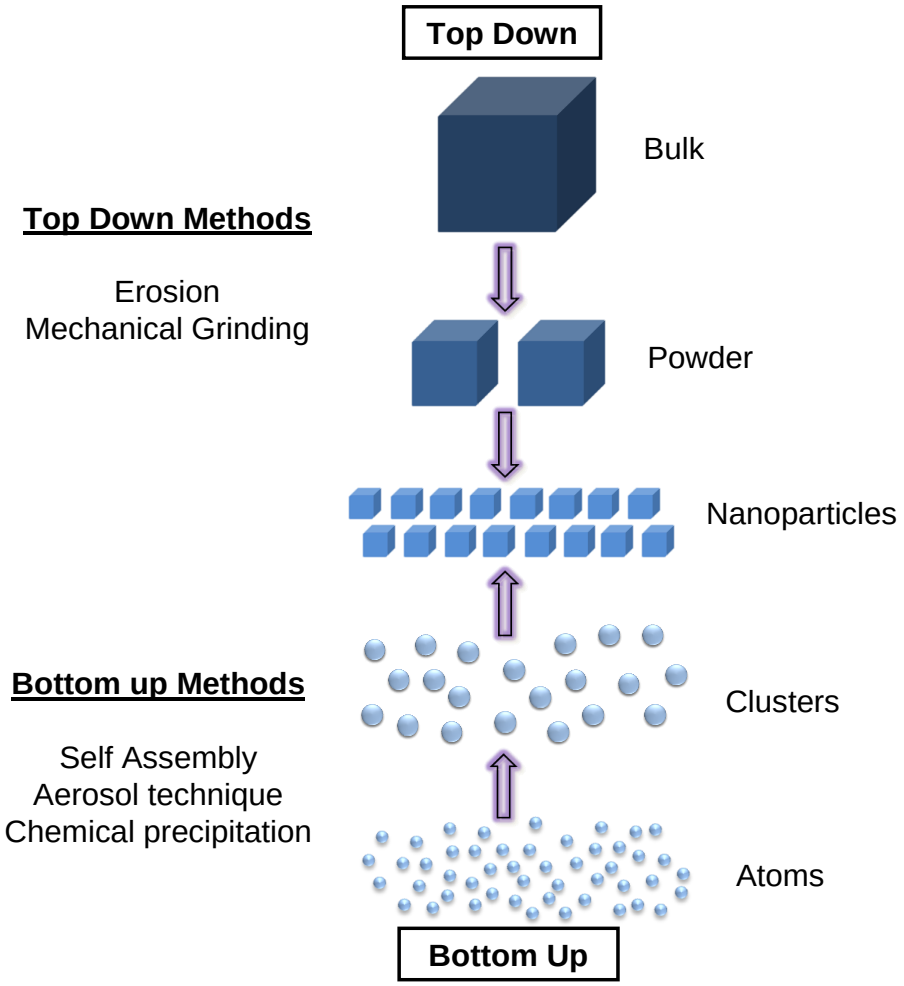

Figure.1.8. Schematic representation of the 'bottom-up' and 'top-down' synthesis processes of nanomaterials with the popular techniques

In this thesis, the bottom-up strategy is applied to synthesise different nanoparticles. Among the different kinds of nanomaterials, noble metal nanoparticles such as mainly Au and Ag are used in the thesis work, therefore the following section describes the synthetic methodologies of these nanoparticles, their stability and important properties.

1.7. Metal nanoparticles formation and their stability

Size and shape of the metal nanoparticles need to be uniform for any of their applications, thus it is important to follow synthetic methods that control the size and shape of the particles. Physical, chemical and biological methods have been developed for the synthesis of various inorganic nanoparticles.[173-193] Among these methods, wet chemical methods are the most promising because it is relatively easier to control the particles size during synthesis. Chemical methods of nanoparticles formation involve the reduction of metal ions by a suitable reducing agent in the presence of a capping agent. It is similar to the conventional colloids preparation, where a precipitating agent is added to induce the colloid formation. In 1875, Faraday published a report on chemical reduction of gold salt in the presence of stabilizing agent to produce zerovalent gold colloids.[194] Later, Turkevich established standard protocol for the synthesis of metal colloids such as 20 nm Au nanoparticles by the reduction of $[AuCl_4]^-$ with sodium citrate.[192, 195, 196]

Stability of synthesized nanoparticles against aggregation is always an important concern before these nanoparticles can be used for any biological or medicinal applications. Stability of these nanoparticles typically depends

on the pH of the medium in which the nanoparticles are dispersed and the electrolyte concentration in the solvent.[197] Nanoparticles synthesized in solvents are inherently unstable and tend to aggregate due to their high surface free energy as a result of their small size.[197-199] Therefore, stabilization of metal nanoparticles in the solution can be achieved by adding shielding, stabilizing or protecting agents which are necessary to prevent agglomeration. The two basic modes of nanoparticles stabilization are electrostatic and steric stabilization, as illustrated in Figure 1.9 (A and B, respectively).

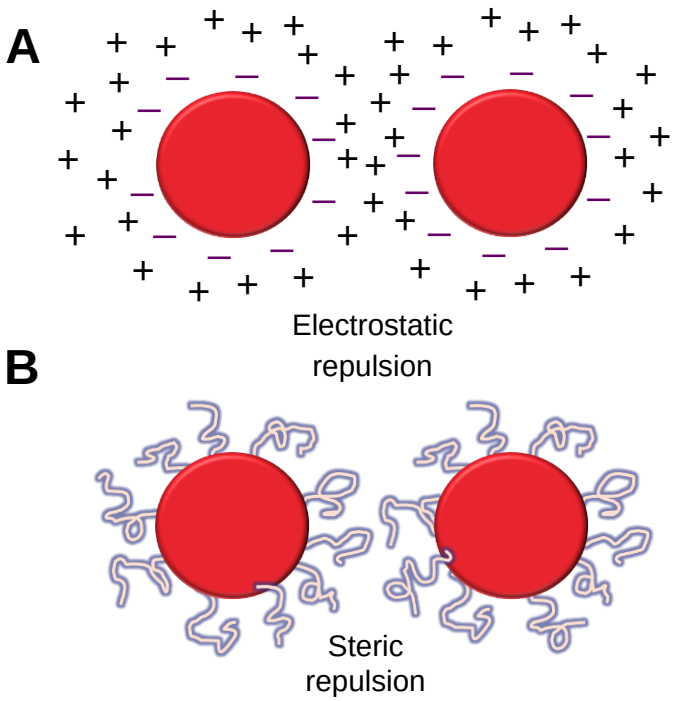

Figure.1.9. Scheme illustrating the stabilization of metal nanoparticles by (A) electrostatic and (B) steric interactions

An electrical double layer is formed by the adsorption of precursor ions and the corresponding counter ions surrounding nanoparticles surface when nanoparticles are synthesized in aqueous medium as shown in Figure 1.9 (A). For example, Au nanoparticles are prepared by the reduction of

$[AuCl_4]^-$ with sodium citrate.[192, 195, 196] These nanoparticles have unreduced $[AuCl_4]^-$ ions and citrate ions on their surface, which renders these nanoparticles surface negative charge. If these nanoparticles come close to each other, due to the same surface charge of each nanoparticle, Coulombic repulsive force would prevent aggregation. Under solution conditions of low ionic strength and moderate surface potentials the electrostatic repulsion between particles is normally sufficient to avert the attractive forces from causing the particle to aggregate.

Conversely, in the case of organic medium where electrostatic forces are less effective, stability of nanoparticles comes from steric interactions.[200] Steric stabilization is achieved by the formation of a protective shield on the metallic nanoparticles surface using sterically demanding organic molecules. In general, polymers, block co-polymers, surfactants and ligands are used as shielding or protecting agents to avoid aggregation using adsorption of these molecules on the surface of nanoparticles by physical or chemical adsorption methods.[198, 199]

1.8. Surface plasmon of metallic Au and Ag nanoparticles

Au and Ag nanoparticles dispersed in solvents exhibit wine red and yellow colours respectively and these materials have very strong intense absorption bands around 520 nm and 400 nm.[201-204] These bands arise from the collective oscillation of the conduction electrons due to the resonant excitation by the incident photos as shown in Figure 1.10 and this phenomenon is known as 'Surface Plasmon Resonance' (SPR). In a bulk metal, presence of free electrons and the cationic cores form a plasma state.

These free electrons can set into oscillations relative to cationic lattice when it interacts with light or any kind of electromagnetic radiation. In this manner a dipolar oscillation of electrons is created (called plasma oscillations) with a certain frequency called bulk plasma frequency that usually falls in the range of ultraviolet frequencies.[205]

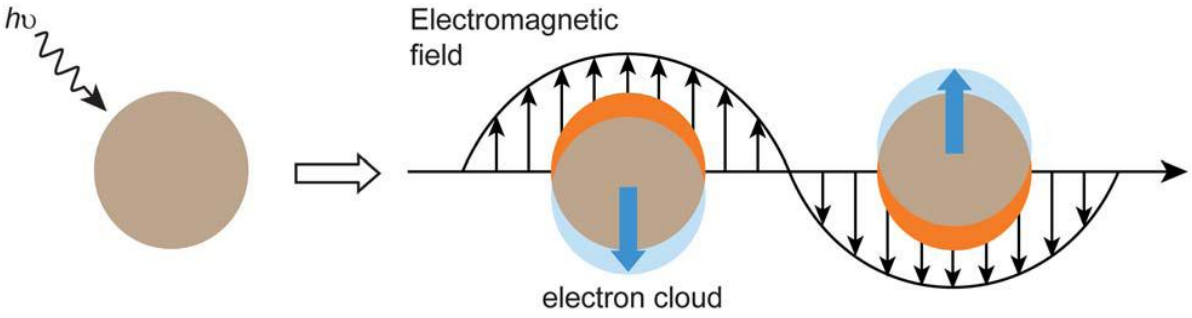

Figure.1.10. Schematic representation of the interaction of light with metal nanoparticles (Adapted from the reference[206])

When the physical dimension of the metal is smaller than the mean free path of the electron, these bulk plasma frequencies are quantized especially in the case of gold, silver and copper and now these frequencies are called Surface Plasmon Resonant (SPR) frequencies. These absorptions are quite strong in the visible region of the electromagnetic spectrum, which becomes the characteristic property of these metal nanoparticles. Furthermore, size, shape, solvent, surface ligand, core charge and temperature also have significant influence on the SPR bands of nanoparticles.[37, 205-208] Significant red-shift of SPR frequency, broadening in SPR band and change in the solution colour from wine red to blue is indication of aggregation due to the inter-particle plasmon coupling.[209]

1.9. Objective of the thesis

Using nanomaterials for a variety of biological applications has become an emerging interdisciplinary area of science; however that raises the need to understand the nanomaterials interaction with different biological components.[29, 140, 210] Understanding of biologically inspired and naturally occurring materials can lead us to develop nanomaterials, nanodevices and processes with desirable functionality, as nature has evolved with desired biological and chemical functionality using commonly found materials.[211] Understanding of biology at molecular level can provide directions in construction and design of nanomaterials with novel applications. The four major fundamental bio-macromolecules are nucleic acid, proteins, lipids and polysaccharides, which are made up of nucleotide, amino acids, fatty acids and sugars respectively.[212]

Therefore, amino acid functionalized nanoparticles have been chosen in the current PhD thesis because their synthetic routes don't involve noxious chemicals, they involve simple purification procedures, available binding sites for different chemical functionalization, multi-valent interactions and stable form of nanoparticles in a wide range of pH. The side functional groups present in the amino acids reduce either single metal ions or two different types of metal ions to form monometallic or bimetallic nanoparticles, respectively, while leaving the amine and carboxylic acid groups intact. Thus, nanomaterials fabricated in this thesis can be considered novel hybrid nanobiomaterials consisting of an inorganic core and amino acid shell/surface, which may be viewed as supported proteins/enzymes.

Moreover, the physicochemical properties of nanoparticles and the biochemical properties of amino acids can be synergistically combined and it will be interesting to evaluate for their enzyme-like behaviour and interaction with bacterial cells because such basic understanding are required for the development of nanomaterial based diagnosis, therapy and medicine. Majority of recent work have focussed on that how the size, shape, surface charge, stability and composition of inorganic nanomaterials control their interaction with the biological systems, while they often overlook the other parameters and synergistic effects of above-mention parameters. Surface chemistry and all the above discussed parameters (Figure1.3) drive the initial interaction and diffusion across the biological world, help in binding with biomolecules, mode of entry and interaction within the cells. Furthermore, the potential of nanomaterials to mimic naturally occurring enzymes has been demonstrated and these intrinsic biocatalyst-like activities can be tuned.[213-218] Still, the influence of amino acid surface functionalized nanoparticles and in combination with different metal composition on their enzymes-like activity has not been studied.

Therefore, the major focus of the thesis is how the variation in surface functionalization in conjunction with nanoparticles composition imparts enzyme-like activity, non-specific or selective toxicity, and total biocompatibility toward biological entities such as bacteria. Furthermore, what happens to the bacterial system after their interaction with functionalized nanoparticles has been attempted to be answered.

1.10. Outline of thesis

This thesis consists of six chapters.

Chapter one provides a brief account of nanosciences, nanobiotechnology and nanotoxicology along with a detailed description about the cell-nanomaterials interaction at nano-bio interface. This chapter demonstrates various dimension and physicochemical properties of nanomaterials involved at the nano-bio interface based on the available literature. Morphology of Gram positive and negative bacterial cells is briefly discussed. Furthermore, in the context of antimicrobial application of nanobiotechnology, mechanisms exerted by nanomaterials to exhibit antibacterial activities are discussed and additional biology relevant applications are illustrated. Towards the end of this chapter, formation of metallic nanoparticles and their important physicochemical properties have been discussed to gain insight toward designing nanomaterials to achieve a control over the nano-bio interface.

Chapter two covers the experimental details on the instruments used in this research work. The underlying physical principles of UV-Visible Spectroscopy (UV-Vis), Fourier Transform Infrared Spectroscopy (FTIR), Transmission Electron Microscopy (TEM), Scanning Electron Microscopy (SEM), X-ray Photoelectron Spectroscopy (XPS), Zeta potential and Cyclic Voltametric methods and their use in the present thesis work are discussed in detail. Additionally, this chapter describes significance of these techniques to understand correlation between various physicochemical properties of synthesized nanoparticles and observed biological applications

(antibacterial, enzyme like activities and gene delivery) presented in the thesis.

Chapter three focuses on development of synthetic methodologies in controlling surface functionality and composition of nanoparticles in a single step using green and eco-friendly synthetic routes. Two different amino acids were employed as reducing and stabilizing agents to synthesize Au, Ag and Au-Ag alloy nanoparticles in a highly controlled manner. Second part of the chapter deals how the individual and synergistic role of the surface bound amino acids and nanoparticles composition enables their action as synthetic nanozymes and antimicrobial active materials. Finally at the interface of nanoparticles-bacterial cells, the correlation between the surface corona and composition of nanoparticles and the observed biological applications has been established.

Chapter four deals with functionalizing the metal nanoparticles surface with polyoxometalates (POMs) and the cationic amino acid lysine to enhance their interaction with bacteria and render them antimicrobial active. Tyrosine reduced Au nanoparticles were non-toxic to Gram negative bacteria and after their sequential surface functionalization with POMs and lysine, due to the enhanced interaction at the nano-bio interface these functionalized nanoparticles turns out to be a potential antibacterial agent. The same sequential surface functionalization approach was extended to Ag nanoparticles, wherein these nanoparticles showed very high antibacterial activity even at smaller concentrations.

Chapter five focuses on constructing self-assembled soft nanostructures of plasmid DNA and biocompatible tri-block copolymer (P-

123) and to understand the nature of interaction between pDNA and tri-block copolymer. Further, transformation studies were performed in cellular environment using *Escherichia coli* as a model microorganism and the integrity of the pDNA in self-assembled soft nanostructures was demonstrated. Additionally, optimum weight ratio of pDNA and P-123 has been screened to achieve highest level of bacterial transformation.

Chapter six provides a summary of the research work presented in the thesis and offers a scope for future work in the area studied.

1.11. References

1. Feynman, R.P., *There's plenty of room at the bottom* Journal of Microelectromechanical Systems, 1992. **1**(1): p. 60-66.
2. Suh, W.H., et al., *Nanotechnology, nanotoxicology, and neuroscience.* Progress in Neurobiology, 2009. **87**(3): p. 133-170.
3. Nirmal, M. and L. Brus, *Luminescence photophysics in semiconductor nanocrystals.* Accounts of Chemical Research, 1999. **32**(5): p. 407-414.
4. Alivisatos, A.P., *Semiconductor clusters, nanocrystals, and quantum dots.* Science, 1996. **271**(5251): p. 933-937.
5. Chan, W.C.W. and S. Nie, *Quantum Dot Bioconjugates for Ultrasensitive Nonisotopic Detection.* Science, 1998. **281**(5385): p. 2016-2018.
6. Dujardin, E. and S. Mann, *Bio-inspired Materials Chemistry.* Advanced Materials, 2002. **14**(11): p. 775-788.

7. Hobson, D.W., *Commercialization of nanotechnology.* Wiley Interdisciplinary Reviews: Nanomedicine and Nanobiotechnology, 2009. **1**(2): p. 189-202.

8. Fortina, P., et al., *Nanobiotechnology: the promise and reality of new approaches to molecular recognition.* Trends in Biotechnology, 2005. **23**(4): p. 168-173.

9. Ragnaill, M.N., et al., *Internal benchmarking of a human blood-brain barrier cell model for screening of nanoparticle uptake and transcytosis.* European Journal of Pharmaceutics and Biopharmaceutics, 2011. **77**(3): p. 360-367.

10. Mahmoudi, M., et al., *Protein-Nanoparticle Interactions: Opportunities and Challenges.* Chemical Reviews, 2011. **111**(9): p. 5610-5637.

11. Mahmoudi, M., et al., *Superparamagnetic Iron Oxide Nanoparticles: Promises for Diagnosis and Treatment of Multiple Sclerosis.* ACS Chemical Neuroscience, 2011. **2**(3): p. 118-140.

12. AMIN, R., S. HWANG, and S.H. PARK, *Nanobiotechnology: An interface between nanotechnology and biotechnology* Nano, 2011. **06**(02): p. 101-111.

13. Niemeyer, C.M. and C.A. Mirkin, eds. *Nanobiotechnology: Concept, Application and perspectives*. 2004, Wiley-VCH verlag GmbH & Co. KGaA.

14. Mirkin, C.A. and C.M. Niemeyer, eds. *Nanobiotechnology II: More concepts and applications* 2007, Wiley-VCH verlag GmbH & Co. KGaA.

15. Rai, M., A. Yadav, and A. Gade, *Silver nanoparticles as a new generation of antimicrobials.* Biotechnology Advances, 2009. **27**(1): p. 76-83.

16. Li, Q., et al., *Antimicrobial nanomaterials for water disinfection and microbial control: Potential applications and implications.* Water Research, 2008. **42**(18): p. 4591-4602.

17. Furno, F., et al., *Silver nanoparticles and polymeric medical devices: A new approach to prevention of infection?* Journal of Antimicrobial Chemotherapy, 2004. **54**(6): p. 1019-1024.

18. Gu, H., et al., *Using Biofunctional Magnetic Nanoparticles to Capture Vancomycin-Resistant Enterococci and Other Gram-Positive Bacteria at Ultralow Concentration.* Journal of the American Chemical Society, 2003. **125**(51): p. 15702-15703.

19. Cao, H. and X. Liu, *Silver nanoparticles-modified films versus biomedical device-associated infections.* Wiley Interdisciplinary Reviews: Nanomedicine and Nanobiotechnology, 2010. **2**(6): p. 670-684.

20. Whitesides, G.M., *The 'right' size in nanobiotechnology.* Nat Biotech, 2003. **21**(10): p. 1161-1165.

21. Whitesides, G.M., *Nanoscience, nanotechnology, and chemistry.* Small, 2005. **1**(2): p. 172-179.

22. Alivisatos, A.P., et al., *From molecules to materials: Current trends and future directions.* Advanced Materials, 1998. **10**(16): p. 1297-1336.

23. Alivisatos, A.P., *Perspectives on the physical chemistry of semiconductor nanocrystals.* The Journal of Physical Chemistry, 1996. **100**(31): p. 13226-13239.

24. Bansal, V., et al., *Galvanic replacement reaction on metal films: A one-step approach to create nanoporous surfaces for catalysis.* Advanced Materials, 2008. **20**(4): p. 717-723.

25. Bansal, V., et al., *Shape dependent electrocatalytic behaviour of silver nanoparticles.* CrystEngComm, 2010. **12**(12): p. 4280-4286.

26. Chrimes, A.F., et al., *Active Control of Silver Nanoparticles Spacing Using Dielectrophoresis for SERS.* Analytical Chemistry, 2012.

27. Plowman, B., et al., *Gold nanospikes formed through a simple electrochemical route with high electrocatalytic and surface enhanced Raman scattering activity.* Chemical Communications, 2009(33): p. 5039-5041.

28. Jin, R., *Super Robust Nanoparticles for Biology and Biomedicine.* Angewandte Chemie International Edition, 2008. **47**(36): p. 6750-6753.

29. Salata, O., *Applications of nanoparticles in biology and medicine.* Journal of Nanobiotechnology, 2004. **2**(1): p. 3.

30. Emerich, D.F. and C.G. Thanos, *Nanotechnology and medicine.* Expert Opinion on Biological Therapy, 2003. **3**(4): p. 655-663.

31. Mahmoudi, M., et al., *Effect of Nanoparticles on the Cell Life Cycle.* Chemical Reviews, 2011. **111**(5): p. 3407-3432.

32. Mahmoudi, M., V. Serpooshan, and S. Laurent, *Engineered nanoparticles for biomolecular imaging.* Nanoscale, 2011. **3**(8): p. 3007-3026.

33. Albanese, A., P.S. Tang, and W.C.W. Chan, *The effect of nanoparticle size, shape, and surface chemistry on biological systems*, in *Annual Review of Biomedical Engineering*2012. p. 1-16.

34. Daniel, M.C. and D. Astruc, *Gold Nanoparticles: Assembly, Supramolecular Chemistry, Quantum-Size-Related Properties, and Applications Toward Biology, Catalysis, and Nanotechnology.* Chemical Reviews, 2004. **104**(1): p. 293-346.

35. Kelly, K.L., et al., *The optical properties of metal nanoparticles: The influence of size, shape, and dielectric environment.* Journal of Physical Chemistry B, 2003. **107**(3): p. 668-677.

36. Sun, Y. and Y. Xia, *Shape-controlled synthesis of gold and silver nanoparticles.* Science, 2002. **298**(5601): p. 2176-2179.

37. Link, S. and M.A. El-Sayed, *Shape and size dependence of radiative, non-radiative and photothermal properties of gold nanocrystals.* International Reviews in Physical Chemistry, 2000. **19**(3): p. 409-453.

38. Narayanan, R. and M.A. El-Sayed, *Shape-dependent catalytic activity of platinum nanoparticles in colloidal solution.* Nano Letters, 2004. **4**(7): p. 1343-1348.

39. Chithrani, B.D., A.A. Ghazani, and W.C.W. Chan, *Determining the size and shape dependence of gold nanoparticle uptake into mammalian cells.* Nano Letters, 2006. **6**(4): p. 662-668.

40. Pal, S., Y.K. Tak, and J.M. Song, *Does the antibacterial activity of silver nanoparticles depend on the shape of the nanoparticle? A study of the gram-negative bacterium Escherichia coli.* Applied and Environmental Microbiology, 2007. **73**(6): p. 1712-1720.

41. Schaeublin, N.M., et al., *Does shape matter? Bioeffects of gold nanomaterials in a human skin cell model.* Langmuir, 2012. **28**(6): p. 3248-3258.

42. Yang, H., et al., *Comparative study of cytotoxicity, oxidative stress and genotoxicity induced by four typical nanomaterials: The role of particle size, shape and composition.* Journal of Applied Toxicology, 2009. **29**(1): p. 69-78.

43. Mehta, M.D., *Nanoscience and Nanotechnology: Assessing the Nature of Innovation in These Fields.* Bulletin of Science, Technology & Society, 2002. **22**(4): p. 269-273.

44. Balzani, V., *Nanoscience and Nanotechnology: A Personal View of a Chemist.* Small, 2005. **1**(3): p. 278-283.

45. Klaine, S.J., et al., *Nanomaterials in the environment: Behavior, fate, bioavailability, and effects.* Environmental Toxicology and Chemistry, 2008. **27**(9): p. 1825-1851.

46. Wang, Y., et al., *Templated synthesis of single-component polymer capsules and their application in drug delivery.* Nano Letters, 2008. **8**(6): p. 1741-1745.

47. Soni, S.K., et al., *Self-assembled enzyme capsules in ionic liquid [BMIM][BF 4] as templating nanoreactors for hollow silica nanocontainers.* Langmuir, 2010. **26**(20): p. 16020-16024.

48. Sivakumar, S., et al., *Degradable, surfactant-free, monodisperse polymer-encapsulated emulsions as anticancer drug carriers.* Advanced Materials, 2009. **21**(18): p. 1820-1824.

49. Farokhzad, O.C. and R. Langer, *Impact of Nanotechnology on Drug Delivery.* ACS Nano, 2009. **3**(1): p. 16-20.

50. Curtis, A. and C. Wilkinson, *Nantotechniques and approaches in biotechnology.* Trends in Biotechnology, 2001. **19**(3): p. 97-101.

51. Schrand, A.M., et al., *Metal-based nanoparticles and their toxicity assessment.* Wiley Interdisciplinary Reviews: Nanomedicine and Nanobiotechnology, 2010. **2**(5): p. 544-568.

52. Colvin, V.L., *The potential environmental impact of engineered nanomaterials.* Nature Biotechnology, 2003. **21**(10): p. 1166-1170.

53. Lewinski, N., V. Colvin, and R. Drezek, *Cytotoxicity of Nanoparticles.* Small, 2008. **4**(1): p. 26-49.

54. Nel, A.E., et al., *Understanding biophysicochemical interactions at the nano-bio interface.* Nature Materials, 2009. **8**(7): p. 543-557.

55. Ashkarran, A.A., et al., *Bacterial Effects and Protein Corona Evaluations: Crucial Ignored Factors in the Prediction of Bio-Efficacy of Various Forms of Silver Nanoparticles.* Chemical Research in Toxicology, 2012. **25**(6): p. 1231-1242.

56. Arruebo, M., *Drug delivery from structured porous inorganic materials.* Wiley Interdisciplinary Reviews: Nanomedicine and Nanobiotechnology, 2012. **4**(1): p. 16-30.

57. Schaeublin, N.M., et al., *Surface charge of gold nanoparticles mediates mechanism of toxicity.* Nanoscale, 2011. **3**(2): p. 410-420.

58. Oberdorster, G., E. Oberdorster, and J. Oberdorster, *Nanotoxicology: An emerging discipline evolving from studies of ultrafine particles.* Environmental Health Perspectives, 2005. **113**(7): p. 823-839.

59. Nel, A., et al., *Toxic potential of materials at the nanolevel.* Science, 2006. **311**(5761): p. 622-627.

60. Borm, P.J.A. and W. Kreyling, *Toxicological hazards of inhaled nanoparticles - Potential implications for drug delivery.* Journal of nanoscience and nanotechnology, 2004. **4**(5): p. 521-531.

61. Borm, P., et al., *Research Strategies for Safety Evaluation of Nanomaterials, Part V: Role of Dissolution in Biological Fate and Effects of Nanoscale Particles.* Toxicological Sciences, 2006. **90**(1): p. 23-32.

62. Yamamoto, A., et al., *Cytotoxicity evaluation of ceramic particles of different sizes and shapes.* Journal of Biomedical Materials Research Part A, 2004. **68A**(2): p. 244-256.

63. Karakoti, A.S., L.L. Hench, and S. Seal, *The potential toxicity of nanomaterials-The role of surfaces.* JOM, 2006. **58**(7): p. 77-82.

64. Kostarelos, K., et al., *Cellular uptake of functionalized carbon nanotubes is independent of functional group and cell type.* Nat Nano, 2007. **2**(2): p. 108-113.

65. Yoshida, K., M. Morita, and H. Mishina, *Cytotoxicity of metal and ceramic particles in different sizes.* JSME International Journal, Series C: Mechanical Systems, Machine Elements and Manufacturing, 2003. **46**(4): p. 1284-1289.

66. Geng, Y., et al., *Shape effects of filaments versus spherical particles in flow and drug delivery.* Nature Nanotechnology, 2007. **2**(4): p. 249-255.

67. Lundqvist, M., et al., *Nanoparticle size and surface properties determine the protein corona with possible implications for biological impacts.* Proceedings of the National Academy of Sciences, 2008. **105**(38): p. 14265-14270.

68. Verma, A. and F. Stellacci, *Effect of Surface Properties on Nanoparticle–Cell Interactions.* Small, 2010. **6**(1): p. 12-21.

69. Cedervall, T., et al., *Detailed Identification of Plasma Proteins Adsorbed on Copolymer Nanoparticles.* Angewandte Chemie International Edition, 2007. **46**(30): p. 5754-5756.

70. Lynch, I., A. Salvati, and K.A. Dawson, *Protein-nanoparticle interactions: What does the cell see?* Nat Nano, 2009. **4**(9): p. 546-547.

71. Ghosh, P.S., et al., *Efficient gene delivery vectors by tuning the surface charge density of amino acid-functionalized gold nanoparticles.* ACS Nano, 2008. **2**(11): p. 2213-2218.

72. Ghosh, P.S., et al., *Binding of nanoparticle receptors to peptide a-helices using amino acid-functionalized nanoparticles.* Journal of Peptide Science, 2008. **14**(2): p. 134-138.

73. Ghosh, P.S., et al., *Nanoparticles Featuring Amino Acid-functionalized Side Chains as DNA Receptors.* Chemical Biology & Drug Design, 2007. **70**(1): p. 13-18.

74. Goodman, C.M., et al., *Toxicity of Gold Nanoparticles Functionalized with Cationic and Anionic Side Chains.* Bioconjugate Chemistry, 2004. **15**(4): p. 897-900.

75. Han, G., P. Ghosh, and V.M. Rotello, *Functionalized gold nanoparticles for drug delivery.* Nanomedicine, 2007. **2**(1): p. 113-123.

76. Hong, R., et al., *Control of Protein Structure and Function through Surface Recognition by Tailored Nanoparticle Scaffolds.* Journal of the American Chemical Society, 2004. **126**(3): p. 739-743.

77. Leroueil, P.R., et al., *Wide varieties of cationic nanoparticles induce defects in supported lipid bilayers.* Nano Letters, 2008. **8**(2): p. 420-424.

78. Mout, R., et al., *Surface functionalization of nanoparticles for nanomedicine.* Chemical Society Reviews, 2012. **41**(7): p. 2539-2544.

79. Moyano, D.F. and V.M. Rotello, *Nano Meets Biology: Structure and Function at the Nanoparticle Interface.* Langmuir, 2011. **27**(17): p. 10376-10385.

80. Verma, A. and V.M. Rotello, *Surface recognition of biomacromolecules using nanoparticle receptors.* Chemical Communications, 2005(3): p. 303-312.

81. You, C.C., et al., *Tunable inhibition and denaturation of alpha-chymotrypsin with amino acid-functionalized gold nanoparticles.* Journal of the American Chemical Society, 2005. **127**(37): p. 12873-12881.

82. Shukla, R., et al., *Biocompatibility of gold nanoparticles and their endocytotic fate inside the cellular compartment: A microscopic overview.* Langmuir, 2005. **21**(23): p. 10644-10654.

83. De, M., P.S. Ghosh, and V.M. Rotello, *Applications of Nanoparticles in Biology.* Advanced Materials, 2008. **20**(22): p. 4225-4241.

84. Shenhar, R. and V.M. Rotello, *Nanoparticles: Scaffolds and building blocks.* Accounts of Chemical Research, 2003. **36**(7): p. 549-561.

85. You, C.-C., A. Verma, and V.M. Rotello, *Engineering the nanoparticle-biomacromolecule interface.* Soft Matter, 2006. **2**(3): p. 190-204.

86. Irwin, P., et al., *Antimicrobial activity of spherical silver nanoparticles prepared using a biocompatible macromolecular capping agent: evidence for induction of a greatly prolonged bacterial lag phase.* Journal of Nanobiotechnology, 2010. **8**(1): p. 34.

87. Leszczynski, J., *Bionanoscience: Nano meets bio at the interface.* Nat Nano, 2010. **5**(9): p. 633-634.

88. Fischer, H.C. and W.C.W. Chan, *Nanotoxicity: the growing need for in vivo study.* Current Opinion in Biotechnology, 2007. **18**(6): p. 565-571.

89. Holl, M.M.B., *Nanotoxicology: a personal perspective.* Wiley Interdisciplinary Reviews: Nanomedicine and Nanobiotechnology, 2009. **1**(4): p. 353-359.

90. Walczyk, D., et al., *What the Cell Sees in Bionanoscience.* Journal of the American Chemical Society, 2010. **132**(16): p. 5761-5768.

91. Lynch, I., K.A. Dawson, and S. Linse, *Detecting Cryptic Epitopes Created by Nanoparticles.* Sci. STKE, 2006. **2006**(327): p. pe14-.

92. Lundqvist, M., et al., *Nanoparticle size and surface properties determine the protein corona with possible implications for biological impacts.* Proceedings of the National Academy of Sciences of the United States of America, 2008. **105**(38): p. 14265-14270.

93. Lynch, I., A. Salvati, and K.A. Dawson, *Protein-nanoparticle interactions: What does the cell see?* Nature Nanotechnology, 2009. **4**(9): p. 546-547.

94. Walczyk, D., et al., *What the cell "sees" in bionanoscience.* Journal of the American Chemical Society, 2010. **132**(16): p. 5761-5768.

95. Prescott, L.M., J.P. Harley, and D.A. Klein, *Microbiology*, ed. 6. 2005: McGraw-Hill.

96. Gram, H., *Uber die isolierte Farbung der Schizomyceten in Schnitt- und Trockenpraparaten (in German).* Fortschritte der Medizin, 1884. **2**: p. 185-189.

97. Bergey, D.H.J.G.H.N.R.K.P.H.A.S., *Bergey's Manual of Determinative Bacteriology* ed. 9. 1994: Lippincott Williams & Wilkins.

98. Austrian, R., *The Gram stain and the etiology of lobar pneumonia, an historical note.* Bacteriological reviews, 1960. **24**(3): p. 261-265.

99. http://www.cehs.siu.edu/fix/medmicro/genmicr.htm.

100. Brogden, K.A., *Antimicrobial peptides: pore formers or metabolic inhibitors in bacteria?* Nat Rev Micro, 2005. **3**(3): p. 238-250.

101. Nederberg, F., et al., *Biodegradable nanostructures with selective lysis of microbial membranes.* Nat Chem, 2011. **3**(5): p. 409-414.

102. Zasloff, M., *Antimicrobial peptides of multicellular organisms.* Nature, 2002. **415**(6870): p. 389-395.

103. Kuroda, K. and G.A. Caputo, *Antimicrobial polymers as synthetic mimics of host-defense peptides.* Wiley Interdisciplinary Reviews: Nanomedicine and Nanobiotechnology, 2013. **5**(1): p. 49-66.

104. Clement, J.L. and P.S. Jarrett, *Antibacterial Silver.* Metal-Based Drugs, 1994. **1**(5-6): p. 467-482.

105. Salem, H.F., K.A.M. Eid, and M.A. Sharaf, *Formulation and evaluation of silver nanoparticles as antibacterial and antifungal agents with a minimal cytotoxic effect.* International Journal of Drug Delivery, 2011. **1**(2): p. 293-304.

106. Amato, E., et al., *Synthesis, Characterization and Antibacterial Activity against Gram Positive and Gram Negative Bacteria of Biomimetically Coated Silver Nanoparticles.* Langmuir, 2011. **27**(15): p. 9165-9173.

107. Taglietti, A., et al., *Antibacterial Activity of Glutathione-Coated Silver Nanoparticles against Gram Positive and Gram Negative Bacteria.* Langmuir, 2012. **28**(21): p. 8140-8148.

108. Zhou, Y., et al., *Antibacterial activities of gold and silver nanoparticles against Escherichia coli and bacillus Calmette-Guerin.* Journal of Nanobiotechnology, 2012. **10**(1): p. 19.

109. Fabrega, J., et al., *Silver nanoparticle impact on bacterial growth: Effect of pH, concentration, and organic matter.* Environmental Science and Technology, 2009. **43**(19): p. 7285-7290.

110. Kim, J.S., et al., *Antimicrobial effects of silver nanoparticles.* Nanomedicine: Nanotechnology, Biology, and Medicine, 2007. **3**(1): p. 95-101.

111. Sondi, I. and B. Salopek-Sondi, *Silver nanoparticles as antimicrobial agent: A case study on E. coli as a model for Gram-negative bacteria.* Journal of Colloid and Interface Science, 2004. **275**(1): p. 177-182.

112. Heinlaan, M., et al., *Toxicity of nanosized and bulk ZnO, CuO and TiO2 to bacteria Vibrio fischeri and crustaceans Daphnia magna and Thamnocephalus platyurus.* Chemosphere, 2008. **71**(7): p. 1308-1316.

113. Jones, N., et al., *Antibacterial activity of ZnO nanoparticle suspensions on a broad spectrum of microorganisms.* FEMS Microbiology Letters, 2008. **279**(1): p. 71-76.

114. Kim, Y.H., et al., *Preparation and characterization of the antibacterial Cu nanoparticle formed on the surface of SiO2 nanoparticles.* Journal of Physical Chemistry B, 2006. **110**(49): p. 24923-24928.

115. Kasemets, K., et al., *Toxicity of nanoparticles of ZnO, CuO and TiO 2 to yeast Saccharomyces cerevisiae.* Toxicology in Vitro, 2009. **23**(6): p. 1116-1122.

116. Zhang, L., et al., *Investigation into the antibacterial behaviour of suspensions of ZnO nanoparticles (ZnO nanofluids).* Journal of Nanoparticle Research, 2007. **9**(3): p. 479-489.

117. Diao, M. and M. Yao, *Use of zero-valent iron nanoparticles in inactivating microbes.* Water Research, 2009. **43**(20): p. 5243-5251.

118. Gong, P., et al., *Preparation and antibacterial activity of Fe3O4@Ag nanoparticles.* Nanotechnology, 2007. **18**(28).

119. Lee, C., et al., *Bactericidal effect of zero-valent iron nanoparticles on Escherichia coli.* Environmental Science and Technology, 2008. **42**(13): p. 4927-4933.

120. Hajipour, M.J., et al., *Antibacterial properties of nanoparticles.* Trends in Biotechnology, 2012. **30**(10): p. 499-511.

121. Feng, Q.L., et al., *A Mechanistic Study of the Antibacterial Effect of Silver Ions on Escherichia Coli and Staphylococcus Aureus.* Journal of Biomedical Materials Research 2000. **52**(4): p. 662-668.

122. Li, W.R., et al., *Antibacterial activity and mechanism of silver nanoparticles on Escherichia coli.* Applied Microbiology and Biotechnology, 2010. **85**(4): p. 1115-1122.

123. Liau, S.Y., et al., *Interaction of silver nitrate with readily identifiable groups: Relationship to the antibacterial action of silver ions.* Letters in Applied Microbiology, 1997. **25**(4): p. 279-283.

124. Lok, C.N., et al., *Proteomic analysis of the mode of antibacterial action of silver nanoparticles.* Journal of Proteome Research, 2006. **5**(4): p. 916-924.

125. Lok, C.N., et al., *Silver nanoparticles: Partial oxidation and antibacterial activities.* Journal of Biological Inorganic Chemistry, 2007. **12**(4): p. 527-534.

126. Panacek, A., et al., *Silver colloid nanoparticles: Synthesis, characterization, and their antibacterial activity.* Journal of Physical Chemistry B, 2006. **110**(33): p. 16248-16253.

127. http://www.snanos.co.th/index.php/how-silver-nanoparticles-kill-bacteria.html.

128. Hirst, S.M., et al., *Bio-distribution and in vivo antioxidant effects of cerium oxide nanoparticles in mice.* Environmental Toxicology, 2013. **28**(2): p. 107-118.

129. Amin, R.M., et al., *Rapid and sensitive microplate assay for screening the effect of silver and gold nanoparticles on bacteria.* Nanomedicine, 2009. **4**(6): p. 637-643.

130. Connor, E.E., et al., *Gold Nanoparticles Are Taken Up by Human Cells but Do Not Cause Acute Cytotoxicity.* Small, 2005. **1**(3): p. 325-327.

131. Gu, H., et al., *Presenting Vancomycin on Nanoparticles to Enhance Antimicrobial Activities.* Nano Letters, 2003. **3**(9): p. 1261-1263.

132. Kim, J.S., et al., *Antimicrobial effects of silver nanoparticles.* Nanomedicine: Nanotechnology, Biology and Medicine, 2007. **3**(1): p. 95-101.

133. http://www.understandingnano.com/medicine.html.

134. Hughes, A.D. and M.R. King, *Nanobiotechnology for the capture and manipulation of circulating tumor cells.* Wiley Interdisciplinary Reviews: Nanomedicine and Nanobiotechnology, 2012. **4**(3): p. 291-309.

135. Cliffel, D.E., B.N. Turner, and B.J. Huffman, *Nanoparticle-based biologic mimetics.* Wiley Interdisciplinary Reviews: Nanomedicine and Nanobiotechnology, 2009. **1**(1): p. 47-59.

136. Clavijo-Jordan, V., et al., *Principles and emerging applications of nanomagnetic materials in medicine.* Wiley Interdisciplinary Reviews: Nanomedicine and Nanobiotechnology, 2012. **4**(4): p. 345-365.

137. Canelas, D.A., K.P. Herlihy, and J.M. DeSimone, *Top-down particle fabrication: control of size and shape for diagnostic imaging and drug delivery.* Wiley Interdisciplinary Reviews: Nanomedicine and Nanobiotechnology, 2009. **1**(4): p. 391-404.

138. Katz, E. and I. Willner, *Integrated Nanoparticle–Biomolecule Hybrid Systems: Synthesis, Properties, and Applications.* Angewandte Chemie International Edition, 2004. **43**(45): p. 6042-6108.

139. Wang, F., et al., *Luminescent nanomaterials for biological labelling.* Nanotechnology, 2006. **17**(1): p. R1-R13.

140. Mailander, V. and K. Landfester, *Interaction of Nanoparticles with Cells.* Biomacromolecules, 2009. **10**(9): p. 2379-2400.

141. Lu, Y. and J. Liu, *Functional DNA nanotechnology: emerging applications of DNAzymes and aptamers.* Current Opinion in Biotechnology, 2006. **17**(6): p. 580-588.

142. Pradeep, T. and Anshup, *Noble metal nanoparticles for water purification: A critical review.* Thin Solid Films, 2009. **517**(24): p. 6441-6478.

143. Bellan, L.M., D. Wu, and R.S. Langer, *Current trends in nanobiosensor technology.* Wiley Interdisciplinary Reviews: Nanomedicine and Nanobiotechnology, 2011. **3**(3): p. 229-246.

144. Raha, S., T. Paunesku, and G. Woloschak, *Peptide-mediated cancer targeting of nanoconjugates.* Wiley Interdisciplinary Reviews: Nanomedicine and Nanobiotechnology, 2011. **3**(3): p. 269-281.

145. Strong, L.E. and J.L. West, *Thermally responsive polymer–nanoparticle composites for biomedical applications.* Wiley Interdisciplinary Reviews: Nanomedicine and Nanobiotechnology, 2011. **3**(3): p. 307-317.

146. Chen, W., et al., *Nanoparticles as magnetic resonance imaging contrast agents for vascular and cardiac diseases.* Wiley Interdisciplinary

Reviews: Nanomedicine and Nanobiotechnology, 2011. **3**(2): p. 146-161.

147. Hu, W. and C.M. Li, *Nanomaterial-based advanced immunoassays.* Wiley Interdisciplinary Reviews: Nanomedicine and Nanobiotechnology, 2011. **3**(2): p. 119-133.
148. Lei, J. and H. Ju, *Nanotubes in biosensing.* Wiley Interdisciplinary Reviews: Nanomedicine and Nanobiotechnology, 2010. **2**(5): p. 496-509.
149. Chang, T.M.S., *Blood replacement with nanobiotechnologically engineered hemoglobin and hemoglobin nanocapsules.* Wiley Interdisciplinary Reviews: Nanomedicine and Nanobiotechnology, 2010. **2**(4): p. 418-430.
150. Dave, S.R. and X. Gao, *Monodisperse magnetic nanoparticles for biodetection, imaging, and drug delivery: a versatile and evolving technology.* Wiley Interdisciplinary Reviews: Nanomedicine and Nanobiotechnology, 2009. **1**(6): p. 583-609.
151. Hu, Y., et al., *Nanodevices in diagnostics.* Wiley Interdisciplinary Reviews: Nanomedicine and Nanobiotechnology, 2011. **3**(1): p. 11-32.
152. Tong, R. and D.S. Kohane, *Shedding light on nanomedicine.* Wiley Interdisciplinary Reviews: Nanomedicine and Nanobiotechnology, 2012. **4**(6): p. 638-662.
153. Singh, V., et al., *A facile synthesis of PLGA encapsulated cerium oxide nanoparticles: release kinetics and biological activity.* Nanoscale, 2012. **4**(8): p. 2597-2605.

154. Das, S., et al., *The induction of angiogenesis by cerium oxide nanoparticles through the modulation of oxygen in intracellular environments.* Biomaterials, 2012. **33**(31): p. 7746-7755.

155. Putnam, D., *Polymers for gene delivery across length scales.* Nat Mater, 2006. **5**(6): p. 439-451.

156. Pridgen, E.M., R. Langer, and O.C. Farokhzad, *Biodegradable, polymeric nanoparticle delivery systems for cancer therapy.* Nanomedicine, 2007. **2**(5): p. 669(12).

157. Check, E., *Gene therapy: A tragic setback.* Nature, 2002. **420**(6912): p. 116-118.

158. Roy, I., et al., *Optical tracking of organically modified silica nanoparticles as DNA carriers: A nonviral, nanomedicine approach for gene delivery.* Proceedings of the National Academy of Sciences of the United States of America, 2005. **102**(2): p. 279-284.

159. Sokolova, V. and M. Epple, *Inorganic Nanoparticles as Carriers of Nucleic Acids into Cells.* Angewandte Chemie International Edition, 2008. **47**(8): p. 1382-1395.

160. Wiesman, Z., et al., *Novel cationic vesicle platform derived from vernonia oil for efficient delivery of DNA through plant cuticle membranes.* Journal of Biotechnology, 2007. **130**(1): p. 85-94.

161. Fusco, S., A. Borzacchiello, and P.A. Netti, *Perspectives on: PEO-PPO-PEO Triblock Copolymers and their Biomedical Applications.* Journal of Bioactive and Compatible Polymers, 2006. **21**(2): p. 149-164.

162. Kakizawa, Y. and K. Kataoka, *Block copolymer micelles for delivery of gene and related compounds.* Advanced Drug Delivery Reviews, 2002. **54**(2): p. 203-222.

163. Moriguchi, R., et al., *A multifunctional envelope-type nano device for novel gene delivery of siRNA plasmids.* International Journal of Pharmaceutics, 2005. **301**(1-2): p. 277-285.

164. Nishiyama, N. and K. Kataoka, *Current state, achievements, and future prospects of polymeric micelles as nanocarriers for drug and gene delivery.* Pharmacology and Therapeutics, 2006. **112**(3): p. 630-648.

165. Luu, Y.K., et al., *Development of a nanostructured DNA delivery scaffold via electrospinning of PLGA and PLA-PEG block copolymers.* Journal of Controlled Release, 2003. **89**(2): p. 341-353.

166. Jeong, J.H. and T.G. Park, *Poly(L-lysine)-g-poly(D,L-lactic-co-glycolic acid) micelles for low cytotoxic biodegradable gene delivery carriers.* Journal of Controlled Release, 2002. **82**(1): p. 159-166.

167. Ghosh, P., et al., *Gold nanoparticles in delivery applications.* Advanced Drug Delivery Reviews, 2008. **60**(11): p. 1307-1315.

168. Zhang, X.-Q., et al., *Polymer-Functionalized Nanodiamond Platforms as Vehicles for Gene Delivery.* ACS Nano, 2009. **3**(9): p. 2609-2616.

169. Luo, D., et al., *Poly(ethylene glycol)-Conjugated PAMAM Dendrimer for Biocompatible, High-Efficiency DNA Delivery.* Macromolecules, 2002. **35**(9): p. 3456-3462.

170. Kwak, M. and A. Herrmann, *Nucleic acid/organic polymer hybrid materials: Synthesis, superstructures, and applications.* Angewandte Chemie - International Edition, 2010. **49**(46): p. 8574-8587.

171. Drexler, K.E. and C. Peterson, *Nanotechnology and Enabling Technologies.* Foresight Briefing, 1989. **2**.

172. Gaffet, E., et al., *Nanostructural materials formation by mechanical alloying: Morphologic analysis based on transmission and scanning electron microscopic observations.* Materials Characterization, 1996. **36**(4â€“5): p. 185-190.

173. Bhattacharya, D. and R.K. Gupta, *Nanotechnology and potential of microorganisms.* Critical Reviews in Biotechnology, 2005. **25**(4): p. 199-204.

174. Ramanathan, R., et al., *Bacterial kinetics-controlled shape-directed biosynthesis of silver nanoplates using morganella psychrotolerans.* Langmuir, 2011. **27**(2): p. 714-719.

175. Chen, X. and S.S. Mao, *Titanium dioxide nanomaterials: Synthesis, properties, modifications and applications.* Chemical Reviews, 2007. **107**(7): p. 2891-2959.

176. Gedanken, A., *Using sonochemistry for the fabrication of nanomaterials.* Ultrasonics Sonochemistry, 2004. **11**(2): p. 47-55.

177. Hulteen, J.C., *A general template-based method for the preparation of nanomaterials.* Journal of Materials Chemistry, 1997. **7**(7): p. 1075-1087.

178. Martin, C.R., *Nanomaterials: A membrane-based synthetic approach.* Science, 1994. **266**(5193): p. 1961-1966.

179. Martin, C.R., *Membrane-based synthesis of nanomaterials.* Chemistry of Materials, 1996. **8**(8): p. 1739-1746.

180. Nam, K.T., et al., *Virus-enabled synthesis and assembly of nanowires for lithium ion battery electrodes.* Science, 2006. **312**(5775): p. 885-888.

181. Wang, X., et al., *A general strategy for nanocrystal synthesis.* Nature, 2005. **437**(7055): p. 121-124.

182. West, J.L. and N.J. Halas, *Engineered nanomaterials for biophotonics applications: Improving sensing, imaging, and therapeutics*, in *Annual Review of Biomedical Engineering*2003. p. 285-292.

183. Jain, D., et al., *Synthesis of plant-mediated silver nanoparticles using papaya fruit extract and evaluation of their anti microbial activities.* Digest Journal of Nanomaterials and Biostructures, 2009. **4**(3): p. 557-563.

184. Bansal, V., et al., *Biosynthesis of zirconia nanoparticles using the fungus Fusarium oxysporum.* Journal of Materials Chemistry, 2004. **14**(22): p. 3303-3305.

185. Bansal, V., et al., *Fungus-mediated biosynthesis of silica and titania particles.* Journal of Materials Chemistry, 2005. **15**(26): p. 2583-2589.

186. Ahmadi, T.S., et al., *Shape-controlled synthesis of colloidal platinum nanoparticles.* Science, 1996. **272**(5270): p. 1924-1926.

187. Huang, X., S. Neretina, and M.A. El-Sayed, *Gold nanorods: From synthesis and properties to biological and biomedical applications.* Advanced Materials, 2009. **21**(48): p. 4880-4910.

188. Dahl, J.A., B.L.S. Maddux, and J.E. Hutchison, *Toward greener nanosynthesis.* Chemical Reviews, 2007. **107**(6): p. 2228-2269.

189. Selvakannan, P.R., et al., *A new method for the synthesis of hydrophobic gold nanotapes.* Journal of Nanoscience and Nanotechnology, 2003. **3**(5): p. 372-374.

190. Selvakannan, P.R., et al., *One-step synthesis of hydrophobized gold nanoparticles of controllable size by the reduction of aqueous chloroaurate ions by hexadecylaniline at the liquid-liquid interface.* Chemical Communications, 2002(13): p. 1334-1335.

191. Selvakannan, P.R., et al., *Synthesis of aqueous Au core-Ag shell nanoparticles using tyrosine as a pH-dependent reducing agent and assembling phase-transferred silver nanoparticles at the air-water interface.* Langmuir, 2004. **20**(18): p. 7825-7836.

192. Turkevich, J., P.C. Stevenson, and J. Hillier, *A study of the nucleation and growth processes in the synthesis of colloidal gold.* Discussions of the Faraday Society, 1951. **11**: p. 55-75.

193. Parikh, R.Y., et al., *Extracellular Synthesis of Crystalline Silver Nanoparticles and Molecular Evidence of Silver Resistance from Morganella sp.: Towards Understanding Biochemical Synthesis Mechanism.* ChemBioChem, 2008. **9**(9): p. 1415-1422.

194. Faraday, M., *The Bakerian Lecture: Experimental Relations of Gold (and Other Metals) to Light.* Philosophical Transactions of the Royal Society of London, 1857. **147**: p. 145-181.

195. Turkevich, J. and G. Kim, *Palladium: Preparation and catalytic properties of particles of uniform size.* Science, 1970. **169**(3948): p. 873-879.

196. Turkevich, J., *Colloidal gold. Part I. Historical and preparative aspects, morphology and structure.* Gold Bulletin, 1985. **18**: p. 86-91.

197. Kallay, N. and S. Zalac, *Stability of Nanodispersions: A Model for Kinetics of Aggregation of Nanoparticles.* Journal of Colloid and Interface Science, 2002. **253**(1): p. 70-76.

198. Bonnemann, H. and R.M. Richards, *Nanoscopic metal particles - Synthetic methods and potential applications.* European Journal of Inorganic Chemistry, 2001(10): p. 2455-2480.

199. Richards, R. and H. Bönnemann, *Synthetic Approaches to Metallic Nanomaterials*, in *Nanofabrication Towards Biomedical Applications*. 2005, Wiley-VCH Verlag GmbH & Co. KGaA. p. 1-32.

200. Templeton, A.C., W.P. Wuelfing, and R.W. Murray, *Monolayer-Protected Cluster Molecules.* Accounts of Chemical Research, 2000. **33**(1): p. 27-36.

201. Jain, P.K., et al., *Calculated absorption and scattering properties of gold nanoparticles of different size, shape, and composition: Applications in biological imaging and biomedicine.* Journal of Physical Chemistry B, 2006. **110**(14): p. 7238-7248.

202. Eustis, S. and M.A. El-Sayed, *Why gold nanoparticles are more precious than pretty gold: Noble metal surface plasmon resonance and its enhancement of the radiative and nonradiative properties of nanocrystals of different shapes.* Chemical Society Reviews, 2006. **35**(3): p. 209-217.

203. Link, S. and M.A. El-Sayed, *Size and temperature dependence of the plasmon absorption of colloidal gold nanoparticles.* Journal of Physical Chemistry B, 1999. **103**(21): p. 4212-4217.

204. Sun, Y. and Y. Xia, *Gold and silver nanoparticles: A class of chromophores with colors tunable in the range from 400 to 750 nm.* Analyst, 2003. **128**(6): p. 686-691.

205. Kelly, K.L., et al., *The Optical Properties of Metal Nanoparticles: The Influence of Size, Shape, and Dielectric Environment.* The Journal of Physical Chemistry B, 2002. **107**(3): p. 668-677.

206. Yeh, Y.C., B. Creran, and V.M. Rotello, *Gold nanoparticles: Preparation, properties, and applications in bionanotechnology.* Nanoscale, 2012. **4**(6): p. 1871-1880.

207. Templeton, A.C., et al., *Solvent Refractive Index and Core Charge Influences on the Surface Plasmon Absorbance of Alkanethiolate Monolayer-Protected Gold Clusters.* Journal of Physical Chemistry B, 2000. **104**(3): p. 564-570.

208. Lee, J.-H., J.-H. Hwang, and J.-M. Nam, *DNA-tailored plasmonic nanoparticles for biosensing applications.* Wiley Interdisciplinary Reviews: Nanomedicine and Nanobiotechnology, 2013. **5**(1): p. 96-109.

209. Su, K.H., et al., *Interparticle Coupling Effects on Plasmon Resonances of Nanogold Particles.* Nano Letters, 2003. **3**(8): p. 1087-1090.

210. McNeil, S.E., *Nanotechnology for the biologist.* Journal of Leukocyte Biology, 2005. **78**(3): p. 585-594.

211. Bhushan, B., *Bioinspired Structured Surfaces.* Langmuir, 2012. **28**(3): p. 1698-1714.

212. Luo, D., *The road from biology to materials.* Materials Today, 2003. **6**(11): p. 38-43.

213. Gao, L., et al., *Intrinsic peroxidase-like activity of ferromagnetic nanoparticles.* Nature Nanotechnology, 2007. **2**(9): p. 577-583.

214. Wei, H. and E. Wang, *Fe 3O 4 magnetic nanoparticles as peroxidase mimetics and their applications in H 2O 2 and glucose detection.* Analytical Chemistry, 2008. **80**(6): p. 2250-2254.

215. He, W., et al., *Au@Pt nanostructures as oxidase and peroxidase mimetics for use in immunoassays.* Biomaterials, 2011. **32**(4): p. 1139-1147.

216. Zhang, K., et al., *Formation of PdPt Alloy Nanodots on Gold Nanorods: Tuning Oxidase-like Activities via Composition.* Langmuir, 2011. **27**(6): p. 2796-2803.

217. Fan, J., et al., *Direct evidence for catalase and peroxidase activities of ferritin-platinum nanoparticles.* Biomaterials, 2011. **32**(6): p. 1611-1618.

218. He, W., et al., *Design of AgM Bimetallic Alloy Nanostructures (M = Au, Pd, Pt) with Tunable Morphology and Peroxidase-Like Activity.* Chemistry of Materials, 2010. **22**(9): p. 2988-2994.

Chapter II

Characterization techniques

Spectroscopic, microscopic and other analytical characterization of nanomaterials are indispensable to correlate their structure, their properties and their interaction with biological systems. Thus the physical principles and instrumentation of different characterization techniques consisting various spectroscopic, electron microscopic and other physicochemical techniques used during the course of the present work are discussed in this chapter.

2.1. Introduction

Nanotechnology and nanoscience are considered as the most important technologies of modern era and the basic of their development lies in the fact that properties of bulk materials changes extensively when their size is reduced to nano-meter scale. However, there are many challenges in the research and development of nano-scale based products and efforts are being made around the globe to create smart, intelligent and multifunctional nanomaterials to exhibit extraordinary applications in the field of catalysis, biology and medicine.[1-5]

It is imperative to understand fundamental key characteristics that contribute to the uniqueness of nanomaterials and ultimately defines their fate in biological entity.[3, 6-8] Size, shape, surface charge, surface area, surface functionality, composition, hydrophilic/hydrophobic nature and structure are the main characteristics on nanomaterials and their for all the synthesised and functionalized nanomaterials prepared in this thesis have been characterized by microscopic and spectroscopic techniques to understand their size, size distribution, shape, physical, chemical and other properties at nano-meter level.

The main emphasis of the thesis is the formation of inorganic and organic nanostructures and investigation of their biological applications. Prior to biological applications, these all the nanomaterials were characterized by UV-Visible, Fourier Transform Infrared (FTIR), X-Ray Photoelectron Spectroscopy (XPS), Transmission Electron Microscopy (TEM), Scanning Electron Microscopy (SEM), Atomic Absorption Spectroscopy (AAS), Inductively Coupled Plasma-Mass Spectroscopy (ICP-MS), Dynamic

Light Scattering (DLS) Zeta Potential and Cyclic Voltammetry (CV) techniques. This chapter is devoted to physical principles and instrumentation of the various characterization techniques employed in this thesis, to characterize nanomaterials and to correlate with observed biological applications.

2.2. Microscopy techniques

Micron sized materials can be observed using optical microscopes with a reasonable resolution but due to lens aberrations and higher wavelength of visible light, higher magnification to image sub-micron materials cannot be achieved or rather difficult. Therefore, powerful imaging techniques like TEM was used in this thesis to characterize nanostructures and surface functionalized nanomaterials. Wherein, SEM imaging was carried out to study morphological changes in bacteria after their treatments with various nanoparticles. Basic principles and applications of these imaging techniques used in this thesis are described below.

2.2.1. Transmission electron microscopy (TEM)

The TEM is used extensively both in materials science and biological sciences. In both the cases, the samples must be very thin and able to bear-up the high vacuum (HV) present inside the instrument. Nanostructures prepared in this thesis for assorted biological applications at nano-bio interface have structural and morphological diversity and the use of TEM enabled the direct imaging of nanostructures. Primary, information about the particles size, shape and surface layers (coatings) were collected from TEM.

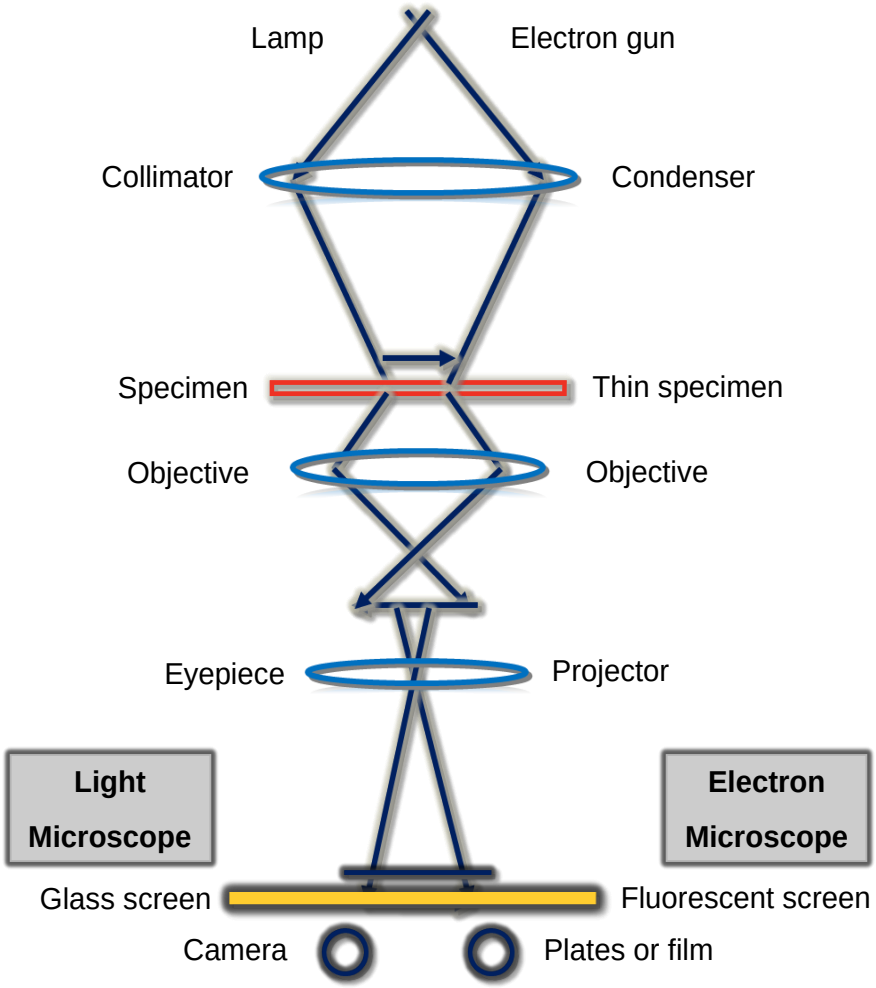

Figure.2.1. Schematic representation of the major components of the optical systems of a TEM (adopted from the reference [9]) (equivalent terms of light and electron microscopy are also shown)

Typically in TEM, a beam of electrons emitted from a cathode (usually tungsten or occasionally lanthanum hexaboride) are accelerated using accelerating voltage (≈100 kV) and directed to a thin sample through the use of magnetic condenser lenses. The sample (specimen) must be prepared as thin as possible so that the electron beam can penetrate through the sample. After the interaction with the thin sample, the incident electron beam have several possible fates such as (i) the electrons may pass thought the sample and remain un-deflected; (ii) it may be elastically scattered

(conserve all energy of incident electron beam) or (iii) it may be in-elastically scattered (a portion of energy is lost of the incident electron beam). If all these three interactions contribute to the obtained image, all the regions would look identical or there would be no contrast, but if the scattered electrons are removed through an aperture after interaction the image formed will therefore be a direct correlation to the thickness and type of the material that the electron beam has passes through.[9] This image, formed by the transmitted electrons (through the specimen), magnified and focused by an objective lens and appears on an imaging screen as shown in Figure 2.1.

All the TEM images presented in this thesis were carried out using a JEOL 1010 TEM instrument operated at an accelerating voltage at 100 KV and samples were prepared by drop caste on to strong carbon coated 200 mesh copper grid and the solvent was allowed to evaporate at room temperature.

2.2.2. Scanning electron microscopy (SEM)

To a certain extent SEM is considered as a limited tool to characterize nanoparticles because sometimes it is not possible to clearly distinguish the nanoparticles from the substrate and this becomes more critical when nanomaterials, which are under study have tendency to adhere strongly to each other, forming agglomerates. Further, in contrast to TEM, SEM cannot determine the inner structure of these domains. In this thesis, microorganism (*Escherichia coli* and *Staphylococcus albus*) were analysed under SEM before and after their treatments with various nanoparticles to

obtain information related to their surface structure or morphological changes with great clarity.

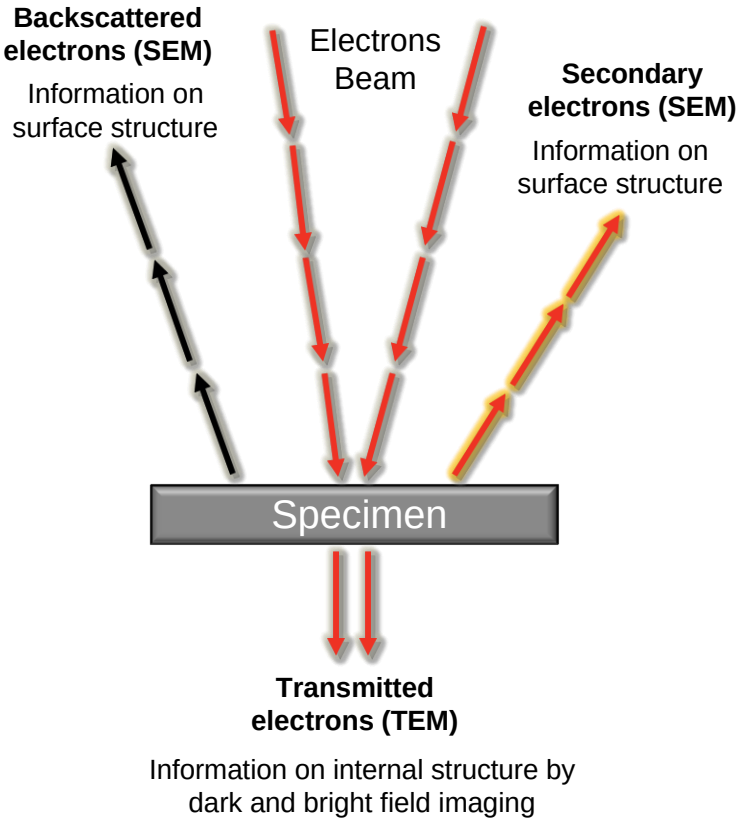

Figure.2.2. Schematic representation of electron-sample interaction in SEM

Similar to TEM, SEM uses a beam of electrons to image surface of the sample. As similar to TEM, which generates electrons through thermionic emission, the SEM also generates electrons through thermionic or using Field Emission Gun (FEG) which operated by holding a sharp pointed tungsten emitter at several kV negative potential relative to a nearby counter electrode. A FEG is able to produce an electron beam that has much greater current density, is smaller in diameter and is more than conventional thermionic emitters. When the beam of electrons strikes on the specimen or sample, signals are generated in the form of secondary electrons (SE), back scattered electrons (BSE) and characteristic X-rays that contains important

information of the specimen's topography and composition. The SEM produces high resolution image of specimen surface, revealing details ≈1-5 nm in size in its primary detection mode for instance SE imaging. Characteristic X-rays in SEM are used to recognize the elemental composition of the specimen by energy dispersive X-ray (EDX) technique. BSE from the specimen may also be used to form an image and this image often used in analytical SEM along with the spectra made from the characteristic X-ray as the confirmation of the elemental composition of the specimen.[10]

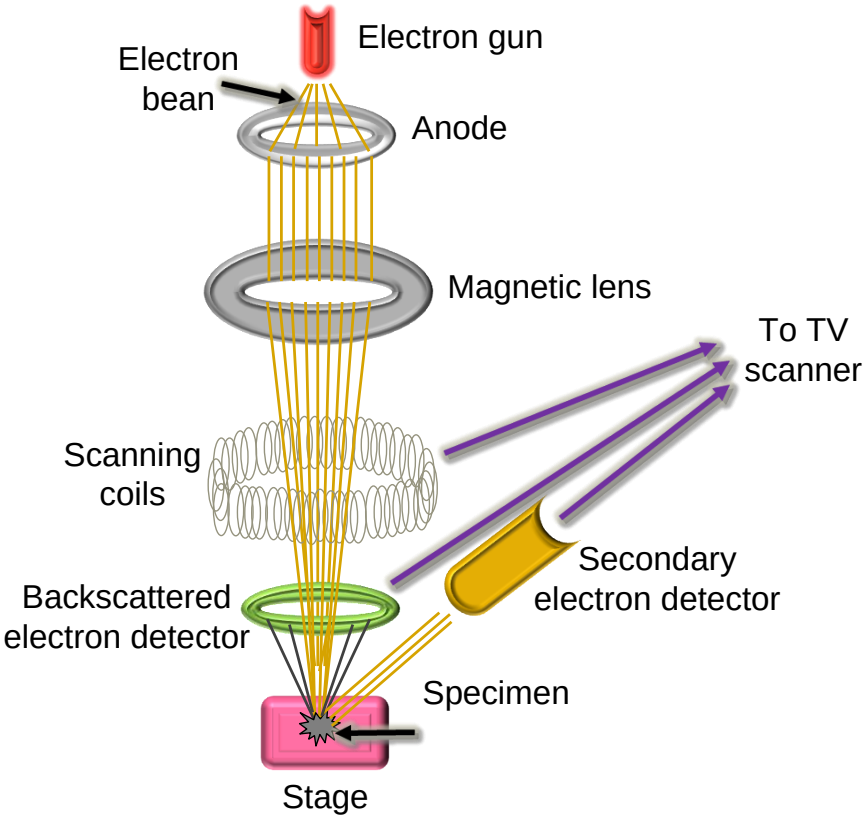

Figure.2.3. Schematic representation of scanning electron microscope

In this thesis, SEM analysis of bacterial cells without any treatment (control) and after their interaction with nanoparticles were performed on a FEI Nova-SEM, operated at an accelerating voltage of 15 kV, 3.5 nm spot

size and 5 mm working distance. The samples were drop casted on glass cover slips, which were mounted on aluminium SEM stub using double-sided carbon tape. SEM requires that the specimen should be conductive for the electron beam to scan the surface and that the electrons have a path to ground for conventional imaging. Therefore, before SEM imaging, all the samples were coated with a 20 Å thick platinum film using precision etching coating system (Gatan model 682). The coatings were done at rock angle 20°, speed 40°/sec, rotation 25 rpm and beam current 5 KeV to avoid sample charging issues.

2.3. Spectroscopy techniques

Electronic, Vibrational and photoelectron spectroscopic techniques are mainly used to study the surface plasmon resonant features of nanoparticles, functional groups bound to the surface of nanoparticles and the chemical state of elements respectively.

2.3.1. Ultraviolet-visible (UV-vis) spectroscopy

UV-vis spectrophotometer is consists of a light source, reference and sample beams, a monochromator and a detector. In the field of nanobiotechnology, UV-vis spectroscopy is being used to characterize the metal nanoparticles based on their distinct SPR features. Primarily, the broadening and peak shift in the absorption spectra of the nanoparticles, how they depend on their size, shape, state of aggregation and the local dielectric environment. Compared to other methods, this is faster, more flexible and less complicated technique, but it is not conclusive and needs to

be performed in association with other complementary spectroscopic and structural investigations.

The magnitude, peak wavelength and spectral bandwidth of the plasmon resonance associated with a nanoparticle are dependent on the particles size, shape, and materials composition as well as the local environment.[11, 12] According to Mie's theory, only a single SPR band is expected in the absorption spectra of spherical metal nanoparticles, whereas anisotropic metal particles could give rise to two or more SPR bands depending on the shape of the particles.

All the UV-visible (UV-vis) spectra presented in this thesis were obtained using Varian Cary 50 Bio Spectrophotometer operated at a resolution of 2 nm over a wavelength of 200-800 nm. In this thesis, we have designed mono and bimetallic alloy nanoparticles of gold and silver and UV-vis spectroscopy was used primary technique to confirm the formation of nanoparticles and nano-alloys.

2.3.2. Fourier transform infrared (FTIR) spectroscopy

In this technique, materials are analysed by observing the atomic vibrations of molecules when exposed to electromagnetic radiation typically in the wavelength ranging from 2.5 to 25 μm, equivalent to 4000-400 cm^{-1} are employed, an order of magnitude greater than those used in UV-vis spectroscopy. Both, RAMAN and FTIR spectroscopy techniques investigate vibrational modes and provides complementary information which can assist molecular interaction studies such as hydrogen bonding and give molecular orientation information for surface studies.[13]

In the field of nano-biotechnology, these spectroscopic methods not only used to detect conformational changes, they also confirm the amino acid functionalization onto nanoparticles through the appearance of additional characteristic bands. In fact, both the techniques have different selection rules and specific advantages and disadvantages for biomedical applications. FTIR spectroscopy has been used to monitor the structure of amino acids bound to the nanoparticles bound protein and also confirm the secondary structure of the proteins on the basis of the absorption of amide bonds. Side chains present in amino acids are fundamentally important in stabilising protein structure and in catalysing enzyme reactions.[14]

In this thesis, FTIR spectroscopy was used to obtain information about the surface properties of amino acid reduced nanoparticles and to detect amino acid binding onto the nanoparticles surface. Also, FTIR analysis was carried out to understand the nature of interaction between plasmid DNA and tri-block copolymer. All the FTIR spectra presented in different chapters of this thesis were recorded in diffuse reflectance spectroscopy (DRS) mode using Perkin-Elmer D100 spectrophotometer with a resolution of 4 cm^{-1}.

2.3.3. Other spectroscopic techniques

2.3.3.1. Atomic absorption spectroscope (AAS)

AAS is an analytical method for the qualitative detection and quantitative determination of elements through the absorption of optical radiation by free atoms in the gas phase. This follows the Beer Lambert Law, which states that absorbance (denoted as A, negative logarithm of the

transmission factor) is proportional to the concentration c of the absorbing substance and the thickness d of the absorbing layer:

$$A = -\log \frac{\phi_t(\lambda)}{\phi_i(\lambda)} = kcd$$

Where $Ø_t$ is the power of transmitted radiation and $Ø_i$ is the power of incident radiation.

AAS analysis of nanoparticles (concentrations of gold and silver, present in nanoparticles) discussed in this thesis were analysed using a Varian PerkinElmer atomic absorption spectrometer after dissolution of samples in freshly prepared aqua regia. Aqua regia is a yellow-reddish coloured corrosive mixture of concentrated nitric acid and hydrochloric acid (HNO_3 + HCl) in a volume ratio of 1:3.

2.3.3.2. Inductively coupled plasma mass spectroscopy (ICP-MS)

ICP-MS is a special type of mass spectroscopy technique, which is capable to determine metals and some non-metals up to the concentration of part per trillion (one part of 10^{-12}). This is accomplished by the ionizing the sample with inductively couple plasma and using a mass spectrometer to separate and quantify those ions. In compare to AAS, ICP-MS has better speed, precision and sensitivity.

In this thesis, ICP-MS analysis was carried out to detect the presence of molybdenum (Mo) and tungsten (W) concentrations qualitatively and quantitatively in surface functionalized gold and silver nanomaterials using Agilent Technologies machine (7700 series ICP-MS) after dissolution of samples in freshly prepared aqua regia.

2.4. X-ray based characterization techniques

2.4.1. X-ray photoemission spectroscopy (XPS)

XPS is also known as electron spectroscopy for chemical analysis (ESCA) and PES (photo emission spectroscopy). This is a quantitative spectroscopic surface chemical analysis technique to estimate the elemental composition, empirical formula and chemical or electronic state (oxidation state) of the element on the surface of a material (up to 10 nm).[15] It also detects the contamination, if any, exist on the surface or the bulk of the sample.

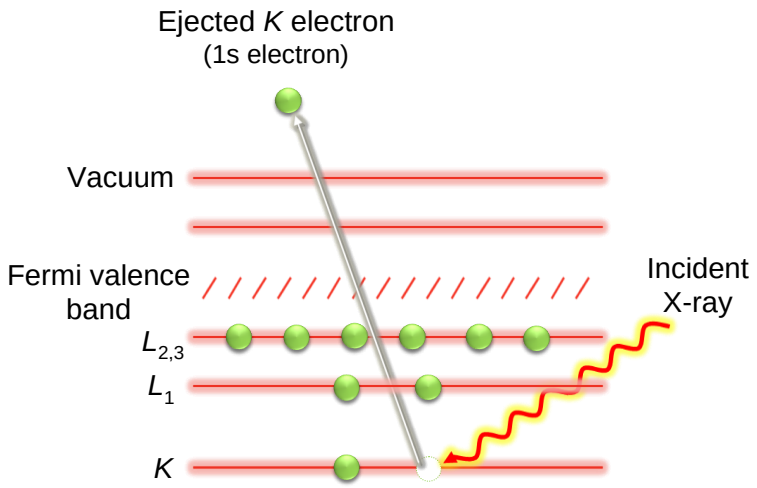

Figure.2.4. Schematic representation of the XPS process, showing photo-ionization of an atom by the ejection of a 1s electron[15]

Under ultra-high vacuum (UHV), X-ray irradiation on a material leads to the emission of electrons from the core orbital of the surface elements. Kinetic energy (KE) measurement and the number of electrons escaping from the surface of the material give the XPS spectrum. From the KE of the electrons, the binding energy (BE) of the electrons can be calculated. This BE (of electrons) reflects the oxidation state of the specific element present

on the surface. The number of electrons reflects the proportion of the specific elements on the surface. As the energy of a particular X-ray wavelength used to excite the electron from a core orbital is a known quantity, electron BE of each of the emitted electrons can be determined using the following equation:

$$E_{\text{binding}} = E_{\text{photon}} - E_{\text{kinetic}} - Ø$$

This equation is based on the work of Ernest Rutherford (1914), where E_{binding} is the energy of the electron emitted from one electron configuration within the atom; E_{photon} is the energy of the X-ray photons being used; E_{kinetic} is the kinetic energy of the emitted electrons as measured be the instrument; and Ø is the work function of the spectrometer (not the material).

All the XPS analysis presented in this thesis were performed using a THERMO K-Alpha XPS machine, at a pressure better than 1 x 10^{-9} Torr (1 Torr = 1.333 × 10^2 Pa). The core level spectra for all the samples studied in this thesis were recorded with un-monochromatized Mg Kα radiation (photon energy of 1253.6 eV) at pass energy of 50 eV and electron take off angle of 90°. The overall resolution was 0.1 eV for XPS measurements. The core level spectra were background corrected using Shirley algorithm,[16] binding energies (BEs) were aligned with adventitious carbon binding energy of 285 eV and chemically distinct species were resolved using a nonlinear least squares fitting procedure.

2.4.2. Energy dispersive X-ray analysis (EDX)

EDX is a useful technique to analyse near surface elements and to estimate their proportion at different positions of the specimen. In general, this technique is employed in the conjugation with SEM and it provides an overall mapping of the specimen. In this technique, an electron beam (typically in the range of 10-20 keV) strikes or interacts with the surface of a specimen and causes X-ray to be emitted from the material. Energy of these emitted X-ray depends on the type of element present in the material. Actually, the X-rays are generated in a region about 2 microns (μm) in depth and therefore EDX is not a true surface technique. By moving the electron beam across the specimen an image of each element in the sample can be obtained. The composition or the amount of nanoparticles near and on the surface can be estimated using the EDX. Elements of low atomic number are difficult to be detected by EDX.

2.5. Particles size analyser

Size and size distribution of the nanomaterials have influence on their biological activities and therefore, size and size distribution study of the nanomaterials in the dispersion as well as suspension is important before applying for any biological or medical application. Particles size and particles size distribution (PSD) can be measured using different techniques like acoustic spectroscopy, laser diffraction methods, electro resistance counting, optical counting, sedimentation techniques or dynamic light scattering (DLS). Although, UV-vis spectroscopy gives an idea about the particle size, while electron microscopy provides direct and visual indication

about the particles size and morphology but DLS is the most commonly used technique to measure particles size and PSD. Therefore, this technique was employed as an additional characterization tool in this thesis for obtaining size distribution of nanomaterials prior to investigate their biological uses.

2.5.1. Dynamic light scattering (DLS)

DLS is an invasive and well-established characterization technique to determine the size distribution profile of colloidal particles. This is also known as photon correlation spectroscopy (PCS) or quasi-elastic light scattering (QELS). Due to the thermal energy of solvent molecules, suspension of particles, emulsions or molecules undergo Brownian motion. If these colloidal particles or molecules are illuminated with a laser light, the intensity of the scattered light fluctuates which is dependent upon the size of the particles (smaller particles move more rapidly than larger particles). Analysis of this intensity fluctuations yield the velocity of the Brownian motion and hence the particles size (hydrodynamic radius) using the stokes-Einstein relationship, as shown below:

$$r_K = K T / 6 \pi \eta D$$

Where K is the Boltzmann's constant; T, the temperature in K; η, the solvent viscosity and D, the diffusion coefficient.

However, it is important to notice that there is often a concentration of ions, or any surface structure around the colloidal particles that can affect how the particles diffuse within the fluid, the diameter that is measured in

DLS is known as the hydrodynamic diameter and can often be larger that measured by electron microscopy.

2.6. Zeta potential measurement (particles charge analyser)

Many nanoparticles in solution bear an electrostatic charge on their surface that hinders the inter particle interaction/aggregation by electrostatic repulsion. However, ions and ionic surfactants in the solution can adsorb onto the nanoparticles surface, modifying the overall surface charge and forming an electrical double layer around each particle. This consists of an inner layer, called Stern layer, more strongly bound to the surface and an outer diffuse layer less firmly bound to the nanoparticles surface. Within the diffuse layer, there is a boundary, the slipping plane, inside which the ions and particles from a stable entity (and travel together under an electric field), and the zeta (ζ) potential measures the electric potential at the slipping plane.

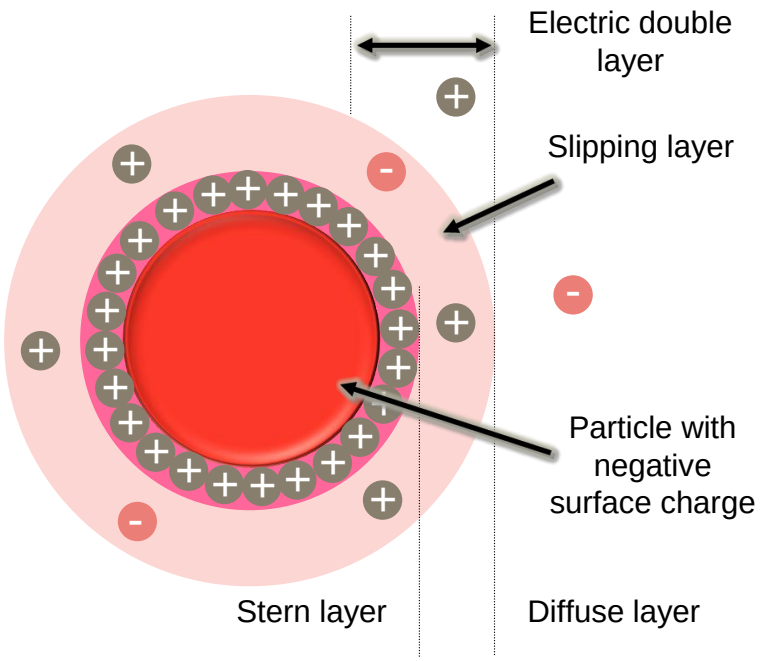

Figure.2.5. Schematic representation of the electrical double layer on the surface of nanoparticle

Generally, nanoparticles characterized by a larger ζ potential repel each other and do not flocculate, thereby forming a stable dispersion. Thus, the ζ potential gives information on the surface charge of the nanoparticles and can be used to detect protein binding to the nanoparticles surface as this will change the overall surface charge. Therefore, the surface charge of the nanomaterials is a standard parameter to be characterized and reported as it is one of the most basic and crucial properties influencing the environmental interactions of nanoparticulate matter.

The initial electrostatic interaction of nanomaterials with biological entity critically depends on the surface charge of nanomaterials and cationic surface charged nanoparticles are reported to have an influence on toxicity on living organisms and the barrier integrity.[17] Also, this is recognized for the stability of the nanoparticles suspension, which is achieved by electrostatic repulsion (or sometimes by the steric hindrance). Therefore, in the field of nano-biotechnology, surface charge analysis of the nanoparticles is essential to achieve assorted and controlled biological applications. Surface charge of nanomaterials developed during this thesis work were determined by the Zeta potential measurements performed in deionized water using a Malvern 2000 Zetasizer.

2.7. Electrochemical studies using cyclic voltammetry (CV)

In analytical chemistry, CV is used to study the electrochemical properties of an analyte in solution. CV is a type of potentiodynamic electrochemical measurement.[18] For CV characterization, analyte has to be redox active and must display reversible wave. Once an analyte is

reduced/oxidized on a forward scan and then reoxidized / rereduced in expected manner on return scan, is known as reversible wave.

In the field of nanobiotechnology, CV studies are relatively new and in this thesis, CV measurements were performed to understand electrochemical behaviour of fabricated nanomaterials to correlate their redox behaviour to the observed biological activities. For CV analysis, 5µL of the relevant nanoparticle solution was drop caste onto an ITO-coated glass electrode surface and allowed to dry at room temperature. CV experiments were conducted using a CH Instruments (CHI 760C) electrochemical analyser in a three electrode setup. A modified 3mm GC (BAS) with nanoparticles was used as the working electrode, which in each case prior to modification was polished with an aqueous 0.3µm alumina slurry on a polishing cloth (Microcloth, Buehler), sonicated in deionized water for 5 min and dried with a flow of nitrogen gas. A Ag/AgCl (3 M NaCl) reference and a Pt wire counter electrode were used. The electrolyte solutions were degassed with nitrogen for 10 min prior to any electrochemical measurement.

2.8. References

1. Sanvicens, N. and M.P. Marco, *Multifunctional nanoparticles - properties and prospects for their use in human medicine.* Trends in Biotechnology, 2008. **26**(8): p. 425-433.
2. Bhattacharya, R. and P. Mukherjee, *Biological properties of "naked" metal nanoparticles.* Advanced Drug Delivery Reviews, 2008. **60**(11): p. 1289-1306.

3. Suh, W.H., et al., *Nanotechnology, nanotoxicology, and neuroscience.* Progress in Neurobiology, 2009. **87**(3): p. 133-170.
4. Niemeyer, C.M. and C.A. Mirkin, eds. *Nanobiotechnology: Concept, Application and perspectives*. 2004, Wiley-VCH verlag GmbH & Co. KGaA.
5. Mirkin, C.A. and C.M. Niemeyer, eds. *Nanobiotechnology II: More concepts and applications* 2007, Wiley-VCH verlag GmbH & Co. KGaA.
6. Nel, A.E., et al., *Understanding biophysicochemical interactions at the nano-bio interface.* Nature Materials, 2009. **8**(7): p. 543-557.
7. Mahmoudi, M., V. Serpooshan, and S. Laurent, *Engineered nanoparticles for biomolecular imaging.* Nanoscale, 2011. **3**(8): p. 3007-3026.
8. Arvizo, R.R., et al., *Intrinsic therapeutic applications of noble metal nanoparticles: past, present and future.* Chemical Society Reviews, 2012. **41**(7): p. 2943-2970.
9. Dawn Chescoe and P.J. Goodhew, *The operation of the transmission electron microscope*. 1984: Oxford University Press.
10. in *http://www.purdue.edu/rem/rs/sem.htm*.
11. Mulvaney, P., *Surface Plasmon Spectroscopy of Nanosized Metal Particles.* Langmuir, 1996. **12**(3): p. 788-800.
12. Jain, P.K., et al., *Noble Metals on the Nanoscale: Optical and Photothermal Properties and Some Applications in Imaging, Sensing, Biology, and Medicine.* Accounts of Chemical Research, 2008. **41**(12): p. 1578-1586.

13. Neil W Barnett, et al., *Industrial Analysis with Vibrational Spectroscopy*. 1997: RSC Publishing

14. Barth, A., *The infrared absorption of amino acid side chains.* Progress in Biophysics and Molecular Biology, 2000. **74**: p. 141-173.

15. John F. Watts and J. Wolstenholme, *An Introduction to Surface Analysis by XPS and AES*. 2003: John Wiley & Sons, Ltd.

16. Shirley, D.A., *High-Resolution X-Ray Photoemission Spectrum of the Valence Bands of Gold.* Physical Review B, 1972. **5**(12): p. 4709-4714.

17. Goodman, C.M., et al., *Toxicity of Gold Nanoparticles Functionalized with Cationic and Anionic Side Chains.* Bioconjugate Chemistry, 2004. **15**(4): p. 897-900.

18. Heinze, J., *Cyclic Voltammetry—"Electrochemical Spectroscopy". New Analytical Methods (25).* Angewandte Chemie International Edition in English, 1984. **23**(11): p. 831-847.

Chapter III

Influence of composition and surface functionalization of nanomaterials towards their biological activities

This chapter first focuses on the development of synthetic methodologies in controlling surface functionality and composition of metal nanoparticles in a single step using green and eco-friendly synthetic routes. Tryptophan and tyrosine amino acids were employed as reducing and stabilizing agents to synthesize gold, silver and their bimetallic alloy nanoparticles in a highly controlled manner. Second part of the chapter shows influence of the individual and synergistic role of the surface bound amino acids and nanoparticle composition on intrinsic enzyme-like and antimicrobial activities. Finally the correlation between the surface corona and metal composition of nanoparticles and the observed biological applications has been established.

3.1. Introduction

Nanomaterials illustrate dimensional similarities with biomolecules such as enzymes, antigens, antibodies and DNA therefore nanomaterial are emerging for myriads of biological applications. Understanding the interface of nanomaterials and biomolecules is imperative because functionalization of nanomaterials with biomolecules can impart unique recognition, catalytic and other properties along with their well-known physicochemical properties (electronic, photonic, optical etc.). Moreover, these hybrid nanomaterials can be employed for several applications in the field of materials science, chemistry, biology and nanomedicine.[1-4] In the context of biology and nanomedicine, designing inorganic nanomaterials requires a deep understanding of interaction between these materials and complex biological systems at the nanometer level to achieve the desired type of selective biological action.[5-9]

In living organisms, nanomaterial interaction with the cell wall, cell membrane, cell organelles, cytoplasm, proteins and genetic material critically depends on many parameters including the size, shape, surface charge, surface functionality, composition, hydrophobicity or hydrophilicity and the surface roughness of nanomaterials as illustrated in Figure 1.3.[10-17] Moreover, either individually or cooperatively all these parameters influence the initial electrostatic adhesion of particles on the cell surface, their cellular uptake or direct penetration inside the cells, and their interaction with cellular components, which ultimately translates into the

level of toxicity posed by inorganic materials towards a specific living organism.[11, 18, 19]

Recently it has been reported that nanomaterials have the potential to mimic natural enzymes as they possess intrinsic biocatalyst-like properties [20-25] and these enzyme-like activities can be tuned in a controlled manner.[23, 26] Especially, nanomaterials are found to function similar to peroxidase- or catalase-like enzymes. Furthermore, it has been documented that nanomaterials which have peroxidase-like activity possess considerable ability to induce production of reactive oxygen species (ROS) thereby exhibiting assorted biological activities. Presence of higher level of ROS in any biological system is harmful due to the significant changes in homeostasis and it may induce cell damage irrevocably while a lesser amount of ROS can be effectively neutralized by natural antioxidants.[27-35] Therefore, to achieve specific applications in the field of biology and nanomedicine, the intrinsic properties, surface chemistry and composition of nanomaterials must be tailored carefully and there is a need to understand their interaction at the nano-bio interface.[36-38]

In this perspective, a range of nanomaterials have been evaluated for antibacterial applications wherein the majority of focus is on the toxicity of the inorganic component [39-47] while relatively few reports discuss the surface charge induced toxicity.[48-51] As highlighted in a recent review, most of the previous studies have utilized as-synthesized metal nanoparticle solutions for antimicrobial studies, without taking into account the contribution of antimicrobial activities originating from unreduced metal ion component in metal nanoparticle solutions; due to this combination it is

rather difficult to unequivocally assign the antimicrobial effect to metal nanoparticles.[39]

In general, toxicity of metal ions or nanoparticles is believed to be arisen through cation induced cell wall rupturing,[9, 52-54] uncoupling of the respiratory chain from oxidative phosphorylation, denaturation of thiol containing membrane proteins and DNA damage.[40, 55-59] In the context of nanoparticles composition, silver nanoparticles (Ag nanoparticles) are typically found to exhibit significantly higher level of toxicity, [40, 44, 55, 57, 58, 60-69] whereas gold nanoparticles (Au nanoparticles) are proven to be biocompatible.[40, 70, 71] The toxicity of Ag nanoparticles is attributed to the partial oxidation of Ag nanoparticles into Ag^+ cations, which leads to rupturing of the negatively charged bacterial cell wall.[55] Further, in an interesting study it was confirmed that cationic Au nanoparticles may also be made moderately toxic causing cell lysis, whereas anionic Au nanoparticles were found nontoxic. This clearly indicates that even the most biocompatible nanomaterials such as Au nanoparticles can be made toxic by tuning its surface charge.[72] Also, functionalization of Au nanoparticles surface by small molecules can render their biocompatible nature to target bacterial cells.[73]

Additionally, it must be noted that most of the nanoparticle-based antimicrobial agents reported in the literature have shown profound toxic effect on Gram negative bacteria, [41, 43, 45, 56, 58, 73-75] whereas those nanomaterials didn't show much antibacterial activity against Gram positive bacteria.[40, 76] This is predominantly because Gram negative bacteria such as *Escherichia coli* containing a negatively charged cell membrane can

be ruptured by interaction with positively charged nanoparticles or cations,[9, 53, 72, 77] whereas Gram positive bacteria such as *Staphylococcus* have stronger defence mechanism due to the thick peptidoglycan cell wall, which is difficult to be decomposed by nanoparticles.[78] However, nature has developed its own defence mechanism against Gram positive bacteria using lysozymes and antimicrobial peptides that are known to hydrolyse the peptidoglycan cell wall.[79, 80]

Lysozymes and antibacterial peptides consisting of simple amino acids are capable of hydrolysing the polymeric linkage between NAG and NAM present in peptidoglycan layer. The structural features, conformation and selectivity of these proteins help in their binding with the bacterial cell wall, thereby enabling amino acids to cooperatively hydrolyse the glycosidic bond to break the cell walls of Gram positive bacteria. Therefore, metal nanoparticles enveloped within a protein or amino acid corona may offer opportunities for the initial interaction of nanomaterials with the peptidoglycan cell wall, followed by hydrolysis and bacterial cell death. This concept is also supported by some of the previous reports which suggest that metal nanoparticulate systems surrounded by a protein corona may mimic natural enzymatic catalysis processes, in which metal nanoparticles act as support to render stability, limited mobility and conformation constraint to the enzymes.[81, 82]

From the above discussion, it is apparent that the guiding principles toward designing an efficient metal nanoparticle-based antibacterial agent for Gram positive bacteria are not clearly understood. Even though

nanoparticle composition and surface charge are considered two major factors influencing antibacterial activity, the additional role of surface functionality in tailoring antibacterial profile of metal nanoparticles has further scope of the study. Furthermore, it is important to use metal ion free nanoparticle solutions for antibacterial studies to unequivocally assign the antibacterial effect to metal nanoparticles. Also, the effect of Au-Ag alloy nanoparticles in comparison with pristine Au or Ag nanoparticles on antibacterial activity has hitherto not been studied. Varying the proportions of two metal components in different compositions of Au-Ag alloy nanoparticles may be a uniquely interesting aspect for controlling intrinsic enzyme-like activity and metal toxicity, since the interaction of these systems is expected to be different from the monometallic Au or Ag nanoparticles.

The major focus of this chapter is to address the aforementioned issues by developing Au, Ag and their bimetallic Au-Ag alloy nanoparticles in a highly facile and controllable manner using amino acids as reducing and functionalizing agents. Although, amino acid based synthesis of nanomaterials is available in literature, [83-86] their application at the nano-bio interface has not been explored widely. Moreover, their capability to produce bimetallic Au-Ag alloy nanoparticles provides an opportunity to investigate their biological applications with different composition and surface functionality.

The amino acids were chosen over conventional reducing agents for metal nanoparticles synthesis because amino acids-mediated synthesis of nanoparticles offers advantages of making alloy nanoparticles of different

compositions in a single step without using any additional stabilizers or toxic chemical reducing agents in contrast to using other reducing agents [87-89] and this is a major step towards greener synthesis of nanomaterials.[90-92] Further, amino acids such as tryptophan and tyrosine have the potential to reduce gold and silver ions into their nanoparticulate forms through their indole and phenol groups, respectively, [84, 85] while their amine and carboxylic acid groups remain intact and may essentially behave the similar manner as amino acids in a protein. Therefore, amino acid-modified nanomaterials may resemble the naturally occurring Gram positive antibacterial agents such as lysozymes and antimicrobial peptides, thereby enabling the formulation of efficient antimicrobial agents against Gram positive bacteria.

Additionally, the availability of amine and carboxyl groups of the amino acids on the nanoparticle surface may provide further opportunities and biological identity to anchor amino acid-functionalized metal nanoparticles to biological surfaces through polyvalent interactions, similar to that in enzymatic interaction with any substrate. Moreover, amino acids are zwitterionic in nature and therefore surface charge of amino acid-functionalized nanoparticles can be easily tuned by varying the solution pH. These properties of amino acids, when combined with the nanoparticle composition in a cooperative manner, amino acid-functionalized nanomaterials have significant potential to be used as generic materials for enzyme-like or antibacterial applications.

3.2. Scheme of the work

In first part of this chapter, a green and eco-friendly synthetic method using amino acid mediated synthesis of Au, Ag and their Au-Ag alloy nanoparticles is described. Tryptophan (Trp or W) and tyrosine (Tyr or Y) amino acids were selected as reducing agent to produce different surface functionalization on nanoparticulate systems due to their similar isoelectric points (tryptophan: 5.89, tyrosine: 5.66) and hydropathy indexes (tryptophan: -0.9, tyrosine: -1.3,), however both the amino acids have different side functional groups (tyrosine: phenol group, tryptophan: indole ring) and these side groups are responsible for the reduction of metal ions. Structures of tryptophan and tyrosine amino acids are illustrated in Figure 3.1.

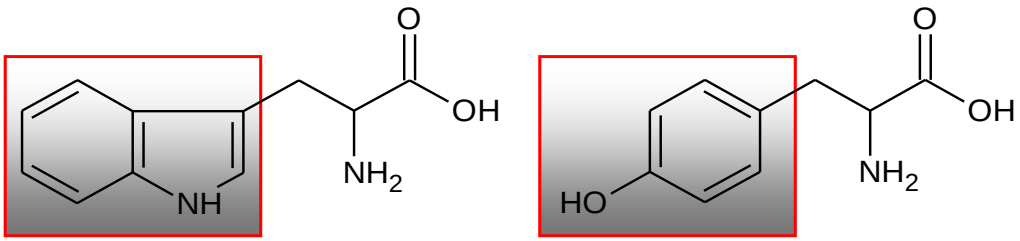

Tryptophan **Tyrosine**

Figure.3.1. Chemical structures of tryptophan and tyrosine amino acids

To achieve control over the composition of bimetallic Au-Ag alloy nanoparticles, three different ratios of precursor gold and silver ions such as 75:25 (in Au rich alloy), 50:50 (in Au=Ag alloy) and 25:75 (in Ag rich alloy) respectively, were introduced in the solution containing amino acids as represented in Figure 3.2. In the next step, all these nanoparticles were subjected to dialysis to remove potentially unbound amino acids and free metal ions, if any. Further, all these mono and bimetallic nanoparticles were

thoroughly characterized using various spectroscopic, microscopic and other analytical techniques.

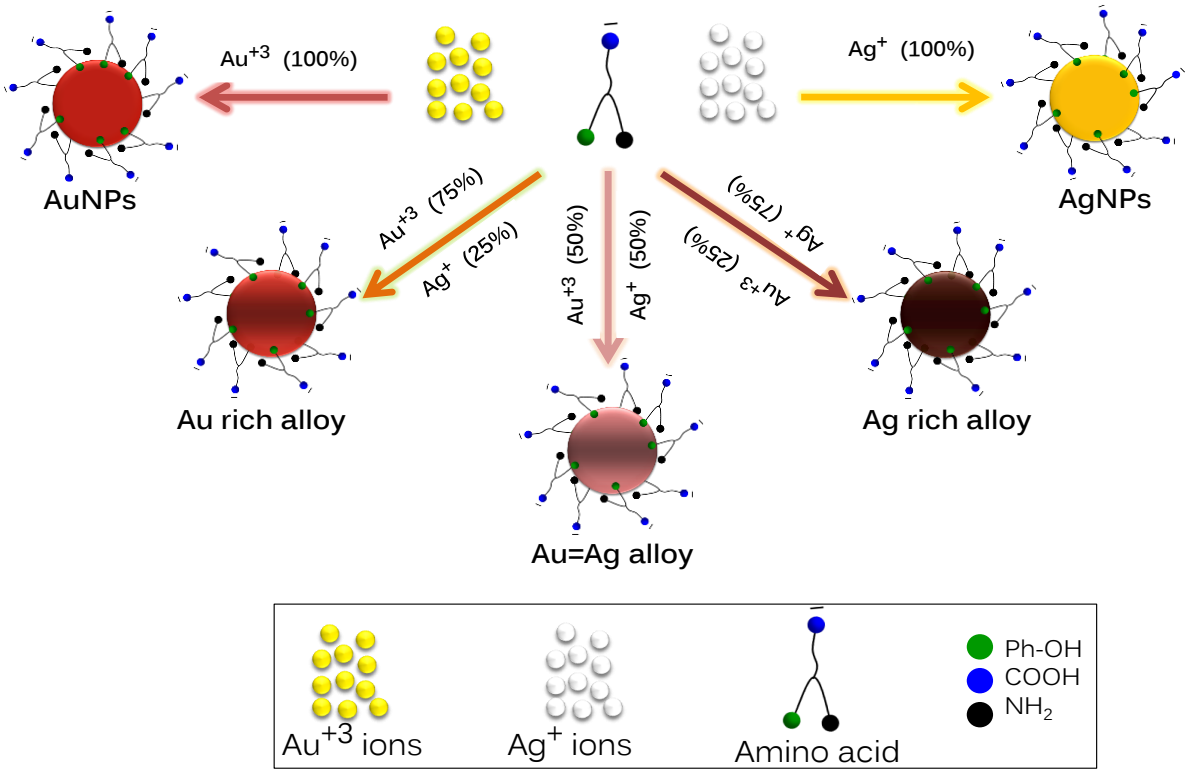

Figure.3.2. Schematic representation of synthesis of Au, Ag and their alloy nanoparticles with different compositions and surface functionality

Next part of the chapter focuses to investigate the biocatalytic properties of amino acid shell present on the surface of nanoparticles and to study how it get affected by the varying metal composition. In this context, intrinsic peroxidase-like activities of these nanoparticles were investigated by catalysing the oxidation of 3,3´,5,5´-tetramethylbenzidine (TMB) substrate. Finally, antibacterial potential of all these nanoparticles were evaluated against model Gram positive bacterium *Staphylococcus albus* and Gram negative bacterium *Escherichia coli*. Nano-SEM imaging was carried out to understand the influence of nanoparticle composition and amino acid

shell towards these bacterial strains and bacterial-nanoparticles interactions.

3.3. Experimental section

3.3.1. Synthesis of Au, Ag and Au-Ag alloy nanoparticles

In a typical experiment, 100 mL aqueous solution containing either 0.5 mM L-tryptophan or 0.1 mM L-tyrosine, along with 1 mM KOH were allowed to boil. To this boiling solution, either $[AuCl_4]^-$ ions, Ag^+ ions or both $[AuCl_4]^-$ and Ag^+ ions were added to obtain pristine Au, pristine Ag and three different compositions of Au-Ag alloy nanoparticles, respectively. The concentrations of metal ions used and details of the reaction products are summarised in Table 3.1.

Terminology	$HAuCl_4$(mM)	$AgNO_3$(mM)	Sample details
Au_{100}^{Trp}	0.20	0.00	Trp-reduced Au
$Au_{75}Ag_{25}^{Trp}$	0.15	0.05	Trp-reduced Au rich Au-Ag alloy
$Au_{50}Ag_{50}^{Trp}$	0.10	0.10	Trp-reduced equimolar Au-Ag alloy
$Au_{25}Ag_{50}^{Trp}$	0.05	0.15	Trp-reduced Ag rich Au-Ag alloy
Ag_{100}^{Trp}	0.01	0.20	Trp-reduced Ag
Au_{100}^{Tyr}	0.20	0.00	Tyr-reduced Au
$Au_{75}Ag_{25}^{Tyr}$	0.15	0.05	Tyr-reduced Au rich Au-Ag alloy
$Au_{50}Ag_{50}^{Tyr}$	0.10	0.10	Tyr-reduced equimolar Au-Ag alloy
$Au_{25}Ag_{50}^{Tyr}$	0.05	0.15	Tyr-reduced Ag rich Au-Ag alloy
Ag_{100}^{Tyr}	0.00	0.20	Tyr-reduced Ag

Table.3.1. Concentration of $HAuCl_4$ and $AgNO_3$ used for the synthesis of Au, Ag and Au-Ag alloy nanoparticles using tryptophan and tyrosine

The total concentrations of metal ions were kept constant at 0.2 mM in all the reactions. Here, it must be noted that although tyrosine amino acid could efficiently synthesize pristine Ag nanoparticles (Ag_{100}^{Tyr}), despite repeated efforts, tryptophan amino acid failed to reduce Ag^{+} ions into Ag nanoparticles. Therefore, a minute amount of $[AuCl_4]^{-}$ ions (10 μM) was added to obtain Ag nanoparticles by tryptophan-mediated reduction (Ag_{100}^{Trp}).

3.3.2. Processing of nanoparticles by concentration and dialysis

All of the ten nanoparticle solutions were heated in water bath to concentrate the nanoparticle solutions (20 times). These solutions were overnight dialysed to remove free metal ions and unbound amino acids from the nanoparticle solutions against deionized water using 12 kDa dialysis membranes. After concentration and dialysis, all the metal nanoparticles solutions remained stable, indicating that these nanoparticles were strongly capped with amino acids. The solutions thus obtained were found stable under standard laboratory storage conditions at room temperature over 6 months, and used as such for materials characterisation and biological studies.

3.3.3. Peroxidase-like activity of Au, Ag and Au-Ag nanoparticles

The peroxidase enzyme-like behaviour of monometallic Au, Ag and bimetallic Au-Ag alloy nanoparticles was examined using 3,3',5,5'-tetramethylbenzidine (TMB) as a chromogenic substrate by catalysing the oxidation of the substrate. Different metal concentrations of mono- and bi-metallic nanoparticles were incubated with TMB substrate in the presence of

H_2O_2 to evaluate effects of nanoparticle concentration and composition on their peroxidise-like activity, in dark.

In dark experimental conditions, the blue colour developed as the reaction proceeded was monitored kinetically using a multimode spectrophotometer. TMB conversion was measured at 650 nm. All these experiments were performed at three different temperatures, 20ºC, 37ºC and 55ºC to investigate effects of temperature on peroxidise-like activities along with surface functionalization and metal composition. Pure tryptophan, tyrosine and precursor metal ions were also evaluated for their peroxidase enzyme-like activities under same experimental conditions for comparison purposes.

3.3.4. Antibacterial assays of Au, Ag and Au-Ag alloy nanoparticles

Quantitative assessment of antimicrobial performance of monometallic Au, Ag and bimetallic Au-Ag alloy nanoparticles was made using colony count methods. Gram positive bacterium *S. albus* and Gram negative bacterium *E. coli* were used as model microorganism for antibacterial studies. Before performing microbiological experiments, all the culture media, glass-wares, containers and micro tips were sterilized by autoclaving at 121°C for 15 min.

To assess antimicrobial activity by colony counting method, 10^4 colony forming units (CFU) of bacteria were incubated with different nanoparticle solutions for 24 hours at 4°C in LB broth, followed by spread-plating of 100 µl aliquots onto nutrient agar (NA) plates. The NA plates were

incubated for 24 hours (*E. coli*) and 48 hours (*S. albus*) at 37 °C and colonies formed after incubation were counted. These colonies correspond to the number of live (viable) bacteria in each suspension at the time of aliquot withdrawal. Plot of the bacterial viability versus the dose of nanoparticles were constructed to visualize the dose dependant bacterial activity. All the bacterial toxicity tests were performed in duplicates and repeated at 3 different times to ensure reproducibility. Further, Nano-SEM was employed to reveal the morphological changes in treated bacterial cells after bacteria-nanoparticles interaction.

3.4. Results and discussion

Tryptophan and tyrosine amino acids can be employed as a reducing agents for gold and silver ions for the synthesis of stable metal nanoparticles in aqueous medium, wherein indole group in tryptophan was found to participate in the metal ions reduction, whereas tyrosine reduces the metal ions through its phenol group.[84, 85]

In this thesis the capability of these amino acids was further explored to form Au-Ag alloy metal nanoparticles of varying composition and surface functionalization. This demonstrated that natural biomolecules such as amino acids can act as green and eco-friendly reducing agents to achieve control over the synthesis of metal alloys in a single step without any requirement of extra additives or special reaction conditions.

3.4.1. UV-visible spectral studies of Au, Ag and Au-Ag alloy nanoparticles

SPR absorption bands are strong characteristic signatures for the noble metal and their alloy nanoparticles.[87] Usually, bimetallic nanoparticles can be either core-shell or alloy type and UV-visible spectrophotometer analysis can differentiate between these two systems. The core-shell nanoparticles give rise to two different SPR bands and the intensities of these individual bands will depend on the relative percentage of each metal present in the core-shell system [93-95] and the similar condition will occur from a dispersion containing separate Au nanoparticles and Ag nanoparticles. Conversely, the single SPR feature of metal alloys will lie between those of two independent metal nanoparticles. Therefore, the formation of alloy nanoparticles can be confirmed using UV-visible absorption spectroscopy.

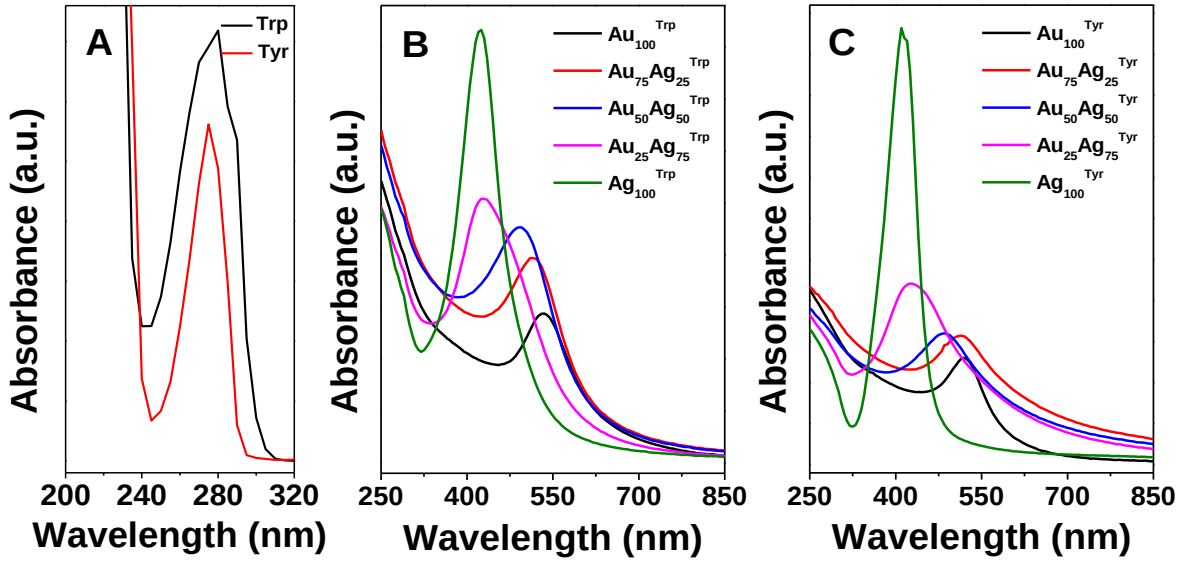

Figure.3.3. UV-visible absorbance spectra of (A) tryptophan (Trp) and tyrosine (Tyr), (B) tryptophan- and (C) tyrosine- reduced Au, Ag and Au-Ag alloy nanoparticles, respectively

In order to examine whether the nanoparticles synthesized using tryptophan and tyrosine amino acids were alloys or core shell particles, UV-visible absorption spectroscopic studies were carried out and presented in Figure 3.3 (B and C). Illustrated in Figures 3.3 A is UV-vis absorbance spectra of pure tryptophan and tyrosine amino acids. Since tryptophan and tyrosine has indole and phenol groups, they have absorbance at 280 and 275 nm, respectively.

A single absorption band was obtained in UV-vis absorbance spectra of Au, $Au_{75}Ag_{25}$ (gold-rich alloy), $Au_{50}Ag_{50}$ (equimolar Au and Ag alloy), $Au_{25}Ag_{75}$ (silver-rich alloy) and Ag nanoparticles obtained from tryptophan and tyrosine mediated reduction of metal ions (Figures 3.3 B and C, respectively). Figures 3.3 B illustrates that tryptophan reduced Au_{100}^{Trp} and Ag_{100}^{Trp} nanoparticles that showed their respective SPR bands at ca. 530 nm and 420 nm, whereas the three alloy nanoparticles showed SPR features at ca. 515 nm ($Au_{75}Ag_{25}^{Trp}$), 495 ($Au_{50}Ag_{50}^{Trp}$) and 425 nm ($Au_{75}Ag_{25}^{Trp}$), respectively. Likewise, tyrosine reduced Au_{100}^{Tyr}, $Au_{75}Ag_{25}^{Tyr}$, $Au_{50}Ag_{50}^{Tyr}$, $Au_{75}Ag_{25}^{Tyr}$ and Ag_{100}^{Tyr} nanoparticles show their respective SPR bands at ca. 520, 510, 485, 425 and 415 nm, respectively (Figures 3.3 C). A clear blue shift of Au SPR features with an increase in Ag content, along with absence of any noticeable additional features in the spectra of alloy nanoparticles provides an evidence towards the formation of a Au-Ag alloy phase, without forming any heterogeneous population of Au and Ag, or a core-shell type structure.[87, 96] Additionally, the positions of the SPR absorption bands of metal and metal alloy nanoparticles observed in this study are very similar to those reported previously.[87]

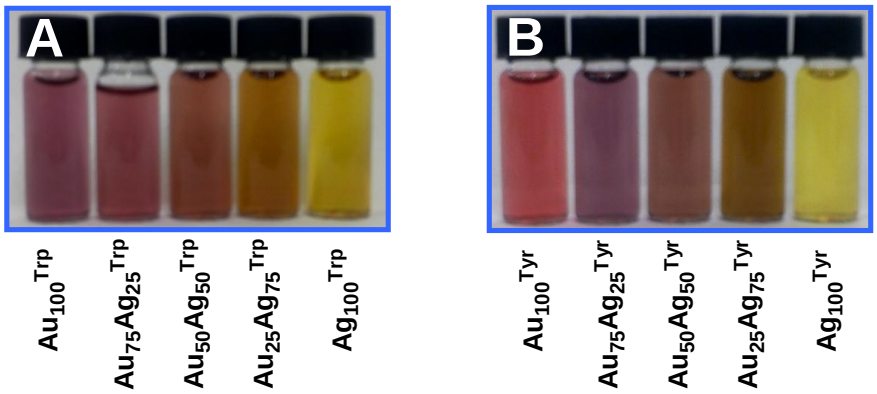

Figure.3.4. Digital photographs of metal nanoparticle solutions synthesised using (A) tryptophan and (B) tyrosine

The digital photographs of metal nanoparticle solutions obtained by tryptophan and tyrosine mediated reduction are illustrated in Figure 3.4 (A and B, respectively), which clearly show a transition in solution colour in both the cases from ruby red (Au) to yellow (Ag), respectively. The intermediate compositions resulted in colours that were varying between ruby red and yellow as can be seen from the digital photographs in Figure 3.4 demonstrating the alloy forming capability of tryptophan and tyrosine amino acids. This is interesting that simple biomolecules such as amino acids can provide a facile handle to control the composition of metal alloys because synthesis of alloys almost always involve a reducing agent along with a capping agent.

Additionally, UV-visible absorbance spectroscopy was employed to compare nanoparticles as-obtained (post-synthesis), and after dialysis as discussed earlier and shown in Appendix C.1. Interestingly, no considerable changes in the position of the SPR plasmon of nanoparticles was observed post- dialysis, except that reduction of π-π* absorption band due to the

aromatic rings of tryptophan and tyrosine at ca. 280 or 275 nm, suggesting that the final nanoparticle solutions are free from unbound amino acids.

Since removal of free metal ions and capping agents from metal nanoparticle solution typically results in nanoparticle aggregation, absence of any such behaviour after dialysis in amino-acid reduced metal nanoparticles indicates that amino acids strongly cap these nanoparticles during synthesis. The stability of amino acid-reduced metal nanoparticles was also evident when these particles showed no evidence of aggregation on storage under standard laboratory conditions in deionized water for over six months. Therefore, synthesis of highly stable, metal ion free, monometallic and alloy nanoparticles is an important advantage of amino acids-mediated synthesis of these nanomaterials.

3.4.2. TEM studies of amino acid reduced Au, Ag and Au-Ag alloy nanoparticles

Illustrated in Figure 3.5 are TEM images, mean particle size and size distribution histogram of tryptophan reduced Au_{100} (A1); $Au_{75}Ag_{25}$ (A2); $Au_{50}Ag_{50}$ (A3); $Au_{25}Ag_{75}$ (A4) and Ag_{100} (A5) nanoparticles, respectively.

As shown in Figure 3.5 (A1-A5), all these nanoparticles are quasi-spherical in shape. The mean particle size of Au_{100}^{Trp} is around 8.2 nm with a standard deviation of 4.4 nm, while Ag_{100}^{Trp} nanoparticles are ~10.8 nm in size with a standard deviation of 5.5 nm. The mean particles size for alloy nanoparticles is ranging from 5 to 6 nm in size.

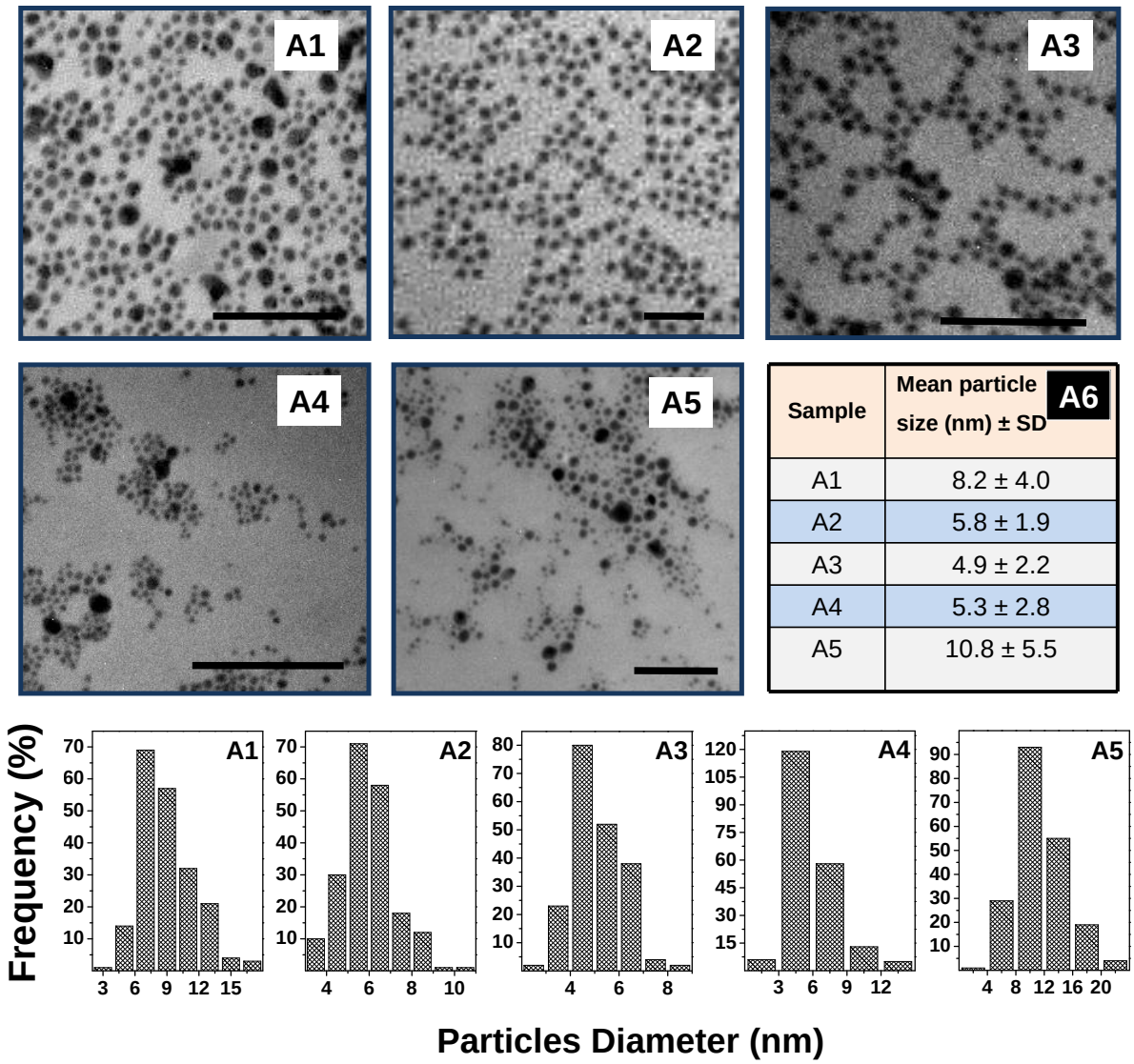

Figure.3.5. TEM images and particle size distribution histogram of tryptophan reduced Au, Ag and their alloy nanoparticles. Scale bars correspond to 100 nm. Average particle sizes along with standard deviations are also shown (A6)

Figure 3.6 shows TEM images, mean particle size and particle size distribution histogram of tyrosine synthesised Au, Ag and their Au-Ag alloy nanoparticles. All these nanoparticles are spherical in shape. As shown in Figure 3.6 (B1-B4), the mean particles size of Au_{100}^{Tyr} and Au containing all the three alloys are ~ 5.5 to 6.5 nm in size with a standard deviation of ~2.5 nm. Conversely, Figure 3.6 (B5) shows that Ag_{100}^{Tyr} are comparatively bigger

in size then all the other nanoparticles synthesised either by tryptophan or tyrosine and the mean particles size of Ag_{100}^{Tyr} is around 26.8 nm with a standard deviation of 5.8 nm.

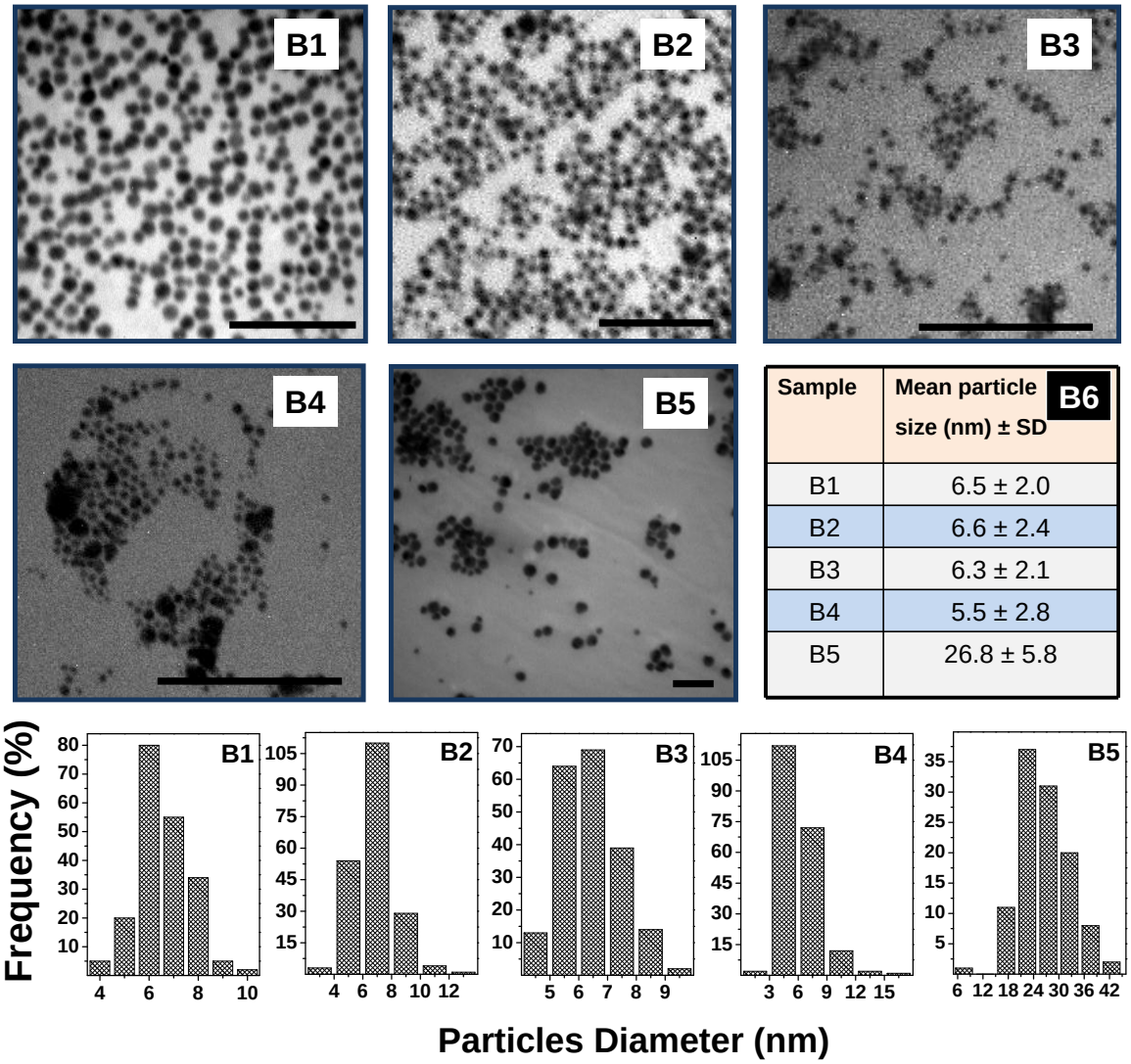

Figure.3.6. TEM images and particle size distribution histogram of tyrosine reduced Au, Ag and Au-Ag alloy nanoparticles. Scale bars correspond to 100 nm. Corresponding average particle sizes along with standard deviations are also shown (B6)

Shape and size of nanoparticles has considerable effects on their biological activities.[31, 74, 97-100] All the nanoparticle synthesised with amino acids are spherical or quasi-spherical in shape and 5 to 10 nm in size

(except Ag_{100}^{Tyr}). This is the size domain where size-dependent toxicity of metal nanoparticles was typically not observed. Hence, shape and size of these nanoparticles does not have significant influence on the biological effects and therefore biological effects of composition and different surface functionalization can be compared confidently.

3.4.3. Estimation of the metal content present in dialysed nanoparticle solutions

Atomic absorption spectroscopy (AAS) was employed to measure the metal content in each sample after nanoparticles synthesis because it is likely that not all of the metal ions employed in the reaction are reduced during metal nanoparticles synthesis, as discussed earlier. Therefore, after nanoparticle formation and purification by dialysis, AAS studies were performed on aqua regia (corrosive mixture of $1HNO_3$ + 3HCl) digested nanoparticle solutions.

AAS results indicated that Au:Ag ratios in finally obtained nanoparticle samples follow a distinct trend as shown in Table 3.2, which is very close to the initial ratios of metal ions used during the synthesis of metal nanoparticles (Table 3.1). Further, AAS results indicated that in different alloy compositions, amino acids have a tendency to form a Ag-rich alloy on the cost of gold ions used during the synthesis. For instance, the initial molar ratios of $[AuCl_4]^-$ and Ag^+ ions used to form $Au_{75}Ag_{25}^{Trp}$ alloy was 75:25, however in the nanoparticles, Au and Ag metal was found to be in 68:32 ratio. Similarly, in the case of $Au_{75}Ag_{25}^{Tyr}$ it was found to be 66:34 for Au:Ag. This is most likely because it is easier to reduce Ag^+ ions in

comparison to $[AuCl_4]^-$ ions, and therefore when both $[AuCl_4]^-$ and Ag^+ ions coexist in a single system, a Ag-rich Au-Ag alloy is obtained.

Sample	% Molar ratios		Zeta potential (mV)
	Au	Ag	
Au_{100}^{Trp}	100	0	-34.6
$Au_{75}Ag_{25}^{Trp}$	68	32	-41.0
$Au_{50}Ag_{50}^{Trp}$	46	54	-21.1
$Au_{25}Ag_{50}^{Trp}$	26	74	-41.6
Ag_{100}^{Trp}	8	92	-36.8
Au_{100}^{Tyr}	100	0	-42.4
$Au_{75}Ag_{25}^{Tyr}$	66	34	-44.4
$Au_{50}Ag_{50}^{Tyr}$	43	57	-42.1
$Au_{25}Ag_{50}^{Tyr}$	23	77	-43.8
Ag_{100}^{Tyr}	0	100	-42.9

Table.3.2: Molar ratios (%) of Au and Ag estimated from AAS and zeta potential measurements of nanoparticle solutions

AAS results further emphasize that by finely controlling the molar ratios of metal ions during amino acid-mediated reduction, Au-Ag alloy composition can be delicately tuned. It is noteworthy that the ratio of Au and Ag in both tyrosine and tryptophan-reduced alloys were very similar, which makes them suitable for comparison during peroxidase-like and antibacterial studies.

3.4.4. Zeta potential measurements of Au, Ag and Au-Ag alloy nanoparticles

Illustrated in Table 3.2 are zeta potential values of different metal nanoparticles. The ζ potential reflects the charge on the surface of

nanomaterials. Interestingly, all the monometallic Au or Ag and bimetallic Au-Ag nanoparticles possess high negative surface charge at physiological pH. The pH of the nanoparticle solutions can indicate about the possible surface charge of the nanoparticles due to the presence of tryptophan and tyrosine amino acids on their surfaces. In principle, if pH of solution is above the isoelectric point of tryptophan or tyrosine (5.89 or 5.66, respectively), relevant nanoparticles must bear a negative surface charge. Conversely, if the pH of the nanoparticles solution is below the isoelectric point of amino acid the nanoparticles must bear a positive surface charge.

The negative zeta potential values were expected since these nanoparticles were stabilized with tryptophan or tyrosine, thus making them negatively charged at physiological pH. A high negative zeta potential value also indicated that these particles have good stability, which is required to prevent these nanoparticles from aggregation in bacterial growth media because inorganic salts and other nutrients may induce aggregation. Further, as all these nanoparticles have similar type of surface charge, it excludes any possibility of surface charge dependent biological activities. It is also imperative to add that charge on the surface of amino acids-capped nanoparticles can be easily controlled by changing the solution pH due to the zwitterionic nature of tryptophan and tyrosine.

3.4.5. X-ray photoemission spectroscopy analysis of Au, Ag and Au-Ag alloy nanoparticles

XPS analysis was carried out to confirm zerovalent state of gold (Au^0) and silver (Ag^0) in mono and bimetallic alloy nanoparticles after reduction of

respective $[AuCl_4]^-$ and Ag^+ ions with tryptophan and tyrosine amino acids. XPS is regarded as a highly surface sensitive technique, therefore presence of amino acid shell on the surface of dialysed nanoparticles samples were also confirmed using XPS. All the spectra discussed in this thesis have been background corrected using Shirley algorithm[101] and their core level binding energies were aligned with respect to the adventitious C1s binding energy (BE) of 285 eV.

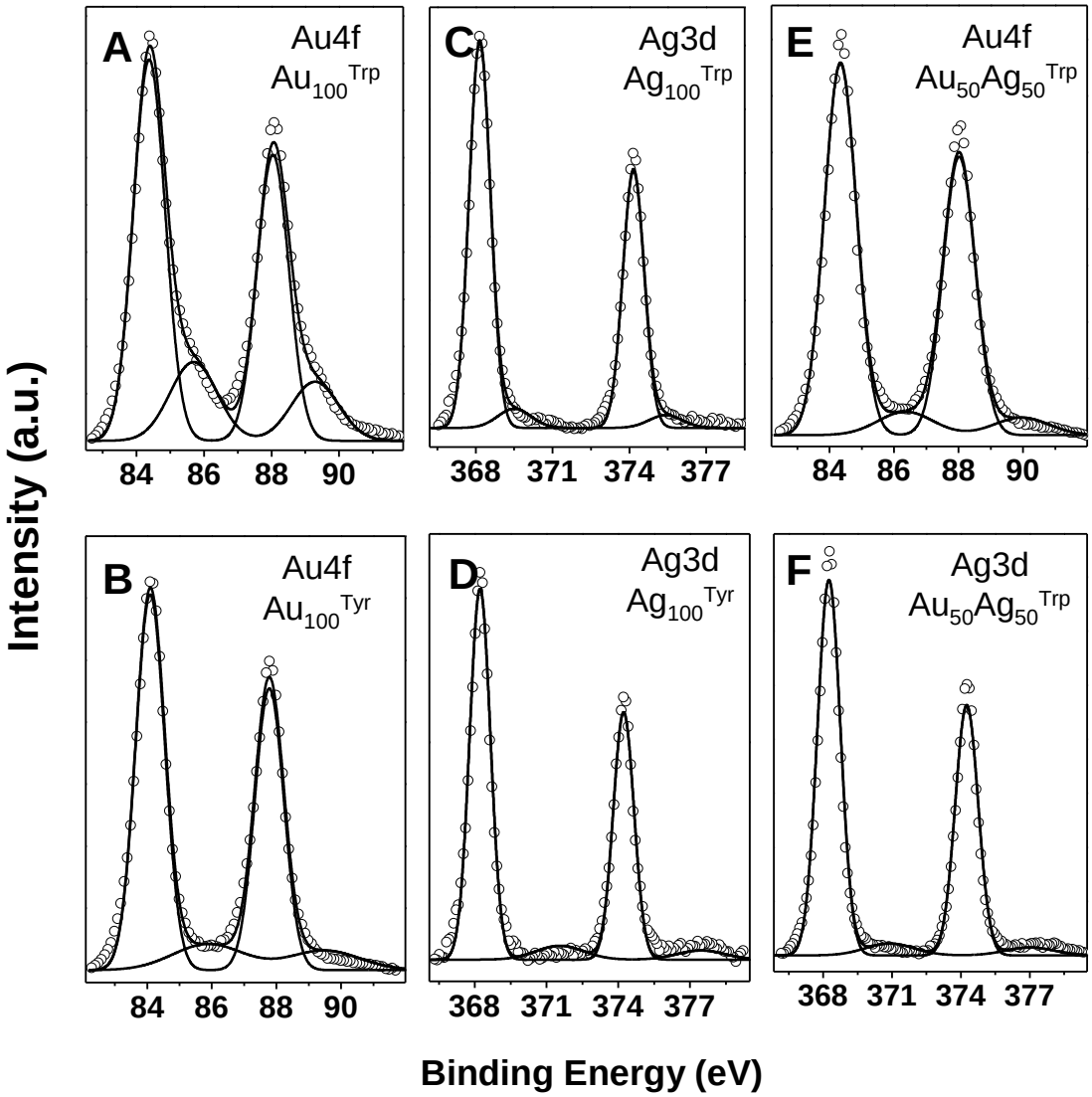

Figure.3.7. Core level Au4f and Ag3d spectra of tryptophan and tyrosine synthesised Au and Ag nanoparticles (A-D) and core level Au4f (E) and Ag3d (F) spectra arising from $Au_{50}Ag_{50}^{Trp}$ alloy nanoparticles, respectively

XPS studies were undertaken for all the 10 different compositions of tryptophan and tyrosine reduced metal and metal alloy nanoparticles. However, selected representative spectra have been shown for brevity. These include Au_{100}^{Trp}, Au_{100}^{Tyr} and $Au_{50}Ag_{50}^{Trp}$. All the Au4f core level spectra presented in Figure 3.7 (A, B and E for Au_{100}^{Trp}, Au_{100}^{Tyr} and $Au_{50}Ag_{50}^{Trp}$, respectively) could be decomposed into two chemically distinct spin-orbit pairs. The chemically distinct components are observed ca. 83.5 eV and 85.8 eV, respectively. The Au4f signal at the lower BE (~83.5 eV) $Au4f_{7/2}$ is attributed to fully reduced metallic Au^0. On the other hand, it is interesting to detect the presence of higher BE component (at ~85.8 eV) in all the samples, which indicated the presence of a small amount of unreduced $[AuCl_4]^-$ ions absorbed on the surface of nanoparticles and even extensive dialysis could not remove these ions due to strong electrostatic complexation of absorbed gold ions with amino acids. Similar Au4f spectra were observed in all the samples containing Au.

The core level XPS spectrum of Ag3d originating from Ag_{100}^{Trp}, Ag_{100}^{Tyr} and $Au_{50}Ag_{50}^{Trp}$ are illustrated in Figure 3.7 C, D and F, respectively. Similar to Au4f core level spectra, the Ag3d spectra also could be decomposed into two chemically distinctive spin-orbit pairs. Two chemically distinct BEs for Ag3d appeared at 368.2 and 371.6 eV, respectively. Here, the low BE component is attributed to metallic silver (Ag^0), whereas the high BE component occurs from the unreduced ions, demonstrating some Ag^+ ions bound on the surface of Ag nanoparticles.

Figure 3.8 (A-B) illustrates spectra of C1s core level recorded for pristine tryptophan and tyrosine amino acids, respectively. Figure 3.8 (C-D)

shows the core level C1s, spectra taken from tryptophan and tyrosine synthesised Au nanoparticles, respectively. N1s and K2p spectra taken from tryptophan synthesised Au nanoparticles (Au_{100}^{Trp}) are presented in Figure 3.8 E and F, respectively.

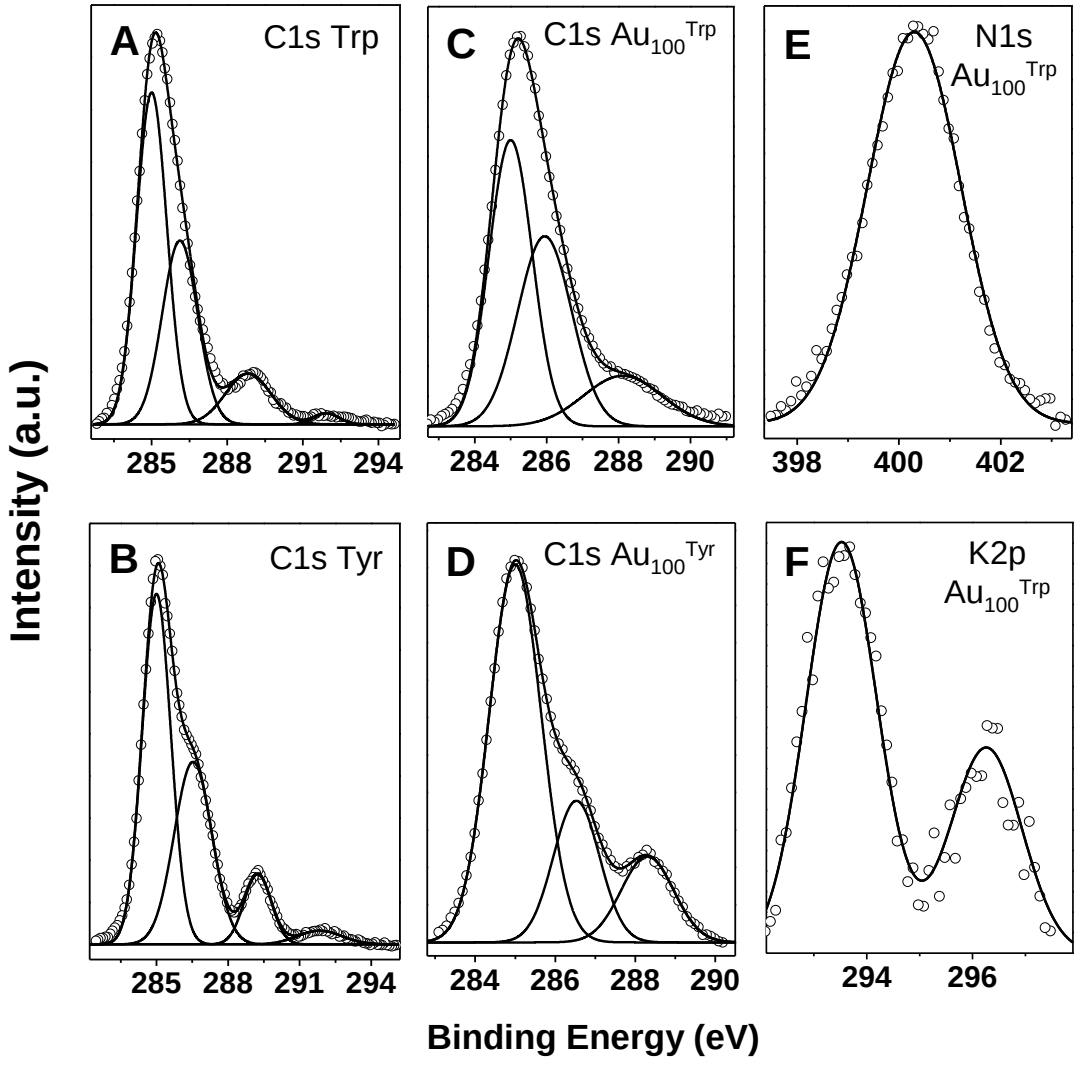

Figure.3.8. Core level XPS spectra of C1s in pristine tryptophan (A), tyrosine (B), Au_{100}^{Trp}(C) and Au_{100}^{Tyr} (D) respectively. Core level N1s (E) and K2p (F) spectra of tryptophan synthesised Au_{100}^{Trp}, respectively

C1s core level spectra recorded for pure tryptophan and tyrosine can be decomposed into four energy levels (Figure 3.8 A-B). BE at 285.0 eV is assigned to alkyl chain and aromatic carbon chain, shoulder of higher BE at

286.4 could be assigned to carbon attached with oxygen and nitrogen (C-O and C-N) species. The high BE at 289.1 eV can be attributed to the corboxylic group present in amino acids. Whereas, additional shaken-up satellite feature at 291.9 eV in both the amino acids arises from the benzyl side chain.[102] Likewise, the C1s core level spectra recorded from the Au_{100}^{Trp} and Au_{100}^{Tyr} Figure 3.8 (C and D, respectively) could be decomposed into three major chemically distinct components at ca. 285, 286.4 and 288.3 eV. The higher BE component observed at 288.3 eV can be assigned to the carboxylate carbon (–COO–) from nanoparticles-bound amino acid molecules (tryptophan or tyrosine), another evidence suggesting why these nanoparticles have very high negative zeta potential. Whereas 286.4 eV BE peak is attributed to the C-N and C-O species again coming from respective amino acid shell present on nanoparticles.

The existence of N1s signals is indicative of surface bound amine groups of amino acids. The representative XPS spectrum of N1s is illustrated in Figure 3.8-E. Furthermore, it was interesting to detect the presence of $K2p_{3/2}$ core levels at ca. 293 eV in the all the samples. Representative, XPS spectrum of K2p recorded for Au_{100}^{Trp} is shown in Figure 3.8 (F). The source of potassium ions in these samples was mainly due to the usage of KOH solution during the synthesis of nanoparticles. Presence of K^+ in nanoparticles even after extensive dialysis of samples suggests that K^+ ions bind strongly to negatively charged nanoparticle to counter balance their surface charges and to maintain electro-neutrality,[10, 11] which leads to highly stable metal nanoparticles in aqueous solutions.

3.4.6. FTIR analysis for the confirmation of amino acid shell

FTIR spectroscopic analysis of Au, Ag and Au-Ag alloy nanoparticles obtained by amino acids was carried out to understand that how the functional groups present in tryptophan or tyrosine amino acids interact with the metal nanoparticles. Furthermore, FTIR analysis provides information about the surface chemistry of nanoparticle. Illustrated in Figure 3.9, identical vibrational frequencies in respective panels (A for tryptophan and B for tyrosine capped nanoparticles) suggested that the functional nature of all these materials must be similar.

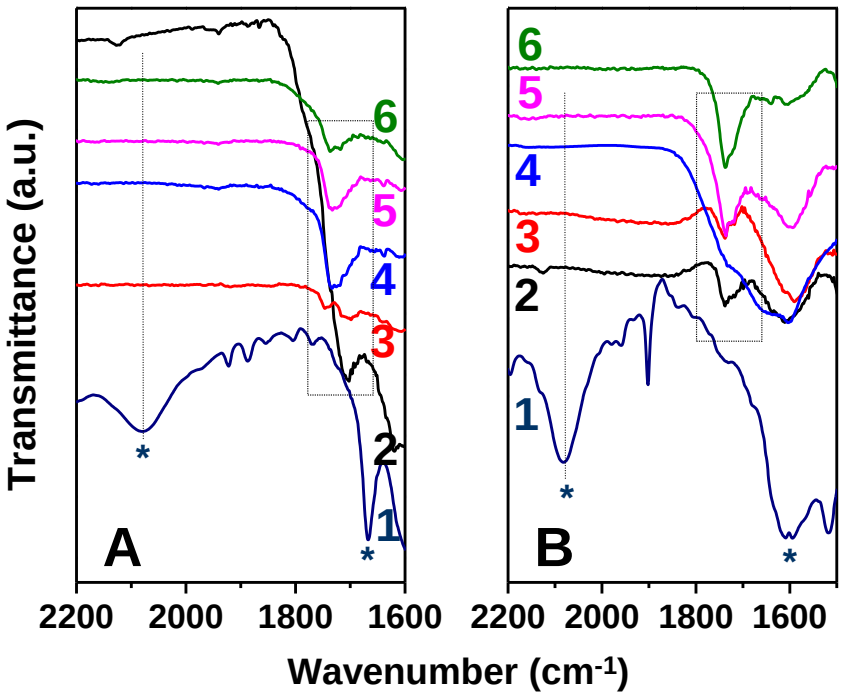

Figure.3.9. FTIR spectral analysis of (A) tryptophan- (curve 1) and (B) tyrosine- (curve 1) reduced Au_{100} (curve 2); $Au_{75}Ag_{25}$ (curve 3); $Au_{50}Ag_{50}$ (curve 4); $Au_{25}Ag_{75}$ (curve 5) and Ag_{100} (curve 6) nanoparticles, respectively

Figure 3.9 (A) shows the FTIR spectra of tryptophan synthesised nanoparticles, wherein the shift of the carbonyl stretching frequency of tryptophan from *1667 cm^{-1} (Figure 3.9 A, curve 1) to 1703 cm^{-1} and 1700

cm^{-1} were observed for Au_{100}^{Trp} and Au rich alloy, as shown in Figure 3.9 A curve 2 and 3, respectively. While in the case of Ag_{100}^{Trp} (Figure 3.9 A curve 6) and Ag rich alloys (Figure 3.9 A, curve 4 and 5) it was observed at 1736 cm^{-1} which can be attributed to the formation of carboxylate ions during the reaction.[103] The difference in the value of shifts observed in different samples correspond to varying degree of carboxylate ion formation in different samples.

As shown in Figure 3.9 B, tyrosine has a carbonyl stretching frequency around *1609 cm^{-1} (Figure 3.9 B, curve 1) that shifted to 1739 cm^{-1} in case of Au_{100}^{Tyr} (Figure 3.9 B, curve 2) or 1737 cm^{-1} in case of Ag_{100}^{Tyr} (Figure 3.9 B, curve 3) after nanoparticles synthesis, due to the carboxylate ion formation. Hence, it was evident from the FTIR spectroscopy that nanoparticles have surface carboxylate groups, which was in support of XPS analysis. Further, the presence of K^+ ions observed in the dialysed samples during XPS analysis supported that carboxylic group of amino acid bound onto metal nanoparticle surface was deprotonated into carboxylate ions. Additionally, presence of surface carboxylate groups also supported the negative surface charge determined by zeta potential measurements.

Moreover, the mechanism of reduction of $[AuCl_4]^-$ ions and Ag^+ ions by tryptophan or tyrosine molecules is clearly understood by comparing FTIR spectra of pristine amino acids and after reduction of metal ions. Heterocyclic amine such as pyrrole and indole undergo oxidative polymerization in the presence of an oxidizing agent and pyrrole is reported to reduce $[AuCl_4]^-$ ions to produce Au nanoparticles.[104] On the other hand, electrochemical methods are documented for oxidative polymerization of

indole through its secondary amine or the α-C of the secondary amine.[105] The amino acid tryptophan has a benzopyrrole (indole) group, which can undergo oxidative polymerization in a similar manner to reduce $[AuCl_4]^-$ ions and Ag^+ ions to create Au and Ag nanoparticles, respectively. Both tryptophan and tyrosine molecules show a peak at *2080 cm^{-1} due to the asymmetrical NH_3^+ bending vibration. The absence of this peak after nanoparticles formation indicates that deprotonation of amine groups during the reduction of metal ions. Further, the similar vibrational features of all these nanoparticles suggest they all have similar amino acid shells on the surface and the symmetry in the vibrational bands indicating that these amino acids were accommodated on the surface of metal in a structured fashion.

3.4.7. Electrochemical behaviour of amino acid capped Au, Ag and their alloy nanoparticles

The binding capacity of amino acids on the surface of metal nanoparticles will have considerable impact on the redox behaviour of Au, Ag and Au-Ag alloy nanoparticles. This kind of fundamental understanding of capping behaviour of tryptophan and tyrosine amino acids on monometallic Au or Ag nanoparticles and on the surface of bimetallic Au-Ag alloy nanoparticles is imperative to design effective nanomaterials for biological activities. Furthermore, it is important to study the distribution of Au and Ag atoms in the bimetallic alloy nanoparticles, which might be affected by the strength of interactions occurring between metallic surface and respective amino acids. Therefore, electrochemical behaviour of Au, Ag

nanoparticles and Au-Ag alloy nanoparticles was studied by employing cyclic voltammetry (CV). CV is an excellent electrochemical technique to study the aforementioned properties and cyclic voltammograms of these nanoparticles were carried out by drop-casting these nanoparticles onto GC substrates and the results are presented in Figure 3.10 (A and B).

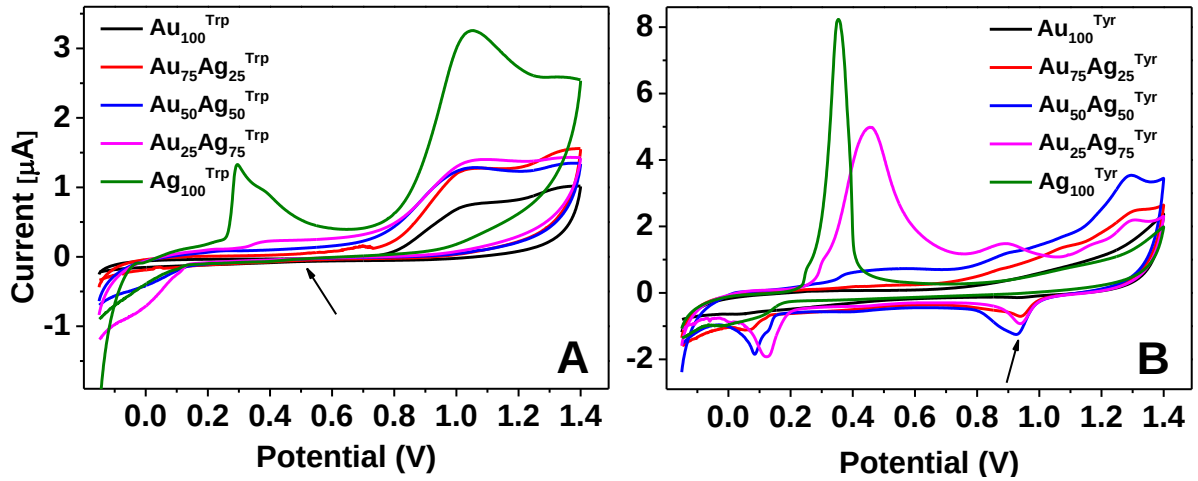

Figure.3.10. Cyclic voltametric profiles of tryptophan- (A) and tyrosine (B) synthesised nanoparticles recorded at 5 mV s^{-1} in 1 M H_2SO_4

In the case of tryptophan-reduced nanoparticles, the CV profile was found to be remarkably similar for the Au_{100}^{Trp}, $Au_{75}Ag_{25}^{Trp}$, $Au_{50}Ag_{50}^{Trp}$ and $Au_{25}Ag_{75}^{Trp}$ samples, all of which contained gold in different proportions. No indication of the CV profile typically observed for gold in acidic solution was seen (Figure 3.10 A), where typical gold-oxide formation and reduction is observed in Figure 3.11 (A). The complete absence of a gold oxide reduction process suggests that the capping by the tryptophan amino acid effectively blocked the underlying metallic surface. However, another broad oxidation process was reflected in Au_{100}^{Trp}, $Au_{75}Ag_{25}^{Trp}$, $Au_{50}Ag_{50}^{Trp}$ and $Au_{25}Ag_{75}^{Trp}$ samples from 0.80 to 1.40 V, which is similar to that recorded for a 1 mM tryptophan solution in 1 M H_2SO_4 recorded at a GC electrode (Figure 3.11-

B). This broad response is most likely due to the oxidation of the tryptophan capping agent on the nanoparticle surface, leading to formation of poly-tryptophan.[83]

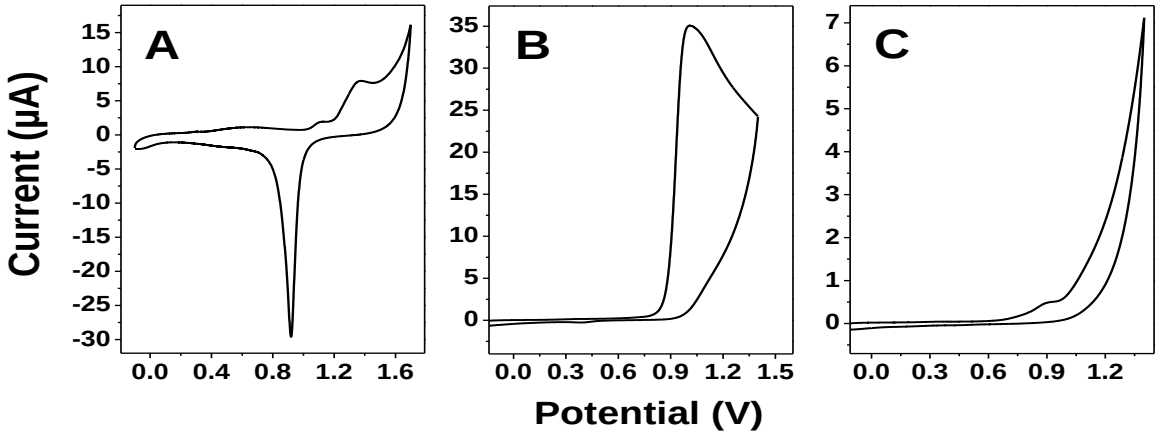

Figure.3.11. Cyclic voltametric profiles of (A) typical gold oxide formation and reduction (B) CV profile of 1 mM tryptophan in 1 M H_2SO_4 and (C) CV profile of tyrosine oxidation

Interestingly, a distinctly different profile is seen for Ag_{100}^{Trp} sample that showed a characteristic Ag oxidative stripping peak at 0.30 V (Figure 3.10-A).[106, 107] This suggests that during tryptophan-mediated synthesis of pristine Ag nanoparticles, a complete compact coverage of the nanoparticle surface with a capping layer does not occur as effectively as in the presence of Au in the sample. Notably, upon increasing the silver content within the alloy, a feature in the range of 0.30 to 0.80 V does begin to emerge, which shifts to more negative potential as the Ag content is increased (highlighted by arrow in Figure 3.10-A). This illustrates the ease with which the nanomaterial can be oxidised, thus indicating a decrease in the blocking ability of the capping agent with increase in Ag content.

In the case of tyrosine-reduced nanoparticles, evidence of the gold-oxide reduction process at 0.90 V was seen in all the alloys containing Au,

including $Au_{75}Ag_{25}^{Tyr}$, $Au_{50}Ag_{50}^{Tyr}$ and $Au_{25}Ag_{75}^{Tyr}$ samples as shown in Figure 3.10 B. However such feature was found absent in Au_{100}^{Tyr} sample, suggesting again a blocking capping layer to electrochemical surface oxide formation. Interestingly, as the Ag fraction is increased across the samples from $Au_{75}Ag_{25}^{Tyr}$, $Au_{50}Ag_{50}^{Tyr}$ and $Au_{25}Ag_{75}^{Tyr}$ to Ag_{100}^{Tyr}, the feature from 0.30 to 0.70 V increases and shifts to a more negative potential indicating a material which is more readily oxidised until sample Ag_{100}^{Tyr}. The broad process recorded from 0.90 to 1.40 V in all the tyrosine-reduced samples most likely consists also of some contribution from tyrosine oxidation, that recorded for a 1 mM tyrosine solution in 1 M H_2SO_4 recorded at a GC electrode (Figure 3.11 C).

Thus, CV analysis suggested that in the case of tryptophan-reduced nanoparticles get very strongly capped due to the formation of poly-tryptophan during synthesis, which interferes with oxidation of Ag present in tryptophan-reduced alloy nanoparticles. Conversely, in the case of tyrosine-reduced nanoparticles they are not as strongly capped, and Ag present in these alloy nanoparticles can be feasibly oxidized during CV experiments. These observations may have significant impact on biological profile of amino acid-reduced nanoparticles due to diverse surface functionality. Moreover, when different metal nanoparticles are exposed to biological system, the ease in oxidation of metal into metal ions may determine the ultimate biological action (toxicity) of these materials.

3.5. Rational behind employing these nanomaterials for biological applications

Tryptophan and tyrosine amino acids utilize their side functional groups to reduce metal ions to form nanoparticles, while retaining their amine and carboxylic acid groups intact on the nanoparticle surface. Hence these tryptophan and tyrosine capped nanoparticles can be viewed as amino acids supported on an inorganic nanoparticle, which can provide biological identity to inorganic nanoparticles. Further, amino acids are the basic building blocks for proteins and enzymes, and they become the active sites of many enzymes for adsorption of selective substrates. The selectivity is induced by the geometrical constraints specified by the structure of enzyme. Therefore, amino acids supported on the surface of an inorganic nanoparticle may function like a synthetic enzyme and it is essential to study the enzymatic-behaviour of these systems in order to use these materials for any other biological application.

In addition to the various properties of amino acids, when they combine with the suitable metal composition of nanoparticles in a cooperative manner, this will modulate their biophysical and biochemical properties. Therefore, these carefully tailored nanoparticles were subjected to investigate their enzyme-like behaviour and antimicrobial applications.

3.5.1. In vitro peroxidase-like behaviour of amino acids capped Au, Ag and Au-Ag alloy nanoparticles

A variety of nanomaterials have been designed to exhibit biological activities which depend on their considerable ability to provoke production

of reactive oxygen species (ROS). High level of ROS present in any biological system is harmful due to the significant changes in homeostasis, which can induce cell damage irrevocably while the lesser amount of ROS can be effectively neutralized by natural antioxidants.[27-34, 108-112] Recently, Ferrum-based (Fe) materials such as iron oxide nanoparticles have been discovered to execute peroxidise enzyme-like activity. This peroxidise-like activity of iron oxide nanoparticles has been attributed due to their close resemblance with Fe present in the heme unit of natural peroxidases.[20, 21, 24, 113] Other nanomaterials have also been employed to explore peroxidases enzyme-like activity or to mimic naturally occurring enzymes besides Fe-based nanoparticles.[22, 26, 114, 115]

Tryptophan and tyrosine amino acids are two important building blocks of natural enzymes and their capping on the surface of Au, Ag and Au-Ag alloy nanoparticles has potential to act as synthetic 'nanozymes'. Therefore, in vitro study of peroxidases enzymes-like activity has been explored to understand the significance of amino acids shell on inorganic nanoparticles support in combination with metal composition in alloy nanoparticles.

Au, Ag and Au-Ag alloy nanoparticles capped with tryptophan and tyrosine amino acids exhibited peroxidise-like activity by catalysing the oxidation of TMB substrate in the presence of H_2O_2 to produce a blue coloured reaction product as shown in Figure 3.12. Prior to peroxidase-like activity, various solutions of tryptophan and tyrosine synthesised nanoparticles showed ruby red (Au nanoparticles) to yellow colour (Ag nanoparticles) (Figure 3.13-A) based on the composition of nanoparticles, as

discussed previously. Intensities of these colours varied because the concentrations employed to investigate peroxidase-like activity were different such as 20, 10 and 5 ppm.

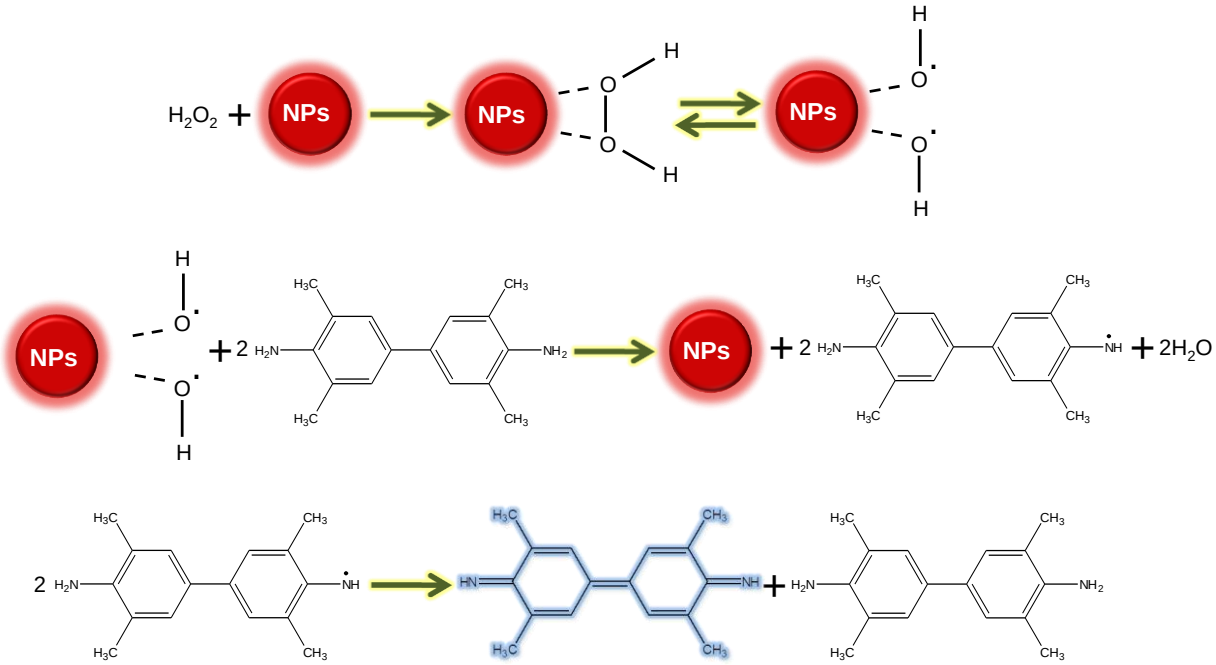

Figure.3.12. Schematic representation of oxidation of TMB by H_2O_2 catalysed by nanoparticles

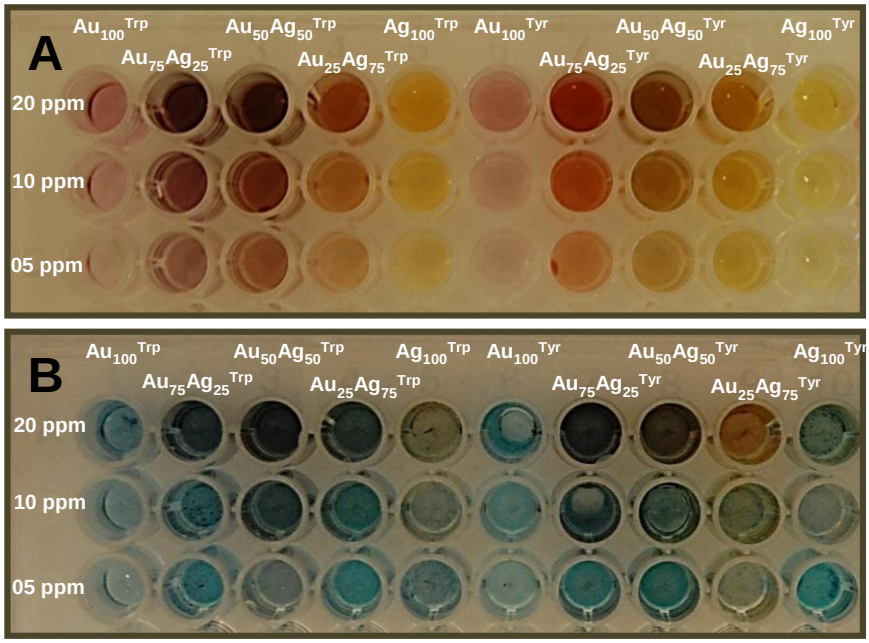

Figure.3.13. Peroxidase-like behaviour of tryptophan- and tyrosine- capped Au, Ag and Au-Ag alloy nanoparticles with different concentrations

Illustrated in Figure 3.13 B is the optical photograph showing blue colour response after peroxidase-like activity of amino acid capped nanoparticles. It was visualized in Figure 3.13 that the peroxidase-like activity of amino acid capped metal nanoparticles were modulated by the composition and the type of amino acid that forms the surface corona around the nanoparticles. Further, quantitative potential of nanoparticles synthesised by amino acids were measured by absorption as a function of reaction time for peroxidase-like behaviour and correlated with temperature, composition and surface functionalization.

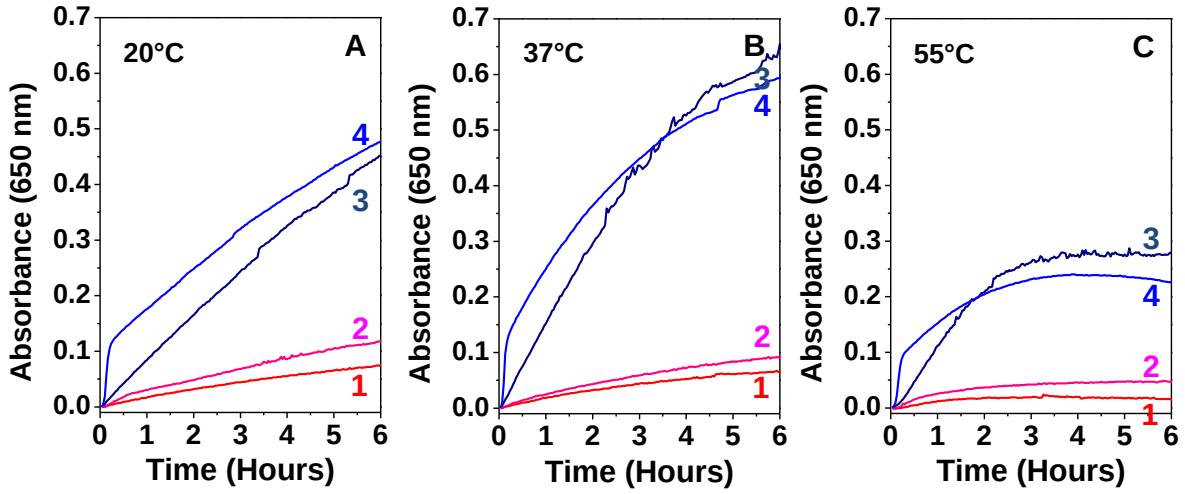

Figure.3.14. Temperature dependent peroxidase-like activity of tryptophan- and tyrosine- capped Au and Ag nanoparticles In all the panels, curve 1, 2, 3 and 4 correspond to Au_{100}^{Trp}, Au_{100}^{Tyr}, Ag_{100}^{Trp} and Ag_{100}^{Tyr}, respectively

Figure.3.14 illustrates the kinetics of peroxidase-like behaviour of monometallic Au and Ag nanoparticles at 5 ppm metal concentration on 20°C, 37°C and 55°C temperatures in panel A, B and C respectively. In all the panels of Figure.3.14, curve 1 and 2 shows peroxidase-like behaviour of tryptophan and tyrosine synthesised Au nanoparticles, whereas, curves 3 and 4 correspond to respective amino acids synthesised Ag nanoparticles.

Relatively, tyrosine capped Au nanoparticles demonstrated higher catalysing potential toward TMB substrate, indicating that tyrosine capping of Au nanoparticles have comparatively higher peroxidase-like activity then tryptophan capped Au nanoparticles. These results show that amino acid shell/corona present on the surface of nanoparticles also had some influence on the peroxidase-like behaviour.

At all the examined temperatures (panels A, B and C), it was seen that the activity of Ag based nanoparticles was significantly higher than Au nanoparticles in both tryptophan and tyrosine capping, while there were slight difference in the catalysing potential of Ag_{100}^{Trp} and Ag_{100}^{Tyr}. This phenomenon suggests that the peroxidase-like behaviour of amino acid capped metal nanoparticles predominantly depends on the core metal, whereas amino acid surface corona has slight influence of peroxidase-like activity. For example, at 20°C (Figure.3.14, panel A) after 4 hour, Ag_{100}^{Trp} illustrated over six time higher oxidation of TMB substrate then Au_{100}^{Trp} in the form of absorbance at 650 nm, signifying impact of core material.

Moreover, temperature has significant influence on the peroxidase-like activity of Ag nanoparticles. As illustrated, at 37°C (Figure.3.14-B) the activity was optimal, whereas at 55°C (Figure.3.14-C) their activity was found to be lowest while moderate activity was reported at 37°C (Figure.3.14-A). Conversely for Au nanoparticles, a slight reduction in peroxidase-like activity was observed with increase in temperature from 20 to 37 to 55°C. There observations demonstrate that temperature plays an influential role in peroxidase-like activity of Ag nanoparticles. These observations revealed the importance of inorganic core metal content and

amino acid surface corona present around the nanoparticles and shows that the peroxidase-like behaviour of nanomaterials depends on both the composition and surface functionalization. These observations, further suggest that the composition and surface chemistry of nanomaterials may have cooperative effects on any biological activity, which is in general overlooked. Therefore, to further understand the role of surface functionality and metal composition along with temperature on peroxidase-like behaviour, tryptophan and tyrosine capped alloys nanoparticles were subjected for investigation under similar experimental conditions. Illustrated in Figure.3.15 is peroxidase-like behaviour of Au-Ag nanoalloys synthesised by tryptophan (Panel A, B and C) and tyrosine (Panel D, E and F) amino acids at 20°C (Panel A and D), 37°C (Panel B and E) and 55°C (Panel C and F) respectively. In all panels, curve 1, 2 and 3 correspond to $Au_{75}Ag_{25}$, $Au_{50}Ag_{50}$ and $Au_{25}Ag_{75}$ composition either prepared by tryptophan or tyrosine, respectively.

Furthermore, Figure.3.15 revealed the significant effect of amino acid corona on peroxidase-like activity. Comparison of same stoichiometric alloys with different amino acids showed different peroxidase-like activity in all the temperatures. Assessment between different panels (such as A with D, B with E and C with F) captivatingly revealed that the presence of surface corona has considerable influence on peroxidise-like behaviour along with temperature and composition. As it could be seen that the core material employed to construct curves 1, 2 and 3 during peroxidise-like activity in all panels are similar but the absorbance is considerably different revealing different catalysing power of these nanomaterials towards TMB. It was

interesting to detect that tyrosine capped alloy nanoparticles have significantly higher peroxidise-like activity then tryptophan capped nanoparticles. For instance, Figure 3.15.panel A, in the case of tryptophan reduced $Au_{75}Ag_{25}^{Trp}$ (curve 1), $Au_{50}Ag_{50}^{Trp}$ (curve 2), $Au_{25}Ag_{75}^{Trp}$ (curve 3) the absorbance was found to be less than 0.2 after 6 hours in all the cases. On the contrary, assessment of similar composition and temperature with different surface functionalization (in case of tyrosine Figure 3.15.panel D), $Au_{75}Ag_{25}^{Tyr}$ (curve 1), $Au_{50}Ag_{50}^{Tyr}$ (curve 2), $Au_{25}Ag_{75}^{Tyr}$ (curve 3) showed 0.3, 0.6 and 0.9 absorbance revealing differential catalysing potential of alloy nanoparticles, respectively.

Peroxidise-like behaviour of amino acid capped alloy nanoparticles was found to be metal composition dependent and with respective increment in the Ag fraction of alloy the peroxidise-like behaviour shows enhancement by catalysing TMB substrate as it shows increment in absorbance at 650 nm. This tendency is widespread in all tested temperatures irrespective to surface functionalization, although the effects were more prominent in the case of tyrosine capped Au-Ag alloy nanoparticles. These results are in good agreement with observations obtained during peroxidise-like behaviour of monometallic Au and Ag nanoparticles. Thus, validating the hypothesis that the peroxidise-like activity of inorganic nanoparticles depends on the core material or composition used to prepare nanoparticles.

Moreover, to validate these results and observations, control experiments were performed in parallel, wherein pure tryptophan, tyrosine and free metal ions were used under same experimental conditions to investigate their effects on peroxidase-like activity. It was interesting to

discover that free amino acids and metal ions alone do not have any peroxidase-like activity as they could not catalyse oxidation of TMB to produce blue coloured reaction product. These control experiments further confirmed that the peroxidase-like activity of amino acid capped nanoparticles were intrinsic nature of nanoparticulate systems which was introduced during their synthesis and controlling nanomaterials composition and surface functionalization has potential to fine tune their biological activity.

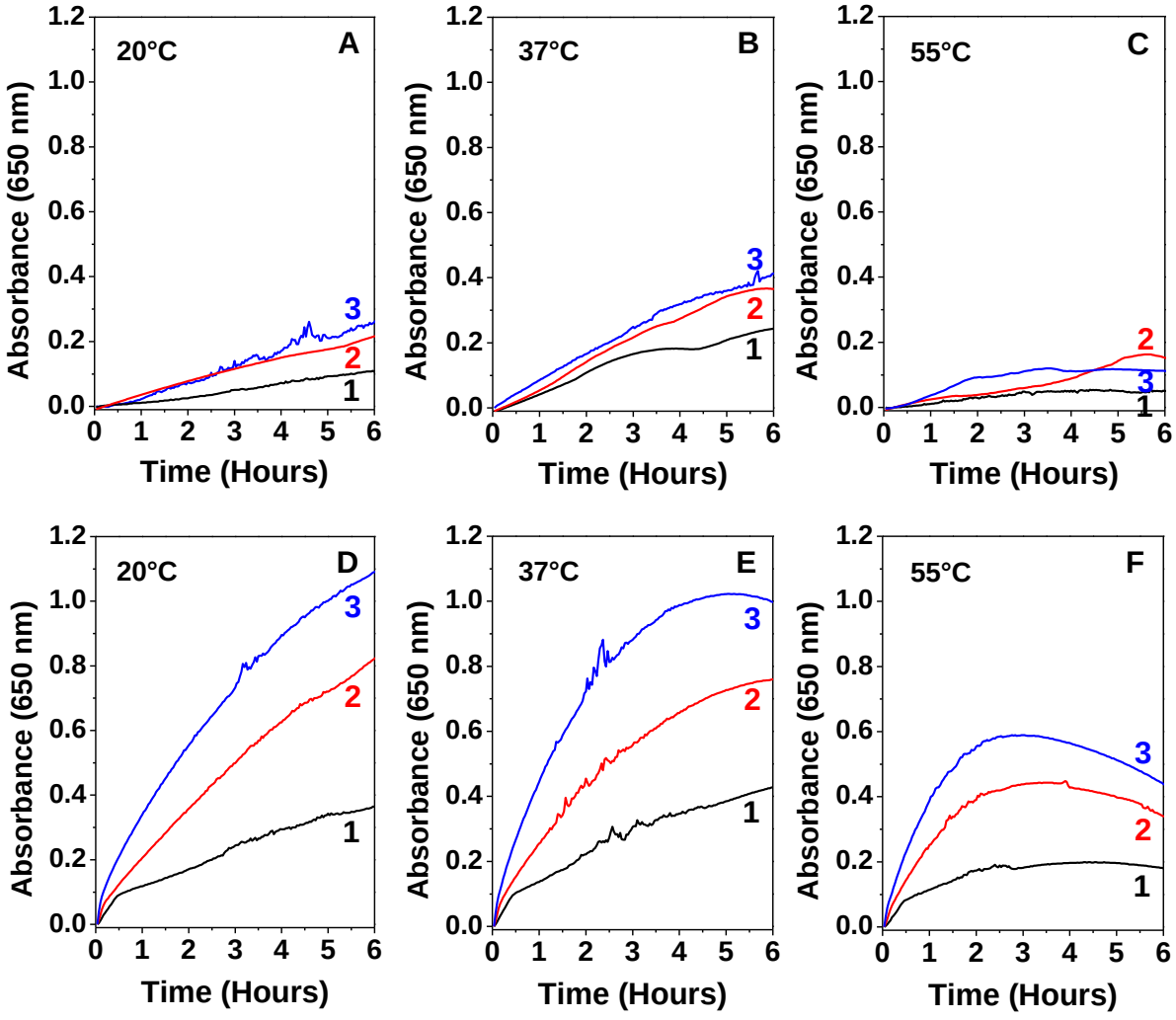

Figure.3.15. Temperature dependent peroxidase-like activity of tryptophan (Panel A, B and C) and tyrosine (Panel D, E and F) capped Au-Ag nanoalloys. In all the panels, curve 1, 2 and 3 correspond to $Au_{75}Ag_{25}$, $Au_{50}Ag_{50}$ and $Au_{25}Ag_{75}$ respectively

These observations on composition and surface-functionality dependent peroxidase-like activity of Au, Ag and Au-Ag alloy nanoparticles are particularly interesting. As discussed in cyclic voltametric studies, due to the presence of poly tryptophan, Ag stripping of alloy nanoparticles was not possible, while in the case of tyrosine capped alloys, Ag stripping was observed. Peroxidase-like activity of alloy nanoparticles was considerably influenced by the Ag stripping from the alloy nanoparticles and therefore tyrosine capped alloy nanomaterials exhibited higher activity. These results suggest that choice of an appropriate biological capping agent can play a major role in cooperative manner with composition in controlling the biological action of nanomaterials. Similar influence of composition, temperature and amino acid corona were obtained when the metal concentrations of nanoparticles were kept 10 and 20 ppm to evaluate peroxidase-like activity. Appendix C (Figure C.2 and C.3) illustrates temperature dependent peroxidase-like activity of tryptophan- and tyrosine-capped Au, Ag and Au-Ag alloy nanoparticles at 10 ppm.

3.5.2. Antibacterial assays of amino acid capped nanoparticles

Peroxidase-like activity of amino acid-functionalized Au, Ag and Au-Ag alloy nanoparticles was found to be composition and surface functionalization dependent. Due to the high intrinsic peroxidase-like behaviour, these amino acid-functionalized nanoparticles are expected to have other biological applications as well. Therefore, composition and surface functionality dependent antibacterial activities of these amino acid-functionalized nanoparticles were investigated against model Gram positive

bacterium *Staphylococcus albus* and Gram negative bacterium *Escherichia coli*. Two different bacterial strains are preferred because these bacterial strains have chemically dissimilar cell walls, which provide first line of defence for these bacterial strains. Hence, the cooperative effect of metal composition and surface functionalization may be entirely different toward different bacterial strains as it was observed in the case of peroxidase-like behaviour.

3.5.2.1. Antibacterial effects of nanoparticles and influence of surface functionalization

A colony counting method was adopted to investigate the antibacterial potential of amino acid functionalized Au and Ag nanoparticles. To evaluate influence of surface functionalization on different bacterial strains, constant metal concentration (25 ppm) was introduced to 10^4 colony forming units (CFU) of bacteria and allowed to interact for 24 hours at 4°C, followed by spread-plating onto nutrient agar plates. Colonies formed after incubation were counted and curves of the bacterial viability versus nanoparticles dose effect were constructed and shown in Figurer 3.16 A and B.

Illustrated in Figurer 3.16 A is antibacterial effect of tryptophan and tyrosine functionalized Au and Ag nanoparticles against Gram negative bacterium *E. coli*. At 25 ppm metal concentration, similar antibacterial activity was observed by both tryptophan and tyrosine capped nanoparticles. In the case of Au nanoparticles, both Au_{100}^{Trp} and Au_{100}^{Tyr} caused minimal cell death as the bacterial viability was found to be over 85% and 95% respectively. Relatively, tryptophan capped Au_{100}^{Trp}

nanoparticles have more toxic effects than tyrosine capped Au_{100}^{Tyr} nanoparticles. Comparative difference in the cell viability shows that amino acid surface functionalization has slight influence on the antibacterial activity against *E. coli* as the core material is identical. Whereas, in the case of amino acid functionalized Ag nanoparticles at the same 25 ppm concentration both Ag_{100}^{Trp} and Ag_{100}^{Tyr} nanoparticles exhibited significantly higher level of toxicity against *E. coli*. In both cases cell viability was found to be less than 5% (Figure 3.16 A). This is expected as Ag nanoparticles are considered as highly efficient Gram negative antibacterial agents and biocompatible nature of Au nanoparticles is well established.[41, 56, 58] These results demonstrates that in the case of Gram negative bacteria (*E. coli*), although the surface functionalization has some influence (shown by Au nanoparticles) on antibacterial activity but predominantly it depends on the metal fraction of nanoparticles (shown by Ag nanoparticles).

Furthermore, shown in Figurer 3.16 B is antibacterial potential of amino acids functionalized Au and Ag nanoparticles against Gram positive bacterium *S. albus*. It was interesting to observe that both tryptophan and tyrosine capped Au and Ag nanoparticles demonstrate significantly higher toxicity (>90%) against Gram positive bacteria. In the case of Ag^+ ions it is expected to perform such a high level of toxicity due to their known interaction with building elements of bacterial cells, DNA and proteins.[77] The ease of Ag^+ ions stripping in both Ag_{100}^{Trp} and Ag_{100}^{Tyr} nanoparticles provide strong rational behind the toxicity of these tryptophan and tyrosine functionalized Ag nanoparticles as discussed during cyclic voltammetry analysis.

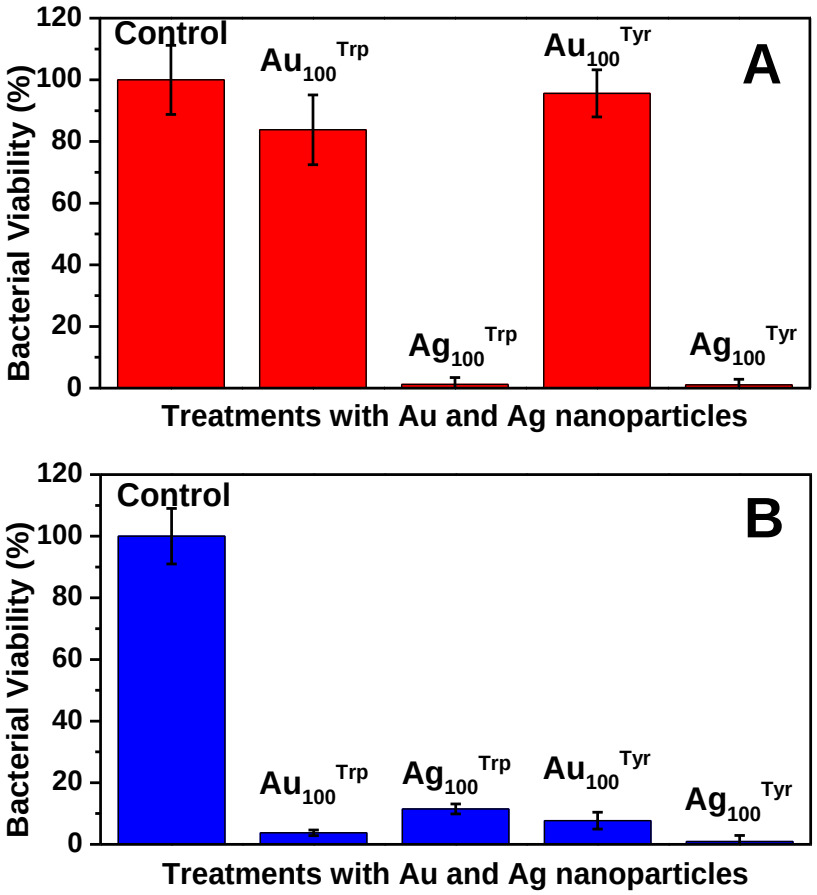

Figure.3.16. Assessment of antibacterial potential of amino acid capped Au and Ag nanoparticles against (A) *E. coli* and (B) *S. albus*, respectively

Recently, Dawson and co-workers established that during interaction, a cell sees the surface corona or other biomolecules present on the surface of nanoparticles rather than bare nanoparticles itself, [36, 116, 117] which gives a rationale behind the unusual toxicity of Au_{100}^{Trp} and Au_{100}^{Tyr} toward *S. albus* that the toxicity is originating through the amino acid surface functionalization toward Gram positive bacteria. Therefore, in the case of Gram positive bacteria, it is believed that the toxicity arises due to the amino acid shell because there was no considerable change in toxicity whether Au or Ag nanoparticles were employed for antibacterial studies. These interesting results suggest that there is a strong interaction between the amino acid shell and the Gram positive bacterial cell wall that causes

disruption of the cell wall. These observations are further confirmed by nano-SEM imaging where the amino acids present on metal nanoparticles act cooperatively to destroy the integrity of Gram positive bacterial cell wall and is discussed in the later part of this chapter.

Additionally, in order to validate this mechanism, control experiments were performed in which pure amino acids were directly added in the bacterial culture, where these amino acids were found to have comparatively higher toxicity towards Gram positive bacteria than Gram negative bacteria. For instant, after treatments with tryptophan amino acid (1mM), *E. coli* bacteria showed 75% cell viability while at the similar concentration, *S. albus* illustrated only 20% cell viability. Likewise, at the similar concentration in the case of tyrosine, *E. coli* and *S. albus* exhibited 68% and 16% bacterial viability, which was in support of the proposed hypothesis. The exact mechanism how amino acids are capable of hydrolysing Gram positive bacterial cells in more effective manner is not clear at this stage and requires further investigations. Therefore, amino acid-reduced metal nanoparticles enveloped within an amino acid corona may offer opportunities against controlling Gram positive bacteria by enabling initial interaction of these nanomaterials with the peptidoglycan cell wall, followed by cell wall lysis and finally bacterial cell death.

3.5.2.2. Effect of metal composition on antibacterial activity employing Au-Ag alloy nanoparticles

Additionally, to evaluate the antibacterial effects of tryptophan and tyrosine synthesised Au-Ag alloy nanoparticles, dilutions were made in such

a way that only Ag fraction present in Au-Ag alloy nanoparticles remain constant. During this approach, Au concentrations were only varied in the Au-Ag alloy nanoparticles, which could explain the effect of increasing amount of Au content with respect to Ag fraction. This strategy made possible to understand the role of metal composition and surface amino acid shell towards antibacterial activity against *E. coli* and *S. albus* as shown in Figure 3.17 (A and B).

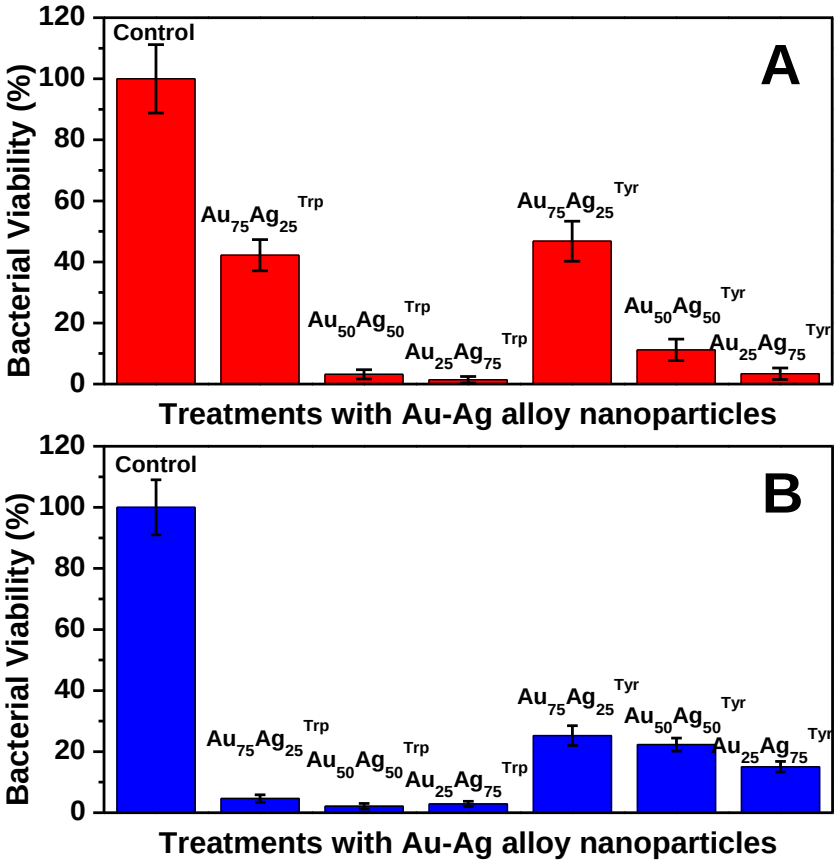

Figure.3.17. Antibacterial activity of Au-Ag alloy nanoparticles synthesized by tryptophan and tyrosine against *E. coli* (A) and *S. albus* (B)

Illustrated in Figure 3.17 (A) is the antibacterial effect of amino acid synthesised Au-Ag alloy nanoparticles against *E. coli*. In the case of *E. coli*, with the decreasing concentration of Au fraction (with respect to the constant Ag content present in alloy nanoparticles, from $Au_{75}Ag_{25}$→

$Au_{50}Ag_{50}$→ $Au_{25}Ag_{75}$), bacterial cell viability decreases significantly and this trend was observed for both tryptophan and tyrosine amino acid capped Au-Ag alloy nanoparticles (Figure 3.17.A). These observations are in strong support that antibacterial activity against Gram negative bacteria arises from the Ag fraction of the nanoparticles, as discussed in previous section. Furthermore, tryptophan capped alloy nanoparticles were found to have relatively more toxic effects than tyrosine capped alloy nanoparticles as reflected in pristine Au_{100}^{Trp} and Au_{100}^{Tyr} nanoparticles as well (Figure 3.16.A). For instance, 40% cell viability was observed in $Au_{75}Ag_{25}^{Trp}$, which increased up to 10% in the case of $Au_{75}Ag_{25}^{Tyr}$ wherein the central material is identical, confirming the influence of surface functionalization. Comparative variation in the cell viability of *E. coli* shows that amino acid surface functionalization has control on the antibacterial activity and validating results discussed in the case of pristine Au and Ag nanoparticles.

Conversely, in the case of *S. albus* (Figure 3.17.B) there were no considerable changes observed in bacterial viability with the decreasing amount of Au fraction present in Au-Ag alloy nanoparticles (from $Au_{75}Ag_{25}$→ $Au_{50}Ag_{50}$→ $Au_{25}Ag_{75}$). However, there is a slight reduction in bacterial cell viability in the case of tyrosine capped alloy nanoparticles, but overall their toxicity was higher than toxicity observed in *E. coli*. These results are also in support that in the case of Gram positive bacteria, composition of Au-Ag alloy nanoparticles do not have significant influence. Additionally, Figure 3.17.B demonstrated that in the case of *S. albus* also, tryptophan capped alloy nanoparticles have significantly higher toxicity compared to tyrosine capped alloy nanoparticles. For instance, $Au_{75}Ag_{25}^{Trp}$ has less than 5%

bacterial viability whereas $Au_{75}Ag_{25}^{Tyr}$ has over 25% cell viability, which clearly explains the effect of surface corona present on nanoparticles in the form of the amino acid.

3.5.2.3. Morphological studies of Au and Ag nanoparticles treated E. coli and S. albus bacterial cells

Towards antimicrobial activities, it is hypothesized that nanomaterials and cations such as Ag^+ ions primarily affect the function of membrane-bound enzymes including enzymes of the respiratory chain. The inhibitory mechanism of nanoparticles on microorganisms shows that after treatment, DNA loses its replication ability; expression of ribosomal subunits proteins and other cellular proteins and enzymes essential for ATP production becomes inactive.[45, 53, 56, 58, 59, 74, 77] However, the mechanism of antibacterial action of nanomaterials is still not clearly understood but reported literature could highlight that bacterial morphology and its membrane integrity is one of the key factors, which is crucial for bacterial survival. Therefore, to understand the effects of amino acid surface functionalized metal nanoparticles on bacterial morphology nano-scanning electron microscopy (Nano-SEM) was employed to visualize changes in bacterial cell wall and morphology after their treatments.

SEM micrographs of *E. coli* bacterial cells before and after their treatments with nanoparticles are illustrated in Figure 3.18. *E. coli* bacterial cells without any treatment (control cells) showed intact cell architecture and the cells are around 3 µm X 1 µm size and appeared as small rod shaped as illustrated in Figure 3.18 A. Bacterial cells exposed to amino

acids capped Au nanoparticles (Au_{100}^{Trp} or Au_{100}^{Tyr}) are shown in Figure 3.18 B and D respectively. These cells revealed that there were no significant changes in their morphology and they had intact cell architecture as untreated *E. coli* cells. Although, these bacterial cells appeared smaller in size compare to untreated cells. Conversely, illustrated in Figure 3.18 C and E are bacterial cells treated with Ag_{100}^{Trp} or Ag_{100}^{Tyr} nanoparticles, respectively. In contrast to untreated or Au nanoparticles treated bacterial cells, Ag nanoparticles treated bacterial cells revealed distinct changes in cell morphology. In lower magnification micrographs of Figure 3.18 C and E it could be seen that treated *E. coli* cells were dissolved and their cellular components were disintegrated, wherein higher magnification images exposed that Ag_{100}^{Trp} (Figure 3.18 c) treated bacterial cell were entirely disintegrated and severely damaged. While in the case of Ag_{100}^{Tyr} (Figure 3.18 e), it could be seen that the bacterial cell were broken in small pieces along with distinct morphology and confirmed patchy bacterial cells.

The components of *E. coli* bacterial cell wall became disorganised and scattered from their original order and close arrangement after their exposure to amino acid coated Ag nanoparticles. Thus confirming that amino acid coated Ag nanoparticles had significant influence on the *E. coli* bacterial cell morphology, while similar surface functionality on Au nanoparticles did not show any influential toxic effect on bacterial cells. These observations revealed that in the case of Gram negative bacterium *E. coli* the toxicity depends on the metal fraction of nanoparticles and presence of either amino acid on the surface of nanoparticles did not exhibited any toxic effect.

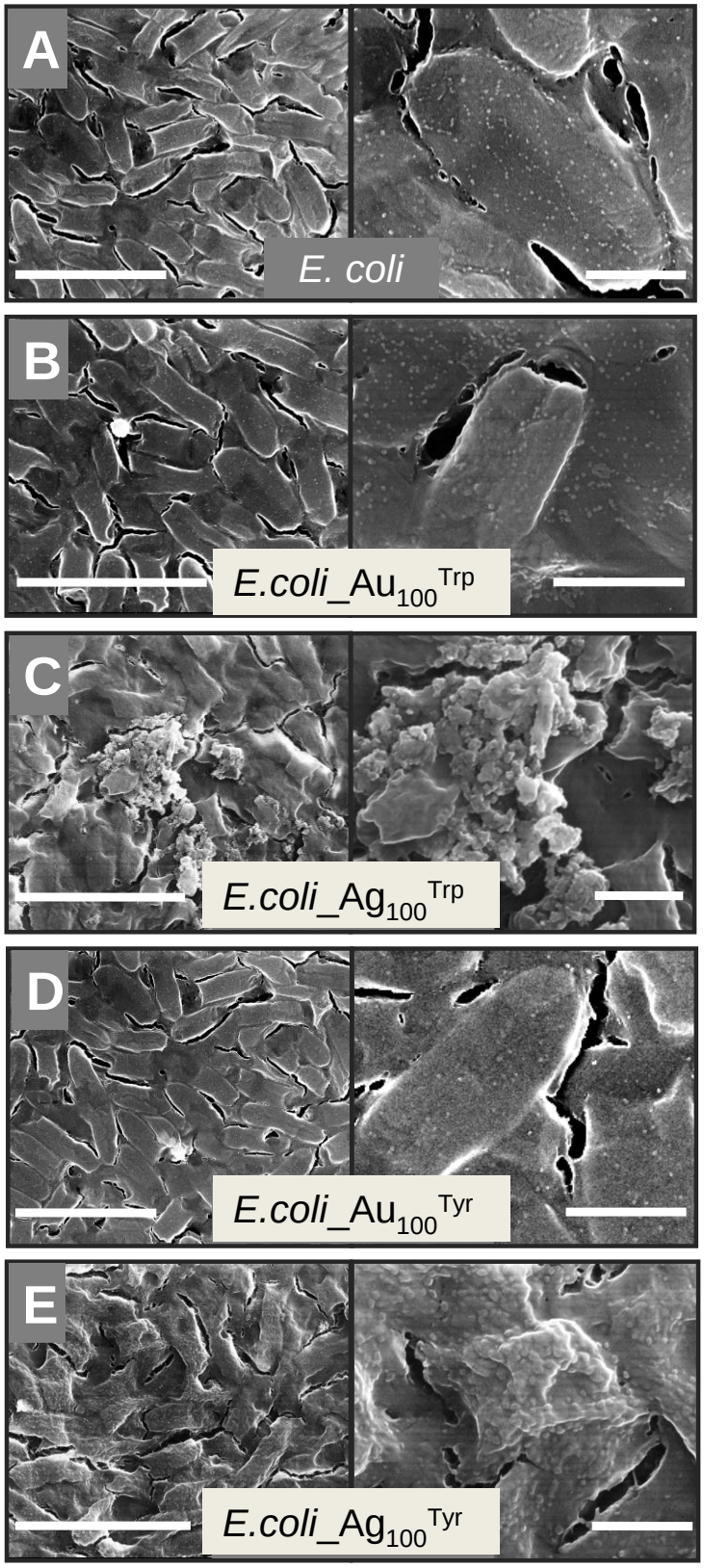

Figure.3.18. SEM micrographs of *E. coli* before and after their treatments with tryptophan and tyrosine synthesised nanoparticles (Scale bar 5 and 1 μM, respectively)

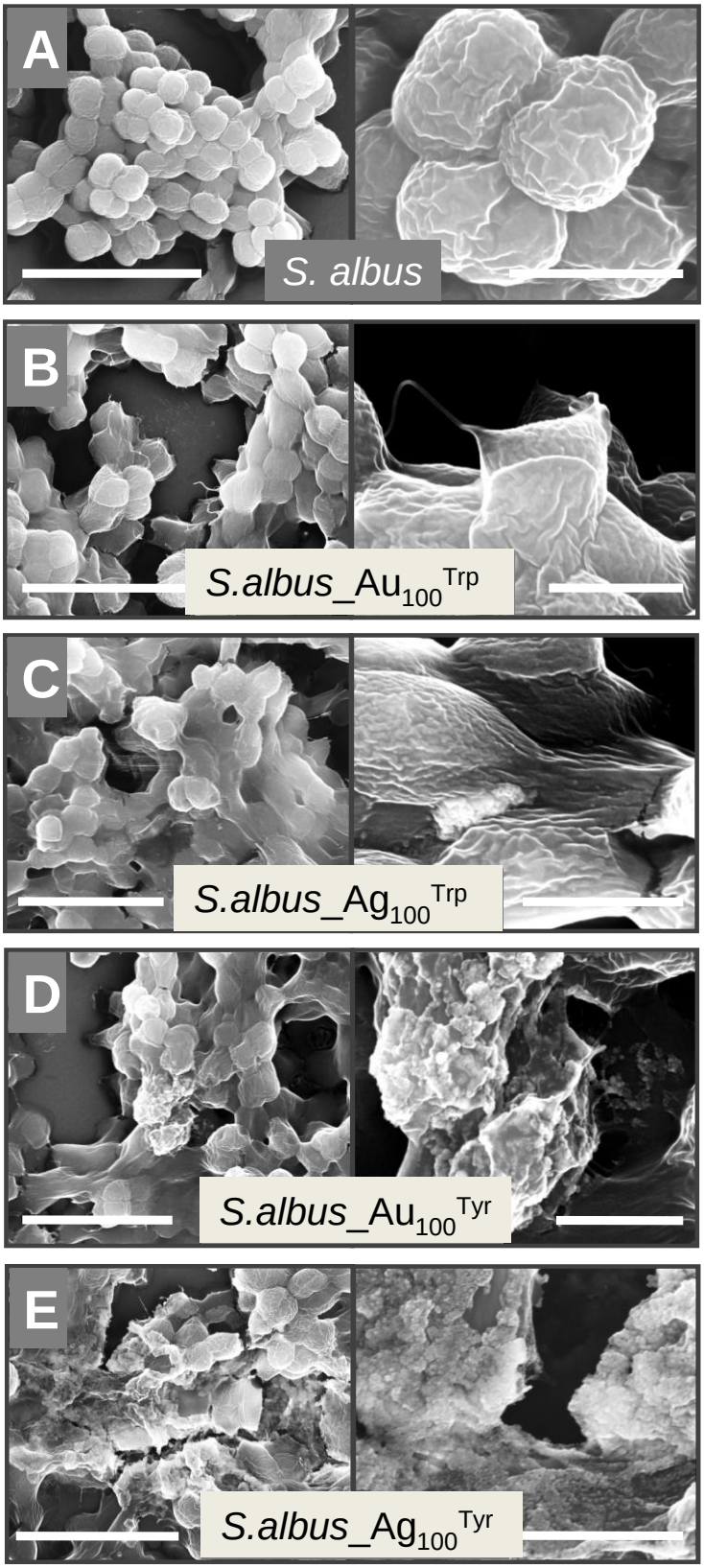

Figure.3.19. SEM micrographs of *S. albus* before and after their treatments with tryptophan and tyrosine synthesised nanoparticles (Scale bar 5 and 1 μM, respectively)

Illustrated in Figure 3.19 (A) are *S. albus* bacterial cells without any treatment showing spherical shape and in lower magnification micrograph the bacterial cluster resembles grapes along with integral cell morphology. Wherein, the higher magnification image shows that these bacterial cells have slightly rough surface. Figure 3.19 B and C, treated with tryptophan coated Au and Ag nanoparticles shows that after treatment *S. albus* cells are dissolved and dispersed. At higher magnification, it could be seen that the bacterial cell wall is peeling out from the bacteria after their exposure to Au_{100}^{Trp} (Figure 3.19 b); while the dispersion effect is clearly evident in bacterial cells treated with Ag_{100}^{Trp} (Figure 3.19 c). Similar, experiments were performed on the tyrosine synthesised nanoparticles, which revealed that these nanomaterials have even more severe morphological changes and along with dissolving bacterial cells tyrosine capped nanoparticles shows significantly higher level of roughness on the bacterial surface (Figure 3.19 D and E). After treatments, the cell wall components became disorganised and scattered from their original ordered and close arrangement. In this sort of morphology and disintegration, it is believed that cell wall possibly lost their natural function which ultimately leads to bacterial cell death. These observations revealed that even the most biocompatible Au nanoparticles may exhibit significant toxicity toward Gram positive bacteria (*S. albus*) by rupturing and collapsing the bacterial cell wall.

The rationale behind this is that in the case of *E. coli* only Ag nanoparticles exhibited significant toxicity compare to the Au nanoparticles because the metal fraction of the nanoparticles was responsible for antibacterial studies as reported in previous studies. Conversely, in case of

S. albus, due to the presence of the amino acids on the surface of nanoparticles these materials caused structural changes which finally lead to cell death. Based on the observed antibacterial activity and existing literature, Figure 3.20 demonstrates various mechanisms by which Au and Ag nanoparticles exhibit antibacterial activities toward Gram positive and Gram negative bacteria.

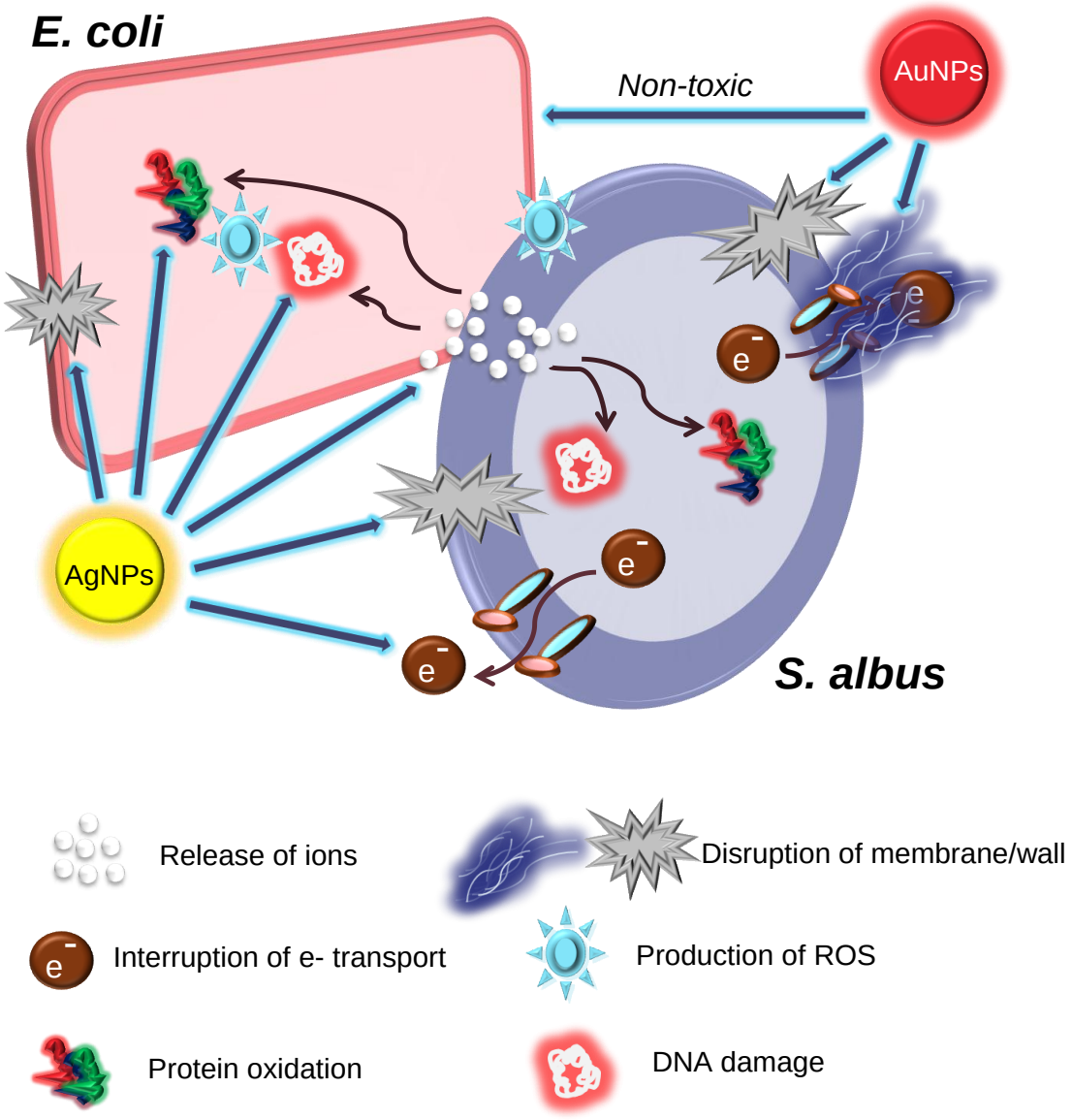

Figure.3.20. Schematic illustration of antibacterial activity of Au and Ag nanoparticles toward *E. coli* and *S. albus*

3.6. Conclusions

In existing literature, stabilizer or toxic chemical reducing agents have been employed to synthesis bimetallic nanoparticles, whereas the method adopted in this chapter provides highly stable, water dispersible metal nanoparticles with different metal composition and surface functionalization without using any additional stabilizer or noxious chemical. [87, 89, 92] In this chapter, a green and eco-friendly method has been developed to prepare Au, Ag and Au-Ag alloy nanoparticles with different metal composition and functionalization using tryptophan and tyrosine amino acids. Indole and phenols groups present in tryptophan and tyrosine are found to reduce gold and silver ions into their respective mono and bimetallic nanoparticulate forms. Thus this is a major step towards greener synthesis of nanomaterials.

Moreover, presence of amino acid corona may provide biological identity to these nanoparticles and these nanomaterials may have significant potential for biological applications. In general, Ag nanoparticles are regarded as toxic by their nature whereas Au nanoparticles are considered as biocompatible.[66, 70, 118] Co-existence of both the metals in Au-Ag alloy nanoparticles in different ratios may have differential biological activity. Therefore, prior to investigate biological activities of these amino acid-functionalized nanoparticles, these nanomaterials were thoroughly characterized by UV-vis, AAS, FTIR, XPS, Zeta potential, TEM and cyclic voltammetry studies to understand their physicochemical nature.

The amino acid-functionalized nanoparticles exhibited intrinsic peroxidase enzyme-like activity, which was found to be metal composition, surface functionalization and temperature dependent. Ag nanoparticles

exhibited higher peroxidase-like activity compared to Au nanoparticles and in the case of alloy nanoparticles; this activity was dependant on the Ag fraction. Presence of tyrosine corona on nanoparticles surface had significant influence on peroxidase-like behaviour. Further, antibacterial potential of these amino acid-functionalized Au, Ag and Au-Ag nanoparticles were investigated on Gram positive (*S. albus*) and Gram negative bacteria (*E. coli*) bacteria. Both, tryptophan and tyrosine synthesised Au, Ag and Au-Ag alloy nanoparticles have significant activity towards *S. albus*, whereas in *E. coli*, only Ag nanoparticles or Ag rich alloy nanoparticles were considerably active. This study indicates that even biocompatible Au nanoparticles can be made toxic. Moreover, it was revealed that toxic effect towards *S. albus* is due to the presence of amino acid shell, wherein the toxicity originates due to the Ag fraction of nanoparticles against *E. coli*. Nano-SEM validated observed antibacterial results and confirmed morphological changes and level of damage in treated bacterial cells.

3.7. References

1. Katz, E. and I. Willner, *Integrated Nanoparticle–Biomolecule Hybrid Systems: Synthesis, Properties, and Applications.* Angewandte Chemie International Edition, 2004. **43**(45): p. 6042-6108.
2. Jain, P.K., et al., *Noble Metals on the Nanoscale: Optical and Photothermal Properties and Some Applications in Imaging, Sensing, Biology, and Medicine.* Accounts of Chemical Research, 2008. **41**(12): p. 1578-1586.

3. Shim, M., et al., *Functionalization of Carbon Nanotubes for Biocompatibility and Biomolecular Recognition.* Nano Letters, 2002. **2**(4): p. 285-288.
4. Liong, M., et al., *Multifunctional inorganic nanoparticles for imaging, targeting, and drug delivery.* ACS Nano, 2008. **2**(5): p. 889-896.
5. Dobrovolskaia, M.A. and S.E. McNeil, *Immunological properties of engineered nanomaterials.* Nature Nanotechnology, 2007. **2**(8): p. 469-478.
6. Colvin, V.L., *The potential environmental impact of engineered nanomaterials.* Nature Biotechnology, 2003. **21**(10): p. 1166-1170.
7. Lewinski, N., V. Colvin, and R. Drezek, *Cytotoxicity of Nanoparticles.* Small, 2008. **4**(1): p. 26-49.
8. Hall, J.B., et al., *Characterization of nanoparticles for therapeutics.* Nanomedicine, 2007. **2**(6): p. 789(15).
9. Leroueil, P.R., et al., *Nanoparticle Interaction with Biological Membranes: Does Nanotechnology Present a Janus Face?* Accounts of Chemical Research, 2007. **40**(5): p. 335-342.
10. Nel, A., et al., *Toxic potential of materials at the nanolevel.* Science, 2006. **311**(5761): p. 622-627.
11. Nel, A.E., et al., *Understanding biophysicochemical interactions at the nano-bio interface.* Nature Materials, 2009. **8**(7): p. 543-557.
12. Xia, T., et al., *Cationic polystyrene nanosphere toxicity depends on cell-specific endocytic and mitochondrial injury pathways.* ACS Nano, 2008. **2**(1): p. 85-96.

13. Weissleder, R., et al., *Cell-specific targeting of nanoparticles by multivalent attachment of small molecules.* Nature Biotechnology, 2005. **23**(11): p. 1418-1423.

14. Brunetti, V., et al., *InP/ZnS as a safer alternative to CdSe/ZnS core/shell quantum dots: In vitro and in vivo toxicity assessment.* Nanoscale, 2013. **5**(1): p. 307-317.

15. Mout, R., et al., *Surface functionalization of nanoparticles for nanomedicine.* Chemical Society Reviews, 2012. **41**(7): p. 2539-2544.

16. Doane, T.L. and C. Burda, *The unique role of nanoparticles in nanomedicine: imaging, drug delivery and therapy.* Chemical Society Reviews, 2012. **41**(7): p. 2885-2911.

17. Schaeublin, N.M., et al., *Does shape matter? Bioeffects of gold nanomaterials in a human skin cell model.* Langmuir, 2012. **28**(6): p. 3248-3258.

18. Walkey, C.D., et al., *Nanoparticle size and surface chemistry determine serum protein adsorption and macrophage uptake.* Journal of the American Chemical Society, 2012. **134**(4): p. 2139-2147.

19. Goethals, E.C., et al., *Decoupling the Effects of the Size, Wall Thickness, and Porosity of Curcumin-Loaded Chitosan Nanocapsules on Their Anticancer Efficacy: Size Is the Winner.* Langmuir, 2013. **29**(2): p. 658-666.

20. Gao, L., et al., *Intrinsic peroxidase-like activity of ferromagnetic nanoparticles.* Nature Nanotechnology, 2007. **2**(9): p. 577-583.

21. Wei, H. and E. Wang, *Fe 3O 4 magnetic nanoparticles as peroxidase mimetics and their applications in H 2O 2 and glucose detection.* Analytical Chemistry, 2008. **80**(6): p. 2250-2254.

22. He, W., et al., *Au@Pt nanostructures as oxidase and peroxidase mimetics for use in immunoassays.* Biomaterials, 2011. **32**(4): p. 1139-1147.

23. Zhang, K., et al., *Formation of PdPt Alloy Nanodots on Gold Nanorods: Tuning Oxidase-like Activities via Composition.* Langmuir, 2011. **27**(6): p. 2796-2803.

24. Fan, J., et al., *Direct evidence for catalase and peroxidase activities of ferritin-platinum nanoparticles.* Biomaterials, 2011. **32**(6): p. 1611-1618.

25. Pirmohamed, T., et al., *Nanoceria exhibit redox state-dependent catalase mimetic activity.* Chemical Communications, 2010. **46**(16): p. 2736-2738.

26. He, W., et al., *Design of AgM Bimetallic Alloy Nanostructures (M = Au, Pd, Pt) with Tunable Morphology and Peroxidase-Like Activity.* Chemistry of Materials, 2010. **22**(9): p. 2988-2994.

27. Banerjee, M., et al., *Heightened Reactive Oxygen Species Generation in the Antimicrobial Activity of a Three Component Iodinated Chitosan-Silver Nanoparticle Composite.* Langmuir, 2010. **26**(8): p. 5901-5908.

28. Premanathan, M., et al., *Selective toxicity of ZnO nanoparticles toward Gram-positive bacteria and cancer cells by apoptosis through lipid peroxidation.* Nanomedicine: Nanotechnology, Biology and Medicine, 2011. **7**(2): p. 184-192.

29. AshaRani, P.V., et al., *Cytotoxicity and genotoxicity of silver nanoparticles in human cells.* ACS Nano, 2009. **3**(2): p. 279-290.

30. Carlson, C., et al., *Unique cellular interaction of silver nanoparticles: Size-dependent generation of reactive oxygen species.* Journal of Physical Chemistry B, 2008. **112**(43): p. 13608-13619.

31. Choi, O. and Z. Hu, *Size dependent and reactive oxygen species related nanosilver toxicity to nitrifying bacteria.* Environmental Science and Technology, 2008. **42**(12): p. 4583-4588.

32. Limbach, L.K., et al., *Exposure of engineered nanoparticles to human lung epithelial cells: Influence of chemical composition and catalytic activity on oxidative stress.* Environmental Science and Technology, 2007. **41**(11): p. 4158-4163.

33. Long, T.C., et al., *Titanium dioxide (P25) produces reactive oxygen species in immortalized brain microglia (BV2): Implications for nanoparticle neurotoxicity.* Environmental Science and Technology, 2006. **40**(14): p. 4346-4352.

34. Xia, T., et al., *Comparison of the Abilities of Ambient and Manufactured Nanoparticles To Induce Cellular Toxicity According to an Oxidative Stress Paradigm.* Nano Letters, 2006. **6**(8): p. 1794-1807.

35. Hirst, S.M., et al., *Bio-distribution and in vivo antioxidant effects of cerium oxide nanoparticles in mice.* Environmental Toxicology, 2013. **28**(2): p. 107-118.

36. Walczyk, D., et al., *What the Cell Sees in Bionanoscience.* Journal of the American Chemical Society, 2010. **132**(16): p. 5761-5768.

37. Walkey, C.D. and W.C.W. Chan, *Understanding and controlling the interaction of nanomaterials with proteins in a physiological environment.* Chemical Society Reviews, 2012. **41**(7): p. 2780-2799.

38. Arvizo, R.R., et al., *Intrinsic therapeutic applications of noble metal nanoparticles: past, present and future.* Chemical Society Reviews, 2012. **41**(7): p. 2943-2970.

39. Neal, A., *What can be inferred from bacterium–nanoparticle interactions about the potential consequences of environmental exposure to nanoparticles?* Ecotoxicology, 2008. **17**(5): p. 362-371.

40. Amin, R.M., et al., *Rapid and sensitive microplate assay for screening the effect of silver and gold nanoparticles on bacteria.* Nanomedicine, 2009. **4**(6): p. 637-643.

41. Baker, C., et al., *Synthesis and antibacterial properties of silver nanoparticles.* Journal of Nanoscience and Nanotechnology, 2005. **5**(2): p. 244-249.

42. Chen, X. and H.J. Schluesener, *Nanosilver: A nanoproduct in medical application.* Toxicology Letters, 2008. **176**(1): p. 1-12.

43. Dror-Ehre, A., et al., *Silver nanoparticle-E. coli colloidal interaction in water and effect on E. coli survival.* Journal of Colloid and Interface Science, 2009. **339**(2): p. 521-526.

44. Jain, D., et al., *Synthesis of plant-mediated silver nanoparticles using papaya fruit extract and evaluation of their anti microbial activities.* Digest Journal of Nanomaterials and Biostructures, 2009. **4**(3): p. 557-563.

45. Cui, Y., et al., *The molecular mechanism of action of bactericidal gold nanoparticles on Escherichia coli.* Biomaterials, 2012. **33**(7): p. 2327-2333.

46. Amato, E., et al., *Synthesis, Characterization and Antibacterial Activity against Gram Positive and Gram Negative Bacteria of Biomimetically Coated Silver Nanoparticles.* Langmuir, 2011. **27**(15): p. 9165-9173.

47. Zhou, Y., et al., *Antibacterial activities of gold and silver nanoparticles against Escherichia coli and bacillus Calmette-Guerin.* Journal of Nanobiotechnology, 2012. **10**(1): p. 19.

48. Sadiq, I.M., et al., *Antimicrobial sensitivity of Escherichia coli to alumina nanoparticles.* Nanomedicine: Nanotechnology, Biology, and Medicine, 2009. **5**(3): p. 282-286.

49. Suresh, A.K., et al., *Cytotoxicity Induced by Engineered Silver Nanocrystallites Is Dependent on Surface Coatings and Cell Types.* Langmuir, 2012. **28**(5): p. 2727-2735.

50. Shai, Y., *Mode of action of membrane active antimicrobial peptides.* Biopolymers - Peptide Science Section, 2002. **66**(4): p. 236-248.

51. Gottenbos, B., et al., *Antimicrobial effects of positively charged surfaces on adhering Gram-positive and Gram-negative bacteria.* Journal of Antimicrobial Chemotherapy, 2001. **48**(1): p. 7-13.

52. Leroueil, P.R., et al., *Wide varieties of cationic nanoparticles induce defects in supported lipid bilayers.* Nano Letters, 2008. **8**(2): p. 420-424.

53. Woo, K.J., et al., *Antibacterial activity and mechanism of action of the silver ion in Staphylococcus aureus and Escherichia coli.* Applied and Environmental Microbiology, 2008. **74**(7): p. 2171-2178.

54. El Badawy, A.M., et al., *Surface Charge-Dependent Toxicity of Silver Nanoparticles.* Environmental Science & Technology, 2011. **45**(1): p. 283-287.

55. Lok, C.N., et al., *Silver nanoparticles: Partial oxidation and antibacterial activities.* Journal of Biological Inorganic Chemistry, 2007. **12**(4): p. 527-534.

56. Sondi, I. and B. Salopek-Sondi, *Silver nanoparticles as antimicrobial agent: A case study on E. coli as a model for Gram-negative bacteria.* Journal of Colloid and Interface Science, 2004. **275**(1): p. 177-182.

57. Lok, C.N., et al., *Proteomic analysis of the mode of antibacterial action of silver nanoparticles.* Journal of Proteome Research, 2006. **5**(4): p. 916-924.

58. Li, W.R., et al., *Antibacterial activity and mechanism of silver nanoparticles on Escherichia coli.* Applied Microbiology and Biotechnology, 2010. **85**(4): p. 1115-1122.

59. Holt, K.B. and A.J. Bard, *Interaction of Silver(I) Ions with the Respiratory Chain of Escherichia coli: An Electrochemical and Scanning Electrochemical Microscopy Study of the Antimicrobial Mechanism of Micromolar Ag+* Biochemistry, 2005. **44**(39): p. 13214-13223.

60. Shrivastava, S., et al., *Characterization of enhanced antibacterial effects of novel silver nanoparticles.* Nanotechnology, 2007. **18**(22).

61. Panacek, A., et al., *Silver colloid nanoparticles: Synthesis, characterization, and their antibacterial activity.* Journal of Physical Chemistry B, 2006. **110**(33): p. 16248-16253.

62. Sharma, V.K., R.A. Yngard, and Y. Lin, *Silver nanoparticles: Green synthesis and their antimicrobial activities.* Advances in Colloid and Interface Science, 2009. **145**(1-2): p. 83-96.

63. Russell, A.D. and W.B. Hugo, *Antimicrobial Activity and Action of Silver*, in *Progress in Medicinal Chemistry*1994. p. 351-370.

64. Nair, L.S. and C.T. Laurencin, *Silver nanoparticles: Synthesis and therapeutic applications.* Journal of Biomedical Nanotechnology, 2007. **3**(4): p. 301-316.

65. Morones, J.R., et al., *The bactericidal effect of silver nanoparticles.* Nanotechnology, 2005. **16**(10): p. 2346-2353.

66. Kim, J.S., et al., *Antimicrobial effects of silver nanoparticles.* Nanomedicine: Nanotechnology, Biology and Medicine, 2007. **3**(1): p. 95-101.

67. Kazachenko, A., et al., *Synthesis and antimicrobial activity of silver complexes with histidine and tryptophan.* Pharmaceutical Chemistry Journal, 2000. **34**(5): p. 257-258.

68. Ashkarran, A.A., et al., *Bacterial Effects and Protein Corona Evaluations: Crucial Ignored Factors in the Prediction of Bio-Efficacy of Various Forms of Silver Nanoparticles.* Chemical Research in Toxicology, 2012. **25**(6): p. 1231-1242.

69. Irwin, P., et al., *Antimicrobial activity of spherical silver nanoparticles prepared using a biocompatible macromolecular capping agent:*

evidence for induction of a greatly prolonged bacterial lag phase. Journal of Nanobiotechnology, 2010. **8**(1): p. 34.

70. Shukla, R., et al., *Biocompatibility of gold nanoparticles and their endocytotic fate inside the cellular compartment: A microscopic overview.* Langmuir, 2005. **21**(23): p. 10644-10654.
71. Connor, E.E., et al., *Gold Nanoparticles Are Taken Up by Human Cells but Do Not Cause Acute Cytotoxicity.* Small, 2005. **1**(3): p. 325-327.
72. Goodman, C.M., et al., *Toxicity of Gold Nanoparticles Functionalized with Cationic and Anionic Side Chains.* Bioconjugate Chemistry, 2004. **15**(4): p. 897-900.
73. Zhao, Y., et al., *Small molecule-capped gold nanoparticles as potent antibacterial agents that target gram-negative bacteria.* Journal of the American Chemical Society, 2010. **132**(35): p. 12349-12356.
74. Pal, S., Y.K. Tak, and J.M. Song, *Does the antibacterial activity of silver nanoparticles depend on the shape of the nanoparticle? A study of the gram-negative bacterium Escherichia coli.* Applied and Environmental Microbiology, 2007. **73**(6): p. 1712-1720.
75. Taglietti, A., et al., *Antibacterial Activity of Glutathione-Coated Silver Nanoparticles against Gram Positive and Gram Negative Bacteria.* Langmuir, 2012. **28**(21): p. 8140-8148.
76. Zhang, Y., et al., *Facile preparation and characterization of highly antimicrobial colloid Ag or Au nanoparticles.* Journal of Colloid and Interface Science, 2008. **325**(2): p. 371-376.

77. Feng, Q.L., et al., *A Mechanistic Study of the Antibacterial Effect of Silver Ions on Escherichia Coli and Staphylococcus Aureus.* Journal of Biomedical Materials Research 2000. **52**(4): p. 662-668.

78. Kim, J.S., et al., *Antimicrobial effects of silver nanoparticles.* Nanomedicine: Nanotechnology, Biology, and Medicine, 2007. **3**(1): p. 95-101.

79. Zasloff, M., *Antimicrobial peptides of multicellular organisms.* Nature, 2002. **415**(6870): p. 389-395.

80. Prescott, L.M., J.P. Harley, and D.A. Klein, *Microbiology*, ed. 6. 2005: McGraw-Hill.

81. Kisailus, D., et al., *Functionalized gold nanoparticles mimic catalytic activity of a polysiloxane-synthesizing enzyme.* Advanced Materials, 2005. **17**(10): p. 1234-1239.

82. Manea, F., et al., *Nanozymes: Gold-nanoparticle-based transphosphorylation catalysts.* Angewandte Chemie - International Edition, 2004. **43**(45): p. 6165-6169.

83. Selvakannan, P.R., et al., *Water-dispersible tryptophan-protected gold nanoparticles prepared by the spontaneous reduction of aqueous chloroaurate ions by the amino acid.* Journal of Colloid and Interface Science, 2004. **269**(1): p. 97-102.

84. Si, S. and T.K. Mandal, *Tryptophan-based peptides to synthesize gold and silver nanoparticles: A mechanistic and kinetic study.* Chemistry - A European Journal, 2007. **13**(11): p. 3160-3168.

85. Selvakannan, P.R., et al., *Synthesis of aqueous Au core-Ag shell nanoparticles using tyrosine as a pH-dependent reducing agent and*

assembling phase-transferred silver nanoparticles at the air-water interface. Langmuir, 2004. **20**(18): p. 7825-7836.

86. Si, S., et al., *A Mechanistic and Kinetic Study of the Formation of Metal Nanoparticles by Using Synthetic Tyrosine-Based Oligopeptides.* Chemistry – A European Journal, 2006. **12**(4): p. 1256-1265.
87. Link, S., Z.L. Wang, and M.A. El-Sayed, *Alloy formation of gold-silver nanoparticles and the dependence of the plasmon absorption on their composition.* Journal of Physical Chemistry B, 1999. **103**(18): p. 3529-3533.
88. Srnova-Sloufova, I., et al., *Bimetallic (Ag)Au Nanoparticles Prepared by the Seed Growth Method: Two-Dimensional Assembling, Characterization by Energy Dispersive X-ray Analysis, X-ray Photoelectron Spectroscopy, and Surface Enhanced Raman Spectroscopy, and Proposed Mechanism of Growth.* Langmuir, 2004. **20**(8): p. 3407-3415.
89. Li, Z.Y., et al., *Structures and optical properties of 4-5 nm bimetallic AgAu nanoparticles.* Faraday Discussions, 2008. **138**: p. 363-373.
90. Dickerson, M.B., K.H. Sandhage, and R.R. Naik, *Protein- and Peptide-Directed Syntheses of Inorganic Materials.* Chemical Reviews, 2008. **108**(11): p. 4935-4978.
91. Dahl, J.A., B.L.S. Maddux, and J.E. Hutchison, *Toward greener nanosynthesis.* Chemical Reviews, 2007. **107**(6): p. 2228-2269.
92. Bhargava, S.K., et al., *Gold nanoparticle formation during bromoaurate reduction by amino acids.* Langmuir, 2005. **21**(13): p. 5949-5956.

93. Hodak, J.H., et al., *Laser-Induced Inter-Diffusion in AuAg Core-Shell Nanoparticles.* The Journal of Physical Chemistry B, 2000. **104**(49): p. 11708-11718.

94. Sun, Y. and Y. Xia, *Gold and silver nanoparticles: A class of chromophores with colors tunable in the range from 400 to 750 nm.* Analyst, 2003. **128**(6): p. 686-691.

95. Chen, D.-H. and C.-J. Chen, *Formation and characterization of Au-Ag bimetallic nanoparticles in water-in-oil microemulsions.* Journal of Materials Chemistry, 2002. **12**(5): p. 1557-1562.

96. Mulvaney, P., *Surface Plasmon Spectroscopy of Nanosized Metal Particles.* Langmuir, 1996. **12**(3): p. 788-800.

97. Yen, H.J., S.H. Hsu, and C.L. Tsai, *Cytotoxicity and immunological response of gold and silver nanoparticles of different sizes.* Small, 2009. **5**(13): p. 1553-1561.

98. Martinez-Castanon, G.A., et al., *Synthesis and antibacterial activity of silver nanoparticles with different sizes.* Journal of Nanoparticle Research, 2008. **10**(8): p. 1343-1348.

99. Mao, Y. and S.S. Wong, *Size- and shape-dependent transformation of nanosized titanate into analogous anatase titania nanostructures.* Journal of the American Chemical Society, 2006. **128**(25): p. 8217-8226.

100. Narayanan, R. and M.A. El-Sayed, *Shape-dependent catalytic activity of platinum nanoparticles in colloidal solution.* Nano Letters, 2004. **4**(7): p. 1343-1348.

101. Shirley, D.A., *High-Resolution X-Ray Photoemission Spectrum of the Valence Bands of Gold.* Physical Review B, 1972. **5**(12): p. 4709-4714.

102. Petoral Jr, R.M. and K. Uvdal, *XPS and NEXAFS study of tyrosine-terminated propanethiol assembled on gold.* Journal of Electron Spectroscopy and Related Phenomena, 2003. **128**(2-3): p. 159-164.

103. Silverstein R.B. and B. G.C., *Spectrometric identification of organic compounds*. second ed. 1967, New York: John Wiley & Sons. 88.

104. Tamil Selvan, S., *Novel nanostructures of gold-polypyrrole composites.* Chemical Communications, 1998(3): p. 351-352.

105. Waltman, R.J., A.F. Diaz, and J. Bargon, *Substituent effects in the electropolymerization of aromatic heterocyclic compounds.* The Journal of Physical Chemistry, 1984. **88**(19): p. 4343-4346.

106. Ivanova, O.S. and F.P. Zamborini, *Size-dependent electrochemical oxidation of silver nanoparticles.* Journal of the American Chemical Society, 2010. **132**(1): p. 70-72.

107. Tominaga, M., et al., *Composition-activity relationships of carbon electrode-supported bimetallic gold-silver nanoparticles in electrocatalytic oxidation of glucose.* Journal of Electroanalytical Chemistry, 2008. **615**(1): p. 51-61.

108. Li, Q., et al., *Antimicrobial nanomaterials for water disinfection and microbial control: Potential applications and implications.* Water Research, 2008. **42**(18): p. 4591-4602.

109. Pulskamp, K., S. Diabate, and H.F. Krug, *Carbon nanotubes show no sign of acute toxicity but induce intracellular reactive oxygen species in*

dependence on contaminants. Toxicology Letters, 2007. **168**(1): p. 58-74.

110. Ratnam, D.V., et al., *Role of antioxidants in prophylaxis and therapy: A pharmaceutical perspective.* Journal of Controlled Release, 2006. **113**(3): p. 189-207.
111. Xia, T., et al., *Comparison of the mechanism of toxicity of zinc oxide and cerium oxide nanoparticles based on dissolution and oxidative stress properties.* ACS Nano, 2008. **2**(10): p. 2121-2134.
112. Lovric, J., et al., *Unmodified cadmium telluride quantum dots induce reactive oxygen species formation leading to multiple organelle damage and cell death.* Chemistry and Biology, 2005. **12**(11): p. 1227-1234.
113. Yu, F., et al., *The artificial peroxidase activity of magnetic iron oxide nanoparticles and its application to glucose detection.* Biomaterials, 2009. **30**(27): p. 4716-4722.
114. Chen, H., et al., *Graphene supported Au-Pd bimetallic nanoparticles with core-shell structures and superior peroxidase-like activities.* Journal of Materials Chemistry, 2011. **21**(44): p. 17658-17661.
115. Ma, M., Y. Zhang, and N. Gu, *Peroxidase-like catalytic activity of cubic Pt nanocrystals.* Colloids and Surfaces A: Physicochemical and Engineering Aspects, 2011. **373**(1-3): p. 6-10.
116. Monopoli, M.P., et al., *Physical-Chemical Aspects of Protein Corona: Relevance to in Vitro and in Vivo Biological Impacts of Nanoparticles.* Journal of the American Chemical Society, 2011. **133**(8): p. 2525-2534.

117. Lynch, I., A. Salvati, and K.A. Dawson, *Protein-nanoparticle interactions: What does the cell see?* Nat Nano, 2009. **4**(9): p. 546-547.

118. Sondi, I. and B. Salopek-Sondi, *Silver nanoparticles as antimicrobial agent: a case study on E. coli as a model for Gram-negative bacteria.* J Colloid Interface Sci, 2004. **275**: p. 177 - 182.

Chapter IV

Sequential surface functionalization of metal nanoparticles using polyoxometalates and lysine to controllably enhance their antibacterial potential

Sequential surface functionalization of metal nanoparticles to improve their antibacterial potential is the major focus of this chapter. In the previous chapter, tyrosine reduced gold nanoparticles were found to be non-toxic toward Gram negative bacteria. Step-wise surface functionalization of biocompatible gold nanoparticles by polyoxometalates (POMs) and the cationic amino acid lysine turned them strong antimicrobial active agent in a sequential manner. The similar strategy was extended to tyrosine capped silver nanoparticles to enhance their antibacterial potential and as a result, these nanoparticles exhibited very high antibacterial activity even at smaller concentrations. This chapter revealed that suitable surface functionalization of nanomaterials either enable them antibacterial active or improve their antibacterial potential.

4.1. Introduction

In the previous chapter, it has been shown that how different amino acid capped metal nanoparticles exhibit antibacterial activities against Gram negative and Gram positive bacteria via different mechanisms. In the case of Gram positive bacteria, it was shown that the surface bound amino acids are responsible for the observed antibacterial activity, whereas composition of nanoparticle played a significant role in rendering them as antibacterial active against Gram negative bacteria. In particular, tyrosine functionalized silver nanoparticles ($AgNPs^{Tyr}$) were found to be toxic; while the same tyrosine functionalized gold nanoparticles ($AuNPs^{Tyr}$) were found to be non-toxic against *E. coli*. Since both the nanoparticles ($AuNPs^{Tyr}$ and $AgNPs^{Tyr}$) have similar surface bound tyrosine ligand shell and similar type of surface charge, these nanoparticles are expected to interact and taken up by the *E. coli* bacterium in a similar manner, though the antibacterial activity was observed only in the case of $AgNPs^{Tyr}$.

Silver (Ag) has long been known for its antimicrobial activities and it has been used in many related applications.[1] Among different nanomaterials, Ag nanoparticles are found to exhibit a significantly higher level of antibacterial activity, [2-4] as they are known to initiate denaturation of proteins and DNA, which instigate toxicity.[3-13] Ag binds to many cellular and membrane components and it is not clearly understood that how the strong binding of Ag to different biological sub-components controls its toxicity.[14] Moreover, antibacterial activity of Ag nanoparticles is size and shape dependent and direct interaction between nanoparticles and

bacterial cells are important to demonstrate antimicrobial activities.[10, 11, 15, 16]

Conversely, AuNPs^{Tyr} didn't demonstrate any appreciable toxicity, which shows that these nanoparticles did not affect bacterial growth. Though, in contrast to Ag nanoparticles, Au nanoparticles are considered as biocompatible,[2, 17, 18] interestingly it was shown that cationic Au nanoparticles may exhibit toxic effects, whereas anionic Au nanoparticles were found to be nontoxic.[19] Furthermore, it has been demonstrated that Au nanoparticles capped with small molecules may work as potential antibacterial agents.[20] In this perspective, Au nanoparticles were chemically surface functionalized with amino-substituted pyrimidine and other drug molecules and it was revealed that these functionalized Au nanoparticles became effective antimicrobial and anticancer agents due to their tailored surface properties.[20-23] Aforementioned arguments are clear evidence of the importance of surface modification / functionalization of nanomaterials for their biological applications and states that even the most biocompatible nanomaterials may be rendered toxic by carefully tuning their surface chemistry.

Therefore, it is believed that appropriate surface functionalization of both tyrosine synthesised Au and Ag nanoparticles may improve their antibacterial activities due to the additional toxic effects created by the surface bound molecules and ions.[24-27] This concept stems from the fact that conventional antibiotics such as ciprofloxacin, doxycycline and ceftazidime selectively penetrate into the bacterial membrane and act on specific target to inhibit bacterial growth. Rather than causing physical

damage to bacterial cell wall, these antibiotics chemically interact with genetic material of bacteria, block cell-division and sometimes trigger autolysins in targeted pathogens. In this manner, bacterial morphology is preserved and therefore, bacterial species have possibility to develop resistance.[28] After discovery of bacterial-resistance through genetic mutations or physical integrity, it was realized that it is a critical issue related to public health[29, 30] and rapid development in the field of nanomedicine may provide an excellent opportunity to control pathogenic microorganisms and bacterial strains.[31-37]

In this context, it has been revealed that many cationic antimicrobial peptides do not have a specific target in bacteria and usually they interact with the bacterial cell wall through an electrostatic interaction which causes physical damage to bacterial cells by forming pores.[38, 39] This physical action prevents microbes from developing resistance against antimicrobial peptides and in fact it is proven that cationic antimicrobial peptides and nanomaterials have potential to overcome bacterial resistance.[13, 28, 38-40] In addition to this, it has been reported that surface coatings of nanoparticles have a significant effect on antimicrobial profiles of functionalized nanoparticles [20, 41-49] and predominantly, polymers and poly-electrolytes are the most commonly used surface coatings to tailor the surface properties of antibacterial nanomaterials. These peripheral coatings can impart charge to the particles (for example positive or negative surface charge) and can stabilize them against aggregation. Furthermore, toxic effects from positively charged nanoparticles have been explored, but these effects were not observed when the same particles were coated with

negatively charged functional groups.[50, 51] The rationale behind this is that if the antimicrobial composition had the same surface charge as the bacterial cells, this induces repulsion and prevents direct contact. Therefore, controlling the surface charge of formulated nanomaterials using surface coatings have considerably possibilities to improve the activity of the formulation[52] because surface charge of antibacterial nanomaterials may be crucial for initial electrostatic attraction and their activity.

Thus, antibacterial activity of nanomaterials involves direct contact between cellular (bacterial) surface and nanoparticles; this suggests that the surface chemistry / functionalization, size and morphology of nanomaterials could be very influential for toxicity against bacteria.[53] Additionally, as shown in previous chapters, biologically inspired understanding of naturally occurring materials can lead to the development of nanomaterials, nanodevices and processes with desirable functionality, as nature has evolved with desired biological and chemical functionality using commonly found materials.[54] Moreover to improve efficiency, nanomaterials can be modified to facilitate their application in different fields such as bacteriology and nanomedicine. Therefore, the major focus of this chapter is design surface functionalized Au and Ag nanoparticles for their step wise improved antibacterial potential, which causes toxicity by physical damage. To achieve this, metal nanoparticles were successively surface functionalized with polyoxometalates (POMs) and the cationic amino acid lysine as illustrated in Figure 4.1 and their antibacterial potential was investigated against model Gram negative bacterium *E. coli*. Inorganic Au nanoparticles were used as inert support to stabilize POMs ions on their surface since Au nanoparticles

are biologically inert and they do not have any direct biological effect. Therefore, Au nanoparticles are the most suitable material for nanomedicine applications. Conversely, Ag nanoparticles are already known for their antibacterial activity, hence their surface functionalization with other molecules such as POMs may enhance their antibacterial potential in synergistic manner, whereas these Ag nanoparticles can also work as active core and support.

To control the surface functionalization of metal nanoparticles, POMs and the cationic amino acid (lysine or lys) were used as functional molecules. POMs are inorganic anionic clusters of early transition metals such as tungsten, molybdenum or vanadium etc, and oxygen, formed by the self-assembly processes.[55-57] Furthermore, these POMs are known to induce ROS and bacterial resistance against inorganic systems are relatively difficult. POMs have molecular diversity which makes them a versatile class of inorganic clusters for surface coating applications.[58] In the field of biomedicine, these inorganic compounds are known for their antibacterial, antiviral and anticancer activities.[55, 58, 59] However, most of the POMs are unstable in aqueous solution at physiological pH and degrade in to mixture of inorganic products, which limits their medicinal and biological applications.[55] Since they are anionic in nature, they can electrostatically bind with any cationic molecules, which can provide additional stability to POMs and at the same time the cationic system may elevate additional toxicity. Therefore, in this regard tyrosine synthesized Au and Ag nanoparticles are employed as discussed earlier. Additionally, lysine is used because it has two amine groups, so it is believed to bind to POMs at one

end and while the other terminal amine group can be used to tether to the negatively charged bacterial wall or membrane faster.

4.2. Scheme of the work

The major part of this chapter focuses on the development of the sequential surface functionalization strategy of tyrosine synthesised metal nanoparticles. As discussed in chapter 3, $AuNPs^{Tyr}$ were synthesised employing tyrosine amino acid and sequentially surface functionalized with POMs and lysine, which resulted in functional $AuNPs^{Tyr@POMs}$ and $AuNPs^{Tyr@POMs\text{-}Lys}$ nanoparticles, respectively (Figure 4.1). The similar strategy was also employed toward tyrosine reduced silver nanoparticles ($AgNPs^{Tyr}$) to develop highly active Ag nanoparticles base antibacterial active agents.

Two different POMs such as 12-phosphotungstic acid (PTA) and 12-phosphomolybdic acid (PMA) were employed for surface functionalization due to their well-known biomedical applications,[58, 60-62] which could be imparted on metal nanoparticles, whereas inorganic metal nanoparticles anchor POMs onto their surface. In this surface functionalization strategy, lysine amino acid was used due to its cationic nature, which can work as guiding molecule toward negatively charged bacterial cells to initiate electrostatic attraction. Physicochemical characterization of these Au and Ag based functional nanoparticles was carried out by UV vis, FTIR, XPS, Zeta potential, AAS, ICPMA and TEM studies. Gram negative bacterium *E. coli* was used as model microorganism to understand the effects of surface functionalization

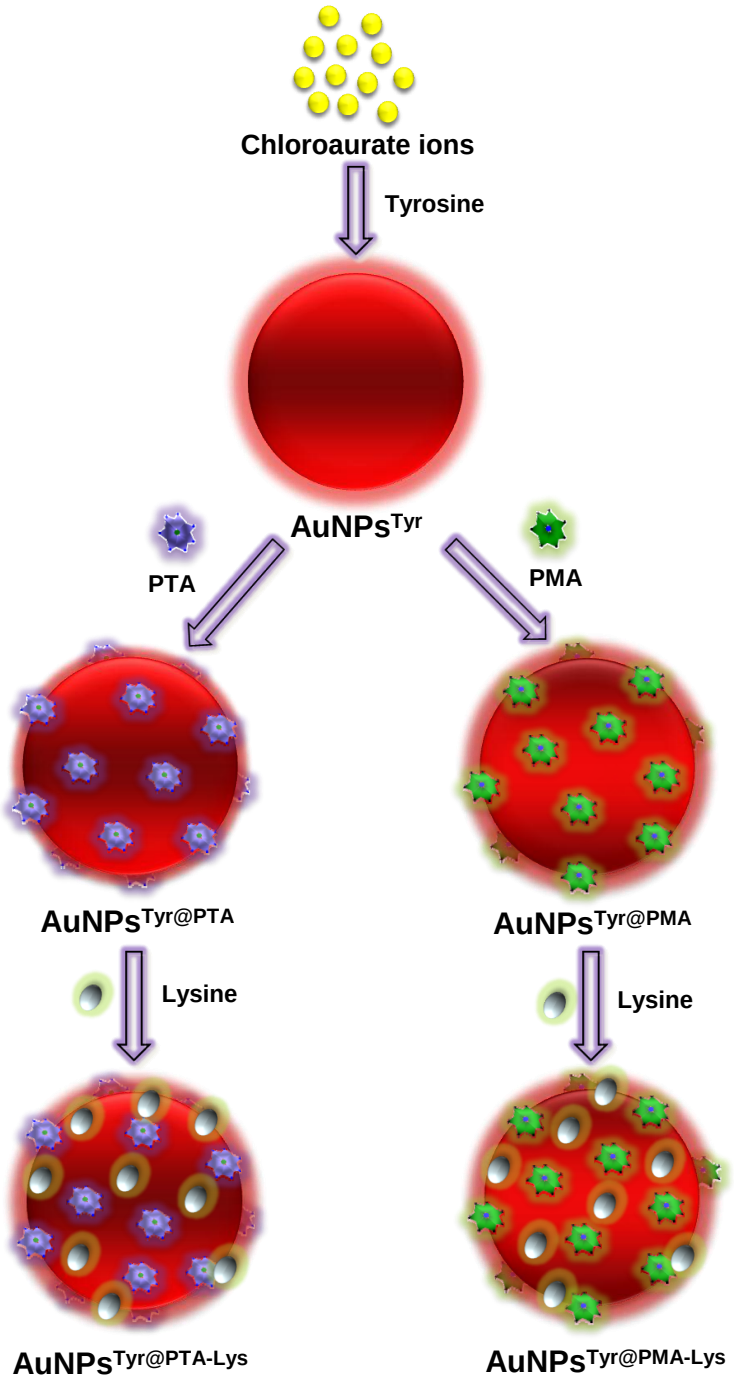

Figure.4.1. Schematic representation of sequential functionalization of tyrosine capped gold nanoparticles by polyoxometalates and lysine

4.3. Experimental section

4.3.1. Synthesis of gold and silver nanoparticles

Tyrosine capped Au and Ag nanoparticles were synthesized as discussed in chapter 3, with slight modifications. Briefly, 300 ml aqueous

solution consisting of 0.1 mM L-tyrosine and 0.1 mM KOH were allowed to boil. Under alkaline boiling conditions, 0.2 mM equivalent of $[AuCl_4]^-$ or Ag^+ ions were added to the above solution. These solutions were further boiled for 5 minutes, which resulted in a ruby-red or yellow coloured solution consisting of tyrosine-reduced $AuNPs^{Tyr}$ or $AgNPs^{Tyr}$ nanoparticles, respectively.

4.3.2. Processing and dialysis of tyrosine capped nanoparticles

To increase the metal concentration of these solutions by the factor of three, these solutions were further allowed to boil to reduce the volume to 100 mL. These colloidal solutions were found to be highly stable even after concentration, signifying that both Au and Ag nanoparticles were strongly capped by tyrosine amino acid. Further, concentrated solutions of $AuNPs^{Tyr}$ and $AgNPs^{Tyr}$ were dialyzed three times against deionized MilliQ water using cellulose dialysis membrane to remove the excess amount of KOH, unreduced metal ions and unbound amino acid, if any.

4.3.3. Sequential surface functionalization with POMs and lysine

After processing and purification of Au and Ag nanoparticles, these materials were successively surface functionalized with POMs and lysine. For surface functionalization of Au and Ag nanoparticles with POMs viz. PTA and PMA, concentrated Au and Ag nanoparticles were separately mixed with aqueous solution of either PTA or PMA to achieve 0.1 mM POMs concentration in these solutions, and incubated for 24 hours under vigorous stirring. Following incubation, these solutions were again subjected to dialysis to remove uncoordinated PTA or PMA molecules; thereby resulting

in POM functionalized Au or Ag nanoparticles ($AuNPs^{Tyr@PTA}$ or $AgNPs^{Tyr@PTA}$ and $AuNPs^{Tyr@PMA}$ or $AgNPs^{Tyr@PMA}$). Subsequently, these POMs functionalized Au and Ag nanoparticles were further modified with a cationic amino acid lysine by adding aqueous solution of L-lysine amino acid to these solutions (final lysine concentration 0.1 mM), incubating for 24 hours under vigorous stirring, followed by dialysis to remove uncoordinated lysine molecules, which resulted in lysine-functionalized nanomaterials viz. $AuNPs^{Tyr@PTA-Lys}$ or $AgNPs^{Tyr@PTA-Lys}$ and $AuNPs^{Tyr@PMA-Lys}$ or $AgNPs^{Tyr@PMA-Lys}$ as represented in Figure 4.1.

4.3.4. Antibacterial activity of POMs and lysine functionalized nanoparticles

Two diverse strategies were employed to investigate antibacterial activities of POMs and lysine functionalized Au and Ag nanoparticles because Au nanoparticles are non-toxic by their nature, while Ag nanoparticles are known to have antibacterial activities. In the case of Au nanoparticles, parent solutions of POMs and lysine functionalized nanomaterials were diluted to obtain stock solutions containing the overall molybdenum (Mo) or tungsten (W) concentrations of 25 µM in solutions to evaluate dose or concentration dependent antibacterial activity. Conversely, in the case of Ag nanoparticles, functionalized parental solutions were diluted to acquire overall silver (Ag) concentration of 25 µM in all the solutions. All the bacterial toxicity tests were performed in duplicate and were performed three times to ensure reproducibility. Before performing antibacterial assay, at each step, dialysis was considered essential to ensure

that the observed antibacterial action is due to nanomaterials, and not from unreduced metal ions, free amino acids and free POMs (PTA or PMA).

To perform antibacterial assessment, different concentrations of Mo or W (present in functionalized Au nanoparticles) or Ag (present in functionalized Ag nanoparticles) were introduced to the bacterial culture containing approximately 10^4 CFU/ml of *E. coli*. Four different concentrations equivalent of 1 µM, 2 µM, 5 µM and 10 µM of W/Mo/Ag were introduced to the bacterial culture (in 1 ml total reaction) and incubated for 15 minutes followed by 100 µl aliquots being spread onto nutrient agar plates. Colonies formed after overnight incubation at 37ºC were counted. These colonies correspond to the number of live bacteria in each suspension at the time of aliquot withdrawal. Plot of the bacterial cell viability versus dose of the nanoparticles (concentrations of W or Mo or Ag present on the surface of functionalized nanoparticles) were constructed to visualize the dose effect on cell viability.

4.4. Results and Discussion

Illustrated in Figure 4.1 are different steps involved in sequential surface functionalization strategy to formulate antibacterial nanoparticles in a highly controlled manner. Initially, $[AuCl_4]^-$ and Ag^+ ions were reduced using tyrosine amino acid under alkaline reaction conditions to form tyrosine-capped $AuNPs^{Tyr}$ and $AgNPs^{Tyr}$, respectively. Under alkaline conditions, phenolic group of tyrosine acts as a reducing functional group,[63] which assists in reduction of metal ions to form tyrosine-capped nanoparticles, and during this reduction process oxidized tyrosine molecules

act as a capping agent to stabilize nanoparticles in the aqueous solution as discussed in chapter 3. These solutions were concentrated and extensively dialyzed followed by their sequential surface functionalization with POMs and lysine to control and enhance their antibacterial performance.

4.4.1. Surface charge measurements of POMs and lysine functionalized Au and Ag nanoparticles using zeta potential

The pH of these $AuNPs^{Tyr}$ and $AgNPs^{Tyr}$ nanoparticles can indicate about the possible surface charge of these nanoparticles due to the presence of tyrosine amino acid on their surfaces. In principle, if the pH of the solution is above the isoelectric point of tyrosine (pI~5.66), respective nanoparticle must bear a negative surface charge and conversely, if the solution pH is below the isoelectric point of amino acid the nanoparticles must bear a positive surface charge. The pH values of the extensively dialyzed solutions containing $AuNPs^{Tyr}$ and $AgNPs^{Tyr}$ nanoparticles were found to be 8.4 and 8.6 respectively, which is well above the isoelectric point of tyrosine amino acid. Therefore, in principle, both the $AuNPs^{Tyr}$ and $AgNPs^{Tyr}$ nanoparticles should bear a negative surface charge, which was further confirmed by the negative zetapotential values of -29 mV and -38.8 mV for $AuNPs^{Tyr}$ and $AgNPs^{Tyr}$, respectively. These high negative zetapotential values further indicated the stability of $AuNPs^{Tyr}$ and $AgNPs^{Tyr}$ nanoparticles, as discussed in pervious chapter.

In the next step of surface functionalization, $AuNPs^{Tyr}$ and $AgNPs^{Tyr}$ were separately surface functionalized with PTA or PMA molecules to obtain $AuNPs^{Tyr@PTA}$ or $AgNPs^{Tyr@PTA}$ and $AuNPs^{Tyr@PMA}$ or $AgNPs^{Tyr@PMA}$ respectively.

Since POMs are highly acidic in nature, when PTA and PMA molecules were added to $AuNPs^{Tyr}$ and $AgNPs^{Tyr}$ nanoparticles solutions, the pH of solutions immediately dropped significantly to ca. 1.5-2.0 ($AuNPs^{Tyr}$) and 2.0-2.5 ($AgNPs^{Tyr}$), which remained 3.7 and 4.2, for $AuNPs^{Tyr@PTA}$ and $AuNPs^{Tyr@PMA}$ and 3.6 and 4.5, for $AgNPs^{Tyr@PTA}$ and $AgNPs^{Tyr@PMA}$, respectively even after extensive dialysis. Since these pH values are well below the pI value of tyrosine, it is expected that as soon as POMs (PTA or PMA) were added to the solutions containing $AuNPs^{Tyr}$ or $AgNPs^{Tyr}$ nanoparticles, the protonation of amine groups in the surface bound tyrosine molecules occurred and this enabled highly negatively charged POM molecules to bind electrostatically to $AuNPs^{Tyr}$ and $AgNPs^{Tyr}$ nanoparticles, resulting in $AuNPs^{Tyr@PTA}$ or $AgNPs^{Tyr@PTA}$ and $AuNPs^{Tyr@PMA}$ or $AgNPs^{Tyr@PMA}$ with zetapotential values of -35.5 and -46.3 ($AuNPs^{Tyr@PTA}$ and $AuNPs^{Tyr@PMA}$), or -35.0 and -38.8 ($AgNPs^{Tyr@PTA}$ and $AgNPs^{Tyr@PMA}$) respectively.

In the last step of surface functionalization (of $AuNPs^{Tyr@PTA}$ or $AuNPs^{Tyr@PMA}$ and $AgNPs^{Tyr@PTA}$ or $AgNPs^{Tyr@PMA}$), when lysine amino acid (pI – 9.74) was introduced to the solutions, the pH of the solutions returned back to 6.1 and 6.4 ($AuNPs^{Tyr@PTA}$ and $AuNPs^{Tyr@PMA}$), or 4.5 and 5.2 ($AgNPs^{Tyr@PTA}$ and $AgNPs^{Tyr@PMA}$) respectively after extensive dialysis. These pH values are significantly lower than the pI of lysine; therefore amine groups of lysine will be protonated at these pH values, which will enable lysine molecules to efficiently functionalize negatively charged $AuNPs^{Tyr@PTA}$ and $AuNPs^{Tyr@PMA}$ to form $AuNPs^{Tyr@PTA-Lys}$ and $AuNPs^{Tyr@PMA-Lys}$, or $AgNPs^{Tyr@PTA}$ and $AgNPs^{Tyr@PMA}$ to form $AgNPs^{Tyr@PTA-Lys}$ and $AgNPs^{Tyr@PMA-Lys}$ respectively. This is evident from a reduction in negative zetapotential values from -35.5 mV to -30.9 mV in

case of AuNPs$^{Tyr@PTA-Lys}$ and from -46.3 mV to -17.9 mV in case of AuNPs$^{Tyr@PMA-Lys}$. However, it should also be noted that the solution pH of lysine-functionalized materials is closer to the pI of tyrosine, which is likely to result in both the negatively and positively charged functional groups of tyrosine residues (zwitterionic state) activated at this pH. This may also potentially result in the rearrangement of the POM and lysine molecules, wherein due to the highly cationic nature of lysine molecules, it is likely that some of the lysine molecules are sequestered between tyrosine and POMs.

4.4.2. Estimation of metal content using AAS and ICP-MS studies

AAS and inductively coupled plasma mass spectroscopy (ICP-MS) analysis were employed to quantify metal content present in dialyzed nanoparticle solutions after their digestion with aqua regia. AAS analysis was carried out to estimate Au or Ag concentrations while ICP-MS was used to quantify tungsten (W) or molybdenum (Mo) concentrations present in functionalized nanoparticles samples. Existence of W and Mo in dialyzed nanoparticle solutions was in support of effective surface functionalization of Au and Ag nanoparticles since unbound POMs (W or Mo) have been removed during the dialysis process.

Furthermore, AAS and ICP-MS studies supported the possibility of molecular rearrangement in the nanoparticle surface corona from the quantification of tungsten (W from PTA) and molybdenum (Mo from PMA) in different samples for fixed amount of Au, which indicates that 27% w/w W (PTA molecules) and 56% w/w Mo (PMA molecules) were lost through lysine functionalization. Similarly, 60% w/w PTA molecules and 31% w/w PMA

molecules were lost during lysine functionalization of $AgNPs^{Tyr@PTA}$ to $AgNPs^{Tyr@PTA\text{-}Lys}$ and $AgNPs^{Tyr@PMA}$ to $AgNPs^{Tyr@PMA\text{-}Lys}$, respectively. Therefore, although it may appear from the zetapotential measurements that these sequentially functionalized nanomaterials bear an overall negative surface charge at the physiological pH (at which antimicrobial activities were assessed), the surfaces of these nanomaterials are rather complex and it is most likely that the amine groups of lysine will be protonated within this complex surface environment and may rather act as guiding molecules to facilitate their interaction with negatively charged bacterial cells.

4.4.3. UV-visible spectroscopic analysis of sequential surface functionalized nanoparticles

UV-visible absorption analysis of $AuNPs^{Tyr}$ and $AgNPs^{Tyr}$ nanoparticles, after their sequential surface functionalization with POMs and lysine, were carried out before and after dialysis. Further, it is noteworthy to mention that all nanoparticle absorbance spectra (Figure 4.2 and 4.3) are normalized against nanoparticle SPR absorbance maxima to have a fair assessment of surface functionalization.

Illustrated in Figure 4.2 are UV-visible absorbance spectra of $AuNPs^{Tyr}$ before and after their surface functionalization with PTA/lysine Figure 4.2 (A) and PMA/lysine Figure 4.2 (B), respectively. In UV-vis, there were no considerable changes in the position of the $AuNPs^{Tyr}$ or $AgNPs^{Tyr}$ plasmon absorption even after extensive dialysis, except the absence of pi-pi* absorption band around 280 nm due to the aromatic rings of tyrosine as discussed in chapter 3. Pristine $AuNPs^{Tyr}$ showed a SPR band with

maximum at 525 nm, which red shifted to 535 nm after their surface functionalization with PTA in AuNPs$^{Tyr@PTA}$, whereas no considerable changes were observed after lysine binding on the surface of AuNPs$^{Tyr@PTA}$ to form AuNPs$^{Tyr@PTA-Lys}$ Figure 4.2 (A). 10 nm shift in SPR band maxima position after PTA functionalization indicated binding of electron-rich PTA molecules to AuNPs^{Tyr} surface. Additionally, after surface functionalization of AuNPs^{Tyr} with PTA, AuNPs$^{Tyr@PTA}$ and AuNPs$^{Tyr@PTA-Lys}$ showed blue shifts in the absorbance maximum of PTA. For instance, pristine PTA molecules exhibited their absorbance maxima at 255* nm, which shifted to 250* nm in AuNPs$^{Tyr@PTA}$ and AuNPs$^{Tyr@PTA-Lys}$.

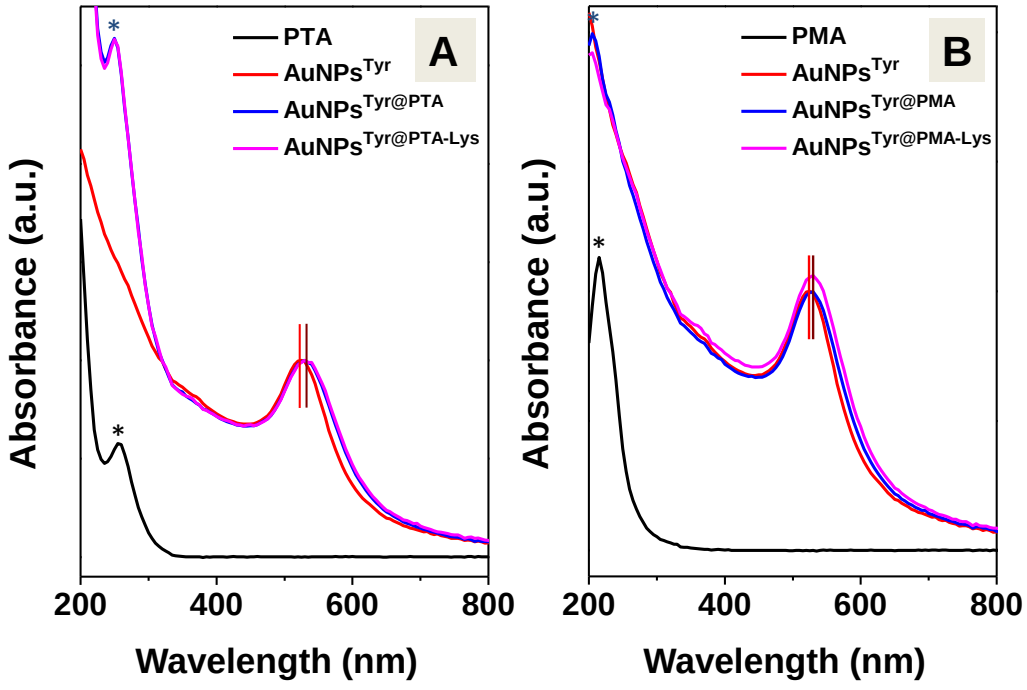

Figure.4.2. UV-visible absorbance spectra of AuNPs^{Tyr} and after their surface functionalization with (A) PTA/lysine and (B) PMA/lysine molecules

Illustrated in Figure 4.2 (B) are UV-visible absorbance spectra of pristine PMA, AuNPs^{Tyr}, AuNPs$^{Tyr@PMA}$ and AuNPs$^{Tyr@PMA-Lys}$, respectively. After surface functionalization of AuNPs^{Tyr} with PMA molecules, a 5 nm red

shift in the SPR band maxima position was observed and it showed an SPR band at 530 nm for both $AuNPs^{Tyr@PMA}$ and $AuNPs^{Tyr@PMA\text{-}Lys}$. This shift indicates surface modification of $AuNPs^{Tyr}$ with electron-rich PMA molecules. The similar blue shift, as discussed in the case of PTA functionalization, was observed in the case of PMA which shifted to 215* nm wherein the original position was found at 205* nm in Pristine PMA. The blue shift in the absorbance maximum of PTA and PMA molecules concomitant with the red shift of $AuNPs^{Tyr}$ SPR affirms the strong association of PTA and PMA molecules with the $AuNPs^{Tyr}$ surface.

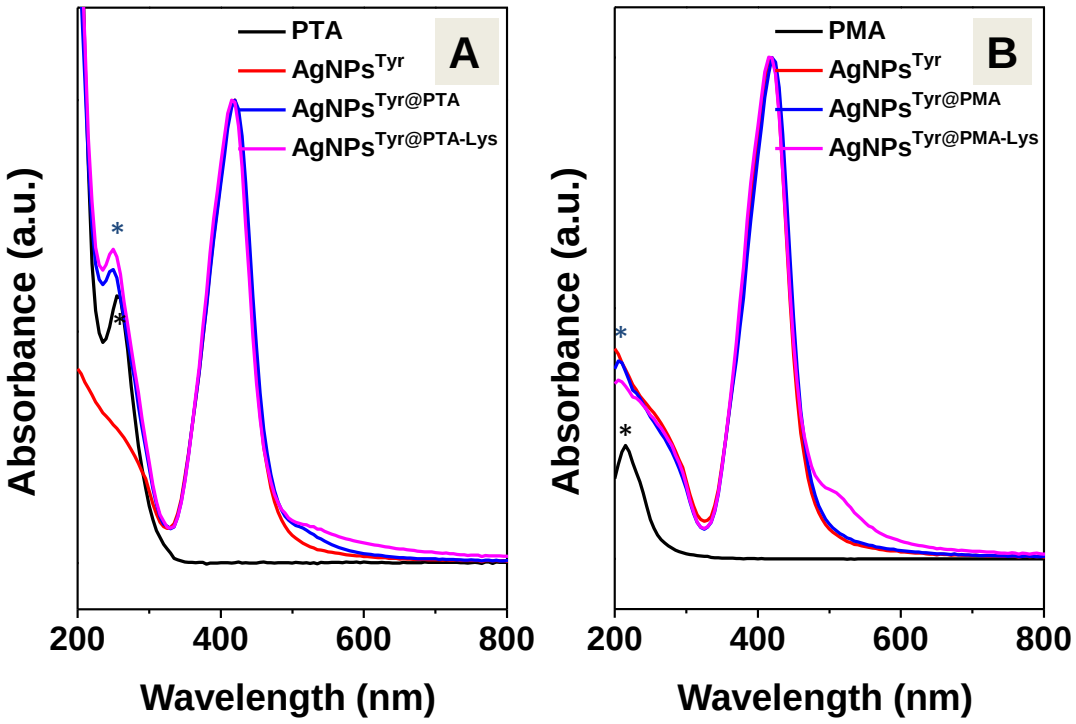

Figure.4.3. UV-visible absorbance spectra of $AgNPs^{Tyr}$ and after their surface functionalization with (A) PTA/lysine and (B) PMA/lysine molecules

UV-visible absorption spectroscopic analysis of $AgNPs^{Tyr}$ before and after dialysis was carried out and dialyzed spectra are presented in Figure 4.3 (A and B). Figure 4.3 (A) illustrates the UV-visible absorption spectra of $AgNPs^{Tyr}$ at different stages of surface functionalization with PTA and lysine

whereas Figure 4.3 (B) shows the similar stages of surface functionalization with PMA and lysine molecules.

Pristine $AgNPs^{Tyr}$ showed their SPR band with maximum at 420 nm, and modification of these $AgNPs^{Tyr}$ with POMs and lysine did not result in any significant spectral shifts in the SPR absorbance maxima. Although, there were no considerable changes in the position of SPR band maxima of $AgNPs^{Tyr}$ before and after their surface functionalization, post-POMs functionalization, all the functionalized nanoparticles displayed 5 to 10 nm blue shifts in the absorbance maximum of POMs. For instance, pristine PTA showed 5 nm shift from 255* nm to 250* nm in $AgNPs^{Tyr@PTA}$ and $AgNPs^{Tyr@PTA\text{-}Lys}$ Figure 4.3 (A), whereas pristine PMA exhibited 10 nm shift from 215* nm to 205* nm in $AgNPs^{Tyr@PMA}$ and $AgNPs^{Tyr@PMA\text{-}Lys}$ Figure 4.3 (B), respectively. Occurrence of additional absorbance bands of PTA and PMA along with the observed blue shift is an indication of the binding of electron-rich POMs molecules on the surface of tyrosine-capped $AgNPs^{Tyr}$.

It is believed that these POMs molecules (PTA or PMA) are strongly associated with the Au and Ag nanoparticle surface even after dialysis as discussed in the previous section during AAS and ICP-MS analysis. This was further confirmed employing FTIR and XPS studies and discussed in the later part of this chapter.

4.4.4. TEM and DLS measurements of functionalized Au and Ag nanoparticles

TEM images corresponding to sequentially surface functionalized $AuNPs^{Tyr}$ and $AgNPs^{Tyr}$ nanoparticles are illustrated in Figure 4.4 and 4.5,

respectively. Corresponding particle size histograms of respective nanoparticles are also illustrated in Figure 4.4 and 4.5, whereas inserted tables showe mean particles size and standard deviation for surface functionalized nanoparticles calculated using ImageJ software.

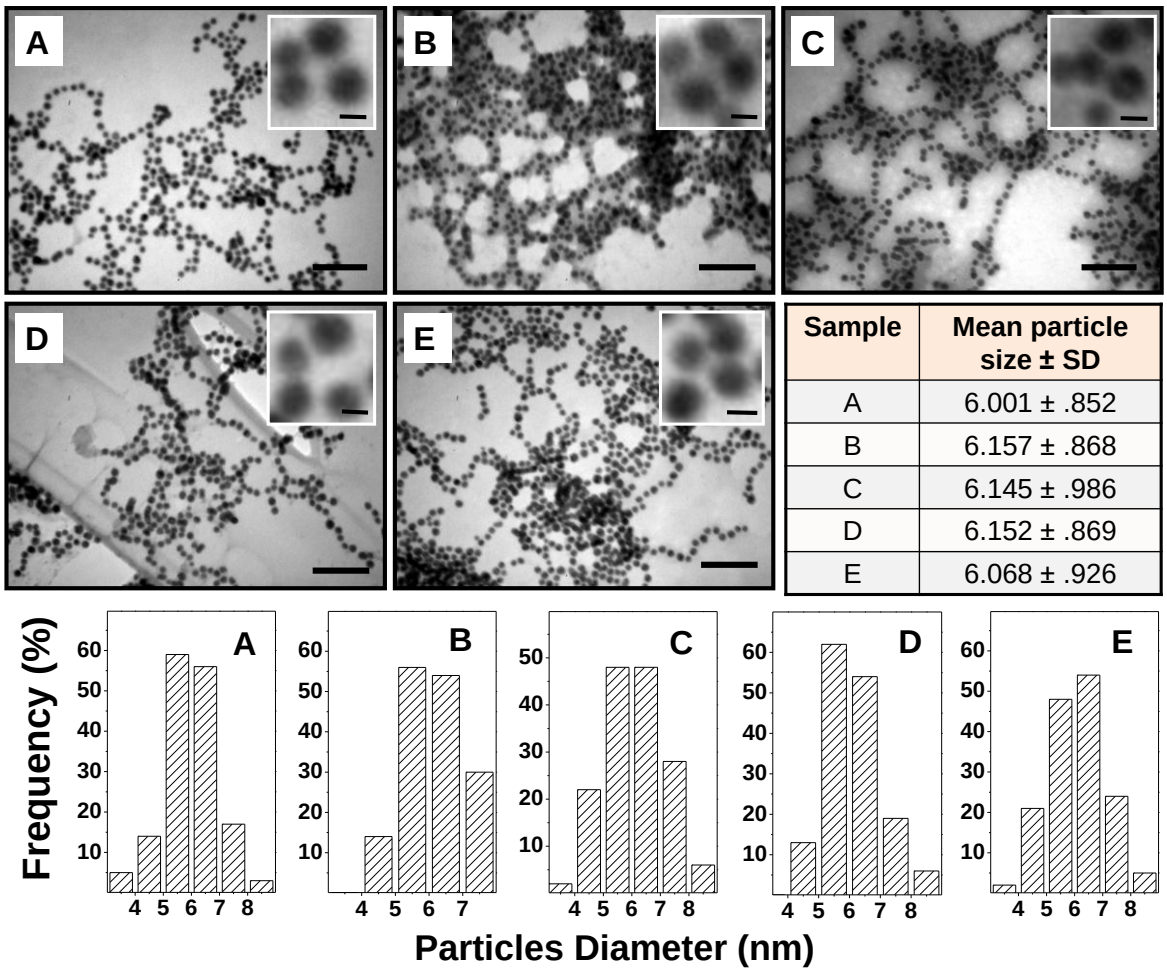

Sample	Mean particle size ± SD
A	6.001 ± .852
B	6.157 ± .868
C	6.145 ± .986
D	6.152 ± .869
E	6.068 ± .926

Figure.4.4. TEM images and particle size distribution histograms of (A) $AuNPs^{Tyr}$, (B) $AuNPs^{Tyr@PTA}$, (C) $AuNPs^{Tyr@PTA\text{-}Lys}$, (D) $AuNPs^{Tyr@PMA}$ and (E) $AuNPs^{Tyr@PMA\text{-}Lys}$. Scale bar correspond to 50 nm (Inset scale bar 5 nm)

TEM images revealed that $AuNPs^{Tyr}$ obtained using tyrosine amino acid as a reducing and capping agent are spherical in shape and these nanoparticles are highly monodispersed. These nanoparticles showed narrow size distribution and average diameter of these $AuNPs^{Tyr}$ is round of 6 nm with 0.85 standard deviation (Figure.4.4, A). It was interesting to

observe that AuNPs^{Tyr} maintained their monodispersity after their surface functionalization with POMs and lysine molecules. Even the size of sequential surface functionalized Au nanoparticles did not exhibit any significant changes in AuNPs$^{Tyr@PTA}$, AuNPs$^{Tyr@PTA-Lys}$, AuNPs$^{Tyr@PMA}$ and AuNPs$^{Tyr@PMA-Lys}$, respectively (Figure.4.4, B-E).

Furthermore, the TEM analysis of all these nanoparticles revealed that there was no aggregation, even after their surface functionalization with lysine, which is in good agreement with UV-vis spectroscopic analysis. The particle size distribution histograms are shown at the bottom of TEM images in Figure 4.4 A-E and average particle diameters are listed in table. It is reported that the shape and size of nanomaterials has considerable effect on nanomaterials biological activities.[16, 64-66] The spherical shape and good monodispersity in the size of all these functionalized Au nanoparticles excluded any such possibility of shape or size dependant antibacterial activity.

Dynamic light scattering (DLS) is an intensive and well-established technique to determine the size distribution profile of nanoparticles and DLS provides information about the hydrodynamic radii of nanoparticles in solution. Therefore, to confirm the hydrodynamic radii and surface functionalization of nanoparticles in solution, DLS analysis was carried out on all the functional Au nanoparticles. Interestingly, DLS measurements revealed that the average hydrodynamic radii of these nanoparticles corresponded to ca. 12-15 nm. Since DLS provides information about the hydrodynamic radii of nanoparticles in solution, an apparent increase in

AuNPs size from DLS over TEM measurements further confirmed successful functionalization of AuNPs with POMs and lysine.

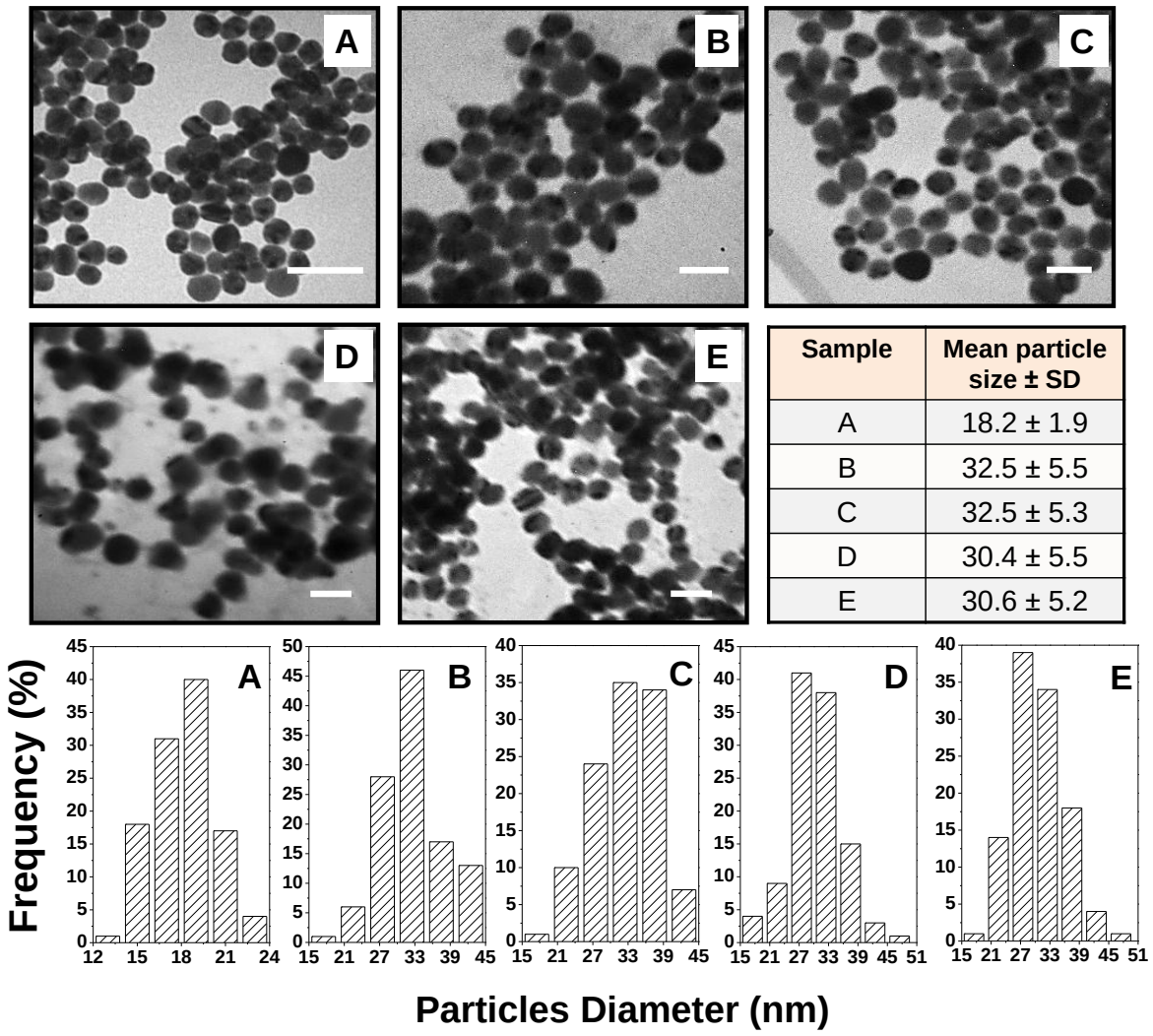

Sample	Mean particle size ± SD
A	18.2 ± 1.9
B	32.5 ± 5.5
C	32.5 ± 5.3
D	30.4 ± 5.5
E	30.6 ± 5.2

Figure.4.5. TEM images and corresponding particle size distribution histograms of (A) $AgNPs^{Tyr}$, (B) $AgNPs^{Tyr@PTA}$, (C) $AgNPs^{Tyr@PTA\text{-}Lys}$, (D) $AgNPs^{Tyr@PMA}$ and (E) $AgNPs^{Tyr@PMA\text{-}Lys}$. Scale bar correspond to 50 nm

TEM images corresponding to step-wise surface functionalization of tyrosine capped $AgNPs^{Tyr}$ are presented in Figure 4.5 (A-E) along with their particle size histograms. The tyrosine reduced $AgNPs^{Tyr}$ are spherical in shape with an average diameter of around 18.2 nm with 1.9 nm standard deviation as illustrated in Figure.4.5, A. After surface functionalization of these $AgNPs^{Tyr}$ with PTA and PMA molecules average diameter of resulted

nanoparticles increase in $AgNPs^{Tyr@PTA}$ and $AgNPs^{Tyr@PMA}$ to 32.5 ± 5.5 and 30.4 ± 5.5 nm for respectively. The increase in the average particles size suggests effective surface functionalization of Ag nanoparticles with PTA and PMA molecules, thus confirming UV-vis absorption spectroscopy results. After lysine functionalization of $AgNPs^{Tyr@PTA}$ and $AgNPs^{Tyr@PMA}$ the average particle size in $AgNPs^{Tyr@PTA\text{-}Lys}$ and $AgNPs^{Tyr@PMA\text{-}Lys}$ were found to be 32.5 ± 5.3 and 30.6 ± 5.2 nm, respectively.

Furthermore, it can be clearly seen in TEM images that there were no signs of aggregation after POMs and lysine binding on the surface of $AgNPs^{Tyr}$. Additionally, DLS analysis was carried out on $AgNPs^{Tyr}$, $AgNPs^{Tyr@PTA}$, $AgNPs^{Tyr@PMA}$, $AgNPs^{Tyr@PTA\text{-}Lys}$ and $AgNPs^{Tyr@PMA\text{-}Lys}$ to validate TEM results. Interestingly, DLS measurements revealed that the average hydrodynamic radii at the initial stage of functionalization was 19.9 nm (hydrodynamic diameter ≈40 nm) in $AgNPs^{Tyr}$, which increased to 28.2 and 21.1 nm in $AgNPs^{Tyr@PTA\text{-}Lys}$ and $AgNPs^{Tyr@PMA\text{-}Lys}$ respectively, at the final stage of surface functionalization. Thus, increase in the hydrodynamic radii confirms surface functionalization of $AgNPs^{Tyr}$.

4.4.5. FTIR spectral analysis to understand surface corona of functionalized nanoparticles

FTIR spectroscopy was employed to elucidate the surface functionalization of different species onto $AuNPs^{Tyr}$ and $AgNPs^{Tyr}$. Additionally, FTIR spectroscopy provides experimental evidence that the amino acids and POMs used for sequential functionalization of Au and Ag

nanoparticles constructs a stable corona that remains present on the surface of nanoparticles even after extensive dialysis.

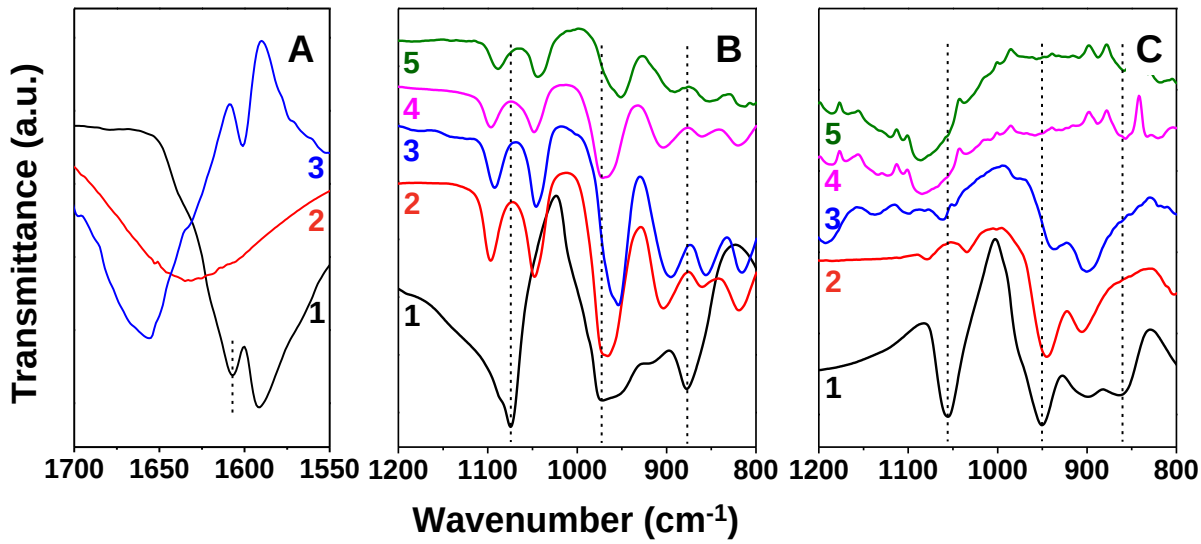

Figure.4.6. FTIR spectra in Panel A: tyrosine, AuNPs^{Tyr} and AgNPs^{Tyr}; in Panel B: PTA, AuNPs$^{Tyr@PTA}$, AuNPs$^{Tyr@PTA-Lys}$, AgNPs$^{Tyr@PTA}$ and AgNPs$^{Tyr@PTA-Lys}$; and in Panel C: PMA, AuNPs$^{Tyr@PMA}$, AuNPs$^{Tyr@PMA-Lys}$, AgNPs$^{Tyr@PMA}$ and AgNPs$^{Tyr@PMA-Lys}$, respectively

Illustrated in Figure 4.6 are FTIR spectra of pure tyrosine amino acid and tyrosine capped Au and Ag nanoparticles (Panel A), pristine PTA and PTA surface functionalized Au or Ag nanoparticles (Panel B) and pristine PMA and PMA surface functionalized Au or Ag nanoparticles (Panel C). FTIR analysis presents clear evidence that the carbonyl stretching vibration from the carboxylate ion in tyrosine shifts from 1608 cm^{-1} (in the case of pristine tyrosine, Figure 4.6-A, curve 1) to 1632 cm^{-1} in AuNPs^{Tyr} (Figure 4.6-A, curve 2) and 1656 cm^{-1} AgNPs^{Tyr} (Figure 4.6-A, curve 3). This shift may be attributed to formation of a quinone type structure on the surface of Au and Ag nanoparticles due to oxidation of the phenolic group in tyrosine while tyrosine molecules act as reducing agent for $[AuCl_4]^-$ and Ag^+ ions, as shown in the Figure 4.7.[63, 67]

Further, binding modes of PTA and PMA molecules on the surface of tyrosine capped Au and Ag nanoparticles were analysed by comparing the FTIR spectra originating from pristine POMs molecules (PTA or PMA respectively) and spectra coming from the POMs functionalized Au and Ag nanoparticles as shown in Figure 4.6 (Panel B and C). The Keggin structures of POMs (PTA – $H_3PW_{12}O_{40}$ and PMA – $H_3PMo_{12}O_{40}$) consist of a cage of either tungsten (W) or Molybdenum (Mo) atoms linked by oxygen atoms with the phosphorus atom at the centre of the tetrahedra.[68-71]

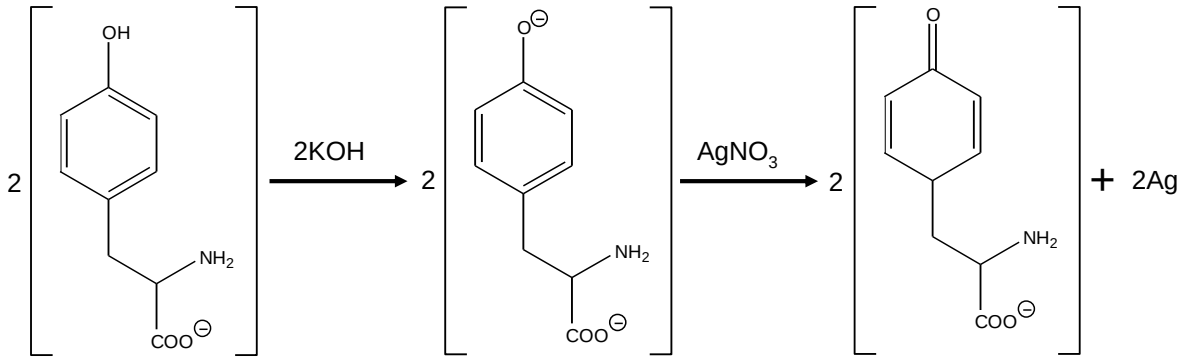

Figure.4.7. Schematic representation of formation of quinone type structure during reduction of Ag^+ ions

Oxygen atoms form distinct bonds both in case of PTA (P–O, W–O–W, and W=O) and PMA (P–O, Mo–O–Mo, and Mo=O) within their Keggin structure, which have distinguishable infrared vibrational frequencies. Wherein, P–O (1075 cm^{-1} and 1058 cm^{-1} for PTA and PMA, respectively) corresponds to an asymmetric stretching vibrational mode between phosphorus and oxygen atoms at the center of the Keggin structure; W–O–W or Mo–O–Mo (874 cm^{-1} or 864 cm^{-1} for PTA and PMA, respectively) corresponds to bending vibrational modes of oxygen atoms that form a bridge between the two W or Mo atoms within the Keggin structure; and

W=O or Mo=O (972 cm^{-1} or 950 cm^{-1} for PTA and PMA, respectively) corresponds to the asymmetric stretching of terminal oxygen atoms.

The binding of PTA and PMA molecules on the surface of tyrosine capped Au and Ag nanoparticles is evident from the shifts observed in the vibrational modes of PTA and PMA molecules originating from POMs surface functionalized Au and Ag nanoparticles. For instance, FTIR spectral signature of pristine PTA for P-O, W-O and W-O-W appeared at 1075, 972 and 874 cm^{-1}, respectively (Figure 4.6-B, curve 1), whereas the FTIR spectral signatures appeared at 1097, 966 and 861 cm^{-1} for $AuNPs^{Tyr@PTA}$ (Figure 4.6-B, curve 2) and at 1097, 971 and 860 cm^{-1} for $AgNPs^{Tyr@PTA}$, respectively (Figure 4.6-B, curve 4). Likewise, notable FTIR spectral signature of pristine PMA for P-O, Mo-O and Mo-O-Mo appeared at 1058, 950 and 864 cm^{-1} (Figure 4.6-C curve 1) whereas the similar FTIR spectral signatures were found at 1078, 944 and 849 cm^{-1} for $AuNPs^{Tyr@PMA}$ (Figure 4.6-C curve 2) and at 1085, 958 and 857 cm^{-1} for $AgNPs^{Tyr@PMA}$, respectively (Figure 4.6-C curve 4).

Subsequently, lysine functionalization of $AuNPs^{Tyr@PTA}$ and $AgNPs^{Tyr@PTA}$ leading to form $AuNPs^{Tyr@PTA-Lys}$ and $AgNPs^{Tyr@PTA-Lys}$ was also established by observed shifts in comparing the FTIR spectra. In case of $AuNPs^{Tyr@PTA-Lys}$ distinguished FTIR spectral signature of PTA molecules showed additional changes and originated at 1062, 938 and 850 cm^{-1} (Figure 4.6-B curve 3), while corresponding signature of $AgNPs^{Tyr@PTA-Lys}$ instigated at 1089, 951 and 852 cm^{-1}, respectively (Figure 4.6-B curve 5). Further functionalization of $AuNPs^{Tyr@PMA}$ with lysine leading to form $AuNPs^{Tyr@PMA-Lys}$ was confirmed by FTIR spectra of these samples since

distinguished features emerged at 1062, 938 and 850 cm^{-1}, respectively(Figure 4.6-C curve 3). These additional shifts observed after lysine functionalization provide evidence that these nanoparticles were effectively surface functionalized with lysine amino acid.

These vibrational shifts were in agreement to those previously reported, indicating the complexation of tyrosine and lysine amino acids with POMs, leading to an amino acid-POM salt-like structure.[72] Therefore, FTIR spectroscopy provides strong evidence that the amino acids and POMs used for sequential functionalization of Au and Ag nanoparticles provide a stable surface corona around nanoparticles.

4.4.6. XPS analysis of POMs and lysine functionalized nanoparticles

XPS analysis was carried out to understand surface chemistry of these functionalized Au and Ag nanoparticles. Furthermore, the presence of zerovalent colloidal gold (Au^0) and silver (Ag^0) in all the samples as well as existence of tungsten (W) or molybdenum (Mo) containing PTA or PMA molecules, were confirmed by XPS analysis. The Au4f, C1s, W4f and Mo4f core levels recorded from the XPS and representative spectra are illustrated in Figure 4.8. All these spectra have been background corrected using Shirley algorithm [73] prior to curve resolution and the core levels are aligned with respect to the adventitious C1s BE of 285 eV.[63, 74-77]

The Au4f core level spectra of all the Au based samples are illustrated in Figure4.8 (A-E) and all these spectra could be stripped into two chemically distinct spin-orbit pairs. The chemically distinct components are

observed at 83.5 eV and 85.7 eV. The Au4f signal at the lower BE $Au4f_{7/2}$ (83.5) is attributed to fully reduced metallic $AuNPs^{Tyr}$. Conversely, is was interesting to detect the presence of a smaller higher BE component (at 85.7 eV) in all the samples, which indicated the presence of small amount of unreduced $[AuCl_4]$- ions absorbed on the surface of metallic $AuNPs^{Tyr}$ and even extensive dialysis could not remove these ions due to strong electrostatic complexation with amino acids.[78]

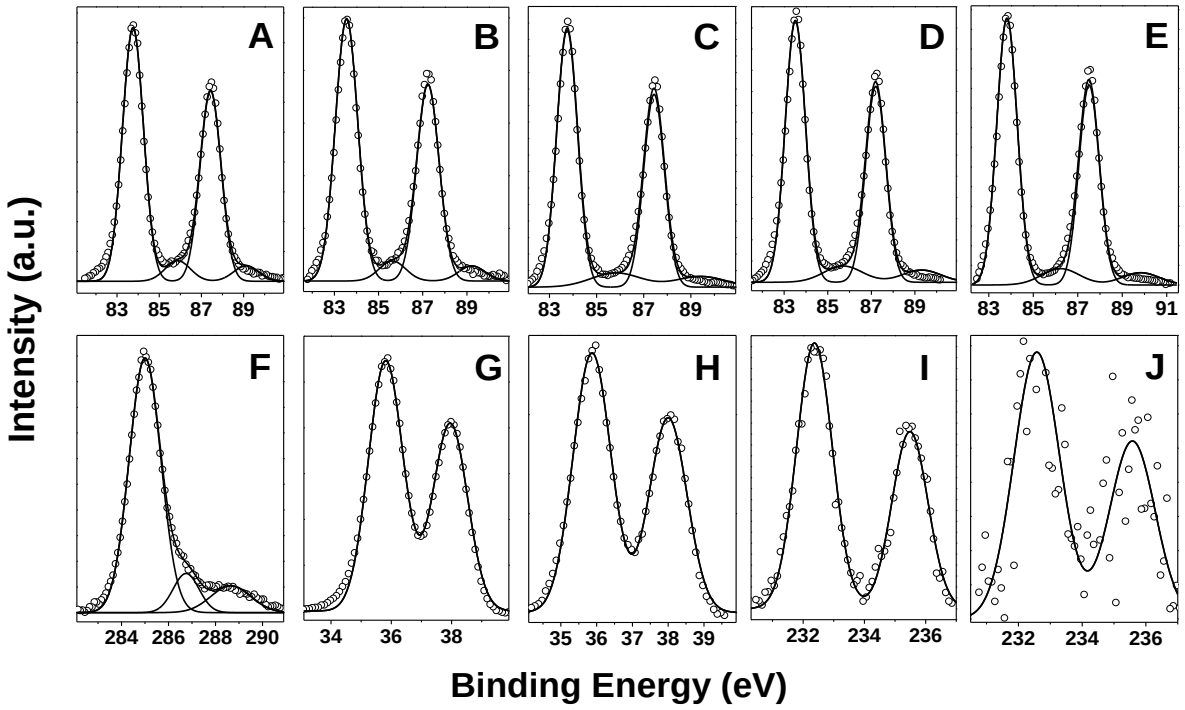

Figure.4.8. Core level spectra of Au4f (A-E), recorded in $AuNPs^{Tyr}$, $AuNPs^{Tyr@PTA}$, $AuNPs^{Tyr@PTA\text{-}Lys}$, $AuNPs^{Tyr@PMA}$ and $AuNPs^{Tyr@PMA\text{-}Lys}$ samples, respectively. Core level spectra of C1s (F), W4f (G-H), Mo4f (I-J) recorded in $AuNPs^{Tyr}$, $AuNPs^{Tyr@PTA}$, $AuNPs^{Tyr@PTA\text{-}Lys}$, $AuNPs^{Tyr@PMA}$ and $AuNPs^{Tyr@PMA\text{-}Lys}$, respectively

The C1s core level spectra recorded from the $AuNPs^{Tyr}$ could be decomposed into three main chemically distinct components at 285, 286.6 and 288.8 eV (Figure 4.8-F). The higher BE component observed at 288.8 eV can be assigned to the carboxylate carbon and 286.6 eV BE peak is

attributed to the C-N and C-O species present in tyrosine amino acid bound to nanoparticle surface. Furthermore, as shown in Figure 4.8 (G-H), W4f signals obtained from PTA functionalized $AuNPs^{Tyr@PTA}$ and $AuNPs^{Tyr@PTA\text{-}Lys}$ nanoparticles, respectively. Similarly, Figure 4.8-I and J illustrate Mo4f signals acquired from PMA surface functionalized $AuNPs^{Tyr@PMA}$ and $AuNPs^{Tyr@PMA\text{-}Lys}$, respectively. Presence of additional signals of W4f and Mo4f in successively functionalized nanoparticles confirmed that tyrosine-capped Au nanoparticles are effectively coated with PTA and PMA molecules in their respective samples.

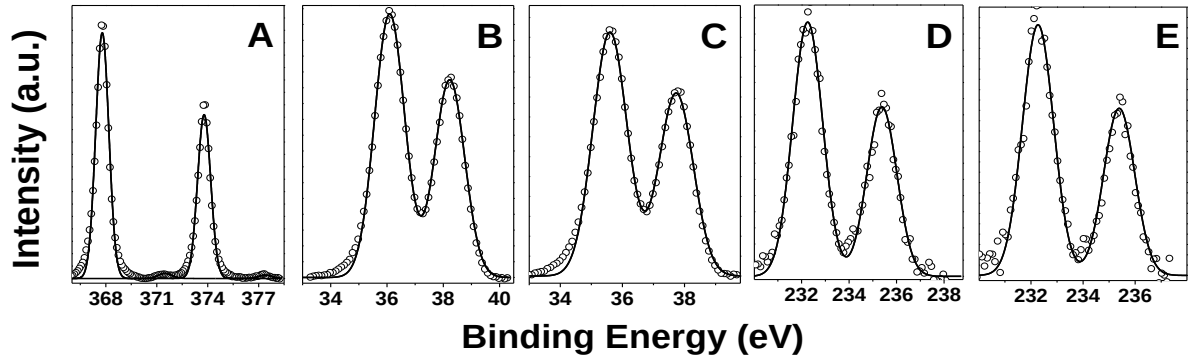

Figure.4.9. Core level spectra of Ag3d (A), W4f (B-C), Mo4f (D-E) recorded in $AgNPs^{Tyr}$, $AgNPs^{Tyr@PTA}$, $AgNPs^{Tyr@PTA\text{-}Lys}$, $AgNPs^{Tyr@PMA}$ and $AgNPs^{Tyr@PMA\text{-}Lys}$ samples, respectively

The core level XPS spectrum of Ag3d originated from the tyrosine capped Ag nanoparticles is illustrated in Figure 4.9 (A). The Ag3d spectrum could be decomposed into two chemically distinctive spin-orbit pairs. Two chemically distinct BEs for Ag3d appeared at 368 and 371.5 eV, respectively. Here, the low BE component is attributed to metallic silver nanocore, whereas the high BE component arises from the unreduced ions, indicating that small fraction of silver ions remain bound to the surface of Ag nanoparticles. Similar to $AuNPs^{Tyr}$, C1s core level spectra recorded from

the surface of $AgNPs^{Tyr}$ could be decomposed into three chemically distinct components, as discussed earlier. Moreover, Figure 4.9 (B-E) showed W4f and Mo4f signals obtained from PTA and PMA functionalized Ag nanoparticles confirming the presence of W and Mo in respective samples which verifies that this functionalized strategy produced effectively and stable surface corona around nanoparticles.

4.5. Antibacterial applications of functionalized nanoparticles

Presence and stability of functional molecules (POMs and lysine) on the surface of Au and Ag nanoparticles were confirmed by various physicochemical characterisation techniques. Once, it was established that strategy employed in sequentially surface functionalization, resulted in well-controlled functional nanoparticulate systems with different surface functionalities, the antibacterial potential of these functionalized nanomaterials were evaluated against Gram negative bacterium *E. coli*.

4.5.1. Assessment of antibacterial activities of gold, silver and their POMs and lysine functionalized nanoparticles

Metallic Au nanoparticles are predominantly considered highly biocompatible as discussed,[17] whereas POMs such as PTA or PMA molecules are considered toxic to the cells due to the presence of toxic heavy metals in their structure such as tungsten (W) and molybdenum (Mo), respectively.[58, 79] It has been reported that in combination with β-lactam, polyoxotungstates, enhance the antibiotic efficiency against otherwise resistance strains of bacteria.[61] Moreover, due to their specific three-dimensional structure and high negative charge, POMs might selectively

bind to the positive patches of proteins. Whereas, presence of cationic lysine molecules in the corona, may guide these nanoparticles toward negatively charged bacterial cells, which may result in higher antibacterial activity. Therefore, it is interesting to investigate the toxicity of sequentially surface functionalized materials in a concentration-dependent manner. Since, $AuNPs^{Tyr}$ did not exhibit any significant toxicity toward *E. coli*, as established in previous chapter (III), the amount of W or Mo were kept constant in different samples to investigate toxicity of surface functionalized Au nanoparticles. Furthermore, since $AuNPs^{Tyr}$ did not contain any W or Mo, the amount of $AuNPs^{Tyr}$ used as respective controls was equivalent to the highest amount of Au present as shown in Table 4.1 below.

Sample Name	Metal concentrations (μM) used for antibacterial studies							
	Au	W or Mo	Au	W or Mo	Au	W or Mo	Au	W or Mo
$AuNPs^{Tyr}$	16.25	0	32.50	0	81.25	0	162.5	0
$AuNPs^{Tyr@PTA}$	1.86	1	3.72	2	9.3	5	18.6	10
$AuNPs^{Tyr@PTA-Lys}$	2.55	1	5.10	2	12.75	5	25.5	10
$AuNPs^{Tyr@PMA}$	7.24	1	14.48	2	36.2	5	72.4	10
$AuNPs^{Tyr@PMA-Lys}$	16.04	1	32.08	2	80.2	5	160.4	10

Table.4.1. Relative concentrations of Au and W or Mo present on the surface of functionalized Au nanoparticles, as used for antibacterial studies

Illustrated in Figure 4.10-A and B are antibacterial activities of nanoparticles at each step of surface functionalization involving PTA or PMA and lysine molecules. $AuNPs^{Tyr}$ were found to be non-toxic to the *E. coli* cells even at the highest concentration (162.5 μM) used for antibacterial studies and bacterial cell viability was found over 93%, indicating that surface capping of AuNPs with oxidized tyrosine amino acid residues during their

synthesis does not significantly manipulate their biocompatible nature. However, surface functionalization of these nanoparticles with POMs rendered them antibacterial active and further surface modification with cationic amino acid lysine enhanced their antibacterial potential significantly (Figure 4.10-A and B). This is evident from comparing the antibacterial activity of different materials at a particular POMs concentration.

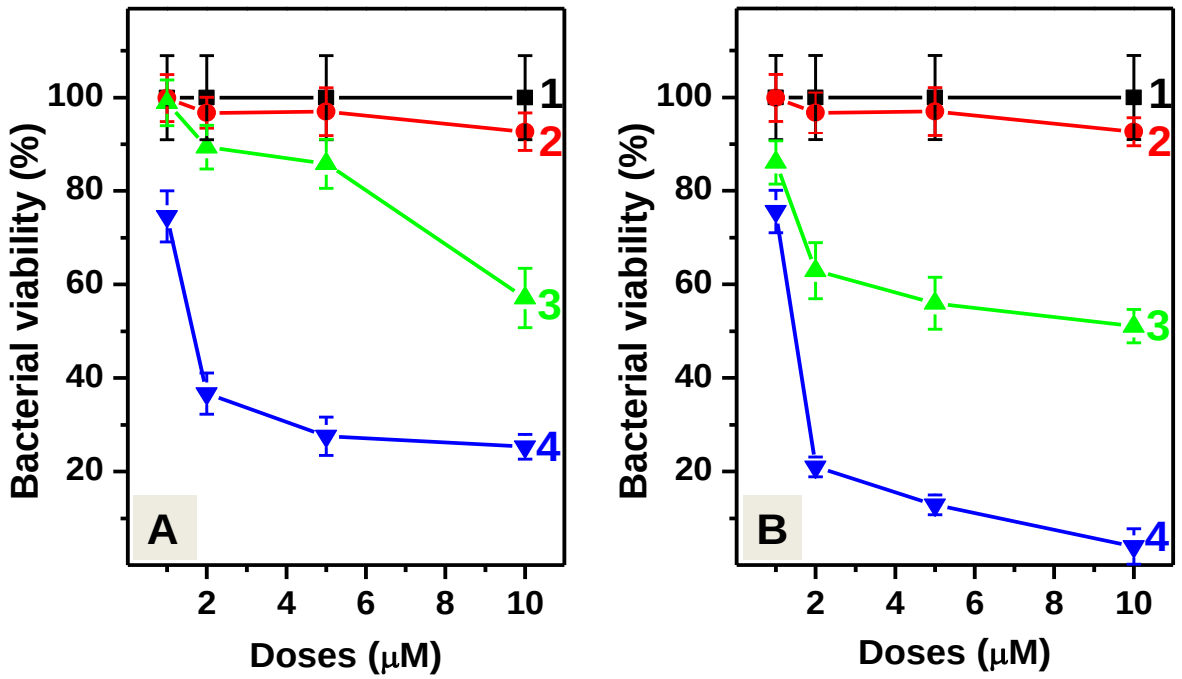

Figure.4.10. Dose dependent antibacterial activity of PTA (Panels A), PMA (Panels B) and lysine functionalized Au nanoparticles

For instance, as shown in Figure 4.10-A at a fixed W concentration of 10 μM, $AuNPs^{Tyr}$ cause ca. 7% bacterial cell death (Figure 4.10-A Curve 2), which increases to 43% in the case of $AuNPs^{Tyr@PTA}$ (Figure 4.10-A Curve 3) with a further increase to more than 75% cell death by $AuNPs^{Tyr@PTA\text{-}Lys}$ (Figure 4.10-A Curve 4). In comparison to PTA, equivalent amount of PMA (10 μM) exhibited higher antibacterial activity as shown in Figure 4.10-B.

$AuNPs^{Tyr@PMA}$ (Figure 4.10-B Curve 3) caused ca. 49% bacterial cell death which increased to 96% after treatments with $AuNPs^{Tyr@PMA-Lys}$ (Figure 4.10-B Curve 4). It is remarkable that at the highest concentration of 10 μM PMA used, the same concentration of lysine functionalization ($AuNPs^{Tyr@PMA-Lys}$) resulted in almost doubling the antibacterial potential of $AuNPs^{Tyr@PMA}$. Captivatingly, the difference in the antibacterial profile of $AuNPs^{Tyr@PTA}$ and $AuNPs^{Tyr@PTA-Lys}$ (Figure 4.10-A) at lower concentration of W (e.g. 2 μM) is even more remarkable suggesting that lysine functionalization may enhance the antibacterial efficiency by almost seven times. Furthermore, to investigate whether this increase in toxicity arises from the cationic nature of lysine which might assist in improving the interaction of nanomaterials with negatively charged bacterial cell wall, control experiments were performed under same experimental conditions wherein bacterial cells were incubated directly with lysine amino acid; however no significant toxicity was observed.

Since POMs and lysine functionalization have capability to modify the biocompatible nature of Au nanoparticles, these molecules may also provide an opportunity to work with Ag nanoparticles in a synergistic manner to enhance their intrinsic antibacterial activity. As discussed, Ag nanoparticles are regarded as antibacterial agent by their nature due to their interaction with cellular proteins, enzymes and nucleic acid. Therefore, it is fascinating to explore their antibacterial potential after their surface functionalization with POMs and lysine molecules. Therefore, toxicity of sequentially surface functionalized Ag nanoparticles has been investigated in a dose-dependent manner. To evaluate antibacterial performance of functionalized Ag

nanoparticles, a different strategy has been adopted compared to functionalized Au nanomaterials. Since $AgNPs^{Tyr}$ are antibacterial active, in this approach amount of Ag was kept constant in all the nanoparticles samples and effect of surface functionalization and stable corona was observed comparatively. The amount of metals present in respective nanoparticles samples used for antibacterial activities are illustrated below in Table 4.2.

Sample Name	Metal concentrations (μM) used for antibacterial studies							
	Ag	W or Mo	Ag	W or Mo	Ag	W or Mo	Ag	W or Mo
$AgNPs^{Tyr}$	1	0	2	0	5	0	0	0
$AgNPs^{Tyr@PTA}$	1	2.38	2	4.76	5	11.9	10	23.8
$AgNPs^{Tyr@PTA-Lys}$	1	1.63	2	3.26	5	8.15	10	16.3
$AgNPs^{Tyr@PMA}$	1	0.51	2	1.02	5	2.55	10	5.10
$AgNPs^{Tyr@PMA-Lys}$	1	0.16	2	0.32	5	0.80	10	3.20

Table.4.2. Relative concentrations of Ag and W or Mo present on the surface of functionalized Ag nanoparticles, as used for antibacterial studies

Illustrated in Figure 4.11-A is antibacterial performance of different Ag nanoparticles involving PTA in one of the functionalization steps while Figure 4.11-B compares those involving PMA in surface functionalization steps. It is not ideal to evaluate the effects of surface functionalization at 5 or 10 μM Ag concentrations since at higher doses $AgNP^{Tyr}$ exhibited significantly high level of antibacterial activity. Whereas, at lower amount of doses (1 or 2 μM) antibacterial performances are significantly different and reveals the effect of surface functionalization. This is evident from comparing the antibacterial activity of different nanoparticles at a particular Ag concentration. For instance, at a fixed Ag dose of 1 μM, $AgNPs^{Tyr}$ cause ca.

36 % bacterial cell death, which increases up to 85 % in the case of $AgNPs^{Tyr@PTA}$ with further slight increase after lysine funtionalization. The similar trend was observed for 2 and 5 μM as shown in Figure 4.11-A.

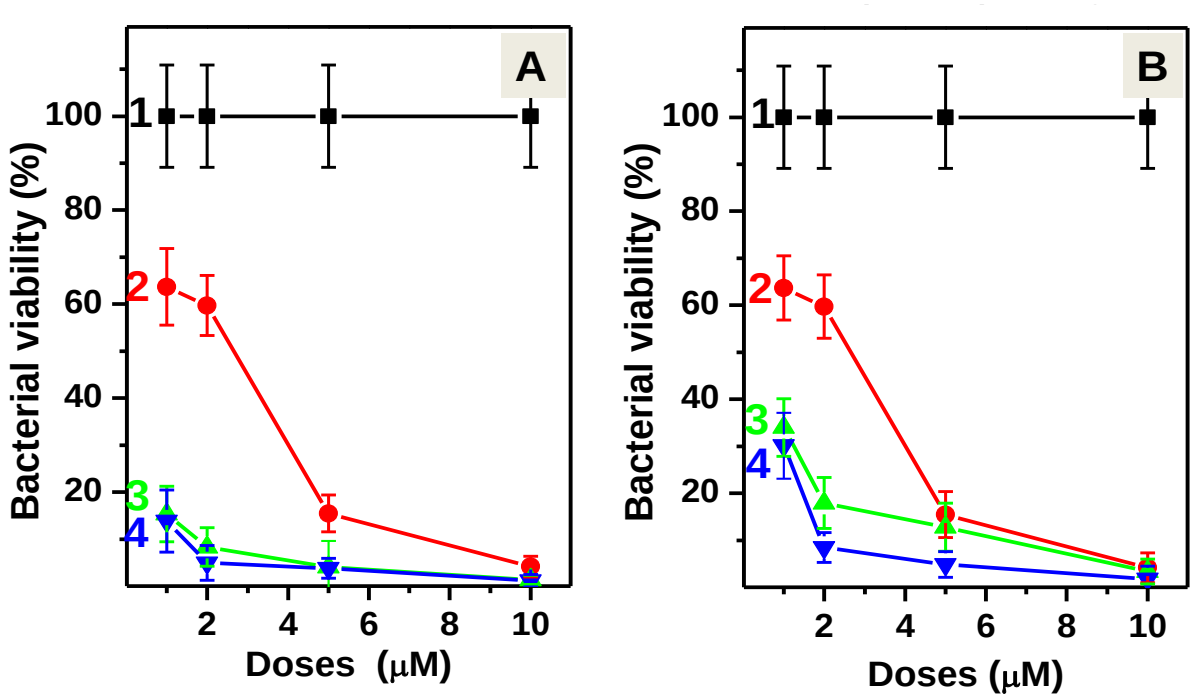

Figure.4.11. Dose dependent antibacterial activity of PTA (Panels A), PMA (Panels B) and lysine functionalized Ag nanoparticles

In comparison to PTA functionalized Ag nanoparticles at constant Ag concentration PMA functionalized Ag nanoparticles exhibited less antibacterial activity, ca. 66 % and 70 % bacterial cell death after treatments with $AgNPs^{Tyr@PMA}$ and $AgNPs^{Tyr@PMA\text{-}Lys}$, respectively. Here, it must be taken in account that loading of PMA molecules on the surface of $AgNPs^{Tyr}$ compared to PTA molecules is comparatively less as illustrated in Table 4.2, hence the amount of PMA present on the identical dose of Ag nanoparticles (ca.1 μM) was comparatively less. Furthermore, the effect of lysine functionalization was not as significant as was observed in the case of functionalized Au nanoparticles. Although, a slight influence of lysine

modification was observed and it was prominent at 2 and 5 μM concentrations in PMA functionalized system as illustrated in Figure.4.11 (B).

4.5.2. Morphological changes in bacterial cell after their treatments with gold, silver and functionalized nanoparticles

Physical integrity of bacterial cell is imperative for its survival and to overcome environmental changes and stress. Therefore, the morphological changes occurring in bacterial cells after their interaction with Au, Ag nanoparticles and their POMs and lysine functionalized nanoparticles, were visualized under Nano-SEM as shown in Figure 4.12 and 4.13.

The SEM images of bacteria without treatment (Figure 4.12-A) and those treated with $AuNPs^{Tyr}$ (Figure 4.12-B) were almost similar, showing an intact cell architecture with an oval morphology, thereby supporting the fact that $AuNPs^{Tyr}$ were non-toxic to bacteria. However treatment of bacteria with POMs- (Figure 4.12 C and E) and lysine-modified nanoparticles (Figure 4.12 D and F) for 20 min reveal distinct morphological changes indicative of significant damage to the bacterial cell integrity. The higher level of damage caused to the bacterial cells by lysine-functionalized materials in comparison to those functionalized only with POMs (PTA or PMA) is also evident.

For example, $AuNPs^{Tyr@PTA}$ (Figure 4.12C) or $AuNPs^{Tyr@PMA}$ (Figure 4.12 E) treatment of bacterial cells resulted in reduction in the bacterial cell thickness (from original ca. 1 μm to ca. 500 nm) along with significant roughening of the bacterial cell, which clearly suggests the disruption of

bacterial cell wall and membrane. In comparison, AuNPs$^{Tyr@PTA-Lys}$ (Figure 4.12 D) and AuNPs$^{Tyr@PMA-Lys}$ (Figure 4.12 F) treatment resulted in further damage to bacteria, wherein sub-cellular components of bacteria discharged due to complete disintegration of the bacterial and bacterial cells become indiscernible. Further, the most prominent effect of AuNPs$^{Tyr@PMA-Lys}$ against *E. coli* in comparison to other nanoparticle systems is also evident from the comparison of these Nano-SEM micrographs. From antimicrobial experiments and Nano-SEM imaging of bacterial cells, it is clear that Au nanoparticles sequentially surface functionalized with POMs and lysine cause irreversible bacterial cell damage and ultimate cell death by disrupting the integrity of bacterial cell wall and membrane.

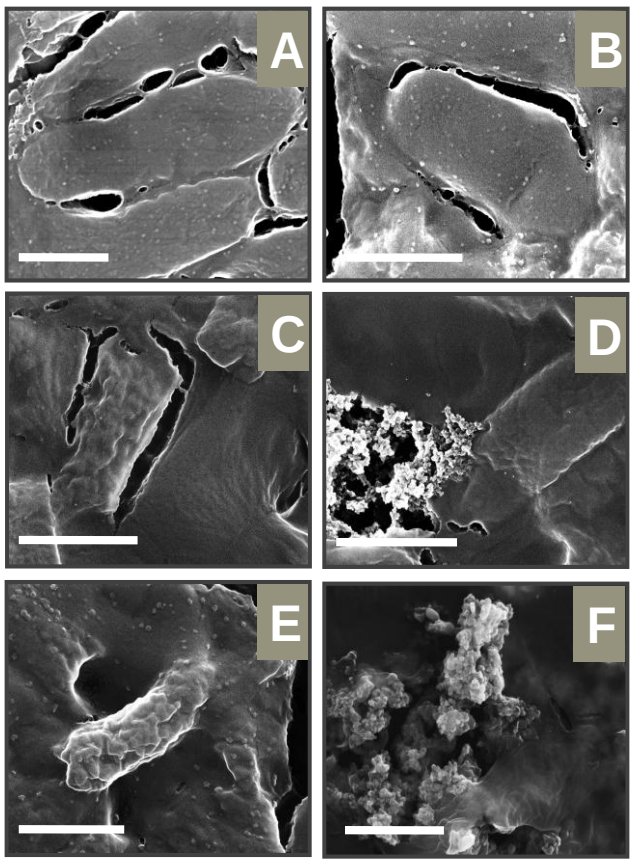

Figure.4.12. SEM micrographs of *Escherichia coli* cells (A) untreated and after their treatments with (B) AuNPs^{Tyr}, (C) AuNPs$^{Tyr@PTA}$, (D) AuNPs$^{Tyr@PTA-Lys}$, (E) AuNPs$^{Tyr@PMA}$, and (F) AuNPs$^{Tyr@PMA-Lys}$. (Scale bars 1 µm)

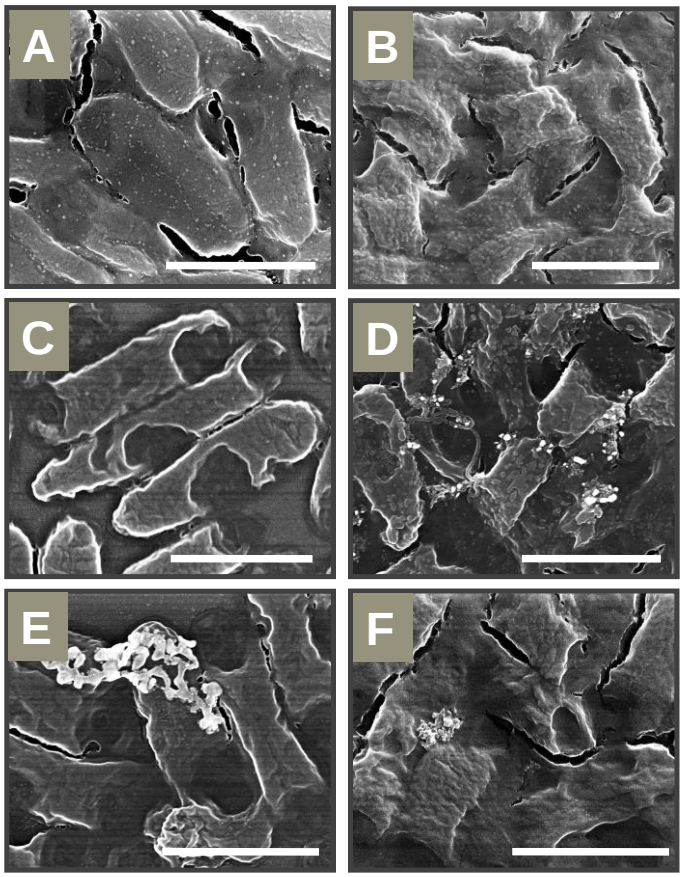

Figure.4.13. SEM micrographs of *Escherichia coli* cells (A) untreated and after treatments with (B) AgNPs^{Tyr}, (C) AgNPs$^{Tyr@PTA}$, (D) AgNPs$^{Tyr@PTA\text{-}Lys}$, (E) AgNPs$^{Tyr@PMA}$, and (F) AgNPs$^{Tyr@PMA\text{-}Lys}$. (Scale bars correspond to 2 µm)

Illustrated in Figure 4.13 are Nano-SEM micrographs of bacterial cells before and after their treatments with different Ag based nanoparticles revealing mode of interaction of different nanomaterials with bacterial cells. AgNPs^{Tyr} treated bacterial cells (Figure 4.13 B) reveal distinct morphological changes, in contrast to untreated bacterial cells (Figure 4.13 A). After treatments with AgNPs^{Tyr}, the cell wall of bacteria was dissolved and significant damage was observed to the bacterial cell integrity. Furthermore, broken bacterial cell are visible with distinct morphology and patchy cells. Functionalization of AgNPs^{Tyr} with PTA molecules created big holes in

bacterial cells (Figure 4.13 C). Additional functionalization of these AgNPs$^{Tyr@PTA}$ nanoparticles with cationic lysine, enhanced level of damage and along with big holes, small broken pieces of bacterial cells and patchy morphology are clearly detectable in nano-SEM micrograph (Figure 4.13 D) Similarly, Figure 4.13 E and F demonstrate bacterial images of AgNPs$^{Tyr@PMA}$ AgNPs$^{Tyr@PMA-Lys}$ treated bacterial cells.

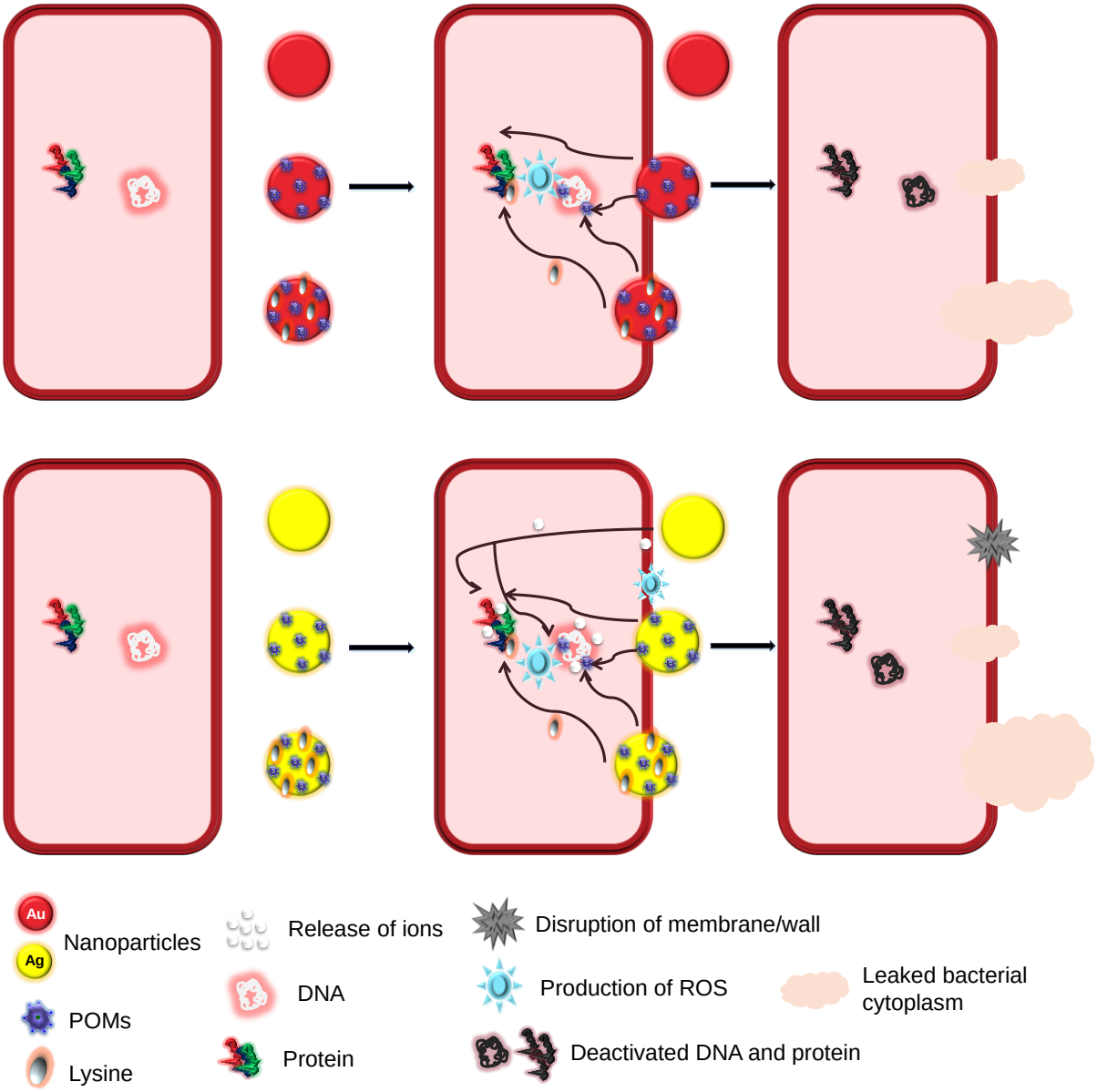

Figure.4.14. Interaction of Au, Ag and their POMs and lysine surface functionalized nanoparticles with *E. coli* bacterial cells

Treatment of bacterial cells resulted in reduction in the bacterial cell thickness along with significant roughening of the bacterial cell, which clearly shows the disruption of bacterial cell wall and membrane, wherein sub-cellular components discharged from bacteria due to complete disintegration of the bacterial cells. Figure 4.14 illustrates interaction of Au, Ag and sequentially surface functionalized nanoparticles with bacterial cells. Since functionalized Au nanoparticles, Ag nanoparticles and functionalized Ag nanoparticles, utilize physical mode of action against bacteria by causing pore formation, cell wall cleavage and cell lysis, it is likely that such nanomaterials may offer significant opportunities to control pathogenic bacteria by preventing them to develop resistance.

4.6. Conclusions

It has been reported that molecules or ions present on the surface of nanomaterials may control or create additional toxic effects because surface functionalization or peripheral coating can impart charge on the surface of nanoparticles and may stabilize them against aggregation.[24, 27, 46] Thus, appropriate formulation of surface corona of nanoparticle is essential to improve their biological activities.[52] In this context, present chapter demonstrated the sequential surface functionalization strategy to control surface corona and surface chemistry of Au and Ag nanoparticles and revealed noteworthy influence of surface bound ions or molecules on antibacterial activities.

Polyoxometalates are known for their biological applications and they have shown antibacterial, anticancer and antiviral activities.[58] Therefore,

two different POMs (PTA and PMA) were employed as functional molecules to impart antibacterial potential on the surface of tyrosine synthesized Au nanoparticles. Sequentially, the cationic amino acid lysine was used as a guiding molecule to target negatively charged bacterial cells for antibacterial activities. Antibacterial studies against *E. coli* showed that after surface functionalization due to the presence of surface bound POMs, biocompatible Au nanoparticles exhibited antibacterial activities and the effect was enhanced in the presence of lysine modified nanoparticles. The similar strategy was extended to tyrosine synthesized Ag nanoparticles and it was found that after surface functionalization with POMs and lysine, antibacterial potential of Ag nanoparticles enhanced significantly and these nanoparticles exhibited antibacterial activity even at smaller concentrations.

Moreover, this chapter provide strong evidence that since Au and Ag nanoparticle-based functional antibacterial agents employ a physical mode of action against bacteria by causing pore formation, cell wall cleavage and cell lysis, it is likely that such designer made functional nanomaterials may offer significant opportunities to control pathogenic microorganisms by preventing them to develop resistance in contrast to most of the conventional antibiotics.

4.7. References

1. Jain, J., et al., *Silver nanoparticles in therapeutics: Development of an antimicrobial gel formulation for topical use.* Molecular Pharmaceutics, 2009. **6**(5): p. 1388-1401.

2. Amin, R.M., et al., *Rapid and sensitive microplate assay for screening the effect of silver and gold nanoparticles on bacteria.* Nanomedicine, 2009. **4**(6): p. 637-643.

3. Lok, C.N., et al., *Silver nanoparticles: Partial oxidation and antibacterial activities.* Journal of Biological Inorganic Chemistry, 2007. **12**(4): p. 527-534.

4. Li, W.R., et al., *Antibacterial activity and mechanism of silver nanoparticles on Escherichia coli.* Applied Microbiology and Biotechnology, 2010. **85**(4): p. 1115-1122.

5. Sondi, I. and B. Salopek-Sondi, *Silver nanoparticles as antimicrobial agent: A case study on E. coli as a model for Gram-negative bacteria.* Journal of Colloid and Interface Science, 2004. **275**(1): p. 177-182.

6. Feng, Q.L., et al., *A Mechanistic Study of the Antibacterial Effect of Silver Ions on Escherichia Coli and Staphylococcus Aureus.* Journal of Biomedical Materials Research 2000. **52**(4): p. 662-668.

7. Baker, C., et al., *Synthesis and antibacterial properties of silver nanoparticles.* Journal of Nanoscience and Nanotechnology, 2005. **5**(2): p. 244-249.

8. Choi, O., et al., *The inhibitory effects of silver nanoparticles, silver ions, and silver chloride colloids on microbial growth.* Water Research, 2008. **42**(12): p. 3066-3074.

9. Kim, J.S., et al., *Antimicrobial effects of silver nanoparticles.* Nanomedicine: Nanotechnology, Biology, and Medicine, 2007. **3**(1): p. 95-101.

10. Martinez-Castanon, G.A., et al., *Synthesis and antibacterial activity of silver nanoparticles with different sizes.* Journal of Nanoparticle Research, 2008. **10**(8): p. 1343-1348.

11. Morones, J.R., et al., *The bactericidal effect of silver nanoparticles.* Nanotechnology, 2005. **16**(10): p. 2346-2353.

12. Nair, L.S. and C.T. Laurencin, *Silver nanoparticles: Synthesis and therapeutic applications.* Journal of Biomedical Nanotechnology, 2007. **3**(4): p. 301-316.

13. Li, Q., et al., *Antimicrobial nanomaterials for water disinfection and microbial control: Potential applications and implications.* Water Research, 2008. **42**(18): p. 4591-4602.

14. Clement, J.L. and P.S. Jarrett, *Antibacterial Silver.* Metal-Based Drugs, 1994. **1**(5-6): p. 467-482.

15. Panacek, A., et al., *Silver colloid nanoparticles: Synthesis, characterization, and their antibacterial activity.* Journal of Physical Chemistry B, 2006. **110**(33): p. 16248-16253.

16. Pal, S., Y.K. Tak, and J.M. Song, *Does the antibacterial activity of silver nanoparticles depend on the shape of the nanoparticle? A study of the gram-negative bacterium Escherichia coli.* Applied and Environmental Microbiology, 2007. **73**(6): p. 1712-1720.

17. Shukla, R., et al., *Biocompatibility of Gold Nanoparticles and Their Endocytotic Fate Inside the Cellular Compartment: A Microscopic Overview.* Langmuir, 2005. **21**(23): p. 10644-10654.

18. Connor, E.E., et al., *Gold Nanoparticles Are Taken Up by Human Cells but Do Not Cause Acute Cytotoxicity.* Small, 2005. **1**(3): p. 325-327.

19. Goodman, C.M., et al., *Toxicity of Gold Nanoparticles Functionalized with Cationic and Anionic Side Chains.* Bioconjugate Chemistry, 2004. **15**(4): p. 897-900.

20. Zhao, Y., et al., *Small molecule-capped gold nanoparticles as potent antibacterial agents that target gram-negative bacteria.* Journal of the American Chemical Society, 2010. **132**(35): p. 12349-12356.

21. Selvaraj, V., et al., *Antimicrobial and anticancer efficacy of antineoplastic agent capped gold nanoparticles.* Journal of Biomedical Nanotechnology, 2010. **6**(2): p. 129-137.

22. Nirmala Grace, A. and K. Pandian, *Antibacterial efficacy of aminoglycosidic antibiotics protected gold nanoparticles-A brief study.* Colloids and Surfaces A: Physicochemical and Engineering Aspects, 2007. **297**(1-3): p. 63-70.

23. Nath, S., et al., *Dextran-Coated Gold Nanoparticles for the Assessment of Antimicrobial Susceptibility.* Analytical Chemistry, 2008. **80**(4): p. 1033-1038.

24. Zhang, Z., et al., *Mussel-inspired functionalization of graphene for synthesizing Ag-polydopamine-graphene nanosheets as antibacterial materials.* Nanoscale, 2013. **5**(1): p. 118-123.

25. Neelgund, G.M. and A. Oki, *Deposition of silver nanoparticles on dendrimer functionalized multiwalled carbon nanotubes: synthesis, characterization and antimicrobial activity.* Journal of nanoscience and nanotechnology, 2011. **11**(4): p. 3621-3629.

26. Li, Z., et al., *Two-level antibacterial coating with both release-killing and contact-killing capabilities.* Langmuir, 2006. **22**(24): p. 9820-9823.

27. Song, J., H. Kong, and J. Jang, *Enhanced antibacterial performance of cationic polymer modified silica nanoparticles.* Chemical Communications, 2009. **0**(36): p. 5418-5420.

28. Nederberg, F., et al., *Biodegradable nanostructures with selective lysis of microbial membranes.* Nat Chem, 2011. **3**(5): p. 409-414.

29. Leeb, M., *Antibiotics: A shot in the arm.* Nature, 2004. **431**(7011): p. 892-893.

30. Norrby, S.R., C.E. Nord, and R. Finch, *Lack of development of new antimicrobial drugs: a potential serious threat to public health.* The Lancet Infectious Diseases, 2005. **5**(2): p. 115-119.

31. Chen, X. and H.J. Schluesener, *Nanosilver: A nanoproduct in medical application.* Toxicology Letters, 2008. **176**(1): p. 1-12.

32. Lee, H.Y., et al., *A practical procedure for producing silver nanocoated fabric and its antibacterial evaluation for biomedical applications.* Chemical Communications, 2007(28): p. 2959-2961.

33. Yacoby, I., H. Bar, and I. Benhar, *Targeted Drug-Carrying Bacteriophages as Antibacterial Nanomedicines.* Antimicrobial Agents and Chemotherapy, 2007. **51**(6): p. 2156-2163.

34. Wong, K.K.Y. and X. Liu, *Silver nanoparticles-the real "silver bullet" in clinical medicine?* MedChemComm, 2010. **1**(2): p. 125-131.

35. Yacoby, I. and I. Benhar, *Antibacterial nanomedicine.* Nanomedicine, 2008. **3**(3): p. 329(13).

36. Hamouda, I.M., *Current perspectives of nanoparticles in medical and dental biomaterials.* Journal of Biomedical Research, 2012. **26**(3): p. 143-151.

37. Amato, E., et al., *Synthesis, Characterization and Antibacterial Activity against Gram Positive and Gram Negative Bacteria of Biomimetically Coated Silver Nanoparticles.* Langmuir, 2011. **27**(15): p. 9165-9173.

38. Brogden, K.A., *Antimicrobial peptides: pore formers or metabolic inhibitors in bacteria?* Nat Rev Micro, 2005. **3**(3): p. 238-250.

39. Shai, Y., *Mode of action of membrane active antimicrobial peptides.* Biopolymers - Peptide Science Section, 2002. **66**(4): p. 236-248.

40. Hancock, R.E.W. and R. Lehrer, *Cationic peptides: A new source of antibiotics.* Trends in Biotechnology, 1998. **16**(2): p. 82-88.

41. Allahverdiyev, A.M., et al., *Coping with antibiotic resistance: Combining nanoparticles with antibiotics and other antimicrobial agents.* Expert Review of Anti-Infective Therapy, 2011. **9**(11): p. 1035-1052.

42. Patil, S.S., et al., *Synthesis and antibacterial studies of chloramphenicol loaded nano-silver against salmonella typhi.* Synthesis and Reactivity in Inorganic, Metal-Organic and Nano-Metal Chemistry, 2009. **39**(2): p. 65-72.

43. Gu, H., et al., *Presenting Vancomycin on Nanoparticles to Enhance Antimicrobial Activities.* Nano Letters, 2003. **3**(9): p. 1261-1263.

44. Huang, W.C., P.J. Tsai, and Y.C. Chen, *Functional gold nanoparticles as photothermal agents for selective-killing of pathogenic bacteria.* Nanomedicine, 2007. **2**(6): p. 777-787.

45. Subash, A.A., et al., *Preparation, characterization, and functional analysis of zinc oxide nanoparticle-coated cotton fabric for antibacterial efficacy.* Journal of the Textile Institute, 2012. **103**(3): p. 298-303.

46. Taglietti, A., et al., *Antibacterial Activity of Glutathione-Coated Silver Nanoparticles against Gram Positive and Gram Negative Bacteria.* Langmuir, 2012. **28**(21): p. 8140-8148.

47. Ashkarran, A.A., et al., *Bacterial Effects and Protein Corona Evaluations: Crucial Ignored Factors in the Prediction of Bio-Efficacy of Various Forms of Silver Nanoparticles.* Chemical Research in Toxicology, 2012. **25**(6): p. 1231-1242.

48. Zhou, Y., et al., *Antibacterial activities of gold and silver nanoparticles against Escherichia coli and bacillus Calmette-Guerin.* Journal of Nanobiotechnology, 2012. **10**(1): p. 19.

49. Irwin, P., et al., *Antimicrobial activity of spherical silver nanoparticles prepared using a biocompatible macromolecular capping agent: evidence for induction of a greatly prolonged bacterial lag phase.* Journal of Nanobiotechnology, 2010. **8**(1): p. 34.

50. Wiesner, M.R., et al., *Assessing the risks of manufactured nanomaterials.* Environmental Science and Technology, 2006. **40**(14): p. 4336-4345.

51. Ozay, O., et al., *P(4-VP) based nanoparticles and composites with dual action as antimicrobial materials.* Colloids and Surfaces B: Biointerfaces, 2010. **79**(2): p. 460-466.

52. Hamouda, T. and J.R. Baker, *Antimicrobial mechanism of action of surfactant lipid preparations in enteric Gram-negative bacilli.* Journal of Applied Microbiology, 2000. **89**(3): p. 397-403.

53. Dror-Ehre, A., et al., *Silver nanoparticle-E. coli colloidal interaction in water and effect on E. coli survival.* Journal of Colloid and Interface Science, 2009. **339**(2): p. 521-526.

54. Bhushan, B., *Bioinspired Structured Surfaces.* Langmuir, 2012. **28**(3): p. 1698-1714.

55. Rhule, J.T., et al., *Polyoxometalates in medicine.* Chemical Reviews, 1998. **98**(1): p. 327-357.

56. Pope, M.T. and A. Muller, *Polyoxometalate chemistry: An old field with new dimensions in several disciplines.* Angewandte Chemie (International Edition in English), 1991. **30**(1): p. 34-48.

57. Hill, C.L. and C.M. Prosser-McCartha, *Homogeneous catalysis by transition metal oxygen anion clusters.* Coordination Chemistry Reviews, 1995. **143**: p. 407-455.

58. Yamase, T., *Anti-tumor, -viral, and -bacterial activities of polyoxometalates for realizing an inorganic drug.* Journal of Materials Chemistry, 2005. **15**(45): p. 4773-4782.

59. Hasenknopf, B., *Polyoxometalates: Introduction to a class of inorganic compounds and their biomedical applications.* Frontiers in Bioscience, 2005. **10**(1): p. 275-287.

60. Yamase, T., H. Fujita, and K. Fukushima, *Medical chemistry of polyoxometalates. Part 1. Potent antitumor activity of polyoxomolybdates on animal transplantable tumors and human cancer xenograft.* Inorganica Chimica Acta, 1988. **151**(1): p. 15-18.

61. Yamase, T., N. Fukuda, and Y. Tajima, *Synergistic effect of polyoxotungstates in combination with β-lactam antibiotics on*

antibacterial activity against methicillin-resistant Staphylococcus aureus. Biological and Pharmaceutical Bulletin, 1996. **19**(3): p. 459-465.

62. Yanagie, H., et al., *Anticancer activity of polyoxomolybdate.* Biomedicine and Pharmacotherapy, 2006. **60**(7): p. 349-352.
63. Selvakannan, P.R., et al., *Synthesis of aqueous Au core-Ag shell nanoparticles using tyrosine as a pH-dependent reducing agent and assembling phase-transferred silver nanoparticles at the air-water interface.* Langmuir, 2004. **20**(18): p. 7825-7836.
64. Albanese, A., P.S. Tang, and W.C.W. Chan, *The effect of nanoparticle size, shape, and surface chemistry on biological systems*, in *Annual Review of Biomedical Engineering*2012. p. 1-16.
65. Chithrani, B.D., A.A. Ghazani, and W.C.W. Chan, *Determining the size and shape dependence of gold nanoparticle uptake into mammalian cells.* Nano Letters, 2006. **6**(4): p. 662-668.
66. Yang, H., et al., *Comparative study of cytotoxicity, oxidative stress and genotoxicity induced by four typical nanomaterials: The role of particle size, shape and composition.* Journal of Applied Toxicology, 2009. **29**(1): p. 69-78.
67. Silverstein R.B. and B. G.C., *Spectrometric identification of organic compounds*. second ed. 1967, New York: John Wiley & Sons. 88.
68. Iliev, V., et al., *Influence of the size of gold nanoparticles deposited on TiO2 upon the photocatalytic destruction of oxalic acid.* Journal of Molecular Catalysis A: Chemical, 2007. **263**(1-2): p. 32-38.

69. Linsebigler, A.L., G. Lu, and J.T. Yates Jr, *Photocatalysis on TiO2 surfaces: Principles, mechanisms, and selected results.* Chemical Reviews, 1995. **95**(3): p. 735-758.

70. Pearson, A., S.K. Bhargava, and V. Bansal, *UV-Switchable Polyoxometalate Sandwiched between TiO2 and Metal Nanoparticles for Enhanced Visible and Solar Light Photococatalysis.* Langmuir, 2011. **27**(15): p. 9245-9252.

71. Pearson, A., et al., *Gold Nanoparticle-Decorated Keggin Ions/TiO2 Photococatalyst for Improved Solar Light Photocatalysis.* Langmuir, 2011. **27**(11): p. 6661-6667.

72. Sanyal, A., S. Mandal, and M. Sastry, *Synthesis and Assembly of Gold Nanoparticles in Quasi-Linear Lysine–Keggin-Ion Colloidal Particles.* Advanced Functional Materials, 2005. **15**(2): p. 273-280.

73. Shirley, D.A., *High-Resolution X-Ray Photoemission Spectrum of the Valence Bands of Gold.* Physical Review B, 1972. **5**(12): p. 4709-4714.

74. Mandal, S., A.B. Mandale, and M. Sastry, *Keggin ion-mediated synthesis of aqueous phase-pure Au@Pd and Au@Pt core-shell nanoparticles.* Journal of Materials Chemistry, 2004. **14**(19): p. 2868-2871.

75. Bansal, V., et al., *Fungus-mediated biosynthesis of silica and titania particles.* Journal of Materials Chemistry, 2005. **15**(26): p. 2583-2589.

76. Joshi, H., et al., *Isothermal titration calorimetry studies on the binding of amino acids to gold nanoparticles.* Journal of Physical Chemistry B, 2004. **108**(31): p. 11535-11540.

77. Ramanathan, R., et al., *Cationic amino acids specific biomimetic silicification in ionic liquid: A quest to understand the formation of 3-D structures in diatoms.* PLoS ONE, 2011. **6**(3).

78. Kumar, A., et al., *Investigation into the interaction between surface-bound alkylamines and gold nanoparticles.* Langmuir, 2003. **19**(15): p. 6277-6282.

79. Kong, Y., et al., *Preparation and antibacterial activity of nanorod-amino acid polyoxometalates.* Materials Letters, 2007. **61**(11-12): p. 2393-2397.

Chapter V

Self-assembled soft nanostructures of plasmid DNA and tri-block copolymer as non-viral DNA delivery vehicle

The major focus of this chapter is to construct self-assembled soft nanostructures of plasmid DNA (pDNA) and biocompatible tri-block copolymer P-123 (PEO_{20}-PPO_{69}-PEO_{20}). A variety of characterization techniques have been discussed, which were employed to understand the nature of interaction between pDNA and PEO_{20}-PPO_{69}-PEO_{20} and how this interaction governed the self-assembly process. Further, these nanostructures were subjected to screen optimum weight ratio of pDNA and PEO_{20}-PPO_{69}-PEO_{20} to achieve highest level of bacterial transformation. Transformation studies of these structures were performed in cellular environment using *Escherichia coli* DH5α as model. During transformation, the integrity and functionality of the pDNA in nanostructures were also demonstrated within the cellular environment by the expression of green fluorescent protein (GFP) gene.

5.1. Introduction

In previous chapters, significance of inorganic metal nanoparticles has been explored for their peroxidase-like behavior and antibacterial activities. Small size of these nanoparticles and easy tailoring of their surface properties provide an opportunity to employ them for a variety of other applications including drug, proteins and even nucleic acids (DNA or RNA) delivery for medicinal purposes.[1-5] In the context of nucleic acid delivery, conventional viral vectors have been used and still considered favorably because of their small particle size, protective core (viral capsid), presence of receptor specific moieties and membrane fusogenic elements. Beside all these important features, viral vectors have potential side effects which limit their application.[6, 7] Therefore, advanced nanomaterials have gained significant attraction within the scientific community for such applications and functional gold nanoparticles, silica materials, quantum dots (QDs), plant based cationic vesicles and cationic polymers are some of the advanced materials currently in use for DNA delivery.[2, 5, 8-23]

Among these advanced nanomaterials due to nanotoxicological properties, inorganic nanomaterials are typically not suitable for DNA delivery applications and moreover, it is not easy to clear inorganic nanomaterials from the living organism due to their strong association with different cellular components. Therefore, it is imperative to utilize organic materials based nanostructures for drug or DNA delivery applications because compared to inorganic nanostructures, organic nanostructures can be easily broken down within the biological system due to enzymatic

reactions. However, applications of such soft organic nanostructures in the field of biology and medicine has not been fully explored and has predominantly been restricted in imaging, screening and sensing [24] while cellular environment and cell itself is a soft object which is composed of organic molecules in complex and functional configurations.[25, 26]

In this perspective, self-assembled vesicles or micelles are at the forefront with possible uses ranging from biomedicine to nano reactors.[27-31] In biomedicine, it is essential to realize that numerous human diseases originate form defective genetic material [11] and gene or antisense therapies are the most frequently used approaches to treat such genetic disorders. In gene therapy, pDNA is introduced into cells of patients to express the pharmaceutical proteins and nucleic acid based drugs and these have emerged as potential new drugs, which could control gene expression. Conversely, in antisense therapy an oligonucleotide could be used to suppress the expression of the disease causing genes. These therapies have remarkable possibilities in cancer treatment because of genetic differences between cancer and normal cells.[32, 33] Therefore, it is necessary to develop efficient non-viral DNA delivery vectors in order to realize the full potential of these therapies and to overcome the safety issues related to viral delivery systems.[34]

In this context, 'polyplexes' have been designed which are typically complex structures of nucleic acids and synthetic polymers formed by self-assembly processes through entropically driven interactions in aqueous solutions. Formation of polyplexes is possible due to the electrostatic interactions between negatively charged DNA and the positively charged

groups of polymers (poly-cations).[7, 35-37] Conventional cationic polymer vehicles very strongly condense genetic material within the polymer vesicle, which result in low transformation efficiency and sometimes cationic polymers illustrate toxicity.[38] Therefore, additionally amphiphilic block copolymers also have been screened to enhance DNA vaccination for therapeutic needs and it has been discovered that appropriate formulation of block copolymer and DNA can reduce the dose of antigen-encoding plasmid.[39-43] Moreover, block copolymer systems have shown thermo reversible gelation around body temperature (37°C) and stimuli responsive (temperature, pH, redox condition etc.) delivery. Therefore, they are particularly attractive for biomedical applications such as drug or DNA delivery and tissue engineering.[12, 13, 41, 44-47]

In addition to aforementioned properties, block copolymer systems have a range of designer made polymers, wherein especially tri-block copolymers have been extensively used in chemical and pharmaceutical industries as detergents, colloidal dispersion stabilizers and even in cosmetic products.[48] Furthermore, these block copolymers are biologically active polymers which can self-assemble into micelle structures and has spontaneous association with poly-anionic DNA to form block copolymer-DNA micelles.[7, 49]

In the context of tri-block copolymers, it is remarkable to know that PEO-PPO-PEO are known to have diverse effects on lipid membrane and activities of these copolymers on bio-membranes mainly depend on the hydrophobic and hydrophilic component of the copolymers. Hydrophobic part (PPO chain) of the PEO-PPO-PEO has potential to insert into the lipid

bilayers while hydrophilic part (PEO chain) of PEO-PPO-PEO weekly adsorb at the membrane surface.[49-51] Thus, depending upon the length of the hydrophobic and hydrophilic chains PEO-PPO-PEO has capability to act as membrane sealant or as membrane permeabilizer to enhance interaction with biological membrane.[7, 50] Further, it has been reported that PEO chain (hydrophilic part) can offer solubility to the block copolymer and mask DNA-block copolymer complex from immune recognition which can efficiently protect DNA from degradation from nucleases.[7, 52, 53]

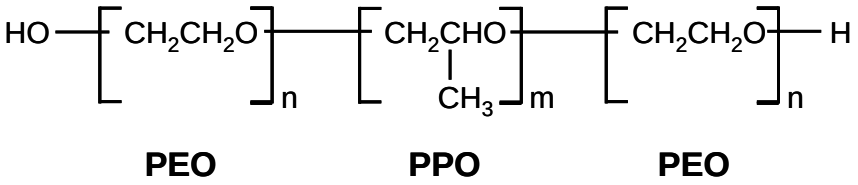

Figure.5.1. Chemical structure of tri-block copolymer (PEO-PPO-PEO)

Therefore, in current chapter, organic tri-block copolymers PEO_{20}-PPO_{69}-PEO_{20} [poly(ethylene oxide)–poly(propylene oxide)–poly(ethylene oxide)] (Figure 5.1) was chosen to understand its interaction with pDNA and for bacterial transformation studies since it has high molecular diversity, well-known physicochemical characteristics and its physicochemical properties can be simply modified for biomedical applications. This tri-block copolymer has basic linear A-B-A type architecture in which the end of one segment is covalently joined to the head of the other segment as illustrated in Figure 5.1. This polymer is also known as P-123 and it has an average molecular weight of 5750, in which PEO contributes 30% of total weight. The studied tri-block copolymer was found capable to self-assemble with pDNA and it created compact soft nano-conjugate system of pDNA and PEO_{20}-PPO_{69}-

PEO_{20} on heating over 31°C (melting point of polymer). These soft self-assembled structures can preserve integrity and functionality of the pDNA and can improve DNA transformation.

5.2. Scheme of the work

The major aim of this chapter is to prepare soft nanostructures of pDNA and tri-block copolymer using self-assembly process. A-B-A type tri-block copolymer (PEO_{20}-PPO_{69}-PEO_{20}) started micellization after heating at 50°C and formed polymer micelles, which on incubation with pDNA lead to pDNA/PEO_{20}-PPO_{69}-PEO_{20} complex as illustrated in Figure 5.2. After encapsulation of pDNA within the complex nanostructures, since very little is known about the physicochemical aspects that govern the association of the negatively charged polyelectrolyte (pDNA) and tri-block copolymer, different techniques including TEM, FTIR, and XPS were employed to understand the interaction between pDNA and PEO_{20}-PPO_{69}-PEO_{20}.

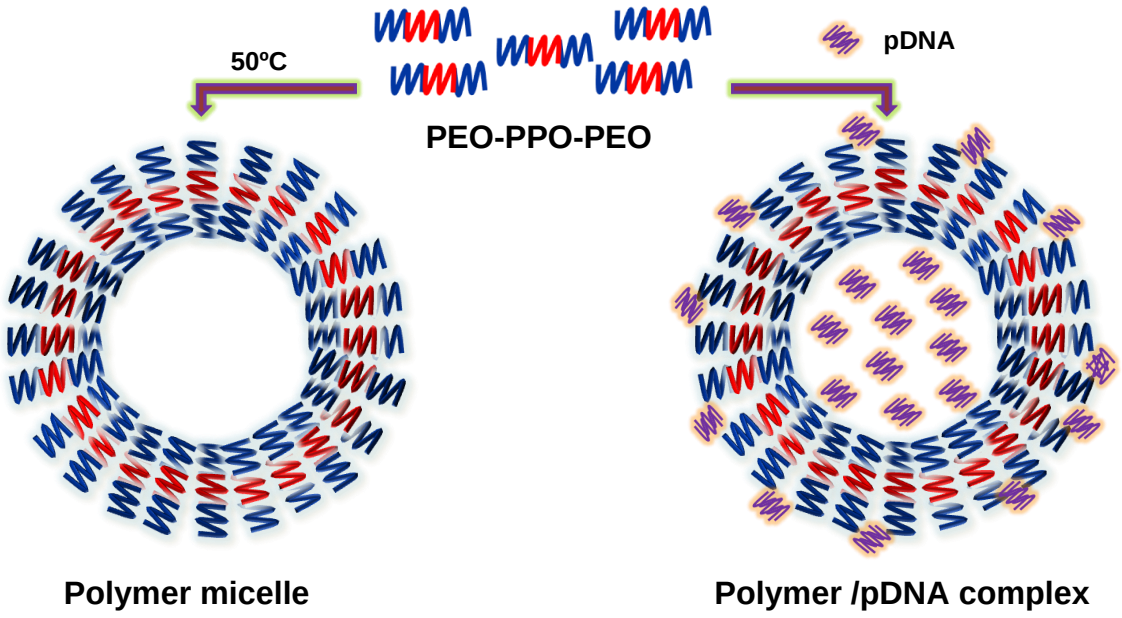

Figure.5.2. Schematic representation of self-assembly process of A-B-A type tri-block copolymer and pDNA

Moreover, these self-assembled nanostructures of pDNA/PEO_{20}-PPO_{69}-PEO_{20} were utilized for bacterial transformation studies in the cellular environment. *Escherichia coli* DH5α was used as a model microorganism to study transformation of these self-assembled complex nanostructures. During transformation studies, optimum weight ratio of pDNA and PEO_{20}-PPO_{69}-PEO_{20} was screened to achieve highest level of transformation. In addition to transformation, the integrity of pDNA in the studied delivery system was demonstrated by the expression of green fluorescence protein (GFP) gene.

5.3. Experimental Section

5.3.1. Isolation of pDNA and purification

pDNA containing green fluorescence protein (GFP) and ampicillin resistance genes was isolated according to the Shambrook *et al.* with some modifications.[54] Briefly, overnight grown fresh culture of *E. coli* DH 5 α was inoculated in LB medium and incubated for 3 hours. Cells were harvested by centrifugation and suspended in chilled Solution I (glucose + Tris + EDTA) followed by vortex. Then, Solution II (NaOH + SDS) and chilled Solution III (potassium acetate + glacial acetic acid) were added sequentially and mixed gently, and supernatant was recovered by centrifugation (c/f) and treated with 20 µl/ml RNase to remove RNA contamination, if any. After that, equal volume of cholophenol : isoamyl alcohol (24:1 V/V) was added and mixed gently and centrifuged. Aqueous phase obtained in this process was transferred in fresh tubes and 0.7 Volume of chilled isopropanol was added and kept in deep freezer for 2 hours and centrifuged. Finally,

precipitated pDNA was washed with 70% ethanol and dissolved in Tris-EDTA (TE) buffer solution.

5.3.2. Preparation of pDNA and PEO-PPO-PEO complex

Under vigorous stirring, 10 g of PEO_{20}-PPO_{69}-PEO_{20} was dissolved in 100 ml deionised miliQ water at 50°C to obtain stock solution of PEO_{20}-PPO_{69}-PEO_{20}. Different volumes of this solution were incubated with fixed amount of pDNA for 2 hours at 37°C to form self-assembled nanostructure. Details of the final weight ratios of pDNA and PEO_{20}-PPO_{69}-PEO_{20} employed for complex nanostructure formation in 1 ml reaction solutions are illustrated in table 5.1. This approach was utilized to screen the optimum weight ratio of pDNA and PEO_{20}-PPO_{69}-PEO_{20} to achieve higher level of bacterial transformation.

S.No.	pDNA	PEO-PPO-PEO	Weight ratio (pDNA : PEO-PPO-PEO)
1	10 µg	-	1:0
2	10 µg	10 µg	1:1
3	10 µg	50 µg	1:5
4	10 µg	100 µg	1:10
5	10 µg	150 µg	1:15
6	10 µg	200 µg	1:20
7	10 µg	500 µg	1:50
8	10 µg	1000 µg	1:100

Table.5.1. Weight ratios of pDNA and PEO_{20}-PPO_{69}-PEO_{20} employed to prepare self-assembled nanostructures

5.3.3. Preparation of competent cells

E. coli DH5α competent cells were prepared by modified $CaCl_2$.$MgCl_2$ mediated method in the presence of tetracycline as illustrated in flow chart given below.[54, 55] These competent cells were employed to study transformation of pDNA and PEO_{20}-PPO_{69}-PEO_{20} complexes at varying weight ratios.

In 10 ml LB medium containing (10 µg/ml tetracycline), single colony of *E. coli* DH 5 α was introduced

↓ Overnight incubation (37°C, 200 rpm)

1 ml fresh inoculum was introduced in 50 ml LB medium

↓ 3 hours incubation at (37° C, 200 rpm)

Kept in ice (1 hour) and transferred into chilled centrifuged tubes

↓ Centrifugation (4,000 rpm, 10 minutes)

Supernatant was discarded; tubes were inverted on paper towel for 1 minute

↓

Cells were suspended in freshly prepared $CaCl_2$/$MgCl_2$ (ice cold) solution

↓ Centrifugation (4,000 rpm, 10 minutes)

Re-suspended bacterial cells in ice cold $CaCl_2$/$MgCl_2$ solution

↓ Centrifugation (4,000 rpm, 10 minutes)

Finally bacterial cells were suspended in 1.5 ml ice cold freshly prepared $CaCl_2$ (100 mM) solution

More specifically, 1 ml of overnight grown fresh bacterial culture was used to inoculate LB broth containing 10µg/ml tetracycline for 3 hours at 37ºC or till optical density reached at 0.5-0.6 at 600 nm. This culture was stored on ice for 1 hour and transferred into sterilized and ice cooled tubes and centrifuged at 4000 rpm for 10 min at 4ºC. The obtained pellet was re-suspended in freshly prepared ice cold $CaCl_2$.$MgCl_2$ solution (20 mM $CaCl_2$ and 80 mM $MgCl_2$). The cells were recovered by centrifugation and re-

suspended in $CaCl_2$.$MgCl_2$ solution. Finally, recovered cells were suspended in ice cold and freshly prepared 100 mM $CaCl_2$ solution and used for transformation studies.

5.3.4. Transformation and gene expression

To perform bacterial transformation, pDNA and PEO_{20}-PPO_{69}-PEO_{20} complexes were mixed with 200 µl of freshly prepared competent cells (*E. coli*) and incubated on ice. After 30 minutes incubation, heat shock was given for 90 seconds at 42°C (to expand the pore size of bacterial cell wall to facilitate DNA uptake) and instantly transferred in ice for 2 minutes (to narrow down the pore size to keep foreign pDNA within the bacteria) followed by addition of 800 µl of LB media. Finally, these bacterial cells were subjected to incubate at 37°C for 1 hour, followed by spreading 100 µl aliquots on nutrient agar plates containing 10 µg/ml ampicillin. Colonies grown after overnight incubation (37°C) were counted and graph was plotted between number of transformed colonies (Y axis) and the ratio of pDNA and PEO_{20}-PPO_{69}-PEO_{20} complex (X axis), respectively. During these experiments, 200 µl of competent cells and 800 µl of LB media was used as negative control, while equal amount of pDNA under same experimental conditions was employed as positive control. Further, integrity and functionality of pDNA after transformation was demonstrated in the *E. coli* cellular environment through the expression of GFP gene.

5.4. Results and Discussion

In aqueous solution, tri-block copolymer (PEO-PPO-PEO) has a tendency to self-assemble into soft spherical micelles like structures. The

size and shape of these soft structures predominantly depends on the concentration of PEO-PPO-PEO present in the solution. Since, PEO-PPO-PEO has the hydrophilic PEO segment, it weakly coordinates to the DNA by electrostatic interactions and form spherical vesicles wherein DNA is entrapped inside [38] as illustrated in Figure 5.2. Soft structures, made up of pDNA and PEO_{20}-PPO_{69}-PEO_{20} were characterized using various techniques to understand interaction between pDNA and PEO_{20}-PPO_{69}-PEO_{20}. Towards the end of this chapter, pDNA and PEO_{20}-PPO_{69}-PEO_{20} complexes were employed for bacterial transformation studies.

5.4.1. TEM studies of self-assembled structures of pDNA and PEO-PPO-PEO with varying weight ratios

It is reported that at a sufficient charge ratio of nitrogen to phosphate (N:P), the polymer can condense DNA to sizes, suitable for cellular uptake and also provides steric protection from degradation.[56] Therefore, different weight ratios of pDNA and PEO_{20}-PPO_{69}-PEO_{20} were prepared to screen optimum size of the complex hybrid nanostructures of pDNA and PEO_{20}-PPO_{69}-PEO_{20} as discussed in section 5.3.2. (Table 5.1).

Figure 5.3 illustrates TEM images of as-formed PEO_{20}-PPO_{69}-PEO_{20} micelles at 0.1 mg/ml (A), 0.5 mg/ml (B), and 1 mg/ml (C) concentrations, and pDNA polymer complexes (pDNA : PEO_{20}-PPO_{69}-PEO_{20}) at 1:1 (D), 1:5 (E), and 1:10 (F), respectively. Pure PEO_{20}-PPO_{69}-PEO_{20} was pseudo-spherical in shape at lower concentration such as 0.1 mg/ml as shown in Figure 5.3 (A). With the increasing concentration of PEO_{20}-PPO_{69}-PEO_{20}, it developed spherical shapes and additionally size of these spherical

structures increased significantly from 0.1 mg/ml to 1 mg/ml from 80 nm to around 3 μm as shown in Figure 5.3 (A and C), which confirmed structural dependence of size of polymer structures on concentration.

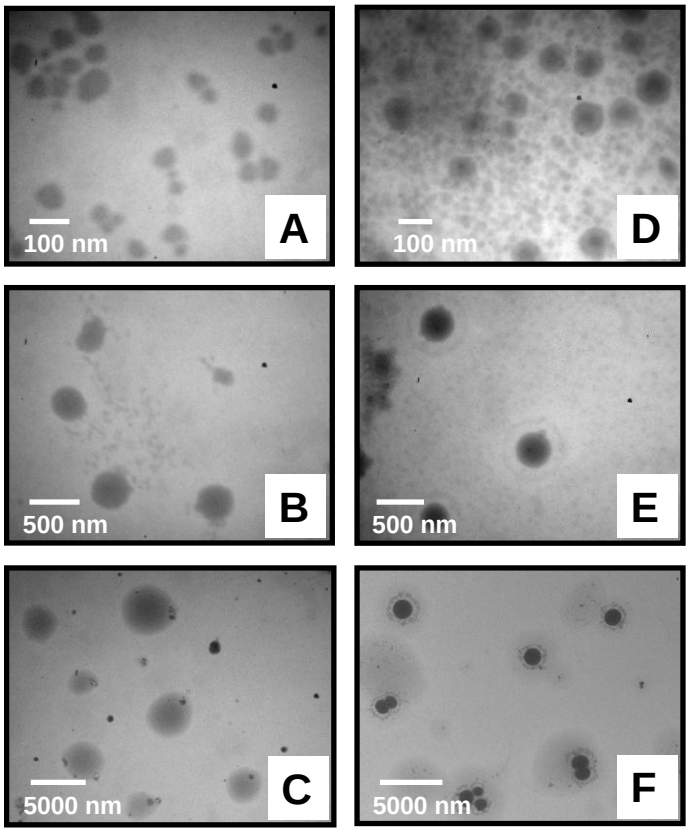

Figure.5.3. TEM images of as-formed (A-C) PEO-PPO-PEO micelles at different concentrations and after their complex formation with pDNA (D-F)

Figure 5.3 (D-F) shows soft nanostructures of pDNA and PEO_{20}-PPO_{69}-PEO_{20} at 1:1 (D), 1:5 (E), and 1:10 (F) weight ratios containing 0.01, 0.05 and 0.1 mg/ml equivalent of polymer, respectively. With the increasing concentration of PEO_{20}-PPO_{69}-PEO_{20} with respect to pDNA, an increase in the complex size was noted. Further, it is interesting to observe that in the complex of pDNA and PEO_{20}-PPO_{69}-PEO_{20}, when samples containing equivalent amount of polymer (A-F) were compared, the organization became compact in the presence of pDNA and relative size of the complex

significantly increased in contrast to pure PEO_{20}-PPO_{69}-PEO_{20}. This increase in size (1-2 μm) is compatible to the size of bacteria and therefore it may be well-suited for parallel bacterial transformation, while further increment in size may decrease transformation efficiency and this hypothesis was further validated during bacterial transformation studies.

5.4.2. FTIR spectral analysis to recognize chemical interaction of self-assembled pDNA and PEO-PPO-PEO complex

FTIR analysis of PEO_{20}-PPO_{69}-PEO_{20}, pDNA and after their complex formation were carried out to understand chemical interaction during self-assembly process. Figure 5.4 shows comparative FTIR spectra of pure PEO_{20}-PPO_{69}-PEO_{20} (curve 1), pure pDNA (curve 2) and after their complex formation at 1:1 (curve 3) and 1:10 concentrations (curve 4).

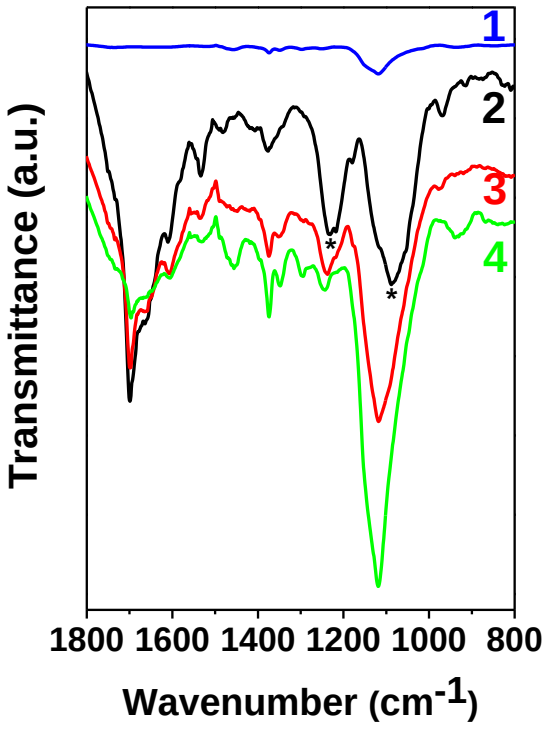

Figure.5.4. FTIR spectra of PEO-PPO-PEO (curve 1), pDNA (curve 2), and after their complexation at 1:1 and 1:10 ratios (curve 3 and 4), respectively

FTIR studies of pure pDNA show specific vibrational frequencies comparable to the nitrogenous bases of DNA in region 1700-1500 cm^{-1} and phosphate (PO_4^{3-}) stretching frequencies in 1250-1050* cm^{-1}. For instance, illustrated in Figure 5.4 curve 2, the two very strong absorption bands located at 1230 and 1088 cm^{-1} (marked with *****) are assigned to the asymmetric and symmetric stretching vibrations of PO_4^{3-} group, respectively. Other vibrational frequencies at 1701, 1661, 1610, 1582 (shoulder), 1534 and 1482 cm^{-1} are assigned to guanine (C7=N stretching), thymine (C2=O stretching), adenine (C7=N stretching), purine stretching (N7), in-plane vibration of cytosine and guanine and in-plane vibration of cytosine, respectively. Additionally, C-C deoxyribose stretching was observed at 969 cm^{-1} while deoxyribose, B-marker frequency was measured at 875 cm^{-1}. The observed pDNA vibrational frequencies were in good harmony with reported literature.[57-60]

Comparative analysis of FTIR spectra provided clear evidence for an interaction between the PO_4^{3-} groups of pDNA and PEO_{20}-PPO_{69}-PEO_{20} during soft complex nanostructure formation. In the case of pristine PEO_{20}-PPO_{69}-PEO_{20} (curve 1), there were no vibrational frequencies in the region between 1700 to 1500 cm-1 but interestingly all these signatures appeared in the self-assembled soft nanostructure of pDNA and PEO_{20}-PPO_{69}-PEO_{20} without any significant changes (curve 3 and 4). Further, FTIR spectroscopy confirmed that PO_4^{3-} groups present in pDNA interacted with PEO_{20}-PPO_{69}-PEO_{20} during self-assembly process to form complex structures of pDNA and PEO_{20}-PPO_{69}-PEO_{20}. As shown in curve 3 and 4 (pDNA and PEO_{20}-PPO_{69}-PEO_{20} ratio 1:1 and 1: 10, respectively) after interaction between pDNA and

PEO_{20}-PPO_{69}-PEO_{20} in the complex, shifts were observed in both the asymmetric and symmetric stretching vibrations of PO_4^{3-} from 1230 to 1237 (1:1) and 1242 (1:10) cm^{-1} and from 1088 to 1118 cm^{-1}, respectively. While there were no considerable changes in vibrational frequencies comparable to other groups. Therefore, FTIR spectroscopy provided strong confirmation that PO_4^{3-} group of pDNA is chemically involved with PEO_{20}-PPO_{69}-PEO_{20} during self-organization process to make soft nanostructures of pDNA and PEO_{20}-PPO_{69}-PEO_{20}.

5.4.3. XPS spectral analysis of self-assembled structures of pDNA and PEO-PPO-PEO

XPS analysis of pDNA, PEO_{20}-PPO_{69}-PEO_{20} and after their self-assembly were carried out to understand surface composition and for qualitative estimation of the presence of the oxygen, carbon and nitrogen. Illustrated in Figure 5.5 are core level XPS spectra of C1s, P2p, N1s and O1s, which are the four basic elements of pDNA. Wherein, Figure 5.6 shows core level XPS spectra of C1s, O1s present in tri-block copolymer and N1s (in pDNA:PEO_{20}-PPO_{69}-PEO_{20} at 1:1 ratio) and C1s (in pDNA:PEO_{20}-PPO_{69}-PEO_{20} at 1:10 ratio), respectively. All these spectra have been background corrected using Shirley algorithm [61] and their core level binding energies were aligned with respect to the adventitious C1s BE of 285 eV.

As shown in Figure 5.5 core level XPS spectra of C1s recorded for pDNA can be decomposed into three energy levels. BE at 285.0 eV is assigned to the aromatic carbon chain whereas the BE at 286.4 eV can be assigned to carbon attached with O and N species. While the higher BE at 287.9 eV can be specified to C=O, present in nitrogenous bases. The core

level XPS spectrum of P2p coming from pDNA shows its BE at 133.4 eV and it can be assigned to phosphate group (PO_4^{3-}) of pDNA. The core level XPS spectra of N1s can be decomposed into two energy levels, in which the lower BE at 399.2 eV can be assigned to –C=N group whereas the higher BE at 400.4 eV can be denoted to -NH_2. Similarly, the O1s recorded for pure pDNA sample can be decomposed into two energy levels. The BEs were observed at 531.3 and 532.75 eV, which may be assigned to phosphate-oxygen and deoxyribose sugar-oxygen respectively.

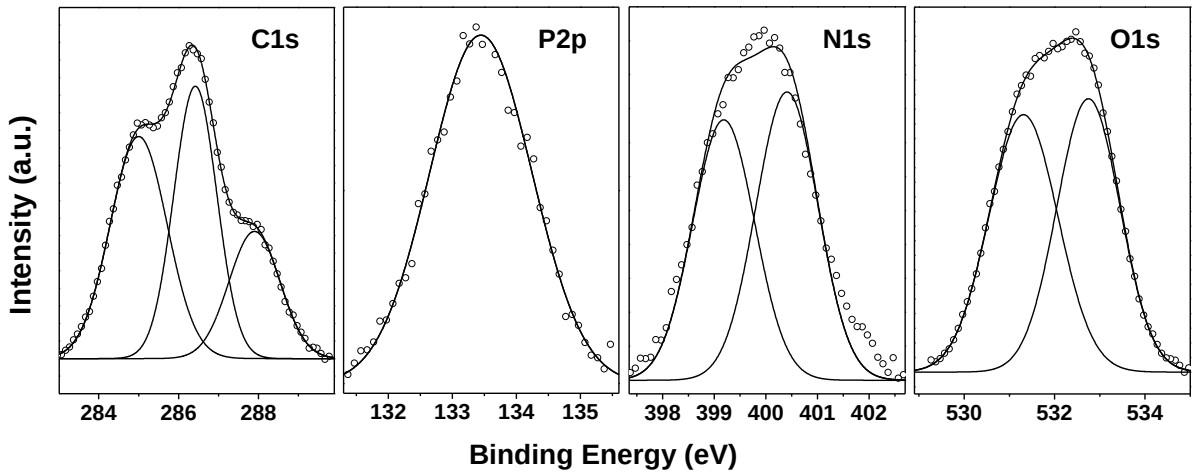

Figure.5.5. Core level XPS spectra of four principal elements present in pDNA

Illustrated in Figure 5.6 are core level XPS spectra of C1s and O1s present in PEO_{20}-PPO_{69}-PEO_{20}. The core level C1s spectrum can be decomposed into two major energy levels at 285.0 eV and 286.5 eV. The lower BE at 285.0 eV is assigned to the alkyl chain present in PEO_{20}-PPO_{69}-PEO_{20} and the higher BE at 286.5 eV can be assigned to carbon attached with oxygen. BE at 532.7 eV was recorded for O1s core level spectrum originating from PEO_{20}-PPO_{69}-PEO_{20}. Since pristine PEO_{20}-PPO_{69}-PEO_{20} did not have nitrogen, N signatures were not seen in XPS analysis, while N

signatures appeared in pDNA and PEO_{20}-PPO_{69}-PEO_{20} structures, suggesting association of pDNA and PEO_{20}-PPO_{69}-PEO_{20}. Representative core level XPS spectra of N1s (in pDNA: PEO-PPO-PEO at 1:1 ratio) is shown in Figure 5.6, which illustrated single BE at 399.6 eV. Furthermore, core level XPS spectra of C1s (in pDNA: PEO-PPO-PEO at 1:10 ratio) is presented in Figure 5.6. It was interesting to observe that there were no significant changes in the binding energies of C1s, even after self-assembly between pDNA: PEO-PPO-PEO at different weight rations. C1s XPS spectra recorded for pDNA: PEO-PPO-PEO (1:10 ratio) can be decomposed into two energy levels. The lower BE is observed at 285.0 eV and the higher BE is recorded at 286.5 eV, are comparable to PEO_{20}-PPO_{69}-PEO_{20}.

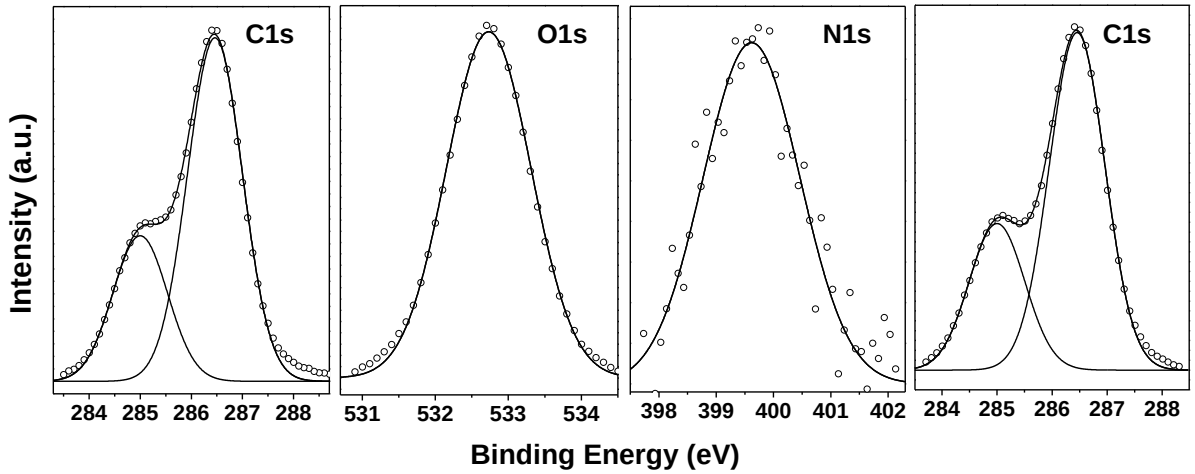

Figure.5.6. XPS spectra of C1s, O1s (tri-block copolymer), N1s and C1s in pDNA: PEO_{20}-PPO_{69}-PEO_{20} at 1:1 and 1: 10 ratios, respectively

Illustrated in table 5.2 are the atomic % of O, C and N present in pDNA, PEO_{20}-PPO_{69}-PEO_{20} and in the complex structures of pDNA and PEO_{20}-PPO_{69}-PEO_{20} (D/P) at different weight ratios, respectively. Coexisting N and P are indicators of DNA since their presence is typically unaffected by surface contaminations, if any. Still, in DNA nucleotides, N atoms are

present in high amount than P, and N has a higher XPS cross section. Therefore, between these P and N, N can provide more reliable reference for composition measurements.[62]

Sample	O atomic %	C atomic %	N atomic %	C/N ratio
PEO-PPO-PEO (P)	12.72	37.28	-	-
DNA (D)	12.12	33.51	04.38	7.65
D/P 1:1	12.77	36.04	1.16	31.07
D/P 1:5	12.16	37.05	0.78	47.50
D/P 1:10	12.45	37.02	.53	69.85

Table.5.2. Atomic % of oxygen, carbon and nitrogen present in pDNA, PEO-PPO-PEO and in the nanostructures of pDNA and PEO-PPO-PEO

It is remarkable to observe that in the complex of pDNA and PEO_{20}-PPO_{69}-PEO_{20}, with the increasing concentration of PEO_{20}-PPO_{69}-PEO_{20} (with respect to pDNA), C/N ratio increased significantly. In case of D/P at 1:1, 1:5 and1:10 ratios, C/N ratio was 31%, 47.5 % and 69.8% respectively. The constant increase in C/N ratio indicates that the pDNA is efficiently encapsulated in the self-assembled complex structures.

5.5. PEO_{20}-PPO_{69}-PEO_{20} mediated transformation and expression of GFP in transformed colonies

Although the major objective of this chapter was to study the chemical interaction of pDNA and PEO_{20}-PPO_{69}-PEO_{20} that drives self-assembly between pDNA and block copolymer, these self-assembled structures were also prepared at varying weight ratios of pDNA and PEO_{20}-PPO_{69}-PEO_{20} to screen the optimum ratio to achieve higher level of transformation. The pDNA and PEO_{20}-PPO_{69}-PEO_{20} are held together in water due the physical

interactions as discussed in previous sections, when these structures come into the contact of bacterial cell, they release pDNA. Moreover, integrity of pDNA during transformation studies is also confirmed and function of pDNA in the cellular environment was demonstrated using *E. coli* DH 5α.

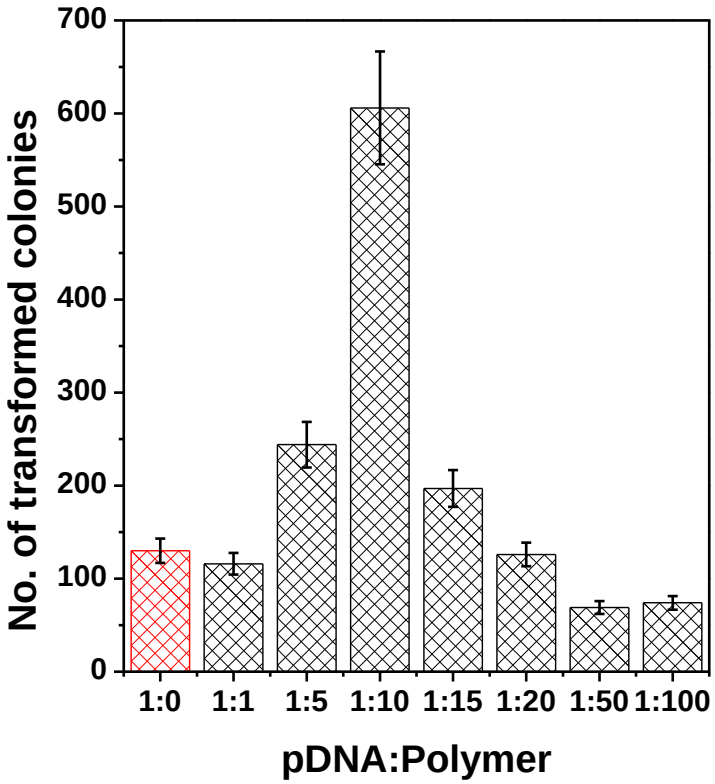

Figure.5.7. Number of transformed colonies grown on ampicillin plates for varying ratios of pDNA and PEO_{20}-PPO_{69}-PEO_{20}

Illustrated in Figure 5.7 are number of transformed colonies grown on ampicillin plates (10 µg/ml) after overnight incubation at 37°C. Ampicillin antibiotic was used during these experiments because *E. coli* DH5α cells originally did not have resistant gene towards ampicillin and therefore, only those competent bacterial cells which have up taken foreign pDNA (with ampicillin resistant gene) during transformation could be able to survive on the antibiotic containing nutrient agar plates. It was interesting to observe that only few competent bacterial cells were able to uptake freely available

pDNA (without employing tri-block copolymer) as some bacterial colonies were grown on antibiotic containing nutrient agar plates (positive control experiments, Figure 5.7 at 1:0 ratio). Conversely, competent bacterial cells themselves could not survive on ampicillin plates due to the lack of the ampicillin resistant gene and no colonies were developed in negative control experiments.

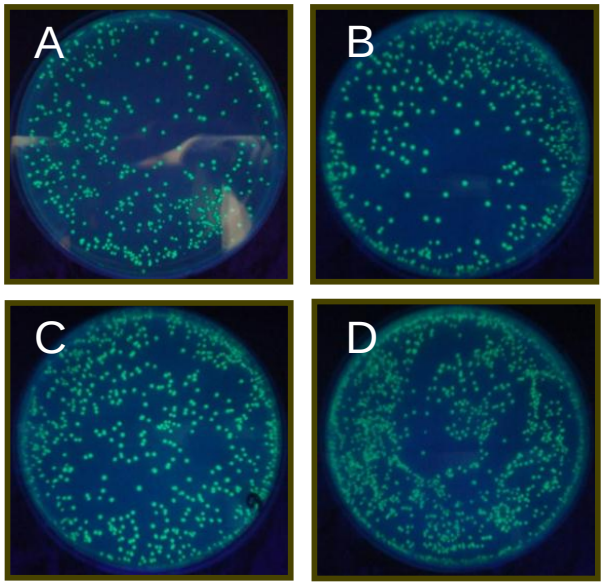

Figure.5.8. Representative transformed colonies grown on ampicillin plates showing expression of GFP gene. pDNA (A), pDNA:PEO_{20}-PPO_{69}-PEO_{20} complexes (B-D) at 1:1 (B), 1:5 (C), and 1:10 (D) ratios, respectively

Transformation studies with soft structures of pDNA and PEO_{20}-PPO_{69}-PEO_{20} revealed that with the increasing ratio of PEO_{20}-PPO_{69}-PEO_{20} (with respect of pDNA), number of transformed colonies exhibited steep rise up to 1:10 weight ratios and reached at the maximum. Further, increment in the PEO_{20}-PPO_{69}-PEO_{20} concentration, present in complex showed significant decline at 1:15 ratio and this feature was continued till the evaluated ratios. It is believed that the number of transformed colonies were maximum at 1:10 ratio because the size of complex at this ratio was the

optimum for parallel transformation and condensation of pDNA. At this ratio, the size of the complex (pDNA+PEO_{20}-PPO_{69}-PEO_{20}) was found to be almost half of the bacterial cells. As illustrated in Figure 5.9, the hydrophilic part of complex (PEO) adsorb on the bacterial cell wall and hydrophobic part (PPO) can insert into the bacterial cell and efficiently delivery pDNA.[49-51] Therefore, at 1:10 ratio of pDNA to PEO_{20}-PPO_{69}-PEO_{20} transformation was maximum and compared to pure pDNA, it showed over 6 folds higher transformation.

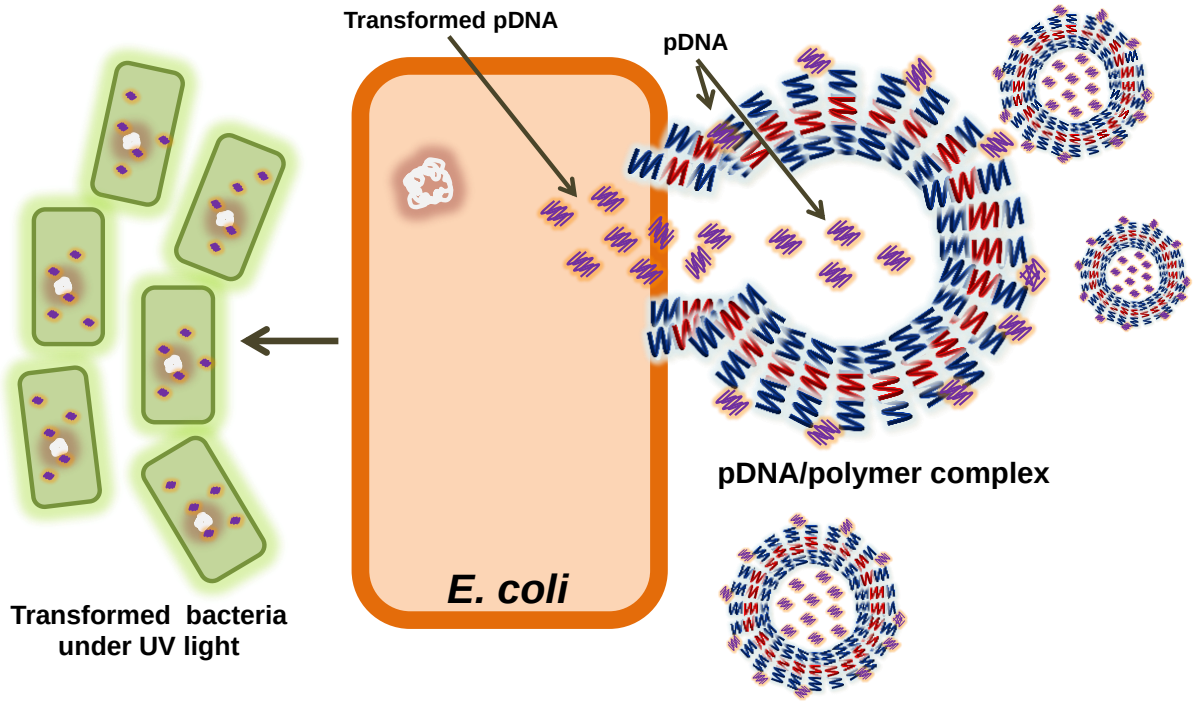

Figure.5.9. Schematic representation of transformation by polymer/pDNA complex

In addition to higher transformation, gene expression is also an important phenomenon to study by which information from a gene (segment of DNA) can be utilized to synthesize a functional gene product. To achieve gene expression it is essential to protect DNA from degradation during DNA

delivery or transformation.[63] Therefore, to confirm the integrity of pDNA in the complex of self-assembled structures (pDNA and PEO_{20}-PPO_{69}-PEO_{20}) and during transformation progression, the capability of transformed pDNA to function as normal, which can synthesize gene product is also demonstrated in the cellular environment *E. coli* DH 5α.

Illustrated in Figure 5.8 is expression of green fluorescence protein (GFP) pDNA in transformed colonies under UV light. In earlier reports it was demonstrated that after transformation, if green fluorescence protein (GFP) pDNA is delivered into cells and stay functional, GFP will be synthesized in the cells through the expression of GFP gene and it will be fluorescent. Figure 5.8 (A-D) exhibit fluorescence originating form transformed bacterial colonies through the expression of GFP gene thus confirming the integrity and functionality of pDNA in cellular environment. Figure 5.9 illustrates mechanism by which pDNA/PEO_{20}-PPO_{69}-PEO_{20} complex release pDNA in to the bacterial cells and gene expression by transferred GFP genes.

5.6. Conclusions

This chapter demonstrates that tri-block copolymer (PEO_{20}-PPO_{69}-PEO_{20}) is capable to self-assemble on heating and it can prepare nanostructures with pDNA. During, self-assembly with pDNA, this polymer encapsulated most of the pDNA. Physicochemical studies of these self-assembled nanostructures revealed that the phosphate group (PO_4^{3-}) of pDNA is involved in self-assembly process. These self-assembled nanostructures are spherical in shape and size of these structures depends on the concentration (or weight ratio) of PEO_{20}-PPO_{69}-PEO_{20}. Moreover, in

this process pDNA condenses and due to the presence of polymer corona, it gets protection from degradation and can efficiently travel and invade bacterial cells to perform transformation. Integrity of pDNA in these self-assembled nanostructures and gene expression in cellular environment is also shown during this chapter. These results revealed that PEO_{20}-PPO_{69}-PEO_{20} has potential to become one of the biocompatible and efficient DNA delivery carriers due to their well-known chemistry and physical characteristics. Moreover, these polymers have molecular diversity and their physicochemical properties can be fine-tuned for biomedical applications.

5.7. References

1. Couvreur, P. and C. Vauthier, *Nanotechnology: Intelligent design to treat complex disease.* Pharmaceutical Research, 2006. **23**(7): p. 1417-1450.
2. Sokolova, V. and M. Epple, *Inorganic Nanoparticles as Carriers of Nucleic Acids into Cells.* Angewandte Chemie International Edition, 2008. **47**(8): p. 1382-1395.
3. Verma, A. and F. Stellacci, *Effect of Surface Properties on Nanoparticle–Cell Interactions.* Small, 2010. **6**(1): p. 12-21.
4. You, C.-C., A. Verma, and V.M. Rotello, *Engineering the nanoparticle-biomacromolecule interface.* Soft Matter, 2006. **2**(3): p. 190-204.
5. Ghosh, P., et al., *Gold nanoparticles in delivery applications.* Advanced Drug Delivery Reviews, 2008. **60**(11): p. 1307-1315.
6. Check, E., *Gene therapy: A tragic setback.* Nature, 2002. **420**(6912): p. 116-118.

7. Gebhart, C.L. and A.V. Kabanov, *Perspectives on polymeric gene delivery.* Journal of Bioactive and Compatible Polymers, 2003. **18**(2): p. 147-166.

8. Ghosh, P.S., et al., *Efficient gene delivery vectors by tuning the surface charge density of amino acid-functionalized gold nanoparticles.* ACS Nano, 2008. **2**(11): p. 2213-2218.

9. Roy, I., et al., *Optical tracking of organically modified silica nanoparticles as DNA carriers: A nonviral, nanomedicine approach for gene delivery.* Proceedings of the National Academy of Sciences of the United States of America, 2005. **102**(2): p. 279-284.

10. Wiesman, Z., et al., *Novel cationic vesicle platform derived from vernonia oil for efficient delivery of DNA through plant cuticle membranes.* Journal of Biotechnology, 2007. **130**(1): p. 85-94.

11. Putnam, D., *Polymers for gene delivery across length scales.* Nat Mater, 2006. **5**(6): p. 439-451.

12. Fusco, S., A. Borzacchiello, and P.A. Netti, *Perspectives on: PEO-PPO-PEO Triblock Copolymers and their Biomedical Applications.* Journal of Bioactive and Compatible Polymers, 2006. **21**(2): p. 149-164.

13. Kakizawa, Y. and K. Kataoka, *Block copolymer micelles for delivery of gene and related compounds.* Advanced Drug Delivery Reviews, 2002. **54**(2): p. 203-222.

14. Moriguchi, R., et al., *A multifunctional envelope-type nano device for novel gene delivery of siRNA plasmids.* International Journal of Pharmaceutics, 2005. **301**(1-2): p. 277-285.

15. Nishiyama, N. and K. Kataoka, *Current state, achievements, and future prospects of polymeric micelles as nanocarriers for drug and gene delivery.* Pharmacology and Therapeutics, 2006. **112**(3): p. 630-648.

16. Luu, Y.K., et al., *Development of a nanostructured DNA delivery scaffold via electrospinning of PLGA and PLA-PEG block copolymers.* Journal of Controlled Release, 2003. **89**(2): p. 341-353.

17. Jeong, J.H. and T.G. Park, *Poly(L-lysine)-g-poly(D,L-lactic-co-glycolic acid) micelles for low cytotoxic biodegradable gene delivery carriers.* Journal of Controlled Release, 2002. **82**(1): p. 159-166.

18. Zhang, X.-Q., et al., *Polymer-Functionalized Nanodiamond Platforms as Vehicles for Gene Delivery.* ACS Nano, 2009. **3**(9): p. 2609-2616.

19. Luo, D., et al., *Poly(ethylene glycol)-Conjugated PAMAM Dendrimer for Biocompatible, High-Efficiency DNA Delivery.* Macromolecules, 2002. **35**(9): p. 3456-3462.

20. Kwak, M. and A. Herrmann, *Nucleic acid/organic polymer hybrid materials: Synthesis, superstructures, and applications.* Angewandte Chemie - International Edition, 2010. **49**(46): p. 8574-8587.

21. Meng, F., Z. Zhong, and J. Feijen, *Stimuli-Responsive Polymersomes for Programmed Drug Delivery.* Biomacromolecules, 2009. **10**(2): p. 197-209.

22. Duncan, R., H. Ringsdorf, and R. Satchi-Fainaro, *Polymer Therapeutics: Polymers as Drugs, Drug and Protein Conjugates and Gene Delivery Systems: Past, Present and Future Opportunities Polymer Therapeutics I.* 2006, Springer Berlin / Heidelberg. p. 1-8.

23. Chen, C.J., et al., *Self-assembly cationic nanoparticles based on cholesterol-grafted bioreducible poly(amidoamine) for siRNA delivery.* Biomaterials, 2013. **34**(21): p. 5303-5316.

24. Whitesides, G.M. and D.J. Lipomi, *Soft nanotechnology: "structure" vs. "function".* Faraday Discussions, 2009. **143**: p. 373-384.

25. Colombo, G., P. Soto, and E. Gazit, *Peptide self-assembly at the nanoscale: a challenging target for computational and experimental biotechnology.* Trends in Biotechnology, 2007. **25**(5): p. 211-218.

26. Hamley, I.W., *Nanotechnology with soft materials.* Angewandte Chemie - International Edition, 2003. **42**(15): p. 1692-1712.

27. Blanazs, A., S.P. Armes, and A.J. Ryan, *Self-Assembled Block Copolymer Aggregates: From Micelles to Vesicles and their Biological Applications.* Macromolecular Rapid Communications, 2009. **30**(4-5): p. 267-277.

28. Zhou, L., et al., *Multifunctional triblock co-polymer mP3/4HB-b-PEG-b-lPEI for efficient intracellular siRNA delivery and gene silencing.* Acta Biomaterialia, 2013. **9**(4): p. 6019-6031.

29. Xiong, X.B., et al., *Amphiphilic block co-polymers: Preparation and application in nanodrug and gene delivery.* Acta Biomaterialia, 2012. **8**(6): p. 2017-2033.

30. Pawar, P.V., et al., *Functionalized polymersomes for biomedical applications.* Polymer Chemistry, 2013. **4**(11): p. 3160-3176.

31. Duncan, R. and M.J. Vicent, *Polymer therapeutics-prospects for 21st century: The end of the beginning.* Advanced Drug Delivery Reviews, 2013. **65**(1): p. 60-70.

32. Pridgen, E.M., R. Langer, and O.C. Farokhzad, *Biodegradable, polymeric nanoparticle delivery systems for cancer therapy.* Nanomedicine, 2007. **2**(5): p. 669(12).

33. Sharma, B., et al., *Selective biophysical interactions of surface modified nanoparticles with cancer cell lipids improve tumor targeting and gene therapy.* Cancer Letters, 2013. **334**(2): p. 228-236.

34. Huang, S., et al., *Tumor targeting and microenvironment-responsive nanoparticles for gene delivery.* Biomaterials, 2013. **34**(21): p. 5294-5302.

35. Boussif, O., et al., *A versatile vector for gene and oligonucleotide transfer into cells in culture and in vivo: Polyethylenimine.* Proceedings of the National Academy of Sciences of the United States of America, 1995. **92**(16): p. 7297-7301.

36. Felgner, P.L., et al., *Nomenclature for synthetic gene delivery systems.* Human Gene Therapy, 1997. **8**(5): p. 511-512.

37. Pack, D.W., et al., *Design and development of polymers for gene delivery.* Nat Rev Drug Discov, 2005. **4**(7): p. 581-593.

38. Wong, S.Y., J.M. Pelet, and D. Putnam, *Polymer systems for gene delivery-Past, present, and future.* Progress in Polymer Science, 2007. **32**(8-9): p. 799-837.

39. McIlroy, D., et al., *DNA/amphiphilic block copolymer nanospheres promote low-dose DNA vaccination.* Molecular Therapy, 2009. **17**(8): p. 1473-1481.

40. Torchilin, V., *Micellar Nanocarriers: Pharmaceutical Perspectives.* Pharmaceutical Research, 2007. **24**(1): p. 1-16.

41. Kataoka, K., A. Harada, and Y. Nagasaki, *Block copolymer micelles for drug delivery: design, characterization and biological significance.* Advanced Drug Delivery Reviews, 2001. **47**(1): p. 113-131.

42. Peng, K.Y., S.W. Wang, and R.S. Lee, *Amphiphilic diblock copolymers based on poly(2-ethyl-2-oxazoline) and poly(4-substituted-ε-caprolactone): Synthesis, characterization, and cellular uptake.* Journal of Polymer Science, Part A: Polymer Chemistry, 2013. **51**(13): p. 2769-2781.

43. Wang, Y. and S.M. Grayson, *Approaches for the preparation of non-linear amphiphilic polymers and their applications to drug delivery.* Advanced Drug Delivery Reviews, 2012. **64**(9): p. 852-865.

44. Du, J. and R.K. O'Reilly, *Advances and challenges in smart and functional polymer vesicles.* Soft Matter, 2009. **5**(19): p. 3544-3561.

45. Onaca, O., et al., *Stimuli-Responsive Polymersomes as Nanocarriers for Drug and Gene Delivery.* Macromolecular Bioscience, 2009. **9**(2): p. 129-139.

46. Li, W., S. Feng, and Y. Guo, *Tailoring polymeric micelles to optimize delivery to solid tumors.* Nanomedicine, 2012. **7**(8): p. 1235-1252.

47. Lee, J.S. and J. Feijen, *Polymersomes for drug delivery: Design, formation and characterization.* Journal of Controlled Release, 2012. **161**(2): p. 473-483.

48. Green, R.J., et al., *Adsorption of PEO-PPO-PEO Triblock Copolymers at the Solid/Liquid Interface: A Surface Plasmon Resonance Study.* Langmuir, 1997. **13**(24): p. 6510-6515.

49. Batrakova, E.V., et al., *Pluronic P85 enhances the delivery of digoxin to the brain: In vitro and in vivo studies.* Journal of Pharmacology and Experimental Therapeutics, 2001. **296**(2): p. 551-557.

50. Wang, J.-Y., J. Marks, and K.Y.C. Lee, *Nature of Interactions between PEO-PPO-PEO Triblock Copolymers and Lipid Membranes: (I) Effect of Polymer Hydrophobicity on Its Ability to Protect Liposomes from Peroxidation.* Biomacromolecules, 2012. **13**(9): p. 2616-2623.

51. Alakhov, V.Y. and A.V. Kabanov, *Block copolymeric biotransport carriers as versatile vehicles for drug delivery.* Expert Opinion on Investigational Drugs, 1998. **7**(9): p. 1453-1473.

52. Batrakova, E.V. and A.V. Kabanov, *Pluronic block copolymers: Evolution of drug delivery concept from inert nanocarriers to biological response modifiers.* Journal of Controlled Release, 2008. **130**(2): p. 98-106.

53. Thomas, M. and A.M. Klibanov, *Non-viral gene therapy: Polycation-mediated DNA delivery.* Applied Microbiology and Biotechnology, 2003. **62**(1): p. 27-34.

54. Sambrook, J. and D. Russell, *Molecular Cloning: A Laboratory Manual* Third Edition ed. 2000.

55. Tu, Z., et al., *An improved system for competent cell preparation and high efficiency plasmid transformation using different Escherichia coli strains*. 2005. 2005.

56. Bielinska, A.U., J.F. Kukowska-Latallo, and J.R. Baker Jr, *The interaction of plasmid DNA with polyamidoamine dendrimers: mechanism of complex formation and analysis of alterations induced in*

nuclease sensitivity and transcriptional activity of the complexed DNA. Biochimica et Biophysica Acta (BBA) - Gene Structure and Expression, 1997. **1353**(2): p. 180-190.

57. Ouameur, A.A. and H.-A. Tajmir-Riahi, *Structural Analysis of DNA Interactions with Biogenic Polyamines and Cobalt(III)hexamine Studied by Fourier Transform Infrared and Capillary Electrophoresis.* Journal of Biological Chemistry, 2004. **279**(40): p. 42041-42054.
58. Ruiz-Chica, J., et al., *Fourier transform Raman study of the structural specificities on the interaction between DNA and biogenic polyamines.* Biophysical Journal, 2001. **80**(1): p. 443-454.
59. Taillandier, E. and J. Liquier, *Infrared spectroscopy of DNA.* Methods in Enzymology, 1992. **211**: p. 307-335.
60. Choosakoonkriang, S., et al., *Biophysical characterization of PEI/DNA complexes.* Journal of Pharmaceutical Sciences, 2003. **92**(8): p. 1710-1722.
61. Shirley, D.A., *High-Resolution X-Ray Photoemission Spectrum of the Valence Bands of Gold.* Physical Review B, 1972. **5**(12): p. 4709-4714.
62. Petrovykh, D.Y., et al., *Quantitative Analysis and Characterization of DNA Immobilized on Gold.* Journal of the American Chemical Society, 2003. **125**(17): p. 5219-5226.
63. Luo, D. and W.M. Saltzman, *Synthetic DNA delivery systems.* Nat Biotech, 2000. **18**(1): p. 33-37.

Chapter VI

Conclusions and scope for the future research

First part of this chapter summarizes the research work presented in this thesis and discusses the major conclusions obtained from this research work. Second part of the chapter emphasizes the scope of the present work and how it can be extended for the potential avenues for future work.

6.1. Summary and Conclusions

In the current literature, majority of the research work at the interface of nano-biology has underestimated, if not overlooked, the role of surface functionalization and its cooperative interaction with the nanoparticle composition, towards the biological activities. The research work presented in this thesis is an attempt to establish the correlation between surface chemical features of nanoparticles with their biological activities. Amino acid functionalized metal nanoparticles have been chosen as model systems to understand the influence of surface corona and metal composition on their peroxidase-like behaviour and antibacterial activity. Amino acids were chosen since the major focus of the thesis is to study the applications of nanomaterials in biology. Therefore, it is imperative to use synthetic methods, which don't use chemical reducing agents, surfactants, organic solvents and harsh reaction conditions in order to obtain the nanomaterials in a green chemical approach.

The synthetic method described here to make mono and bimetallic nanoparticles employs amino acids as reducing groups for the metal ions, which are fundamental building blocks of proteins. Side groups present in amino acids were utilized as reducing agents while retaining amine and carboxylic acid groups, enabling bio-functionalized nanoparticles synthesis at ambient conditions. The as-formed nanoparticles were capped instantaneously by a shell of amino acids, enabling the nanoparticle surface to appear like a polymer of amino acids pseudo-protein, stabilizing the nanoparticles against aggregation, providing sites for further

functionalization and pH dependant surface charge control. Importantly, cell and cellular components appear to approach these nanoparticles in a similar manner how they approach a supported enzyme. Moreover, presence of amino acids on the surface of nanoparticles can provide biological identity to the nanomaterials.

In first part of the thesis, tryptophan and tyrosine amino acids were used to make gold, silver and their bimetallic alloy nanoparticles, wherein respective metal ions were reduced by indole (tryptophan) or phenol (tyrosine) groups. These nanoparticles are highly stable, water dispersible with controlled metal composition in bimetallic system. All these nanoparticles were found to have intrinsic peroxidase enzyme-like activities. Peroxidase-like behaviour of these nanoparticles was found to be temperature, composition and amino acid surface functionalization dependant. Tyrosine capped nanoparticles exhibited higher peroxidase-like activity compare to tryptophan capped nanoparticles. In mono metallic system, Ag nanoparticles show more peroxidase-like behaviour compared to Au nanoparticles, irrespective of amino acid coating. In bimetallic alloy systems, with the increment in Ag fraction (with respect to Au), the peroxidase-like activity increases and a steep rise in the activity of tyrosine capped Au-Ag alloy nanoparticles was observed due to the ease of Ag stripping. Further, to understand interaction of these nanomaterials with bacteria, assessments were performed on Gram positive (*Staphylococcus albus*) and Gram negative (*Escherichia coli*) bacterial strains. Interestingly, all the nanoparticles were proven to be highly toxic to *S. albus* irrespective of their composition such that even Au nanoparticles, which are typically

considered as biocompatible, were found to be toxic. Conversely, only Ag and Ag rich alloy nanoparticles were found to be toxic to *E. coli*, while Au nanoparticles didn't illustrate much toxicity. Amino acid surface corona, present around the nanoparticles raised toxicity towards Gram positive bacteria similar to lysozymes and other antimicrobial peptides, whereas composition dependant toxicity was revealed against Gram negative bacteria and capping of amino acids had little influence. This work is the first attempt to show that how an amino acid shell on a nanoparticles surface and their metal composition may function like a selective antibiotic.

Second part of the thesis was focussed on fine-tunning the antimicrobial profile of non-toxic tyrosine reduced Au nanoparticles by sequential surface functionalization with appropriate molecules. Polyoxometalates (POMs) and cationic amino acid lysine were shown to impart antibacterial activity on the surface of Au nanoparticles to change their inherent biocompatible nature. In this case, presence of POMs and lysine renders these Au nanoparticles active by their tendency to create oxidative stress and attacking the negatively charged bacterial cell membrane, respectively. Moreover, presence of lysine molecules can initially guide Au nanoparticles toward negatively charged bacterial cells through electrostatic forces, which improves the direct contact between bacterial cells and nanomaterials enabling further interaction, ultimately leading to cell death due to the cationic nature of lysine. These results clearly demarcated the effect of surface composition of nanoparticles on the overall antibacterial activity of these materials. The same sequential functionalization was extended to silver nanoparticles, wherein these

nanoparticles have shown very high antibacterial activity even at smaller concentrations due to the synergistic effects of silver and POMs.

All the nanomaterials used in this thesis for antibacterial studies, employed physical mode of action against both the bacterial strains. These nanomaterials caused cell wall degradation, cell lysis and created big pores (holes) within the studied bacterial strains. With such morphological changes, bacterial cells could not maintain their physical integrity and were unable to perform their biological reactions, which is important for their survival. Therefore, the nanomaterials fabricated in this thesis grant an opportunity to control pathogenic bacteria and moreover these nanomaterials can prevent bacterial strains to develop resistance.

In the last part of the thesis, formation of complex of plasmid DNA-tri block copolymer nanostructures has been demonstrated. The electrostatic interaction between negatively charged phosphate groups present in pDNA and positively charged groups of block copolymer governs the self-assembly process to make their combined structures. During self-assembly, the pDNA encapsulated in the micelles of block copolymer and the size of these micelles depends on the weight ratio of pDNA and block copolymer. Due to the encapsulation of pDNA these micelles preserve integrity of pDNA during transformation, and show high transformation efficiency for a green fluorescent protein (GFP) expressing plasmid.

6.2. Scope for Future work

Materials utilized for peroxidase-like behaviour and antibacterial activities in the present research work can be explored further in the

following ways. Utilizing more two amino acids to reduce the metal ions to form nanoparticles, which contain multiple amino acids on their surface. This combination of different amino acid on the surface of nanoparticles can form numerous materials and the potential materials to be considered as "nanozymes". Making artificial enzymes is an emerging field of research, synthesizing these nanozymes and studying their enzyme-like properties will have significant scope in the future. Moreover, by varying the amino acid shell composition, toxicity of these materials can be tailored in such a way to create materials with wide range of controlled toxicities and biomedical applications. Their interaction with different proteins, enzymes, DNA and other cell components can be a broad area to explore. Further, uptake of nanoparticles within bacteria, cancer and mammalian cells can be followed by where these nanoparticles can be localized within the specific cellular space.

Au nanoparticles are inherently biocompatible and their biological profile can be controllably fine-tuned by their surface functionalization with appropriate molecules, as demonstrated using POMs and lysine. Although antibacterial activities of these functionalized nanoparticles have been discussed in this thesis but in near future these nanomaterials can be employed as potential anticancer and antiviral agents due to the presence of active POMs. Preliminary, work has been done in this aspect, where these nanomaterials exhibited similar toxicity pattern against human lung carcinoma cells (data not included for brevity). Furthermore, the sequential surface functionalization strategy can be expanded from POMs and lysine to other biomolecules or chemical moieties to realize the full potential of

surface functionalized nanomaterials, which might go beyond current expectations.

Tri block copolymer can be used as safe and efficient carrier to deliver drug and genes. The principle forces and chemical interactions developing DNA-polymer structures have been established in this thesis. In future, it will be interesting to investigate the principle forces governing destabilization of DNA-polymer or drug-polymer structures. Also, it will be of particular interest to explore the effects of external stimuli including temperature, pH and redox conditions on drug and gene delivery using polymer based nanocarriers.

Appendices

Appendix -A. Author's achievements and professional activities

Appendix-B. List of publications

Appendix-C.

Appendix -A. Author's achievements and professional activities

Profile was added to the Victorian Government website
http://www.studymelbourne.vic.gov.au/living_in_melbourne/student-stories/hemant-daima

STUDY MELBOURNE
VICTORIA AUSTRALIA

Live Study Apply FAQs Fast Facts Contact

Home > Living > Student Stories > A gold step forward in healthcare

A gold step forward in healthcare

In the laboratories of RMIT University's Advanced Materials and Industrial Chemistry Group in Melbourne, Hemant Daima is pursuing his PhD that involves synthesising very small particles of precious metals such as gold, silver and platinum, for use in healthcare.

This new field of nanobiotechnology draws together expertise from a wide range of scientific disciplines to develop new nanostructures that can help improve drug delivery, gene delivery, cancer treatment and other health tools.

"I could not dream of a better research group to work with in the field of nanobiotechnology," Mr Daima said.

"Very few groups in the world are working in nanobiotechnology and I have the opportunity to work in a reputed group - so I have the advantages of gaining expertise in materials science, chemistry, biology and physical sciences, all available through a single platform."

Mr Daima's interest in nanobiotechnology began when he took a project on nanomaterials synthesis as part of his Master of Science degree at the University of Rajasthan in Jaipur, India, and decided he wanted to know more about life under the microscope.

"I found that this is a pretty interesting area with lots of opportunities," Mr Daima said.

"I decided to pursue my doctoral work in the field of nanobiotechnology to capitalise on my full potential, educational background and past research experience."

After being awarded a National Overseas Scholarship from the Government of India to pursue his doctoral studies overseas, he searched the world for opportunities in nanobiotechnology, eventually finding RMIT University.

The research project is examining ways to control the synthesis of gold, silver and platinum nanoparticles through green chemistry. Once these key inorganic materials are successfully synthesised, Mr Daima will examine ways they can be applied to different biological applications.

"I absolutely love my time at RMIT University. The University campus is located right in the heart of the city and I have been trained on the most sophisticated and advanced instruments in my research field," Mr Daima said.

"I found that Melbourne is the most vibrant and multicultural city in Australia. I had the opportunity to interact with students from different cultural backgrounds and nationalities. It is also a great place to experience festivals!"

Research and Professional Skill Development Training/Courses

2012: Research Commercialisation
Queensland University of Technology, Brisbane (Australia)

2012: Project Management
University of Technology, Sydney (Australia)

2012: Entrepreneurship
University of South Australia, Adelaide, (Australia)

2012: Leadership and Communication
Curtin University, Sydney (Australia)

2012: Advanced FTIR and UV-Vis spectroscopic training
2010: Spectroscopic training

Honour, Awards and Fellowships

1. Awarded with *DVC (R&I)'s PGRS International Conference fund* to attend ICCMPP-2012 held at Lucknow, India (26 October 2012).

2. Recipient of *PerkinElmer Pty Ltd Award* for the most outstanding contribution to the field of FTIR spectroscopy (14 May 2012).

3. Awarded with *DVC (R&I)'s PGRS International Conference fund* and *School Conference Fund* to attend Nanotech 2012 held at California, USA (4 April 2012, 1 June 2012).

4. Recipient of the *PerkinElmer Research Excellence Award* for academic achievements in 2011 (28 March 2012).

5. Selected for *the Australian Nanotechnology Network (ANN) Bursary* to attend ICONN 2012 held at Perth, Australia.

6. Commendation in Vision to reality: Higher Degrees by Research Conference 2011 held at RMIT University, Melbourne, Australia (21 October, 2011).

7. Awarded with *RACI Travel Bursary* to attend 41st CHEMECA 2011 held at Sydney, Australia (20 September 2011) and

8. Granted with *RACI Travel Bursary* to attend 40th CHEMECA 2010 held at Adelaide, Australia (27 September 2010).

9. Recipient of *National Overseas Scholarship* from the Government of India, New Delhi to pursue doctoral studies abroad in Nanotechnology, Biotechnology & Genetic Engineering (2007-08).

Appendix-B. List of publications

Referred journal publications

1. PR. Selvakannan, R. Ramanathan, B. J. Plowman, Y. Sabri, **H. Daima**, A. O'Mullane, V. Bansal, S. K. Bhargava. Probing the effect of charge transfer enhancement in off resonance mode SERS via conjugation of the probe dye between silver nanoparticles and metal substrates. 2013 (Accepted in Physical Chemistry Chemical Physics, Manuscript ID: CP-ART-04-2013-051646 (Impact factor-3.573).
2. A. F. Chrimes, K. Khoshmanesh, P. R. Stoddart, A. A. Kayani, A. Mitchell, **H. Daima**, V. Bansal, K. Kalantar-zadeh. Active control of silver nanoparticles spacing using dielectrophoresis for SERS. Analytical Chemistry 84(9), 2012, pp. 4029-4035. Publisher: American Chemical Society, Print ISSN: 0003-2700, Web ISSN: 1520-6882 (Impact factor-5.874, Cited>13).
3. D. Jain, **H. K. Daima**, S. Kachhwala, S. L. Kothari. Synthesis of plant-mediated silver nanoparticles using papaya fruit extract and evaluation of their antimicrobial activities. Digest Journal of Nanomaterials and Biostructures 4 (3), 2009, pp. 557-563. Publisher: National Institute R&D Materials Physics, ISSN 1842-3582 (Impact factor-2.078, Cited>93).
4. **H. K. Daima**, J. Anitha, P. Manivachakam, S. Marimuthu, S. Murugesan. Isolation, analysis and identification of phytochemicals of Cynodon dactylon (L.) Pers.; Poaceae using AAS, HPLC and GC-M S methods. Pestology 31 (8), 2007, pp. 60-67. Publisher: Scientia Publications, ISSN: 09703012 (Cited>1).
5. **H. K. Daima**, PR. Selvakannan, R. Shukla, S. K. Bhargava, V. Bansal. Fine-tuning the antimicrobial profile of biocompatible gold nanoparticles by their sequential surface functionalization using polyoxometalates and lysine (Under review in Langmuir, Manuscript ID: la-2013-01391b (Impact factor-4.186).
6. **H. K. Daima**, PR. Selvakannan, A. E. Kandjani, S. K. Bhargava, V. Bansal. Tyrosine-capped, lysine-guided Ag nanoparticle-polyoxometalate composites as efficient antibacterial agents. (Will be communicated to RSC Advances).
7. **H. K. Daima**, PR. Selvakannan, R. Shukla, V. Mistry, A. P.O' Mullane, S. K. Bhargava, V. Bansal. Amino acids mediated synthesis of gold, silver and their alloy nanoparticles: Influence of surface functionlization and metal

composition on antibacterial activity. (Will be communicated to Nature Nanotechnology).

8. **H. Daima**, S. Shankar, PR. Selvakannan, S. K Bhargava, V. Bansal. Self-assembled nanostructures of triblock co-polymer and plasmid DNA and their applications as non-viral DNA delivery vector. (Under preparation).

Refereed conference publications

1. **H. K. Daima**, PR. Selvakannan, S. Shankar, Ravi Shukla, S. K. Bhargava, V. Bansal. Amino acid and gold nanoparticles modified mesoporous silica materials synthesis and their applications in DNA transformation. *Proceedings of CHEMECA 2012: Quality of Life through Chemical Engineering* (Wellington, New Zealand) 23-26 September 2012, pp. 160-164.
2. **H. K. Daima**, PR. Selvakannan, R. Shukla, S. K. Bhargava, V. Bansal. Stabilization of polyoxometalates on gold nanoparticles surface using amino acid linker to control their toxicity. *Proceedings of CHEMECA 2012: Quality of Life through Chemical Engineering* (Wellington, New Zealand) 23-26 September 2012, pp. 1628-1634.
3. **H. K. Daima**, PR. Selvakannan, S. K. Bhargava, V. Bansal. Sequential surface functionalization by polyoxometalates and lysine renders non-toxic gold nanoparticles strong antibacterial agents. *Technical Proceedings of Nanotech 2012 TechConnect World Conference and Expo* (Santa Clara, USA) 18-21 June 2012, Vol. 3, pp.154-158**.**
4. **H. K. Daima**, S. Shankar PR. Selvakannan, S. K. Bhargava, V. Bansal. Self assembled nanostructures of triblock co-polymer and plasmid DNA and their applications as non-viral DNA delivery vector. *Technical Proceedings of Nanotech 2012 TechConnect World Conference and Expo* (Santa Clara, USA) 18-21 June 2012, Vol. 3, pp.178-181**.**
5. **H. K. Daima**, PR. Selvakannan, S.K. Bhargava, V. Bansal. Rendering the gold nanoparticles surface antibacterial active by sequential surface-modification with polyoxometalates and lysine amino acid. *Proceedings of ICONN 2012* (Perth, Australia) 5-9 February 2012, pp. 1-2**.**
6. **H. K. Daima**, PR. Selvakannan, Z. Homan, S. Bhargava, V. Bansal**.** Tyrosine mediated gold, silver and their alloy nanoparticles synthesis: Antibacterial activity toward Gram positive and Gram negative bacterial strains. *Proceedings of 2011 International Conference on Nanoscience, Technology and*

Societal Implications (NSTSI) (Bhubaneswar, India) 8-10 December 2011, pp.1-6.

7. **H. K. Daima**, PR. Selvakannan, S. K. Bhargava, V. Bansal**.** Metal/polyoxometalate/amino acid as functional nanoconjugates for potential antibacterial activity**.** *Proceedings of CHEMECA 2011: Engineering a Better World* (Sydney, Australia) 18-21 September 2011, pp. 1971-1980**.**
8. **H. K. Daima**, PR. Selvakannan, S. K. Bhargava, V. Bansal. Threonine amino acid mediated photochemical synthesis of Au, Ag and bimetallic Au-Ag nanoparticles with antibacterial activity. *Proceedings of CHEMECA 2011: Engineering a Better World* (Sydney, Australia) 18-21 September 2011, pp. 365-374.
9. **H. K. Daima**, PR. Selvakannan, V. Bansal, S. K. Bhargava**.** Surface functionality driven antimicrobial activity: Case study of amino acid reduced nanoparticles with different bacterial strains. *Proceedings of CHEMECA 2010: Engineering at the Edge* (Adelaide, Australia) 26-29 September 2010, pp. 2934-2943.

Appendix-C.

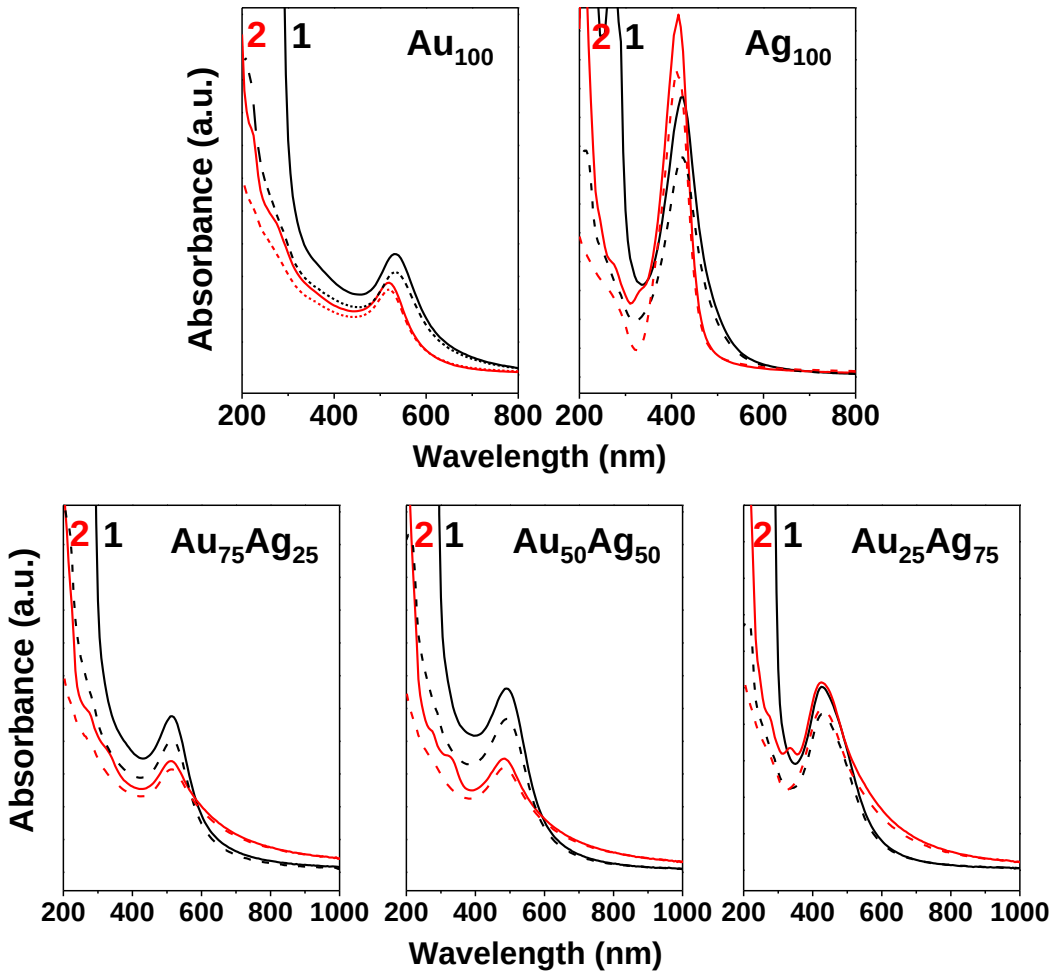

Figure.C.1. UV-visible absorbance spectra of as-obtained nanoparticles (solid lines) and post-dialysis (dotted lines) wherein curve 1 and 2 corresponds to tryptophan and tyrosine reduced nanoparticles, respectively

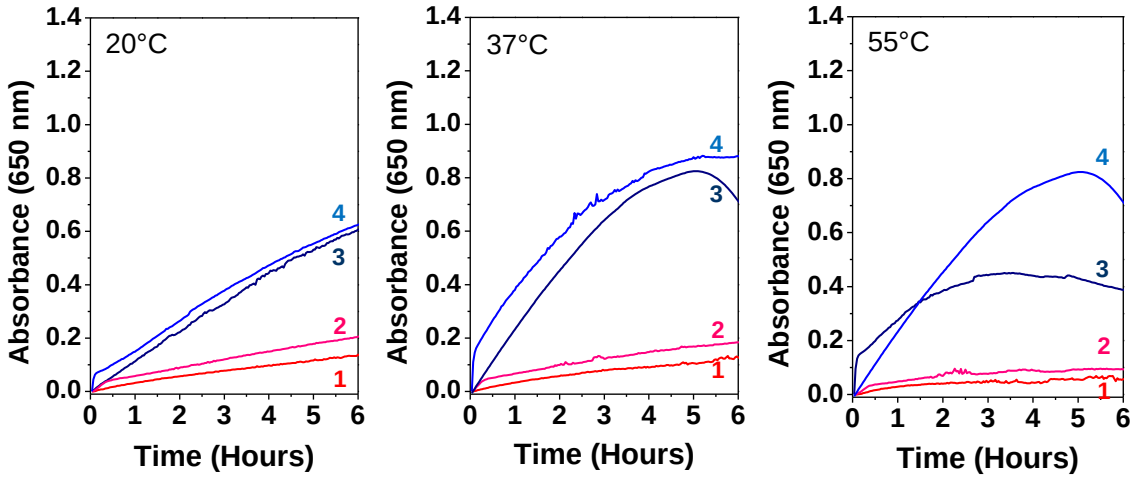

Figure.C.2. Temperature dependent peroxidase-like activity of tryptophan- and tyrosine- capped Au and Ag nanoparticles (10 ppm). Curve 1, 2, 3, and 4 correspond to Au_{100}^{Trp}, Au_{100}^{Tyr}, Ag_{100}^{Trp} and Ag_{100}^{Tyr} nanoparticles, respectively

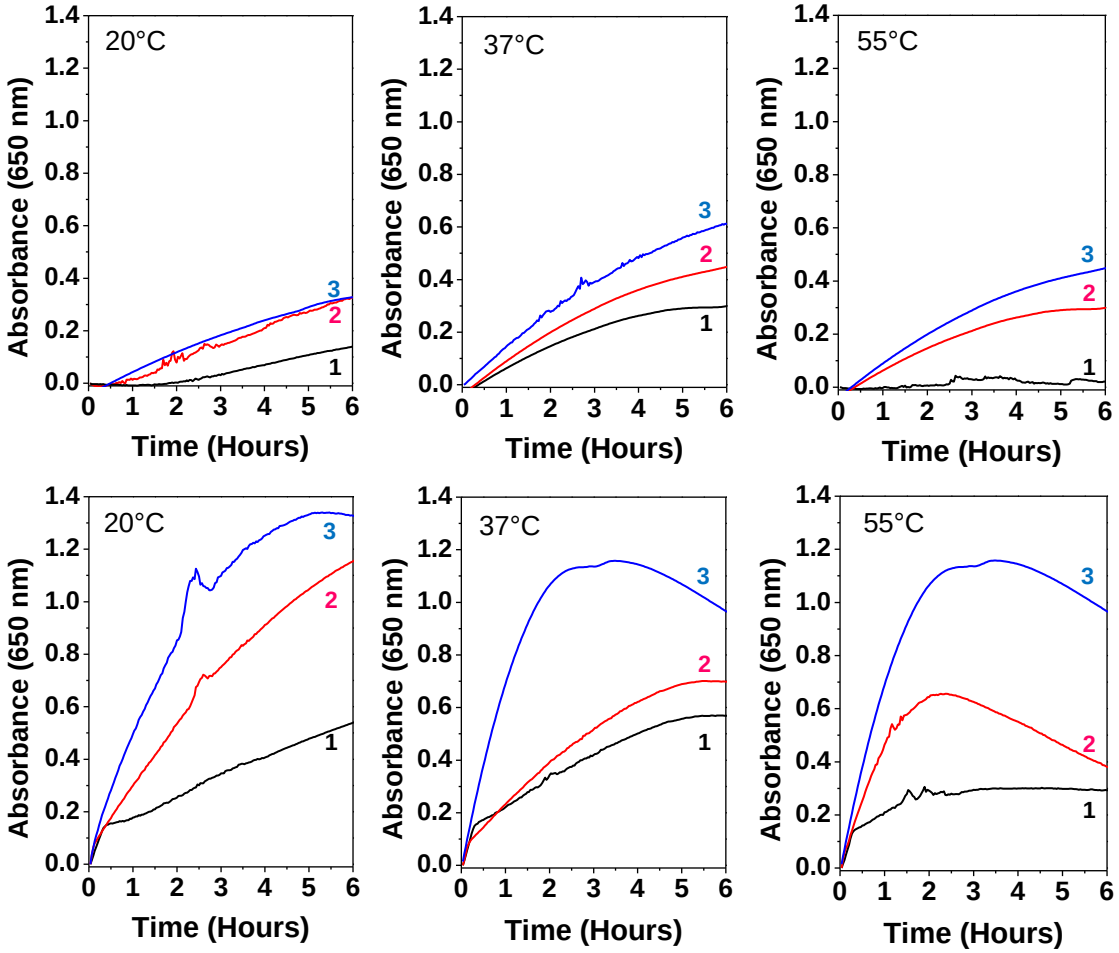

Figure.C.3. Temperature dependent peroxidase-like activity of tryptophan- (top) and tyrosine- (bottom) capped Au-Ag alloy nanoparticles. Curve 1, 2, and 3 correspond to $Au_{75}Ag_{25}$, $Au_{50}Ag_{50}$, $Au_{25}Ag_{75}$ nanoparticles, respectively